MECHANISMS AND ANALYSIS OF THE CNS DISTRIBUTION OF CEDIRANIB, A MOLECULARLY-TARGETED ANTI-ANGIOGENIC AGENT

A DISSERTATION
SUBMITTED TO THE FACULTY OF THE GRADUATE SCHOOL
OF THE UNIVERSITY OF MINNESOTA
BY

Tianli Wang

IN PARTIAL FULFILLMENT OF THE REQUIREMENTS
FOR THE DEGREE OF
DOCTOR OF PHILOSOPHY

Dr. William F. Elmquist

August 2011

Acknowledgements

First and foremost, I want to extend my deepest appreciation to my advisor, Dr. William Elmquist, for his continuous support, thoughtful guidance, endless patience and helpful advice. I am greatly indebted to him for giving me the freedom to explore my research interests. I could not have achieved my goals without him. His enthusiasm for research and optimistic attitude during the difficult times has motivated me and will be my example in the rest of my life.

I would also like to share my gratefulness to the other members of my thesis committee, Dr. Ronald Sawchuk, Dr. Richard Brundage and Dr. Carolyn Fairbanks, for their time, comments and help. In particular, I would like to thank the many people who have taught me pharmacokinetics, including Dr. Ronald Sawchuk, Dr. William Elmquist, Dr. Richard Brundage and Dr. Cheryl Zimmerman, whose inspiring teaching first made pharmacokinetics/pharmacometrics so fascinating to me.

I also want to express my appreciation to my former and present labmates in the Elmquist lab: Naveed Shaik, Nagdeep Giri, Guoyu Pan, Ying Chen, Li Li, Sagar Agarwal, Ramola Sane, Rajneet Oberoi, Shruthi Vaidhyanathan and Rajendar Mittapalli, for providing a friendly environment in which to learn and grow. Special thank goes to Sagar Agarwal for his collaboration with me. I would also like to thank my former classmate, Kyle Baron, for his knowledge sharing and collaboration.

I am appreciative of the Department of Pharmaceutics for providing me the opportunity to fulfill my dream in pursuing this PhD. My thanks also go to Candice McDermott and Erica Stapic for their kindly support during my stay in the department.

Lastly, and most importantly, I am extremely thankful to my parents, Kebing Guo and Guozhen Wang, for their infinite love and unwavering encouragement in every imaginable way throughout my educational endeavor. I also want to express my utmost gratitude to my husband, Wei Zhong, for his understanding and extraordinary support in all my pursuits, and for his companionship which has made my years in graduate school enjoyable. To them I dedicate this thesis.

Tianli Wang

August 2011

Abstract

The role of vascular endothelial growth factor (VEGF) in brain tumor angiogenesis via stimulation of its receptor (VEGFR) is well established, indicating that the tumor endothelium may be a potential target for brain tumor treatment. However, the current angiogenesis inhibitors used in clinical trials so far have shown limited effects on tumor growth and improvement in survival. Cediranib is an orally available small-molecule kinase inhibitor of all three VEGFR isoforms, with additional activity against PDGFRß and c-KIT. Its broad activities against critical targets, especially the anti-angiogenic activity, make cediranib an attractive option for therapy in central nervous system (CNS) tumors. Cediranib has shown promising anti-angiogenic efficacy in early clinical trials in glioblastoma (GBM), but its anti-tumor mechanisms and its effect on the efficacy of concurrent chemotherapies remain unclear.

ATP-binding cassette transporters p-glycoprotein (P-gp) and breast cancer resistance protein (BCRP) have been shown to work in concert to restrict brain penetration of several tyrosine kinase inhibitors. This study investigated the influence of P-gp and BCRP at the blood-brain barrier (BBB) on the CNS penetration of cediranib. Although *in vitro* studies suggest that both P-gp and BCRP significantly affect intracellular delivery of cediranib, *in vivo* data indicated that P-gp is a dominant efflux transporter for cediranib and BCRP plays a minor role in limiting transport of cediranib across the BBB. The interaction of cediranib with these brain efflux transporters could limit the anti-angiogenic and anti-tumor action in cells in the brain parenchyma and might lead to poor

outcomes in clinical trials. A more thorough understanding of the mechanisms controlling the delivery of cediranib to its targets will allow more efficacious use of this drug in GBM.

To better understand the brain distributional kinetics, simulation strategies were employed to explore the appropriate ways to compare the true brain partitioning among different transporter deficient transgenic mouse groups, which, in general, helps in exploring the contribution of each drug transporter to the brain drug delivery. There are two partial-areas analyses utilized to determine the exit rate constant from the brain, the performances of which were evaluated and compared in the current study. The requirement for accurate determination of the brain-to-plasma ratio of the area under the concentration-time curve (AUC) also warrants the investigation of a Bayesian approach to estimate the variability around the AUC_o^∞ and the tissue-to-plasma AUC_o^∞ ratio obtained by destructive sampling.

Since anti-angiogenic agents are commonly used in combination therapy for GBM, the influence of anti-angiogenic therapy on tumor delivery of traditional chemotherapy and molecularly-targeted agents was examined using a xenograft GBM model. It has been shown that restoration of the BBB integrity by cediranib and bevacizumab could decrease the tumor site delivery of both temozolomide and erlotinib, and even the delivery of cediranib itself, which could also be one of the reasons for the limited efficacy of cediranib in clinical trials.

These findings provide insight into improvement of the molecularly-targeted tumor delivery of cediranib and proper strategies for effective combination therapy of anti-angiogenic agents and chemotherapeutics for GBM.

Table of Contents

Acknowledgements……...i
Abstract……...iii
Table of Contents……..……..…..vi
List of Tables……...x
List of Figures…….....xi
CHAPTER 1 INTRODUCTION…..……1
1.1 Introduction……2
1.1.1 Brain tumor and glioma angiogenesis……...2
1.1.2 Mechanisms limiting CNS drug delivery…….5
1.1.2.1 Tight junctions……...5
1.1.2.2 ABC Transporters……..…6
1.1.2.3 Abnormal glioma BBB…….....10
1.1.2.4 The brain-tumor cell barrier……11
1.1.3 Anti-angiogenic therapies for glioma and its influence on chemotherapy drug delivery……...……12
1.1.4 Evaluation of transporter function……...…...…16
1.2 Statement of the problem……..……17
1.3 Specific aims……..17
CHAPTER 2 DETERMINATION OF CEDIRANIB IN MOUSE PLASMA AND BRAIN TISSUE USING HIGH-PERFORMANCE LIQUID CHROMATOGRAPHY-MASS SPECTROMETRY……..……..20
2.1 Introduction…….....21
2.2 Materials and Methods……...23
2.2.1. Chemicals and reagents……..23
2.2.2 Preparation of stock and working solutions, calibration standards, and quality controls……24
2.2.3 Sample pretreatment……..…….25
2.2.4 Chromatographic and mass-spectrometic conditions……..…25
2.2.5 Calibration curve…….....26
2.2.6 Method validation……...27
2.2.6.1 Accuracy and precision…….....27
2.2.6.2 Limit of quantitation……..27
2.2.6.3 Recovery……28
2.2.6.4 Analyte stability……28
2.2.7 Method application……...……..28
2.3 Results and Discussion……..29
2.3.1 Chromatography……29
2.3.2 Linearity, accuracy, precision and sensitivity……..…..30
2.3.3 Recovery……31
2.3.4 Stability……...……31
2.3.5 Method application……32
2.4 Conclusion…….……....33

2.5 Footnotes……..…….....…..34
CHAPTER 3 BRAIN DISTRIBUTION OF CEDIRANIB IS LIMITED BY ACTIVE EFFLUX AT THE BLOOD-BRAIN BARRIER……..43
3.1 Introduction…….....44
3.2 Material and methods…….47
3.2.1 Chemicals and reagents……...….48
3.2.2 *In vitro* studies……...…48
3.2.2.1 Cell lines……..…..48
3.2.2.2 Intracellular accumulation…….....49
3.2.2.3 Directional flux assays……..…….....50
3.2.2.4 P-gp and BCRP inhibition assays…….……51
3.2.3 *In vivo* studies……...….51
3.2.3.1 Animals…….…52
3.2.3.2 Plasma and brain pharmacokinetics following intravenous or oral administration……..…….……53
3.2.3.3 Steady-state brain distribution of cediranib……...…54
3.2.3.4 Influence of P-gp and BCRP on brain distribution of cediranib…….....55
3.2.3.5 Quantitative analysis of cediranib by liquid chromatography-tandem mass spectrometry……...55
3.2.3.6 Statistical analysis……..…..55
3.3 Results…….....55
3.3.1 *In vitro* studies…….55
3.3.1.1 Intracellular accumulation of cediranib in MDCKII cells…….....55
3.3.1.2 Directional permeability of cediranib across MDCKII cells…….....56
3.3.1.3 Cediranib as a P-gp or BCRP inhibitor……..……57
3.3.2 *In vivo* studies……..58
3.3.2.1 Cediranib brain and plasma pharmacokinetics…….…….58
3.3.2.2 Effect of P-gp and BCRP on steady-state brain and plasma pharmacokinetics of cediranib……59
3.3.2.3 Influence of P-gp and BCRP inhibitors on brain distribution of cediranib……....60
3.4 Discussion……..61
3.5 Conclusion…….……65
3.6 Footnotes……..…….....65
CHAPTER 4 MODELING AND SIMULATION OF BRAIN DISTRIBUTIONAL KINETICS…….87
4.1 Introduction…….....….89
4.1.1 Distributional kinetics of brain partitioning……..….....89
4.1.2 Partial-areas analysis…….....……....91
4.1.3 Bayesian approach to estimate AUC and brain-to-plasma AUC ratio for sacrifice design data……...…….....…93
4.2 Methods……...…99
4.2.1 Distributional kinetics of brain partitioning…….99
4.2.1.1 Isee systems STELLA ®…….100

4.2.1.2 Construction of models……...100
4.2.1.3 An illustration using a cediranib study in mice……...102
4.2.2 Partial-areas analysis……103
4.2.3 Bayesian approach to estimate AUC and brain-to-plasma AUC ratio for sacrifice design data……104
4.2.3.1 Model specification……..104
4.2.3.1.1 Likelihood distribution……..105
4.2.3.1.2 Priors on parameters ($\bar{\mu}_j$ and Σj)……106
4.2.3.2 AUC estimation……106
4.2.3.3 Posterior distribution of terminal elimination rate constant……107
4.2.3.4 Model convergence……108
4.2.3.5 Method validation……108
4.2.3.5.1 Simulation……..109
4.2.3.5.2 Model application to real data……110
4.3 Results and discussion……111
4.3.1 Distributional kinetics of brain partitioning……111
4.3.1.1 Effect of efflux clearance on the brain T_{max}……111
4.3.1.2 Brain-to-plasma concentration ratio vs time profile……114
4.3.2 Partial area analysis……115
4.3.3 Bayesian approach to estimate AUC and brain-to-plasma AUC ratio for sacrifice design……118
4.3.3.1 Simulated serial sacrifice design……118
4.3.3.2 Cediranib i.v. study in mice……119
4.4 Conclusions……122
4.4.1 Distributional kinetics of partition coefficient……122
4.4.2 Partial-areas analysis……123
4.4.3 Bayesian approach to estimate AUC and brain-to-plasma AUC ratio for sacrifice design data……124
4.5 Footnotes……124
CHAPTER 5 EFFECT OF ANTI-ANGIOGENIC THERAPY ON DRUG DELIVERY TO BRAIN TUMOR SITE……166
5.1 Introduction……167
5.2 Material and methods……171
5.2.1 Chemicals and Mayo GBM xenograft model……171
5.2.1.1 Chemicals……171
5.2.1.2 Mayo GBM xenograft model……171
5.2.2 Determine the effect of anti-angiogenic treatment on drug delivery to tumor sites……172
5.2.3 Quantitative Analysis by Lipid Chromatography-Tandem Mass Spectrometry.172
5.2.3.1 Temozolomide……173
5.2.3.2 Erlotinib……174
5.2.3.3 Cediranib……174
5.2.4 Statistical analysis……175
5.3 Results……175

5.3.1 Effect of anti-angiogenic therapy pre-treatment on temozolomide delivery to tumor sites……....175
5.3.2 Effect of anti-angiogenic therapy pre-treatment on erlotinib delivery to tumor sites……..176
5.3.3 Effect of cediranib pre-treatment on its own delivery to tumor sites…….…...177
5.4 Discussion……177
5.5 Conclusion.…….....……....…179
5.6 Footnotes…….....……...180
CHAPTER 6 RECAPITULATION……..186
BIBLIOGRAPHY……....193
Appendix I Partial Area Analyses……...……..219
Appendix II Derivation of Time to Attain Peak Concentration in the Brain……221
Appendix III Derivation of Terminal Phase Brain-to-Plasma Concentration Ratio….223

List of Tables

Table 2-1 Sub-stock solutions were diluted with MeOH from the stock solutions and used to prepare calibration standards and QC samples……..36
Table 2-2 Within-assay and between-assay variabilities and accuracy of the HPLC-MS/MS assay for cediranib in mouse plasma and brain homogenate……...39
Table 2-3 Absolute recoveries for cediranib and ISTD in the mouse plasma and brain homogenate. a. cediranib; b. AG1478……...40
Table 2-4 Cediranib stability of the plasma and brain homogenate samples. a. stability in mouse plasma; b. stability in mouse brain homogenate……41
Table 3-1 P_{app} of cediranib across wild-type and MDR1-transfected MDCKII cell monolayers, in the presence and absence of P-gp selective inhibitor LY335979….81
Table 3-2 P_{app} of cediranib across wild-type and Bcrp1-transfected MDCKII cell monolayers, in the presence and absence of BCRP selective inhibitor Ko143…….82
Table 3-3 Plasma and brain oral non-compartmental PK parameters in wild-type and Mdr1a/b(-/-) Bcrp1(-/-) mice…….83
Table 3-4.A One-compartment plasma PK parameters following i.v. dosing in wild-type, *Mdr1a/b (-/-)*, *Bcrp1 (-/-)* and *Mdr1a/b (-/-) Bcrp1 (-/-)* mice……....84
Table 3-4.B Brain and plasma non-compartmental PK parameters following i.v. dosing in wild-type, *Mdr1a/b (-/-)*, *Bcrp1 (-/-)* and *Mdr1a/b (-/-) Bcrp1 (-/-)* mice…….85
Table 3-5 Steady-state brain and plasma concentrations and apparent plasma cleances and the brain-to-plasma concentration ratios…….86
Table 4-1 Parameters of the STELLA model for partial-areas analysis……130
Table 4-2 Model parameters of the simulated two-compartment model……...132
Table 4-3 The observed brain T_{max} in four genotypes of transporters……...135
Table 4-4 The estimated values of kout by the two partial-areas analysis……143
Table 4-5 Estimated values of kout by the two partial-areas analysis when concentration data had 5%, 10%, and 20% error……150
Table 4-6 Statistical comparison of the estimated k_{out} values by two methods when residual error was set to be (a) 5%, (b) 10%, and (c) 20%.....151
Table 4-7 Evaluation of the robustness of posterior estimators of $AUC^{\infty}_{0,pl}$, $AUC^{\infty}_{0,br}$ and the ratio of them obtained by the Bayesian approach based on 100 Monte Carlo simulations……...157
Table 4-8 Bayesian posterior mean and 95% credible interval (C.I.) of the plasma and brain AUC^{∞}_{0} s and their ratios and the comparison with the point estimate and 95% confidence interval (C.I.*) estimated by the Bailer's approximation extended by Yuan……164
Table 4-9 Comparisons of Bayesian posterior mean, standard deviation (SD) and 95% credible interval (C.I.) for partial AUCs (the AUC up to the last sampling time point) in four genotypes of transporters with Bailer-Satterthwaite approximation of mean, SD and 95% confidence interval (C.I.*) estimated by Phoenix WinNonlin……....165
Table 5-1 List of agents being studied in combination with avastin in GBM…….....181

List of Figures

Figure 1.1 Anti-angiogenic mechanisms of anti-angiogenic agents currently in clinical evaluation……...19
Figure 2.1 Chemical structures of cediranib and the ISTD. a, cediranib; b, AG1478….35
Figure 2.2 Representative HPLC-MS/MS chromatograms of extracts of a) the highest plasma and brain homogenate calibrator samples; b) plasma and brain homogenate LLOQ samples: 1, plasma; 2, brain homogenate……...37
Figure 2.3 Mouse plasma and brain pharmacokinetic profiles of cediranib following 5 mg/kg oral administration……..42
Figure 3.1.A Accumulation of cediranib in wild-type and *MDR1*-transfected MDCKII cells with and without presence of the P-gp selective inhibitor, 1 μM LY335979, and the P-gp and BCRP dual inhibitor, 5 μM GF120918…….66
Figure 3.1.B Accumulation of cediranib in wild-type and *Bcrp1*-transfected MDCKII cells with and without presence of the BCRP selective inhibitor, 200 nM Ko143, and the P-gp and BCRP dual inhibitor, 5μM GF120918……..67
Figure 3.2 Directional flux of cediranib across MDCKII cell monolayers. (Wildtype: ◇, transport from Apical-to-Basolateral chamber; □, transport from Basolateral chamber; *MDR1*-transfected: ▲, transport from Apical-to-Basolateral chamber; ●, transport from Basolateral-to-Apical chamber; ⊠, transport from Basolateral-to-Apical chamber with the treatment of LY335979.)…….....68
Figure 3.3 Directional flux of cediranib across MDCKII cell monolayers. (Wildtype: ◇, transport from Apical-to-Basolateral chamber; □, transport from Basolateral chamber; *Bcrp1*-transfected: ▲, transport from Apical-to-Basolateral chamber;● , transport from Basolateral-to-Apical chamber; ⊠, transport from Basolateral-to-Apical chamber with the treatment of Ko143.)…….....69
Figure 3.4.A Accumulation of ^{3}H-vinblastine in *MDR1*- transfected cells in presence of increasing concentrations of cediranib ranging from 0 to 40 μM…….....70
Figure 3.4.B Accumulation of ^{3}H-prazosin in *Bcrp1*- transfected cells in presence of increasing concentrations of cediranib ranging from 0 to 40 μM……..71
Figure 3.5.A Cediranib brain and plasma concentrations in wild-type mice after oral dosing (dose = 5 mg/kg)……..……72
Figure 3.5.B Cediranib brain and plasma concentrations in *Mdr1a/b(-/-) Bcrp1(-/-)* mice after oral dosing (dose = 5 mg/kg)…….73
Figure 3.6.A Cediranib brain and plasma concentrations in wild-type mice by i.v. injection (dose = 4 mg/kg)…….74
Figure 3.6.B Cediranib brain and plasma concentrations in Bcrp1(-/-) mice by i.v. injection (dose = 4 mg/kg)…….75
Figure 3.6.C Cediranib brain and plasma concentrations in Mdr1a/b(-/-) mice by i.v. injection (dose = 4 mg/kg)…….76
Figure 3.6.D Cediranib brain and plasma concentrations in Mdr1a/b(-/-)Bcrp1(-/-) mice by i.v. injection (dose = 4 mg/kg)……..77
Figure 3.6.E Cediranib brain-to-plasma concentration ratio after i.v. injection (dose = 4 mg/kg)……78

Figure 3.7.A Brain-to-plasma concentration ratios at 90 minute post oral dose of 5mg/kg cediranib into the wild-type, *Bcrp1(-/-)*, *Mdr1a/b(-/-)*, and *Mdr1a/b(-/-)Bcrp1(-/-)* mice……79
Figure 3.7.B Brain-to-plasma concentration ratios at 90 minute post oral dose of 5 mg/kg cediranib into the wild-type mice pretreated with vehicle control, 10 mg/kg BCRP inhibitor Ko143, 25 mg/kg P-gp inhibitor LY335979, and 10 mg/kg dual inhibitor GF120918……80
Figure 4.1 Correlation between plasma and brain concentrations after intravenous injection of 4mg/kg cediranib into four genotypes of FVB mice……126
Figure 4.2 STELLA simulation model to illustrate the effect of efflux transport on brain-to-plasma partitioning in four genotypes. A. Wild-type mice (WT); B. BCRP knockout mice (BCRP KO); C. P-gp knockout mice (Pgp KO); D. Triple knockout mice (TKO)……..127
Figure 4.3 STELLA model for partial area analysis simulation……129
Figure 4.4 Simulated two-compartment PK model for Bayesian model validation…..131
Figure 4.5 The brain concentration vs. time profiles of four genotypes……133
Figure 4.6 At the time when C_{brain} achieves the maximum, the C_{brain}/C_{plasma} ratio equals to the brain-to-plasma AUC_0^∞ ratio, which exactly reflects the CL_{in}/CL_{out} ratio…134
Figure 4.7 The simulated brain-to-plasma concentration ratio vs. time profiles of four genotypes……136
Figure 4.8 The relationship between the concentration ratio, partial AUC ratio, and clearance ratio. A. Wild-type mice (WT); B. BCRP knockout mice (BCRP KO); C. P-gp knockout mice (Pgp KO); D. Triple knockout mice (TKO)……...…137
Figure 4.9 The brain-to-plasma concentration ratio vs. time profiles in a real-world experiment – cediranib brain-to-plasma concentration ratio after i.v. injection (dose = 4 mg/kg)……139
Figure 4.10 Influence of k1 on (A) Cc and (B) Ct. 1: k1= 0.1, 2: k1= 0.5, 3: k1= 0.9..140
Figure 4.11 Influence of k1 on (A) $AUC_{0,C}^t$ and (B) $AUC_{0,T}^t$. 1: k1= 0.1, 2: k1= 0.5, 3: k1= 0.9……141
Figure 4.12 Influence of k1 on (A) $AUC_{0,T}^t / AUC_{0,C}^t$ and (B) R ($AUC_{0,T}^\infty / AUC_{0,C}^\infty$). 1: k1= 0.1, 2: k1= 0.5, 3: k1= 0.9……..……..…..142
Figure 4.13 Linear regression by (A) cumulative and (B) internal partial-areas analysis when nominal $k_{out} = 2hr^{-1}$……144
Figure 4.14 Linear regression by (A) cumulative and (B) internal partial-areas analysis when nominal $k_{out} = 0.2hr^{-1}$……..145
Figure 4.15 Linear regression by (A) cumulative and (B) internal partial-areas analysis when nominal $k_{out} = 0.02hr^{-1}$……146
Figure 4.16 Linear regression by (A) cumulative and (B) internal partial-areas analysis when concentration data have 5% error……...……147
Figure 4.17 Linear regression by (A) cumulative and (B) internal partial-areas analysis when concentration data have 10% error……...……..148
Figure 4.18 Linear regression by (A) cumulative and (B) internal partial-areas analysis when concentration data have 20% error……...……..149

Figure 4.19 Linear regression by cumulative partial-areas analysis when time-interval was (A) 1hr and (B) 15 min……153
Figure 4.20 Linear regression by internal partial-areas analysis when time-interval was (A) 1hr and (B) 15 min……154
Figure 4.21 Traceplots of the posterior parameters for the simulated data (A: $AUC^{\infty}_{0,pl}$, B: $AUC^{\infty}_{0,br}$ C: $AUC^{\infty}_{0,br} / AUC^{\infty}_{0,pl}$)……155
Figure 4.22 Auto-correlation plots of the posterior parameters for the simulated data……156
Figure 4.23 Gelman-Rubin diagnostics of the posterior parameters for the simulated data……157
Figure 4.24 Traceplots of the posterior parameters for the FVB mice with the i.v. dose of cediranib. A. Wild-type mice; B. *Bcrp1(-/-)* mice; C. *Mdr1a/b(-/-)* mice; D. *Mdr1a/b(-/-)Bcrp1(-/-)* mice……159
Figure 4.25 Posterior distributions of the plasma AUC^{∞}_{0} in four genotypes of brain efflux transporters. Black: wild-type mice; Blue: *Bcrp1(-/-)* mice; Red: *Mdr1a/b(-/-)* mice; Green: *Mdr1a/b(-/-)Bcrp1(-/-)* mice……160
Figure 4.26 Posterior distributions of the brain AUC^{∞}_{0} in four genotypes of brain efflux transporters……161
Figure 4.27 Posterior distributions of the brain-to-plasma AUC ratio ($AUC^{\infty}_{0,br} / AUC^{\infty}_{0,pl}$) in four genotypes of brain efflux transporters……162
Figure 4.28 Posterior distributions of the brain drug targeting indexs for the three transporter knockout mice……163
Figure 5.1 Chemical structure of temozolomide, an alkylating agent…….....182
Figure 5.2 Chemical structure of erlotinib, a selective tyrosine kinase inhibitor against EGFR……182
Figure 5.3 Impact of AATs (cediranib and avastin) on temozolomide uptake into tumor core, rim, and normal brain at 1 hour and 4 hours post dose of temozolomide…...183
Figure 5.4 Impact of AATs (cediranib and avastin) on erlotinib uptake into tumor core, rim, and normal brain at 1 hour and 4 hours post dose of erlotinib……184
Figure 5.5 Impact of once daily treatment of cediranib on its own uptake into tumor core, rim, and normal brain at 1 hour and 4 hours post dose……185

CHAPTER 1

INTRODUCTION

1.1 Introduction

1.1.1 Brain tumor and glioma angiogenesis

Every year, there are approximately 200,000 brain tumors diagnosed in North America, of which 50,000 originate in the brain and 150,000 metastasize from extracranial tumors (Davis et al., 2001; Weil et al., 2005). Glioblastoma multiforme (GBM), a WHO grade IV malignant glioma, is the most common primary brain tumor, with a median survival of approximately 18 months, despite aggressive progress in radiotherapy, chemotherapy, and surgery (Stupp et al., 2005; Zhang et al., 2008). Besides maximum debulking surgery and radiation therapy, the current standard therapy for newly diagnosed GBM includes concurrent temozolomide during radiotherapy and adjuvant temozolomide followed by 6-months of post-radiotherapy (Stupp et al., 2005; Goellner et al., 2011; Theeler and Groves, 2011). Temozolomide is a CNS permeable compound used in conjunction with and after radiotherapy, the therapeutic benefit of which depends on its ability to yield a monofunctional alkylating agent binding to the O^6 position of guanine via chemical decomposition (Newlands et al., 1992). Clinical trials demonstrated that adjuvant temozolomide to radiation therapy was associated with an improved median survival from 12.1 months to 14.6 months (Chamberlain, 2011). However, the overall 5-year survival rate for GBM is still as low as 9.8% (Stupp et al., 2009). Tumor recurrence was found at the original tumor location in more than 90% of patients with glioma and 5% may develop new lesions at distant sites (Choucair et al., 1986). The ability of glioma cells to migrate and promote angiogenesis makes the treatment of GBM challenging and demands further investigation into novel therapies that potentially target these processes.

Infiltrative phenotype of the highly infiltrative gliomas leads to relapse and lethality of GBM. Glioma cells can either migrate by co-option of normal blood vessels or infiltrate through the extracellular matrix and then hide in apparently normal brain tissue surrounding the core tumor mass (Bergers and Hanahan, 2008; Agarwal et al., 2011a). This infiltration is difficult to be immediately detected by conventional magnetic resonance imaging (MRI) techniques and hence becomes a big challenge in brain tumor treatment (Gagner et al., 2005). It has been shown that invasive GBM cells can spread up to several centimeters away from the contrast-enhancing regions of tumor and the margins of surgical resection into adjacent normal brain parenchyma, causing tumor recurrence which typically occur within 18 months of diagnosis (Kuratsu et al., 1989; Silbergeld and Chicoine, 1997). Therefore, effective drug delivery to the invasive glioma cells co-opting blood supply from mature brain capillaries in normal brain parenchyma is critical for the treatment of GBM (Agarwal et al., 2011a).

Moreover, gliomas are able to recruit and proliferate blood vessels to support growth by overexpressing pro-angiogenic ligands, such as vascular endothelial growth factor (VEGF, otherwise known as vascular permeability factor), platelet derived growth factor (PDGF) (Mrugala et al., 2004), and fibroblast growth factors (FGF) (Bergers and Hanahan, 2008; Rahman et al., 2010). GBM is characterized by a marked increase in endothelial cell proliferation and migration (Takano et al., 1996; Fischer et al., 2005; Reardon et al., 2011). Angiogenesis is a physiologic process of blood vessel sprouting from existing vasculature by endothelial cell migration and proliferation. Pathologically,

once tumor grows beyond 1-2 mm, continued survival of the tumor would require tumor angiogenesis to overcome hypoxia and limits of nutrient diffusion (Fidler et al., 2002). During tumor angiogenesis, vascular basement membrane is disrupted and structurally changed, and extracellular matrix of tissues is remodeled (Cai et al., 2011). To date, role of the vascular endothelial growth factor (VEGF) family of ligands (VEGF-A, VEGF-B, VEGF-C, VEGF-D, VEGF-E, VEGF-F, and PlGF) and receptors (VEGFR-1, -2 and -3) in the regulation of angiogenesis has been recognized (Carmeliet and Jain, 2000; Hoeben et al., 2004). It has been shown that VEGF is secreted by GBM cell lines (Masi et al., 2005). VEGF and VEGFR-1 and -2 are present in all types of brain tumors (Mentlein et al., 2004; Huang et al., 2005). For brain tumors, in particular gliomas, angiogenesis is mainly driven by VEGF-A-mediated signaling via VEGFR-2 (also known as KDR), which leads to the proliferation, migration and survival of tumor endothelium, and the abnormal microvascular permeability (Carmeliet and Jain, 2000). The hyperpermeability of blood vessels causes vasogenic cerebral edema which results in morbidity and mortality, and increased interstitial fluid pressure which contributes to tumor hypoxia and prevents adequate tumor penetration of chemotherapeutics (Gerstner et al., 2009). The potent tyrosine kinase VEGFR-2 is overexpressed both on the luminal (blood side) and abluminal (stromal side) aspect of tumor endothelial cells, but the kinase domain is exclusively found inside the endothelial cells (Hormigo et al., 2011; Sikkema et al., 2011). Therefore, tumor vasculature has been investigated as a potential target for disrupting tumor-associated angiogenesis by inhibition of VEGF signaling (Demeule et al., 2004). It has also been reported that VEGFR inhibitors may result in a marked decrease in tumor

cell proliferation due to parenchymal tumor cell apoptosis (Prewett et al., 1999; Sasaki et al., 2008) and invasiveness (Du et al., 2008). Thus, a number of VEGF/VEGFR inhibitors such as tyrosine kinase inhibitors (TKIs) and monoclonal antibodies have been developed as potential therapeutics against many tumor types (Sharma et al., 2011).

1.1.2 Mechanisms limiting CNS drug delivery

Despite aggressive therapy, the majority of primary and metastatic brain tumor patients have a poor prognosis with low survival rates, in part due to the protection of the blood-brain barrier (BBB) that prevents toxins, including chemotherapy, from reaching the brain. The BBB is a physical and metabolic barrier between the brain and the systemic circulation, composed of a monolayer of brain capillary endothelial cells, which are surrounded by extracellular matrices, pericytes, astrocytes, and neurons, all of which may influence formation and function of the BBB (Loscher and Potschka, 2005), (Haseloff et al., 2005; Hawkins and Davis, 2005). The BBB can prevent transfer and accumulation of therapeutic agents from the systemic circulation into the brain parenchyma and can significantly limit efficacy of systemic therapies for GBM, a primary brain tumor. Major mechanisms of the BBB that influences drug transport include the restriction of paracellular brain uptake through the tight junctions between the endothelial cells of the brain microvasculature, and the efflux function of the ATP-binding cassette (ABC) drug transporters expressed on the luminal side of the capillary endothelial cells.

1.1.2.1 Tight junctions

Tight junctions are occluding seals between adjacent endothelial cells within the brain microvasculature, with which passive drug diffusion out of the vasculature is limited to hydrophilic molecules under 500kDa and lipophilic molecules which can readily diffuse across the lipid bi-layer (Loscher and Potschka, 2005). Tight junctions are formed by occludin, junctional adhesion molecules 1-3, claudins, cingulin and the zonula occludens family members (ZO-1/2/3) (Colgan et al., 2008). Claudins work as the backbone of tight junction strands and bind to claudins on adjacent cells to produce the primary seal of the tight junction. Occludin is correlated with increased electrical resistance across the membrane and decreased paracellular permeability. The ZOs serve as recognition proteins for tight junctional placement and as a support structure for signal transduction proteins. Cingulin binds ZO proteins with other cingulin molecules. The primary cytoskeletal protein, actin, can bind to all of the ZO proteins, claudin and occludin (Huber et al., 2001). It has been demonstrated that the flux across tight junctions can be significant and that the permeability and selectivity of the junctions can be regulated (Ban and Rizzolo, 2000; Huber et al., 2001).

1.1.2.2 ABC Transporters

It is well-known that lipophilic compounds or small nonpolar molecules pass through the BBB by transcellular passive diffusion. But it was demonstrated that the BBB permeability of a number of lipophilic compounds is not proportional to their lipophilicity, attributed to the presence of efflux transporters at the BBB (Levin, 1980; Pardridge, 1998). Multiple efflux transporter proteins are members of the ABC family.

They are expressed on the luminal side of plasma membranes of a number of tissue cells such as the capillary endothelial cells of the BBB and the epithelial cells of the choroid plexus in the blood-cerebrospinal fluid barrier (Kusuhara and Sugiyama, 2001a; Kusuhara and Sugiyama, 2001b). These transporters utilize the energy from ATP hydrolysis to drive the transport of substrates against a concentration gradient and out of cells. The blood-brain barrier efflux proteins, such as p-glycoprotein (P-gp/MDR1), breast cancer resistance protein (BCRP/ABCG2) and the multidrug resistance protein (MRP) family, form a barrier for delivery of CNS disease therapeutics to target cells in the brain parenchyma. It has been suggested that over-expression of ABC drug efflux transporters such as P-gp and BCRP on the endothelial cells of the BBB may be one of the mechanisms of the poor response of CNS tumors to chemotherapy. Therefore, modulation of drug efflux transporters at the BBB forms a novel strategy to enhance the penetration of drugs into the brain and may yield new therapeutic options for drug-resistant CNS diseases (Loscher and Potschka, 2005).

P-gp is typical of ABC proteins and is located at the luminal surface of the microvessel endothelial cells that line the blood vessels and the newly formed capillaries around the brain tumors (Cordon-Cardo et al., 1989; Decleves et al., 2002). It has been reported that there is a 17-fold higher expression of P-gp in rat luminal membranes compared to brain capillaries and a 400-500-fold increase compared to whole brain membranes (Beaulieu et al., 1997). In mice, P-gp is encoded by the *mdr1a* and *mdr1b* genes. A number of *in vivo* studies have also been conducted to study the efflux function of P-gp

at the BBB using transgenic mice to examine the role of P-gp at the BBB (Schinkel et al., 1994; Schinkel et al., 1996; van Asperen et al., 1996; Kawahara et al., 1999). In rodents, murine P-gp is coded by two isoforms, mdr1a and mdr1b genes, but only *mdr1a* is localized in brain capillaries (Demeule et al., 2002). In absence of Pgp at the BBB in *mdr1a* knockout mice, the brain penetration of P-gp substrates can increase up to 10- to 100-fold, and blockade of BBB P-gp by P-gp inhibitors can also significantly increase the brain concentration of various drugs (Loscher and Potschka, 2005).

BCRP was first detected in a chemotherapy-resistant breast cancer cell line MCF-7 but it is expressed in a variety of tissues including the intestine, kidney, placenta, brain endothelium and hematopoietic cells (Sharom, 2008) as well as solid tumors (Diestra et al., 2002). In the brain, BCRP has been detected mainly at the luminal surface of capillary endothelial cells. Murine BCRP is encoded by Bcrp1/Abcg2 gene. It shares some substrates with P-gp and MRPs (Sharom, 2008), and the tissue distribution of BCRP shows extensive overlap with that of P-gp (Schinkel and Jonker, 2003). In contrast, the role of BCRP in drug efflux transport from the brain is a controversy. BCRP expression at the BBB may not lead to visiblely low brain penetration of all its *in vitro* substrates, such as abacavir and zidovudine (Pan et al., 2007; Giri et al., 2008), dehydroepiandrosterone sulfate and mitoxantrone (Lee et al., 2005), as well as topotecan (de Vries et al., 2007).

Furthermore, P-gp and BCRP have been shown to team up to restrict the transport of several therapeutic agents into the brain, thereby influencing drug efficacy. It has been shown that there is an overlapping substrate specificity for these two efflux pumps, and a number of drugs, including many anti-cancer tyrosine kinase inhibitors (TKIs), are reported to be dual substrates for P-gp and BCRP (Dai et al., 2003; de Vries et al., 2007; Polli et al., 2008; Chen et al., 2009; Agarwal et al., 2010; Agarwal et al., 2011b; Tang et al., 2011). It has been shown that absence of both P-gp and BCRP may result in a significantly larger enhancement in brain uptake than the additive effects seen from absense of only one of the transporters, for several dual P-gp and BCRP substrates, such as topotecan (de Vries et al., 2007), lapatinib (Polli et al., 2009), dasatinib (Chen et al., 2009), gefitinib (Agarwal et al., 2010), sorafinib (Agarwal et al., 2011b), erlotinib, flavoperidol, mitoxantrone (Kodaira et al., 2010), imatinib (Breedveld et al., 2005), and tandutinib (Yang et al., 2010). Compensation with the respective other transporter has been suggested as a plausible explanation. Thus dual inhibition of both transporters by combination therapy with TKIs may have a great impact on the brain tumor treatment.

The relative activity of P-gp and BCRP at the BBB is relevant to the relative substrate-transporter affinities and the relative transporter expression levels. It has been demonstrated that, at the mouse BBB, P-gp expression was approximately 5-fold higher than BCRP (Kamiie et al., 2008). This finding may explain the observation that P-gp is dominant in restricting the brain penetration of many dual P-gp/BCRP substrates while cooperating with BCRP (Lee et al., 2005; Zhao et al., 2009; Agarwal et al., 2011b).

Nevertheless, for those dual substrates with a considerably higher BCRP affinity than P-gp, such as sorafenib (Agarwal et al., 2011b) and dantrolene (Kodaira et al., 2010), a pronounced BCRP effect was observed.

Since VEGFR-2 and efflux transporters are expressed in endothelial cells and variably in GBM tumor cells, the interaction between VEGFR inhibitors and these efflux transporters may limit the achievable intracellular drug levels within these target cells and specifically reduce the efficacy of AATs. First of all, the activity of P-gp and BCRP in endothelial cells limit the accumulation of a VEGFR inhibitor to target receptor signaling in the same cells. The limited BBB penetration may impair the anti-angiogenic efficacy of these molecules in CNS malignancies. In addition, reduced accumulation within glioma cells may also impair the anti-tumor efficacy of VEGFR inhibitors. Furthermore, VEGFR-2 signaling through Src and PKC-beta suppresses P-gp expression and/or activity in brain capillary endothelial cells such that inhibition of VEGFR-2 can upregulate P-gp expression and possibly enhance drug exclusion from endothelial cells (Liu et al., 2009; Hawkins et al., 2010).

1.1.2.3 Abnormal glioma BBB

GBM development is associated with a partial disruption of the blood-brain barrier within the core tumor mass where the tumor is highly angiogenic. During gliomagenesis, expression of VEGF and other pro-angiogenic factors such as PDGF promotes abnormal development of an immature tumor vasculature by promoting loss of robust tight

junctions between endothelial cells. The tortuous and highly permeable endothelial wall allows intra-tumoral accumulation of radiographic contrast and provides graphic evidence for disruption of the BBB in essentially every GBM. However, at the growing edge of the tumor and the vascular niche for invasive glioma cells, the BBB is intact (Gilbertson and Rich, 2007). Therefore, GBM consists of regions of relatively open BBB (tumor 'core') and other regions with an intact BBB (tumor 'rim'). Since tumor may recur from either region, anti-tumor agents must be adequately delivered in different regions of a brain tumor, especially in the non-contrast enhancing areas (tumor rim/ normal brain).

1.1.2.4 The brain-tumor cell barrier

Despite the disrupted BBB in tumor core, there is a second barrier contributing drug resistance of gliomas, called the brain-tumor cell barrier (BTB), with ABC transporters expressed on glioma cell membrane. The presence of P-gp in glioma cell lines has been found heterogenously in high-grade gliomas (Decleves et al., 2002), even though some argued that P-gp is mainly expressed on glioma-associated endothelial rather than glioma cells (Bahr et al., 2003). BCRP has also been reported to be expressed on a stem cell like side-population of tumor cells and plays a role in multidrug resistance in glioma cells (Zhou et al., 2001; Dean et al., 2005). Moreover, an enhanced expression of MRPs, especially MRP1, has also been observed in malignant glioma cells (Mohri et al., 2000; Bahr et al., 2003; Benyahia et al., 2004). Therefore, both BBB and BTB can restrict the molecularly-targeted drug delivery to the intracellular targets at the tumor cells.

1.1.3 Anti-angiogenic therapies for glioma and its influence on chemotherapy drug delivery

Since endothelial proliferation with hypoxia and necrosis is a hallmark of GBM, treatment with anti-angiogenic agents is promising in blocking its growth (Hormigo et al., 2011). The effects of anti-angiogenic therapies (AATs) targeting growth factors like VEGF, or growth factor receptors like VEGFR, epidermal growth factor receptor (EGFR) and platelet-derived growth factor receptor (PDGFR) in delaying tumor progression and lengthening survival in recurrent GBM have been evaluated in clinical trials, either alone or in combination with proven effective therapies (Wurdinger and Tannous, 2009). The first generation of antiangiogenic therapies evaluated for treatment of GBM were thalidomide, lenalidomide, carboxyamidotriazole and penicillamine. However, these agents were not sufficiently potent and lack of significant clinical benefits compared with cytotoxic chemotherapies (Chamberlain, 2011). Therefore, more recent investigations have focused on newer, more potent anti-angiogenic agents including VEGF-blocking antibodies such as bevacizumab (Genentech, San Francisco, CA), fusion protein soluble decoy receptors such as VEGF-trap (Regeneron, Tarrytown, NY), and multitarget tyrosine kinase inhibitors such as cediranib (AstraZeneca, London, UK), vatalanib (Novartis, Basel, Switzerland), vandetanib (AstraZeneca, London, UK), pazopanib (GlaxoSmithKline, Middlesex, UK), sorafenib (Bayer, West Haven, CT and Onyx, Richmond, CA), and sunitinib (Pfizer, La Jolla, CA), the mechanisms of which are summaried in Figure 1.1 (Sathornsumetee et al., 2007). In spite of drugs interfering with

the VEGF pathway, there are other antiangiogenic agents currently in preclinical and clinical development, such as inhibitors to PDGFs, FGFs, angiopoietins/Tie-2 system, protein kinase C and integrins (Sathornsumetee and Rich, 2007).

A humanized monoclonal antibody that blocks VEGF-A, bevacizumab (Avastin), was the first anti-angiogenic agent approved by FDA for the treatment of recurrent GBM following prior temozolomide-based chemoradiotherapy (Chamberlain, 2011). Bevacizumab, either alone or in combination with chemotherapy (most commonly irinotecan), has shown an improvement in response rate and 6-month progression-free survival in recurrent GBM (Friedman et al., 2009; Vredenburgh et al., 2011). Potential mechanisms have been suggested for the anti-GBM action of bevacizumab, such as antivascular activity by normalization of the GBM vasculature, disruption of vascular niche for glioma stem cells, as well as direct antitumor activity (Vredenburgh et al., 2007; Chamberlain, 2011). However, updated data indicate that bevacizumab treatment in glioma may improve survival through the alleviation of peri-tumoral brain edema, without effect on tumor growth (Verhoeff et al., 2010). The result conflicts with the initial enthusiasm based on the concept that angiogenesis is a key event in tumor progression. Further studies are needed to confirm the anti-tumor mechanisms of anti-VEGF agents.

Moreover, recent preclinical studies in three different orthotopic mouse models of glioblastoma indicate the same is true for cediranib (AZD2171, Recentin), the anti-angiogenic molecularly-targeted tyrosine kinase inhibitor against all VEGF recepter

subtypes (VEGFR-1, -2, and -3), PDGFR and c-KIT (a stem cell factor receptor) (Jain et al., 2007; Kamoun et al., 2009; Brave et al., 2011). Cediranib is an indole-ether quinazoline orally available and highly potent to VEGFRs with a subnanomolar EC50 (Batchelor et al., 2010; Rahman et al., 2010). Multitargeted kinase inhibition helps overcome the adaptive treatment resistance of malignant gliomas by blocking multiple co-activated or compensatorily signaling pathways (Sathornsumetee et al., 2007; Sathornsumetee and Reardon, 2009; Sathornsumetee, 2011). Additionally, the activity against PDGFR may help disturb the normalization of blood vessels by disrupting pericyte supported evasive therapeutic resistance (Bergers and Hanahan, 2008). Furthermore, as a potent inhibitor of those crytical receptors such as VEGFRs and PDGFRs, cediranib has been anticipated to convey more direct anti-tumor benefits in addition to its anti-angiogenic effect, since overexpression and activation of PDGFRs may be another important factor involved in malignancy of gliomas (Mrugala et al., 2004). However, a recent clinical study showed that cediranib significantly abated tumor vessel permeability and diameter and caused other vascular changes that led to edema alleviation after 24 hours post treatment, without inducing true tumor regression (Batchelor et al., 2007). Preclinical studies have confirmed this effect in three different orthotopic mouse GBM models (Kamoun et al., 2009). A phase II trial in patients with recurrent GBM also showed that cediranib monotherapy resulted in a positive radiographic response of 56% and a prolonged 6-month progression-free survival from 10 weeks (Wong et al., 1999) to 117 days (Jain et al., 2007), as well as a steroid-sparing effect, due to reduced edema (Jain et al., 2007; Batchelor et al., 2010). A reduction in the

number of circulating endothelial cells and progenitor cells was also demonstrated (Sorensen et al., 2009). These encouraging data point to the promise of the use of AATs in glioma treatment, even though several questions remain on mechanism and actual tumor effect.

Since AATs function to normalize the aberrant tumor vasculature, they may influence the delivery of selected combination therapies to the invasive glioma cells in the perivascular niche. The influence might depend on properties of the drug and the mechanisms that limit its delivery across the BBB. As the vasculature normalizes, tight junctions reform, blood flow is enhanced, and drugs that are typically more permeable in the normal BBB could have enhanced delivery, due to their ability to diffuse transcellularly across an intact barrier, when used in conjunction with anti-angiogenic therapy like bevacizumab or cediranib. It has been investigated in a recent study that cediranib enhanced the effectiveness of temozolomide in two U87 GBM xenografts expressing EGFR (Wachsberger et al., 2011). In contrast with the positive findings, the benefit of combination therapy may be controversial in that another antiangiogenic agent, TNP-470, may reduce tumor concentrations and effectiveness of temozolomide in GBM xenograft models (Ma et al., 2001). It has also been hypothesized that drugs that do not cross the BBB readily may have their delivery diminished to the tumor when co-treated with antiangiogenic agents, due to a reformed vascular integrity and a restored efficient efflux by transporters such as P-gp and BCRP. Inadequate drug delivery to the intracellular targets may explain why many of these novel therapeutic strategies have failed to provide clinical benefits. Furthermore, the BBB integrity restroration by anti-VEGF agents might

increase the invasiveness of tumor cells (Rubenstein et al., 2000). This may be another possible reason for the lack of efficacy. Therefore, a more informed understanding for how AATs might influence the delivery of standard and molecularly-targeted therapeutics and how to use combination therapy more effectively and intelligently to treat brain tumors is critical and desirable.

1.1.4 Evaluation of transporter function

There are generally two *in vivo* approaches to manipulate the magnitude of transporter-mediated drug exclusion from the CNS or other tissues: one is genetic modulation of transporter expression such as transporter gene knockout mice; and the other is through co-treatment of chemicals which modulate specific or overlapping transporter functions. Effect of transporters on brain exposure can be evaluated by comparison of brain distribution in these animal models and the corresponding wildtype strain. The most commonly used estimators for brain drug uptake are the brain-to-plasma concentration ratio (C_{brain}/C_{plasma}) and the area under the concentration curve ratio for brain versus plasma (AUC_{brain}/AUC_{plasma}) from zero to infinity. However, unlike the ratio of AUC_{brain}/AUC_{plasma} from 0 to infinity which reflects the overall relative exposure of drug in brain, the C_{brain}/C_{plasma} ratio is a function of time. Only at some distributional scenarios the C_{brain}/C_{plasma} ratio can be considered as a good estimate of brain distribution. This study discussed the accurate determination of partition coefficient for an examined tissue (i.e., brain) by simulation strategies. In order to statistically compare the transporter functions, a novel approach has been applied to estimate the variation of

AUC_{brain}/AUC_{plasma} ratio from 0 to infinity. Besides C_{brain}/C_{plasma} or AUC_{brain}/AUC_{plasma} ratios, another indirect method to evaluate transporter functions by determining the total rate constant out of the brain is via a partial areas analysis. Evaluation and comparison of two similar partial area-based analyses was also discussed based on simulations.

1.2 Statement of the problem

An intact BBB can prevent transfer and accumulation of therapeutic agents from the systemic circulation into the brain parenchyma and therefore can significantly limit efficacy of systemic therapies in GBM. Despite the leaky BBB at tumor core, invasive tumor cells commonly co-opt blood supply and infiltrate into brain parenchyma at regions distant from contrast enhancement, resulting in possible recurrence. Thus, successful therapeutic strategies for GBM, a whole brain disease, must adequately deliver effective treatment to the tumor core, the tumor growing edge, and even the normal brain tissues. As a molecularly-targeted antiangiogenic agent, cediranib targets to the brain angiogenic capillaries as well as glioma cells. However, the possible interaction of cediranib and efflux transporters at the BBB may limit cediranib distribution into different tumor regions and prevent its possible clinical benifits. Moreover, given their effect on the restoration of the BBB integrity, AATs, including cediranib, may have a detrimental impact on the delivery of concomitantly administered chemotherapeutics to the brain tumor.

1.3 Specific aims

1. In order to explore possible reasons for limited efficacy of cediranib in GBM treatment, specific aim one is to identify and characterize the interaction of cediranib with two important efflux transporters present at the BBB, P-gp and BCRP, by using cell culture models and transporter transgenic mice models. Following the validation of an LC-MS assay for cediranib (chapter 2), a description of studies directed at this aim is found in chapter 3.

2. In order to quantify the impact of efflux transporters on brain kinetics of CNS compounds, specific aim two is to suggest accurate estimators of partition coefficient for an examined tissue (i.e., brain) and the way to estimate its variability by simulation strategies, as well as evaluate two similar partial area-based analyses which can also be used to determine the transporter effect. This aim is addressed by the studies described in chapter 4.

3. In order to test the hypothesis that concomitant AAT may influence the regional delivery and hence the efficacy of combination treatments for GBM, specific aim three is to examine the effect of AAT (bevacizumab and cediranib) on site-specific pharmacokinetics for two relevant agents with different mechanisms of distribution across the BBB (temozolomide and erlotinib), as well as cediranib itself, to tumor core, tumor growing edge (rim) and the normal brain parenchyma in a murine xenograft model of GBM. We have outlined a preliminary study that addresses this aim in chapter 5.

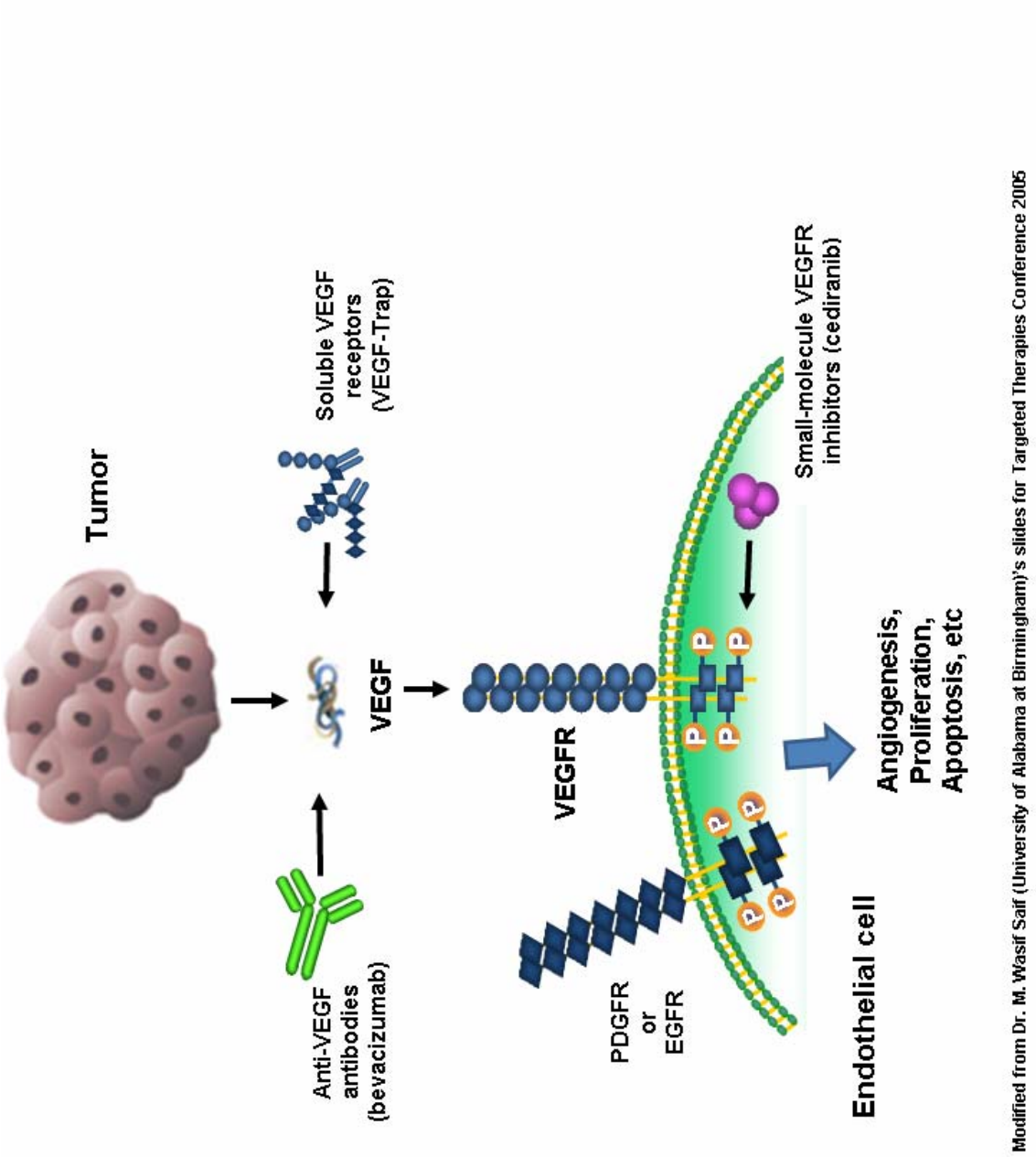

Figure 1.1 Anti-angiogenic mechanisms of anti-angiogenic agents currently in clinical evaluation.

CHAPTER 2

DETERMINATION OF CEDIRANIB IN MOUSE PLASMA AND BRAIN TISSUE USING HIGH-PERFORMANCE LIQUID CHROMATOGRAPHY-MASS SPECTROMETRY

A new high performance liquid chromatography coupled with tandem mass spectrometry (HPLC-MS/MS) assay for cediranib, a tyrosine kinase inhibitor for VEGFRs, was developed and validated, for the determination of plasma and brain levels of cediranib in small specimen volumes. Tyrphostin was used as internal standard. Mouse plasma and brain homogenate samples were prepared using liquid-liquid extraction. The assay was validated for a 2.5-2500 ng/mL concentration range for plasma, and for 1-2000 ng/mL range for brain homogenate. For these calibration ranges, within-assay variabilities were 1.1-14.3% for plasma and 1.5-9.4% for brain homogenate; between-assay variabilities were 2.4-9.2% for plasma, and 4.9-10.2% for brain homogenate. Overall accuracy ranged from 101.5 to 107.0% for plasma and 96.5 to 100.2% for brain homogenate, for all target concentrations. The developed assay has been successfully applied to a cediranib brain distribution study in mice at an oral dose of 5 mg/kg.

2.1 Introduction

The vascular endothelial growth factor (VEGF) and receptors (VEGFR-1, -2, -3) have been recognized as one of the critical mediators of pathological angiogenesis and are involved in the regulation of vascular endothelial cell proliferation, survival, migration, and tumor cell invasion. Numerous solid tumors overexpress VEGF, the role of which in tumor angiogenesis is via stimulation of VEGFR. VEGFRs are also highly expressed in many types of human solid tumors, including glioma, lung, breast, renal, ovarian and gastrointestinal tract carcinomas (Sharma et al., 2011). Inhibition of the VEGFR-mediated signal transduction pathways stabilizes the progression of tumors by disrupting

angiogenesis - the formation of new blood vessels that tumors need to grow and spread. There have been at least two potential therapeutic strategies for cancers via blocking VEGFR signaling, which have been clinically validated with FDA-approvals: (i) anti-VEGF monoclonal antibodies (e.g., bevacizumab) and (ii) tyrosine kinase inhibitors (TKI, e.g., sorafenib and suntinib). TKIs are a class of small molecules blocking intracellular signals involved in growth and angiogenesis.

Cediranib, 4-[(4-Fluoro-2-methyl-1H-indol-5-yl)oxy]-6-methoxy-7-[3-pyrrolidin-1-yl)propoxy]quinazoline (RECENTIN™, AZD2171) (Figure 2.1a), is an orally active pan-VEGFR inhibitor with additional activity against platelet-derived growth factor ß and c-Kit (Batchelor et al., 2010). Cediranib has exhibited antitumor and antiangiogenic activity in various cell lines (Wedge et al., 2005; Takeda et al., 2007; Siemann et al., 2009) and xenografts including colon, lung, prostate, breast and ovary (Wedge et al., 2005; Medinger et al., 2009). Its pharmacological effect has been evaluated in Phase II/III clinical trials for advanced non-small cell lung cancer, advanced colorectal cancer, metastatic renal cell carcinoma, and recurrent glioblastoma, etc. (Dietrich et al., 2009). However, due to the physiological structures of the brain capillary endothelium, i.e., blood-brain barrier (BBB), the brain delivery of cediranib may be limited and lead to limited pharmacological effects when used as a CNS anti-tumor therapeutic.

To comprehensively characterize the preclinical pharmacokinetics (PK) of cediranib and the brain disposition of cediranib, a highly sensitive, accurate and reproducible

quantitation assay is required. To date there are no published methods for the analysis of cediranib in biological samples, except for one study using HPLC with radiochemical detection (HPLC-RAD), UV (HPLC-UV) and mass spectrometric (HPLC–MS^n) to characterise [^{14}C]-cediranib and its biosynthetic N+-glucuronide metabolite in hepatocytes from human and pre-clinical species (Lenz et al.). The method described here quantifies cediranib in mouse plasma and brain homogenate utilizing high performance liquid chromatography coupled with mass spectrometry (HPLC-MS/MS) equipped with electrospray positive ionization interface following a liquid-liquid extraction. This method allows the evaluation of compound concentrations in both the plasma and the whole brain at a range of time points in mice specimens, and employs tyrphostin (AG1478, 4-(3-Chloroanilino)-6,7-dimethoxyquinazoline, as shown in Figure 2.1b), a structurely-similar tyrosine kinase inhibitor, as the internal standard (ISTD).

2.2 Materials and Methods

2.2.1 Chemicals and reagents

Cediranib (98% purity) and internal standard tyrphostin AG1478 (free base, >99% purity) were purchased from Selleck Chemicals LLC (Houston, TX, USA) and LC Laboratories (Woburn, MA, USA), respectively. HPLC grade acetonitrile (ACN), methanol (MeOH), ethyl acetate (EtOH) and dimethyl sulfoxide (DMSO) were obtained from Fisher Scientific (Fair Lawn, NJ, USA). Ammonium formate and formic acid were of analytical grade and supplied from Sigma-Aldrich (St. Louis, MO, USA). Bovine serum albumin (BSA; ≥96% pure from agarose gel electrophoresis) was also obtained from Sigma-

Aldrich (St. Louis, MO, USA). All other chemicals used were HPLC or reagent grade. Drug-free mouse plasma was obtained from Valley Biomedical (Catalog# AP3054, Winchester, VA, USA). Deionized water was obtained from a Milli-Q-UF system (Millipore, Milford, MA, USA) and used throughout. The mobile phase was vacuum-filtered through a 0.45 μm filter (Millpore, Milford, MA, USA).

2.2.2 Preparation of stock and working solutions, calibration standards, and quality controls

The stock solution of cediranib at 1 mg/mL was prepared by dissolution of 1.14 mg cediranib in 1.14 mL DMSO. Sub-stock solutions were prepared by dilution of the stock solution into 100, 10, and 1 μg/mL in MeOH. The stock solutions were stored at -20℃ in glass vials, with caps tightly wrapped with Parafilm®. Working solutions were diluted with MeOH from the stock and sub-stock solutions as indicated in Table 2-1. The working solutions were diluted in blank mouse plasma or brain homogenate on each day of analysis to provide nine calibration standards containing cediranib for plasma samples at the following concentrations: 1, 2.5, 5, 10, 25, 50, 500, 1000, 2500 ng/mL, and for brain homogenate samples at 1, 2.5, 5, 10, 25, 50, 500, 1000, 2000 ng/mL.

Quality control (QC) samples were prepared independently by adding the appropriate volume of working solution diluted with blank plasma or brain homogenate at four different concentrations: for plasma, 2.5 ng/mL, the lower limit of quantitation (LLOQ); 15 ng/mL, the low QC; 200 ng/mL, the medium QC; and 800 ng/mL, the high QC; for

brain homogenate, 1 ng/mL, the LLOQ; 5 ng/mL, the low QC; 50 ng/mL, the medium QC; and 200 ng/mL, the high QC. The QC samples were stored at -80℃ until used.

The ISTD compound (AG1478) was dissolved in MeOH to a concentration of 400 ng/mL.

2.2.3 Sample pretreatment

Prior to drug extraction, frozen samples were thawed in a water bath at ambient temperature. Brain tissues were homogenized with a tissue homogenizer (Power Gen 125, Fisher Scientific, Pittsburgh, PA) in 3 volumes of ice-cold 5% (w/v) BSA in phosphate-buffered saline (PBS) solution. A 50 μL aliquot of plasma and a 100 μL aliquot of brain homogenate samples were dispensed into disposable borosilicate glass culture tubes (13mm×100 mm) containing AG1478 (400 ng/mL in 10μL MeOH) and vigorously mixed for 5 s on a vortex-mixer. The liquid-liquid extraction procedures were as follows: 800 μL EtOH was added to each tube and vortexed vigorously for 30 s then centrifuged at 300 rpm for 10 min at 4℃ (SORVALL® LEGEND RT, Kendro). A volume of 600 μL of the top organic layer was transferred to a glass culture tube and dried under a gentle stream of nitrogen. The samples were reconstituted in 75 μL mobile phase and transferred to autosampler vials for injection. A volume of 10 μL was injected at 10℃ using a temperature-controlled autosampling device.

2.2.4 Chromatographic and mass-spectrometic conditions

HPLC analysis was performed using an Agilent Model 1200 separation system (Santa Clara, CA, USA). Separation was achieved on a ZORBAX Eclipse XDB-C_{18} RRHT threaded column (4.6 x 50 mm, 1.8 μm; Agilent Technologies). Column temperature was set to be 30℃. The mobile phase was composed of 10 mM ammonium acetate containing 0.1% formic acid: acetonitrile (62:38 v/v). The flow rate was maintained at 0.25 mL/min and the chromatographic run time was 9 minutes.

The HPLC system was interfaced to a TSQ® Quantum 1.5 triple quadrupole mass spectrometer (Thermo Finnigan, San Jose, CA, USA) equipped with an electrospray ionization (ESI) source. The samples were analyzed using an electrospray probe in the positive ionization mode operating at an ion spray voltage of 4000V for both cediranib and the ISTD. Selected reaction monitoring (SRM) was employed for mass spectrometric quantitation. Data acquisition and analysis was controlled by the Xcalibur version 2.0.7 data system. The spectrometer was programmed to allow the [MH]+ ion of cediranib at m/z 451.7 and that of ISTD at m/z 317 to pass through the first quadrupole (Q1) and into the collision cell (Q2). The collision gas was argon (1.5 mTorr) and the collision energy was set at 17 volts for cediranib and 16 volts for AG1478. The transitions monitored were m/z 451.7 -> 112.2 for cediranib, m/z 317->301 for the ISTD, and monitored through the third quadrupole (Q3). The scan width for the two product ions was set 1.5 unit with 0.5 second of scan time.

2.2.5 Calibration curve

Calibration curves for cediranib were computed with the peak area ratios of analyte and ISTD using weighted quadratic regression, with a weighting factor of 1/concentration. Parameters of each calibration curve were used to compute concentrations for the QC samples and unknown samples by interpolation. Data acquisition, peak integration and quantification were performed by Xcalibur software (Thermo Fischer Scientific Inc, Waltham, MA, USA).

2.2.6 Method validation

2.2.6.1 Accuracy and precision

The method developed for cediranib quantitation in mouse plasma and brain homogenate was validated for 5 different days by repeated analysis (n=5) of QC samples. The low, median and high QC levels correspond to the drug levels anticipated in most mouse samples. Precision and accuracy for the three quality controls were calculated by a single factor analysis of variance (ANOVA) to determine accuracy as well as within- and between-assay variability. The within-assay and between-assay precision was expressed as the relative standard deviation (RSD%), and the total accuracy as the percentage of mean measured (back-calculated) to nominal concentration.

2.2.6.2 Limit of quantitation

Replicate analysis of the lower limits of quantitation (LLOQ, i.e., the lower calibration level) samples was also performed. The assay LLOQ was determined following the criteria that the accuracy and precision were less than 20% with the ratio of signal/noise

greater than 10, according to the FDA (US Food and Drug Administration, 2001) guidance for bioanalytical method validation. Calculations of the signal/noise ratio were based on peak areas. The peak area for background noise was measured in the plasma blank and the brain homogenate blank at the corresponding retention time window.

2.2.6.3 Recovery

The plasma and homogenate samples were extracted in triplicate according to the liquid-liquid extraction procedure described previously. The extraction efficiency was determined by comparing the absolute peak areas of drug extracted from biomatrices with those of non-extracted samples in the reconstitution solvent (mobile phase). The extraction efficiency of the ISTD was assessed with an identical procedure. Analyses were performed in triplicate with three levels of cediranib (10, 100 and 1000 ng/mL) and 40 ng/mL ISTD (the concentration used in the assay).

2.2.6.4 Analyte stability

The long-term stability over five freeze-thaw cycles was evaluated for the QC samples stored at -80℃ up to 223 days for plasma and up to 3 weeks for brain homogenate. The freeze-thaw stability was expressed as a percentage of the drug concentration measured after those freeze-thaw cycles compared to the concentration on day one. Frozen samples were thawed at a 37℃ water bath and refrozen each day at -80℃.

2.2.7 Method application

The described analytical method has been applied to the brain and plasma pharmacokinetic study of cediranib in mice. 28 wild-type FVB mice were randomly assigned to seven groups. Mice in each group were dosed via oral gavages with 5mg/mL cediranib suspended in 10% (w/v) Tween 80 aqueous solution as vehicle. At various time points (0.25, 0.5, 1, 2, 4, 8, 20 h postdose), mice (n=4) were euthanized. Blood samples (~400 μL) were immediately harvested into plastic tubes containing 100 unit/mL heparinized saline via cardiac puncture and whole brain was collected within 3 min and rinsed with ice-cold saline to remove extraneous blood. At the end of the experiment, plasma was separated from blood by centrifugation at 3500 rpm for 10 min at 4℃. Plasma and whole brain samples were stored at -80℃ until analysis. All studies were approved by the Institutional Animal Care and Use Committee of the University of Minnesota. Pharmacokinetic data analysis was performed using Phoenix WinNonlin 6.1® (Pharsight, CA).

2.3 Results and Discussion

2.3.1 Chromatography

Some TKIs have similar structures and physicochemical properties, hence we chose AG1478 as the ISTD for cediranib since deuterated analogues of cediranib were not available. Optimal resolution of analyte and ISTD peaks from one another and from the void volume was achieved with 62% aqueous mobile phase when run isocratically at 0.25 mL/min. Using the chromatographic conditions as we described above, retention time ranges were 3.8-4.0 min for cediranib and 6.3-6.9 min for the ISTD AG1478. Typical

chromatograms of the highest calibrator sample in plasma and brain homogenate are shown in Figure 2.2a using the SRM detection mode. Figure 2.2b shows representative chromatographic profiles obtained from extracts of LLOQ plasma and homogenate samples. The low background from the biological matrix and the sharp and symmetrical resolution of the peaks gave good selectivity for cediranib and AG1478.

2.3.2 Linearity, accuracy, precision and sensitivity

Calibration curves over the entire ranges of concentrations (2.5-2500 ng/mL for plasma samples; 1-2000 ng/mL for brain samples) were adequately described by 1/x weighted quadratic regression of the peak-area ratios of cediranib to its ISTD and the nominal cediranib concentrations, with regression coefficient r^2 always greater than 0.9990 in all analytical runs. The weighting factor was selected based on evaluation of the r^2 value and the deviation of back-calculated calibrators from nominal values (% Diff). The assay LLOQ was determined in five aliquots to be 2.5 ng/mL for cediranib in plasma and 1 ng/mL in brain homogenate. The ANOVA performed on the three QCs from 5×5 validation runs resulted in twenty and four degrees of freedom for within- and between-assay comparisons, respectively. The levels of QCs were selected to reflect the range of concentrations found in mouse plasma and brain homogenate after typical dosing. Accuracy and precision (RSD%) assessments are shown in Table 2-2. For plasma samples, within-assay variabilities ranged from 1.1 to 1.3% and between-assay variabilities ranged from 2.4 to 6.0%. Additionally, for brain homogenate samples, within-assay variabilities ranged from 1.5 to 3.7% and between-assay variabilities ranged

from 4.9 to 6.0%. Overall accuracy was described by the percentage of the grand mean of each calculated concentration to the nominal concentration, and ranged from 102.1 to 107.0% for plasma and 96.5 to 99.8% for brain homogenate, respectively, for all target concentrations. Both within-assay and between-assay variabilities were within ±10% for QCs and within ± 20% for LLOQs. These results satisfied the acceptance criteria in the FDA guidance and the assay was suitable in terms of accuracy and precision.

2.3.3 Recovery

The recovery of cediranib from spiked plasma samples and brain homogenate samples were calculated by comparing the peak area of extracted samples at 10, 100 and 1000 ng/mL, using the extraction conditions described above, with those from corresponding unextracted samples in mobile phase. Recovery for ISTD at 40 ng/mL was also assessed. High and similar recoveries using this extraction method were obtained for both compounds. Average recoveries for cediranib at all three evaluated concentration levels and the ISTD were above 80% in both plasma and brain homogenate. These recoveries allowed quantitation of cediranib down to 1 ng/mL from a sample volume of 100 µL. The recovery results are summarized in Table 2-3.

2.3.4 Stability

Some QC samples (n=5 for each concentration level) were extracted on day one and the rest of them were frozen at -80℃, then thawed, extracted and refrozen each day for further studies. Cediranib concentrations at -80℃ undergoing four freeze-thaw cycles in

mouse plasma for up to 222 days and in brain homogenate for up to 20 days were all within ±15% of the starting concentrations, indicating that cediranib can be considered stable in stored plasma and homogenate samples at all three concentration levels and that there was no concentration-dependent degradation observed. Percentage recoveries for cediranib at each level and in both biological matrices are summarized in Table 2-4a and 2-4b. Evaluation of more than one freeze-thaw cycle was performed in case that occasionally samples will be analyzed more than once. Evaluation of bench-top stability at room temperature was not deemed necessary as all samples were kept on the bench for less than 15 minutes.

2.3.5 Method application

The established HPLC-MS/MS assay was applied to study the brain and plasma pharmacokinetics of cediranib in FVB mice following a single oral dose of 5 mg/kg cediranib suspension. The assay was found to be sufficiently sensitive and accurate for determining cediranib in plasma and brain samples in order to characterize its pre-clinical pharmacokinetics and brain distribution in mice. Figure 2.3 shows the plasma and brain concentration-time profiles (means±S.D.) at 0.25, 0.5, 1, 2, 4, 8, 20 hours post-dose. All measured concentrations were above the LLOQ. The maximum plasma concentration (C_{max}) achieved was 510 ± 205 ng/mL and was reached at 4 hour after oral dosing; the apparent oral clearance and terminal half-life of cediranib in the plasma were determined to be 28.8 mL/hour and 3.5 hours, respectively. However, the brain delivery of cediranib was limited. The brain area under the curve from time zero to the last time point (AUC)

was 849 ± 80 hour×ng/mL, and only 21.8% compared with that in the plasma, which was 3892 ± 434 hour×ng/mL. The restriction in the brain uptake of cediranib implies drug efflux transporter activity at the BBB. A study in wild-type mice does not provide sufficient information on the distribution of cediranib across the BBB. Further studies have been done in transporter-genetic knockout mice to fully understand the mechanistic interpretation of the brain penetration. The present assay has also been successfully utilized in our recent studies exploring the influence of drug efflux transporters on the brain penetration of cediranib.

2.4 Conclusion

In conclusion, a robust and reproductible HPLC-MS/MS assay for quantitation of cediranib in mouse plasma and brain homogenate samples has been developed and validated. This is the first report for quantitation of cediranib in plasma and whole brain samples. The liquid-liquid extraction precedure gives a high extraction yield and is simple to apply. The quantitation range of 2.5-2500 ng/mL is sufficient to allow both plasma and tissue pharmacokinetic studies. The assay is sensitive and specific, with high accuracy and precision. It was successfully used to quantify plasma and whole brain concentrations of cediranib in a preclinical pharmacokinetic study. Furthermore, given the sensitivity and the relatively small sample volume (50μL for plasma and 100μL for brain homogenate), the present assay is feasible for and has been applied in our laboratory to *in vitro* studies of cediranib (e.g., intracellular uptake studies). It may help

fill the current knowledge gaps in preclinical pharmacokinetic studies of cediranib in small specimens.

2.5 Footnotes

We thank James Fisher (Clinical Pharmacology Analytical Services Laboratory, Department of Experimental and Clinical Pharmacology, University of Minnesota) for his assistance with the method development. This work was supported by National Institutes of Health grant R01 CA 138437.

a.

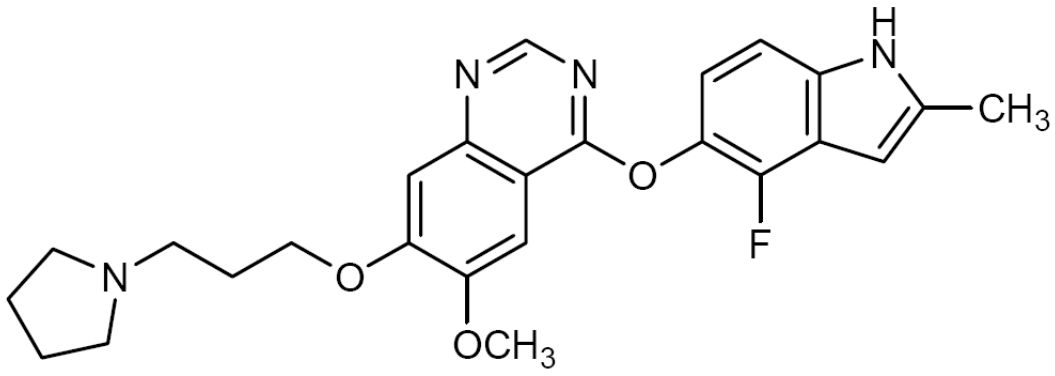

b.

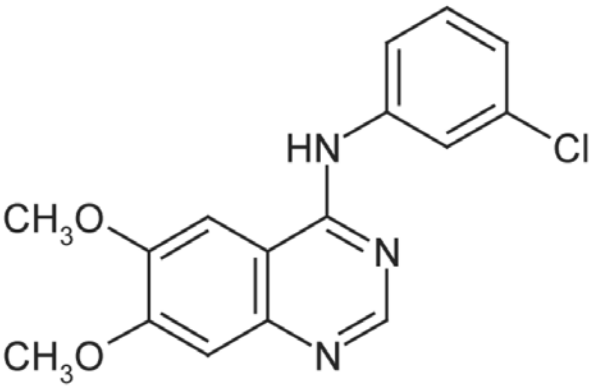

Figure 2.1 Chemical structures of cediranib and the ISTD. a, cediranib; b, AG1478.

Table 2-1 Sub-stock solutions were diluted with MeOH from the stock solutions and used to prepare calibration standards and QC samples as follows.

	Target concentration (μg/mL)	Initial concentration (μg/mL)	Solution (mL)	Final volume (mL)	Final concentration (μg/mL)
Substock 1	100	1000	0.5	5	100
Substock 2	10	100	0.5	5	10
Substock 3	1	10	0.5	5	1

1.

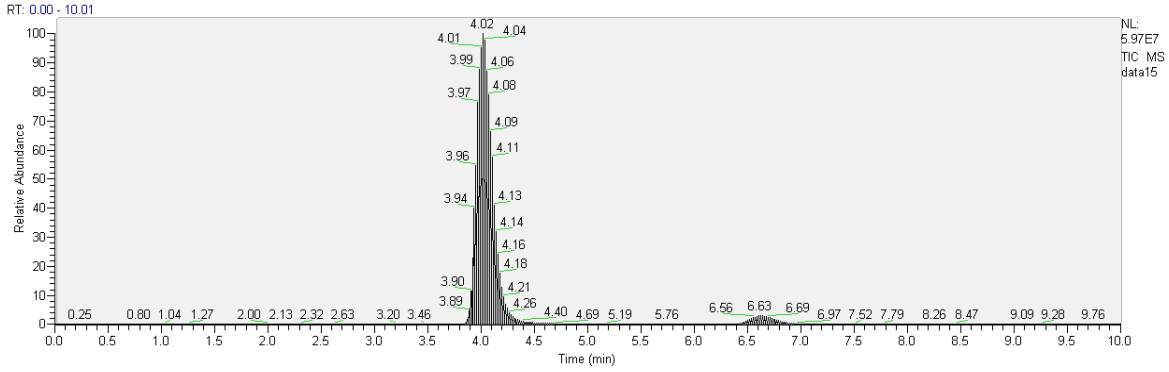

2.

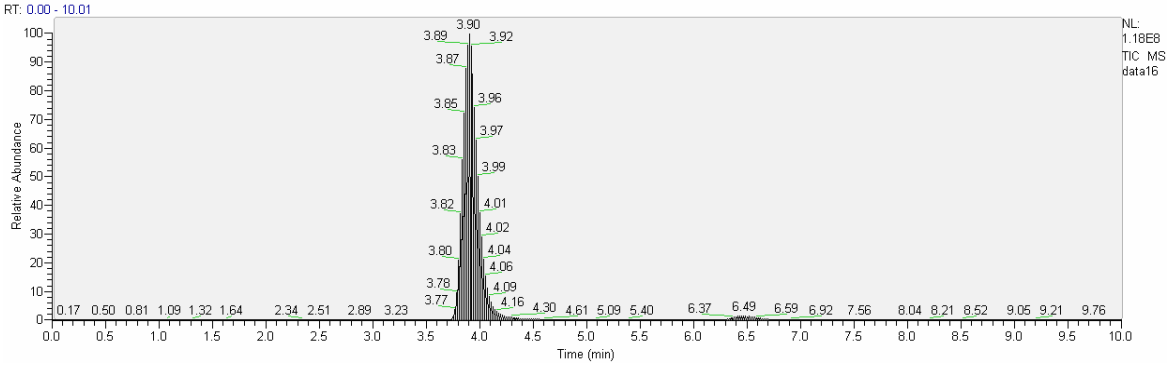

Figure 2.2.a Representative HPLC-MS/MS chromatograms of extracts of the highest plasma and brain homogenate calibrator samples: 1, plasma; 2, brain homogenate. Cediranib: retention time at around 4 min; AG1478: retention time at around 6.5 min.

1.

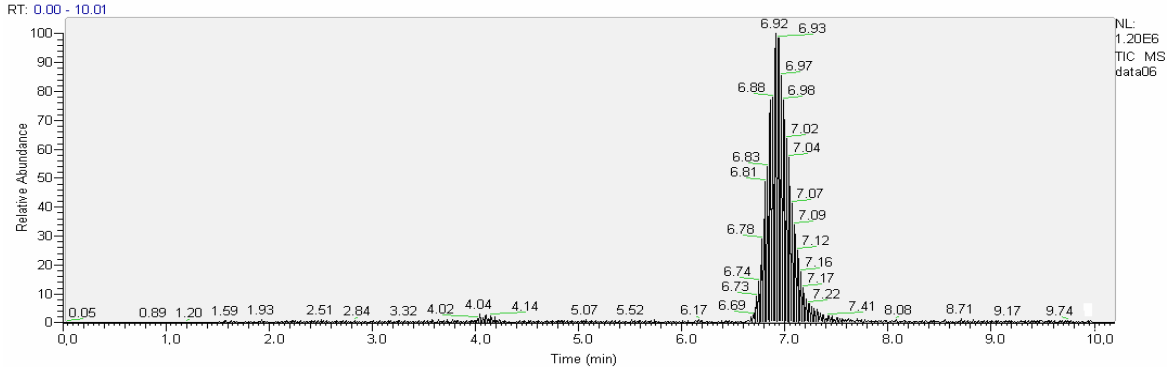

2.

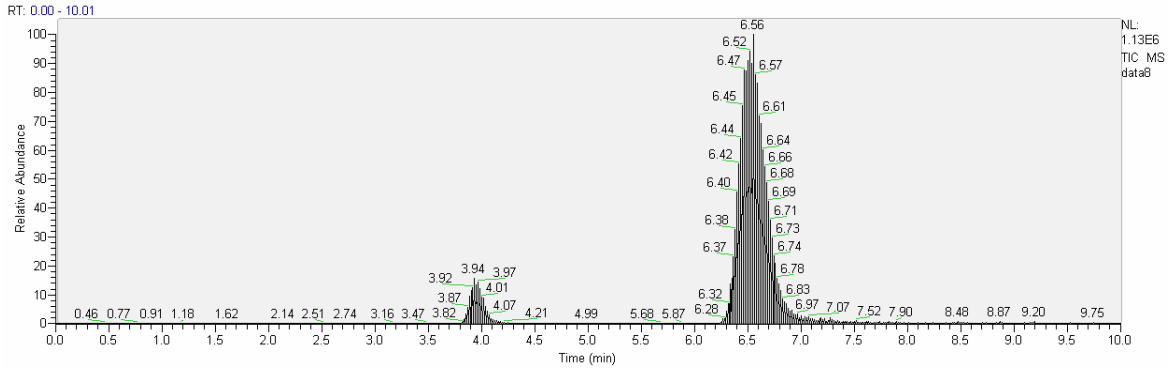

Figure 2.2.b Representative HPLC-MS/MS chromatograms of extracts of plasma and brain homogenate LLOQ samples: 1, plasma; 2, brain homogenate. Cediranib: retention time at around 4 min; AG1478: retention time at around 6.5 min.

Table 2-2 Within-assay and between-assay variabilities and accuracy of the HPLC-MS/MS assay for cediranib in mouse plasma and brain homogenate.

Matrix	Nominal (ng/mL)	RSD (%)		Accuracy (%)
		Within-assay	Between-assay	
Plasma	2.5 (LLOQ)	14.3	9.2	101.5
	15 (Low QC)	1.3	6.0	107.0
	200 (Medium QC)	1.1	4.7	104.0
	800 (High QC)	1.2	2.4	102.1
Brain	1 (LLOQ)	9.4	10.2	100.2
	5 (Low QC)	3.7	4.9	96.5
	50 (Medium QC)	1.5	6.0	99.8
	200 (High QC)	1.7	5.5	98.2

Table 2-3 Absolute recoveries for cediranib and ISTD in the mouse plasma and brain homogenate.

a. Cediranib recoveries

ng/mL	Recovery in Plasma	Recovery in Brain Homogenate
10	83.2% ± 1.1%	101.6% ± 2.0%
100	79.0 % ± 0.7%	80.0% ± 0.6%
1000	83.5% ± 2.4%	89.5% ± 3.4%

b. AG1478 recovery

ng/mL	Recovery in Plasma	Recovery in Brain Homogenate
40	85.7% ± 3.6%	81.7% ± 0.6%

Table 2-4 Cediranib freeze-thaw (FT) cycle stability of the plasma and brain homogenate samples. a. stability in mouse plasma; b. stability in mouse brain homogenate.

a.

ng/mL	1st FT cycle recovery	2nd FT cycle recovery	3rd FT cycle recovery	4th FT cycle recovery	5th FT cycle recovery
15	100.0%	103.8%	108.2%	99.1%	114.4%
200	100.0%	103.6%	108.9%	98.3%	97.1%
800	100.0%	97.8%	103.8%	98.8%	99.1%

b.

ng/mL	1st FTcycle recovery	2nd FT cycle recovery	3rd FT cycle recovery	4th FT cycle recovery	5th FT cycle recovery
5	100.0%	93.8%	98.9%	103.0%	110.4%
50	100.0%	92.5%	93.7%	106.7%	102.3%
200	100.0%	89.1%	93.6%	99.7%	102.0%

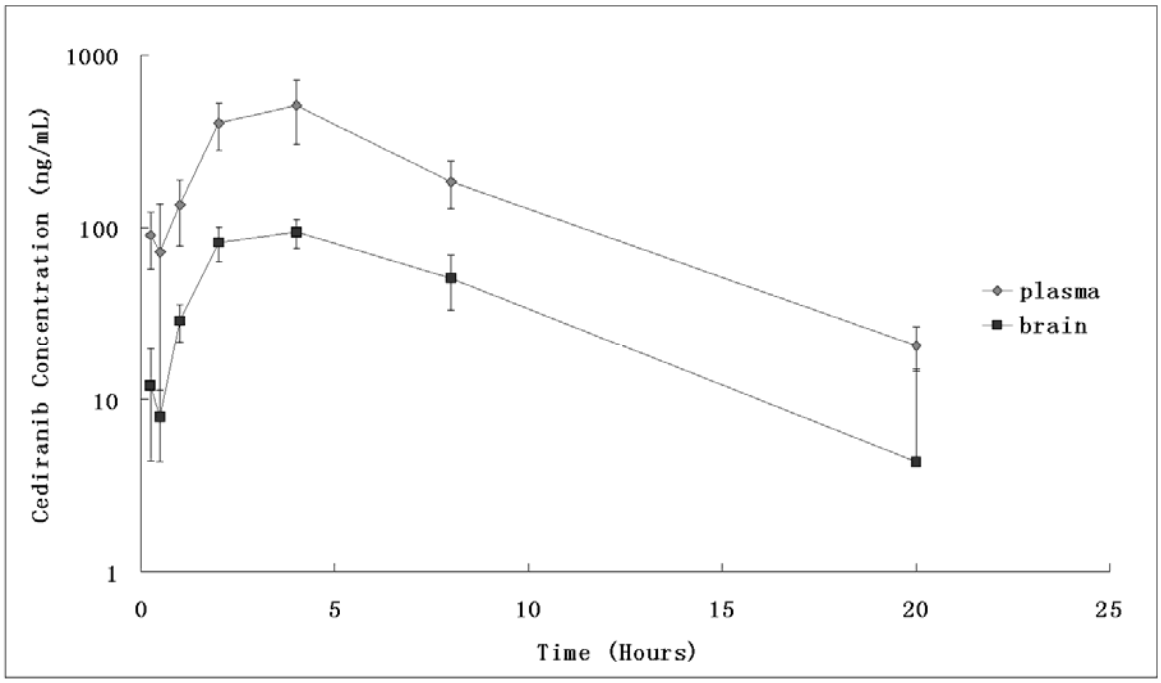

Figure 2.3 Mouse plasma (—◆—) and brain (—■—) pharmacokinetic profiles of cediranib following 5 mg/kg oral administration.

CHAPTER 3

BRAIN DISTRIBUTION OF CEDIRANIB IS LIMITED BY ACTIVE EFFLUX AT THE BLOOD-BRAIN BARRIER

Cediranib is a highly potent and orally active tyrosine kinase inhibitor mainly targeting VEGFRs. Its anti-angiogenic and direct anti-tumor activities make it an attractive option for the treatment of glioma, a primary brain tumor. This study investigated the influence of two important efflux transporters at the BBB, P-glycoprotein (P-gp) and breast cancer resistance protein (BCRP), on the brain delivery of cediranib. In vitro studies indicated cediranib as a dual substrate for P-gp and BCRP. However, upon examining the effect of cediranib on the cellular accumulation of prototypical P-gp and BCRP substrates, no competitive inhibition of BCRP was observed. An in vivo mouse disposition study conclusively showed that P-gp is the dominant transporter restricting the brain distribution of cediranib. The brain-to-plasma partitioning (AUC_{brain}/AUC_{plasma}) and the steady-state brain-to-plasma concentration ratio of cediranib were approximately 20-fold higher in Mdr1a/b(-/-) and Mdr1a/b(-/-)Bcrp1(-/-) mice, compared with wild-type and Bcrp1(-/-) mice. Moreover, there was no significant difference between wild-type and Bcrp1(-/-) mice, and between Mdr1a/b(-/-) and Mdr1a/b(-/-)Bcrp1(-/-) mice in cediranib brain distribution. Furthermore, pharmacokinetic studies also showed that cediranib plasma clearance was not influenced by either P-gp or BCRP, but the oral bioavailability was reduced by P-gp and BCRP. These finding s are clinically relevant to the efficacy of cediranib chemotherapy in glioma.

3.1 Introduction

Delivery of drugs through the blood-brain barrier (BBB) is one of the fundamental challenges in treating diseases of the central nervous system (CNS). The BBB is an

anatomical barrier due to the presence of endothelial tight junctions, and a functional one due to the expression of active drug efflux transporters. Together these two aspects restrict the passage of many small and large molecules into the brain making the barrier effectively impermeable to many desirable compounds. ATP-binding cassette (ABC) transporters, P-glycoprotein (P-gp, ABCB1) and breast cancer resistance protein (BCRP, ABCG2), are two important efflux transporters that work together at the BBB, limiting the transport of several therapeutic agents into the brain. It has been shown that there are overlapping substrate specificities for these two efflux pumps, and a number of drugs, including many anti-cancer tyrosine kinase inhibitors (TKIs), are reported to be dual substrates for both P-gp and BCRP (Dai et al, 2003; de Cries st al., 2007; Polli et al., 2008; Chen et al., 2009; Agarwal et al., 2010; Agarwal et al., 2011; Tang et al., 2011). Furthermore, it has been reported that P-gp is dominant in restricting the brain penetration of many dual P-gp/BCRP substrates although it can work in concert with BCRP (Lee et al., 2005; Zhao et al., 2009; Agarwal et al., 2011).

Cediranib (AZD2171, Recentin™) is a highly potent and orally active inhibitor of the vascular endothelial growth factor family of receptors (VEGFR-1, -2 and -3) (Batchelor et al., 2007). The role of VEGFRs as primary mediators of angiogenesis is well established in many tumors of the CNS, especially glioblastoma multiforme (GBM) (Huang et al., 2005). In gliomas, angiogenesis is mainly driven by VEGF-A-mediated signaling via VEGFR-2, which leads to the proliferation, migration and survival of tumor endothelium, and abnormal microvascular permeability (Carmeliet and Jain, 2000).

VEGFR-2 is commonly overexpressed in tumor endothelial cells in gliomas (Hormigo et al., 2011; Sikkema et al., 2011). Therefore, tumor vasculature has been investigated as a potential target for disrupting tumor-associated angiogenesis by inhibition of VEGF signaling (Demeule et al., 2004). Cediranib has been evaluated in clinical trials for the treatment of various tumors either alone or in combination with standard or experimental therapeutics, including recurrent glioblastoma multiforme (GBM) (Batchelor et al., 2010), non-small cell lung cancer (Ramalingam et al., 2010), colorectal cancer (Satoh et al., 2011), and others. Preclinical studies in glioblastoma mouse models have shown its effect in reducing tumor blood vessel formation and normalizing the aberrant glioma vasculature, leading to an improvement in progression-free survival. However, this survival benefit is thought to be due to alleviation of edema, rather than a true anti-tumor effect (Kamoun et al., 2009). A recently concluded phase II clinical study also reported that cediranib significantly decreased tumor vessel permeability and diameter, as well as induced other vascular changes that led to edema alleviation, but did not affect tumor growth (Batchelor et al., 2010).

As mentioned earlier, delivery of drugs across the BBB into the brain, to the intracerebral targets, is a requirement for efficacy of these drugs. Restricted delivery of a variety of TKIs across the BBB can significantly hamper their efficacy against brain tumors (Agarwal et al., 2010; Kodaira et al., 2010; Polli et al., 2008). We therefore hypothesized that cediranib may also be a substrate for either P-gp or BCRP, or for both. If this is true, interaction with these active efflux transporters present at the BBB could limit cediranib

brain distribution and result in poor efficacy in treatment of brain tumors such as GBM. In a recent review, we discussed how efficacy of molecularly-targeted agents in GBM can be limited by several factors that affect drug delivery to the target (Agarwal et al., 2011). Glioma is a very invasive disease and glioma cells infiltrate normal brain areas centimeters away from the tumor core and remain shielded behind an intact BBB (Kuratsu et al., 1989; Silbergeld and Chicoine, 1997; Lucio-Eterovic et al., 2009). Even though tumor core blood vessels may show poor barrier function, it may still be difficult for cediranib to achieve therapeutic concentrations in the brain endothelium and the invasive tumor cells in order to target the infiltrative tumor growth. The limited delivery of cediranib to its target sites may be one of the reasons for the poor effectiveness seen in GBM. There have been no published reports investigating the distribution of cediranib to the CNS. Similarly, the interaction of cediranib with drug efflux transporters has not been characterized. In the current study, we investigated whether cediranib is a substrate for the efflux pumps, P-gp and BCRP and whether this restricts delivery of cediranib across an intact BBB.

The objective of the current study was to characterize the interaction of cediranib with the two important ABC transporters at the BBB, and to examine their influence on delivery of cediranib across the BBB. Cediranib is currently being evaluated for therapy in glioma, a very invasive tumor of the brain, and restricted delivery to the invasive glioma cells could significantly limit its effectiveness against this lethal disease.

3.2 Material and methods

3.2.1 Chemicals and reagents

Cediranib and tyrphostin (AG1478) were procured from Selleck Chemicals LLC (Houston, TX, USA) and LC Laboratories (Woburn, MA), respectively. ^{3}H-vinblastine (18.2 Ci/mmol, purity - 97.4 %) was purchased from Moravek Biochemicals (La Brea, CA) and ^{3}H-prazosin (70 Ci/mmol, purity - 97 %) was purchased from Perkin Elmer (Waltham, MA). Elacridar (GF120918, N-[4-[2-(6, 7-Dimethoxy-3,4-dihydro-1H-isoquinolin-2-yl)ethyl]-5-methoxy-9-oxo-10H-acridine-4-carboxamide) was purchased from Toronto Research Chemicals, Inc. (Ontario, Canada). Ko143((3S,6S,12aS)-1,2,3,4,6,7,12,12a-Octahydro-9-methoxy-6-(2-methylpropyl)-1,4-dioxopyrazino[1',2':1,6] pyrido [3,4- b]indole-3-propanoic acid 1,1-dimethylethyl ester) was generously provided by Dr. Alfred Schinkel (The Netherlands Cancer Institute, Amsterdam, The Netherlands) and zosuquidar (LY335979, (*R*)-4-((1a*R*,6*R*,10b*S*)-1,2-difluoro-1,1a,6,10btetrahydrodibenzo-(*a*,*e*) cyclopropa(*c*) cycloheptan-6-yl)-α-((5-quinoloyloxy) methyl)-1-piperazine ethanol, trihydrochloride) was a gift from Eli Lilly and Co. (Indianapolis, IN). All other reagents and chemicals were purchased from Sigma Chemical Co (St. Louis, MO).

3.2.2 *In vitro* studies

3.2.2.1 Cell lines

In vitro studies were conducted in epithelial Madin-Darby Canine Kidney (MDCKII) cells that expressed either human P-gp (MDCKII-*MDR1* cell line) or murine BCRP (MDCKII-*Bcrp1* cell line). These cells were generously provided by Dr. Piet Borst and

Dr. Alfred H. Schinkel (The Netherlands Cancer Institute, The Netherlands). Cells were cultured in DMEM media containing 10% fetal bovine serum (Sigma-Aldrich, St. Louis, MO), penicillin (100U/ml), streptomycin (100µg/ml) and amphotericin B (250 ng/mL) (all Sigma-Aldrich, St. Louis, MO) and maintained at 37°C with 5% CO2 under humidifying conditions.

3.2.2.2 Intracellular accumulation

For the intracellular accumulation studies, cells were grown in 12-well polystyrene plates (Thermo Fisher Scientific Inc., Rochester, NY) that were seeded at a density of 2 x 10^5 cells/well. Growth medium was changed on alternate days until the cells formed confluent monolayers. On the day of the experiment cells were equilibrated for 30 mins with 1 mL of growth medium with or without transporter inhibitors. After the preincubation step, the experiment was initiated by addition of 1 ml of cediranib working solution (1 µM) and the plates were incubated in an orbital shaker maintained at 37º C. The experiment was terminated after a 3-hour accumulation period by aspirating the drug solution from the wells and washing the cells with ice-cold phosphate-buffered saline. Cells were then solubilized by addition of 0.5 ml of M-PER® mammalian protein extraction reagent (Thermo Scientific Inc., Rockford, IL) to each well and the protein concentration in the solubilized cell fractions was determined by the BCA protein assay (Thermo Scientific Inc., Rockford, IL). Cediranib concentration associated with a 100 µL sample was determined by high-performance liquid chromatography coupled with mass spectrometry (HPLC-MS/MS). The intracellular uptake of cediranib was expressed as a

percentage of accumulated cediranib (nanogram per microgram of protein) measured in the transfected cells versus wild-type cells. For inhibition studies, the cells were treated with the dual inhibitor GF120918 (5 μM) and the selective inhibitors LY335979 (1 μM) for P-gp or Ko143 (200 nM) for BCRP during both the preincubation and the accumulation periods. The stock solutions for all the inhibitors used were prepared in dimethyl sulfoxide and diluted using cell growth medium to obtain working concentrations. ^{3}H-vinblastine and ^{3}H-prazosin were included in the accumulation studies as positive controls for P-gp and BCRP, respectively. Radioactivity (dpm) associated with a 150 μL sample was determined by liquid scintillation counting (LS-6500, Beckman Coulter Inc., Fullerton, CA). The radioactivity in the cell fractions was normalized by the respective protein concentrations and drug accumulation in the cells was expressed as a percentage of accumulated radioactivity (dpm per microgram of protein) in the transfected cells versus the WT control cells.

3.2.2.3 Directional flux assays

Transepithelial transport of cediranib was assessed using MDCKII wild-type, *MDR1*-, and *Bcrp1*- transfected cells. Transport assays were performed in 6-well Transwells (Corning Inc., Corning, NY). The cells were seeded at a density of 2×10^5 cells/well until they formed confluent polarized monolayers. The experiment was conducted by applying a 900 ng/mL solution of cediranib (in complete growth medium) to the donor compartment. The receiver compartment was then sampled (200 μL aliquot) at 2 and 3 hours after addition of cediranib to the donor side and immediately replaced with fresh

growth medium. Transport of cediranib was assessed in two directions: apical-to-basolateral (A-to-B) and basolateral-to-apical (B-to-A). The amount of cediranib transported over time was determined by measuring cediranib concentrations in the samples by HPLC-MS/MS. The apparent permeability (P_{app}) of cediranib was calculated by the following equation,

$$P_{app} = \frac{\frac{dQ}{dt}}{A \times C_0}$$

where, *dQ/dt* is the rate of mass transport (determined from the slope of the amount transported vs time plot), *A* is the apparent surface area of the cell monolayer (4.67 cm^2), and C_0 is the initial donor concentration. The efflux ratio, defined as the ratio of P_{app} in the B-to-A direction to the P_{app} in the A-to-B direction, was used to estimate the magnitude of transporter-mediated efflux.

3.2.2.4 P-gp and BCRP inhibition assays

The ability of cediranib to inhibit P-gp and BCRP was evaluated by examining the intracellular accumulation of prototypical probe substrates ^{3}H-vinblastine for P-gp and ^{3}H-prazosin for BCRP in presence of varying concentrations of cediranib ranging from 0 to 40μM. The accumulation was carried out for 2 hours as described earlier and the amount of accumulated radioactivity associated with the probe substrates (dpm per microgram protein) were measured and plotted versus cediranib concentration.

3.2.3 *In vivo* studies

3.2.3.1 Animals

In vivo studies were conducted in wild-type, *Mdr1a/b (-/-)* [P-gp knockout], *Bcrp1(-/-)* [BCRP knockout] and *Mdr1a/b (-/-) Bcrp1 (-/-)* [triple knockout] mice of a FVB genetic background from Taconic Farms, Inc.(Germantown, NY). All animals were maintained under temperature-controlled conditions with a 12-h light/dark cycle and unlimited access to food and water and were between 8 to 10 weeks old at the time of experiment. Mice were handled according to the guidelines set by the *Principles of Laboratory Animal Care* (National Institutes of Health) and were approved by The Institutional Animal Care and Use Committee (IACUC) of the University of Minnesota.

3.2.3.2 Plasma and brain pharmacokinetics following intravenous or oral administration

Wild-type and *Mdr1a/b(-/-)Bcrp1(-/-)* mice were administered a 5 mg/kg dose of cediranib (1.0 % w/v Tween 80) by oral gavage. Mice were euthanized using a CO_2 chamber at desired time points for up to 24 hours post-dose (n = 4 at each time point) and then blood and brain were harvested.

For the intravenous administration of cediranib, the dosing solution was prepared on the day of the experiment by dissolving cediranib in a vehicle containing DMSO, propylene glycol and saline (5:3:2 v/v/v) to yield a concentration of 2 mg/mL. Wild-type, *Mdr1a/b (-/-)*, *Bcrp1(-/-)* and *Mdr1a/b (-/-) Bcrp1 (-/-)* mice, received an intravenous dose of 4 mg/kg cediranib by tail vein injection. Blood and brain were sampled at different time points up to 24 hours post-dose, *n* = 4 at each time point.

Plasma was isolated from blood by centrifugation at 3500 rpm for 10 min at 4˚C. The brain was rinsed with ice-cold saline to remove extraneous blood and flash frozen in liquid nitrogen. Plasma and brain specimens were stored at -80˚C until analysis by HPLC-MS/MS. At the time of analysis, brain tissues were homogenized in 3 volumes of ice-cold 5% (w/v) BSA in phosphate-buffered saline solution. Brain concentration was corrected for the residual drug in the brain vasculature by using a correction factor as described by Dai et al (Dai et al., 2003).

Non-compartmental and one-compartmental PK analyses using Phoenix WinNonlin 6.1® (Pharsight, CA) were carried out to estimate the pharmacokinetic parameters. The area under the curve (AUC) was calculated using the trapezoidal rule. The maximum drug concentration (C_{max}) and the time to reach peak concentration (T_{max}) were estimated from the observed data. Volume of distribution based on the plasma concentration (V_d), drug clearance (CL) and elimination rate constant (k_e) were estimated utilizing an one-compartment model.

3.2.3.3 Steady-state brain distribution of cediranib

The partition coefficient of cediranib in brain was determined by measuring concentrations in brain and plasma at steady-state in wild-type, *Mdr1a/b (-/-)*, *Bcrp1 (-/-)* and *Mdr1a/b (-/-) Bcrp1 (-/-)* mice. Cediranib was administered as a constant rate intraperitoneal infusion of 50 μg/hr by using Alzet osmotic minipumps (Durect Corporation, Cupertino, CA). A 50 mg/ml solution of cediranib in DMSO was filled in the minipumps (model 1003D) and the pumps were equilibrated by soaking them

overnight in sterile saline solution at 37ºC. The primed pumps were surgically inserted into the peritoneal cavity of anesthetized mice (ketamine 100 mg/kg, xylazine 10 mg/kg) and the animals were allowed to recover for an hour on a heated pad. The animals were euthanized 72 hours post surgery and brain and blood was collected as described earlier. Plasma and brain specimens were stored at -80˚C until analysis by HPLC-MS/MS. The pumps operated at a constant flow rate of 1 µL/hr resulting in an intraperitoneal infusion rate of 50 ug/hr.

The apparent plasma clearance (CL_{app}) following infusion to steady state was calculated as follows,

$$CL_{app} = \frac{R_0}{C_{ss}}$$

where, R_0 is the constant rate of infusion (ng/hr) and C_{ss} is the steady-state plasma concentration (ng/mL).

3.2.3.4 Influence of P-gp and BCRP on brain distribution of cediranib

The influence of pharmacological inhibition of P-gp and BCRP on brain distribution of cediranib was examined by concurrent administration of selective and non selective inhibitors along with cediranib. Wild-type mice received an intravenous dose of blank vehicle (control), 25 mg/kg LY335979, 10 mg/kg Ko143, or 10 mg/kg GF120918 , 30 minutes prior to a 5 mg/kg oral dose of cediranib. Brain and plasma were collected at 90 minutes after the cediranib dose. Similarly, brain distribution of cediranib was determined in a separate group of wild-type, *Mdr1a/b (-/-)*, *Bcrp1 (-/-)* and *Mdr1a/b (-/-) Bcrp1 (-/-)* mice that were dosed orally with 5 mg/kg cediranib. The effect of

pharmacological inhibition was then compared with genetic deletion of transporter genes at the same time point.

3.2.3.5 Quantitative analysis of cediranib by liquid chromatography-tandem mass spectrometry

Quantitation of cediranib in cell lysate, cell culture media, mouse plasma and mouse brain homogenate were all conducted by HPLC-MS/MS according to the validated assay described in Chapter 2.

3.2.3.6 Statistical analysis

The two sample t-test was employed for statistical testing of two groups using SigmaStat, version 3.1 (Systat Software, Inc., Point Richmond, CA). Significance was declared at $p < 0.05$. Multiple groups were compared by one-way analysis of variance (ANOVA) with the Holm-Sidak post-hoc test at a significance level of $p < 0.05$.

3.3 Results

3.3.1 *In vitro* studies

3.3.1.1 Intracellular accumulation of cediranib in MDCKII cells

Intracellular accumulation of cediranib in MDCKII wild-type and *MDR1*- or *Bcrp1*-transfected cells was examined. ^{3}H-vinblastine and ^{3}H-prazosin, prototypical substrates for P-gp and BCRP, respectively, were included as positive controls. As seen in Fig. 3.1A, accumulation of the P-gp substrate vinblastine was significantly reduced in the *MDR1*-

transfected cells compared with wild-type control (~24% of wild-type). Likewise, cediranib accumulation in the *MDR1*-transfected cells was 44% lower compared with the wild-type cells ($p<0.05$). Accumulation in the *MDR1*-transfected cells increased upon treatment with the P-gp specific inhibitor LY335979 and the P-gp/BCRP dual inhibitor GF120918 (Fig. 3.1A), such that it was not significantly different from the accumulation in wild-type cells. This suggested that P-gp is involved in efflux of cediranib from the cells. In the Bcrp1-transfected cells, there was significantly lower accumulation of the BCRP substrate prazosin compared with wild-type control (~44% of wild-type, Fig. 3.1B). Similarly, cediranib accumulation in the *Bcrp1*-transfected cells was statistically lower than that in wild-type cells (~68% of wild-type). The efflux activity of BCRP can be abolished upon treatment with the BCRP-selective inhibitor Ko143 (Fig.3.1B), which suggests that BCRP also limits intracellular accumulation of cediranib.

3.3.1.2 Directional permeability of cediranib across MDCKII cells

Transcellular transport of cediranib was determined in MDCKII wild-type and *MDR1*- or *Bcrp1*-transfected cells. In the *MDR1*-transfected cells, the rate of cediranib transport was significantly increased in the B-to-A direction compared to that in the A-to-B direction (Fig. 3.2, $p < 0.05$). The apparent permeability of cediranib in the B-to-A direction was 2–fold greater than the A-to-B permeability in the *MDR1*-transfected cells. The P-gp inhibitor LY339579 effectively inhibited P-gp mediated efflux transport in the *MDR1*-transfected cells, such that there was no significant difference in the permeability of cediranib transported in both directions (Fig. 3.2). The directional permeabilities of

cediranib in wild-type and *MDR1*-transfected cells are shown in Table. 3-1. Directional flux experiments in the *Bcrp1*-transfected cells showed increased directionality in the flux of cediranib (Fig. 3.3), with the apparent permeability in the B-to-A direction being 4–fold greater than the A-to-B permeability (Table. 3-2). The BCRP inhibitor Ko143 reversed the BCRP-mediated efflux transport in that there was no difference in the permeability of cediranib transported in the two directions (Fig. 3.3). These studies suggest that cediranib is a substrate of both P-gp and BCRP and is efficiently transported by both transporters.

3.3.1.3 Cediranib as a P-gp or BCRP inhibitor

Figure 3.4 shows the effect of cediranib on accumulation of ^{3}H-vinblastine in *MDR1*-transfected cells (Figure 3.4.A) and ^{3}H-prazosin *Bcrp1*-transfected cells (Figure 3.4.B). Increasing concentrations of cediranib enhanced the intracellular accumulation of vinblastine in the *MDR1*-transfected cells (Fig. 3.4.A). However, cytotoxicity associated with cediranib restricted the maximum dose to 40 μM. Thus we were not able to accurately estimate the IC_{50} of cediranib for inhibition of P-gp. But these results clearly show that cediranib inhibits the P-gp-mediated transport of vinblastine. Interestingly, cediranib treatment did not increase prazosin accumulation in the *Bcrp1*-transfected cells (Fig. 3.4.B), indicating that cediranib does not inhibit BCRP-mediated efflux, even though it is a substrate for BCRP. This suggests that cediranib may be transported by BCRP via binding to a different site than the prazosin binding site.

3.3.2 *In vivo* studies

3.3.2.1 Cediranib brain and plasma pharmacokinetics

Since cediranib is an orally administered compound, cediranib pharmacokinetics in plasma and brain was first examined after oral administration in wild-type and *Mdr1a/b(-/-)Bcrp1(-/-)* mice. Cediranib brain concentrations in the wild-type mice were significantly lower than the plasma concentrations (Figure 3.5A), indicating restricted transport of cediranib across the BBB. In comparison, in the *Mdr1a/b(-/-)Bcrp1(-/-)* mice, cediranib brain exposure were 26–fold higher than plasma (Table 3-3 and Figure 3.5B), showing the influence of P-gp and/or BCRP on cediranib transport across the BBB. There was no significant difference in plasma $AUC_{(0\text{-}20hr)}$ between these genotypes (Table 3-3), suggesting that P-gp and BCRP do not influence the apparent systemic clearance of cediranib.

In order to further investigate whether the limited brain penetration of cediranib is mediated by either P-gp or BCRP or both, brain and plasma pharmacokinetics of cediranib were studied following intravenous injection into wild-type, *Mdr1a/b (-/-)*, *Bcrp1 (-/-)* and *Mdr1a/b (-/-) Bcrp1 (-/-)* mice (Figure 3.6.A~D). Plasma pharmacokinetics of cediranib in all the four genotypes followed one-compartment kinetics. Table 3-4.A shows the one-compartment pharmacokinetic parameters of cediranib in mouse plasma for all four genotypes. There was not an obvious difference in the means of volume of distribution (V_d) of cediranib among different mice groups, although the V_d in *Mdr1a/b (-/-) Bcrp1 (-/-)* mice was a little higher than the other mice.

It was also shown that the means of total body clearance (CL) of cediranib in those transporter-knockout mice were not quite different, although the plasma CL in wild-type mice was to some extent lower than transporter-knockout mice.

It has been shown in Table 3-4.B that brain concentrations were significantly lower than the plasma concentrations yielding an AUC_{brain} / AUC_{plasma} of around 0.2 in wild-type and *Bcrp1-/-* mice, but brain exposure increases dramatically in both *Mdr1a/b-/-* and *Mdr1a/b-/-Bcrp1-/-* mice (AUC ratio $\approx$ 6). Interestingly, the absence of BCRP in the *Bcrp1(-/-)* mice does not result in any change in the BBB permeability of cediranib. Similarly, there was no significant difference in the brain exposure of cediranib in *Mdr1a/b(-/-) and Mdr1a/b(-/-) Bcrp1(-/-)* mice. These *in vivo* results differ from the *in vitro* observations that cediranib was shown as a dual substrate for P-gp and BCRP. Thus, we concluded that cediranib brain distribution *in vivo* is dominantly limited by P-gp-mediated efflux. BCRP might play an insignificant role in pumping cediranib out of the BBB.

3.3.2.2 Effect of P-gp and BCRP on steady-state brain and plasma pharmacokinetics of cediranib

The role of P-gp and BCRP in transporting cediranib out of the brain was also investigated by determining the steady-state brain distribution of cediranib in wild-type, *Mdr1a/b(-/-), Bcrp1(-/-), and Mdr1a/b(-/-)Bcrp1(-/-)* mice. The brain-to-plasma steady-state concentration ratios ($C_{ss,brain}/C_{ss,plasma}$) were compared across the four genotypes

(Table 3-5). From the intravenous studies described above, the half-life of cediranib in the plasma was determined to be ~ 1.8 to 3 hours, and ~3 to 7 hours in the brain, suggesting that an infusion lasting 72 hours would be sufficient to attain steady-state in both plasma and brain. There was no significant difference in $C_{ss,plasma}$ or CL_{app} between the four genotypes, confirming our earlier results that P-gp and BCRP do not influence the systemic elimination of cediranib. However, $C_{ss,brain}$ of cediranib was pronouncedly enhanced in the *Mdr1a/b(-/-) and Mdr1a/b(-/-) Bcrp1(-/-)* mice, compared to wild-type and *Bcrp1(-/-)* mice, leading to a 20.8- and 25-fold higher steady-state brain-to-plasma ratio, respectively. These results were consistent with the AUC ratios seen in both of the oral and i.v. PK studies.

3.3.2.3 Influence of P-gp and BCRP inhibitors on brain distribution of cediranib

There are generally two in vivo approaches to quantify the magnitude of transporter-mediated drug exclusion from the CNS: one is through use of transporter-deficient animal models; and the other is through co-treatment of chemical modulaters of transporter function. In this experiment, we examined the consistency of these experimental approaches. Results from the transporter-deficient animal models showed that the brain-to-plasma concentration ratios at 90 minutes after an oral cediranib dose were 0.14 ± 0.055, 0.16 ± 0.032, 2.20 ± 0.36, 2.32 ± 0.20 in wild-type, *Mdr1a/b(-/-), Bcrp1(-/-), and Mdr1a/b(-/-) Bcrp1(-/-)* mice, respectively (Figure 3.7A). Concurrent administration of the selective P-gp inhibitors LY335979 and the dual P-gp and BCRP inhibitor GF120918 resulted in an enhancement in brain-to-plasma concentration ratios of cediranib (2.35 ±

0.89 and 3.15 ± 1.92, respectively) at the same time point in the wild-type mice, compared with the vehicle control (0.18 ± 0.025) (Figure 3.7B). However, similar to what we saw in the *Bcrp1(-/-)* mice, pretreatment of BCRP specific inhibitor Ko143 has no significant effect on the brain distribution of cediranib in the wild-type mice, with the brain-to-plasma ratio being 0.17 ± 0.072. The pharmacological inhibition recapitulates our findings in the genetic knockouts and confirms that P-gp is the main efflux transporter that limits the brain distribution of cediranib. Coadministration of the pharmacological inhibitors for the two transporter proteins, especially for P-gp, may have the potential to enhance the brain delivery of cediranib by inhibiting the efflux function.

3.4 Discussion

Cediranib is a pan-inhibitor of VEGFR family and other regulators of tumor growth and angiogenesis such as PDGFR and c-KIT. These targets of cediranib are expressed on glioblastoma vasculature (Batchelor et al., 2007). Moreover, cediranib can inhibit tumor cell migration and invasion by inhibiting VEGF/VEGFR autocrine signaling (Morelli et al., 2009). The VEGFR-blockade by cediranib may also lead to the tumor cell apoptosis (Kamoun et al., 2009). Thus, cediranib has been an attractive option for brain tumor therapy (Batchelor et al., 2007; Batchelor et al., 2010). However, clinical trials for cediranib and other anti-angiogenic agents fail to attain anti-tumor efficacy. The reasons for their failures remain unclear. Gioma, in particular, is an infiltrative and malignant brain tumor, where invasive tumor cells may be protected from anti-cancer therapeutics by an intact BBB. We hypothesize that the restricted delivery of cediranib to its target

sites (brain tumor endothelial cells and invasive glioma cells) in the brain might be one of possible reasons for its failure in GBM therapy. Thus, the aim of the current study was to investigate the interaction of cediranib with active efflux transporters at the BBB. We have been the first to show that cediranib is a P-gp and BCRP dual substrate. Furthermore, our *in vivo* findings conclusively show that the brain delivery of cediranib is mainly limited by P-gp rather than BCRP.

In vitro accumulation and directional transport studies showed that cediranib is a substrate for both P-gp and BCRP. Inhibition of P-gp and BCRP by their inhibitors can increase the restricted intracellular accumulation of cediranib in the transporter-overexpressed cell lines to the wild-type level. Interestingly, cediranib inhibits the P-gp activity, rather than BCRP. These findings can be clinically relevant since inhibition of P-gp by cediranib may alter tissue pharmacokinetics of concurrently administered drugs which are potential P-gp substrates. The finding that cediranib is transported by BCRP, but it does not inhibit the BCRP efflux transport of other substrates, like prazosin, is similar to the behavior of another TKI sorafinib, as reported by Agarwal (Agarwal et al., 2010b). This is yet another possible example of multiple binding sites on BCRP for drug transport.

The results of our animal studies showed that P-gp has a leading impact in limiting the brain delivery of cediranib and that BCRP does not have a significant effect in keeping it out of the brain, although in vitro studies indicated cediranib as a dual substrate for both

P-gp and BCRP. To date, there are a number of findings reported about the cooperation of P-gp and BCRP in restricting TKIs across the BBB, such as imatinib (Breedveld et al., 2005), dasatinib (Chen et al., 2009), gefitinib (Agarwal et al., 2010a), lapatinib (Polli et al., 2009), erlotinib (Kodaira et al., 2010), and sunitinib (Tang et al., 2011), with P-gp as their dominant transporter. Cediranib is different in that P-gp and BCRP do not have a combined effect on its brain distribution *in vivo*. Our data suggested that P-gp might compensate for the absence of BCRP, but BCRP did not compensate for the loss of P-gp. Even if P-gp was absent or inhibited, BCRP activity still did not become apparent. The BCRP-mediated transport of cediranib does not show any *in vitro-in vivo* correlation. A similar finding was reported by Giri et al. for zidovudine (AZT) (Giri et al., 2008). A possible mechanism behind the subdued BCRP effect might be the 5-fold lower amount of BCRP at the mice BBB than P-gp (Kamiie et al., 2008). Our results are consistent with the finding by Kodaira et al. that P-gp-mediated efflux transport was greater than BCRP for many dual substrates (Kodaira et al., 2010).

Mouse pharmacokinetic studies also indicated that P-gp and BCRP may influence the oral absorption of cediranib by reducing the oral bioavailability and absorption rate, with a prolonged absorption peak and a slightly increased F in *Mdr1a/b(-/-)Bcrp1(-/-)* mice compared with wild-type mice. However, the plasma clearance of cediranib remained unchanged no matter the presence or absence of the transporters. The mean of volume of distribution was increased in *Mdr1a/b(-/-)Bcrp1(-/-)* mice compared with the other groups. We have postulated that since P-gp and BCRP restrict cediranib from getting into

some tissues, the simultaneous absence of these transporters may result in a better distribuion of cediranib into those tissues or organs. Our current studies are also the first to report the pharmacokinetics of cediranib in mice, which will be helpful for other studies such as a constant rate infusion and a multiple oral administration in animal models treated with cediranib.

We also compared the brain-to-plasma C_{ss} ratio in the four genotypes. The results were consistent with results of the single dose pharmacokinetic studies following both i.v. and oral administration in that cediranib exposure in *Mdr1a/b(-/-)* and *Mdr1a/b(-/-)Bcrp1(-/-)* mice was ~20-fold higher than that in wild-type and *Bcrp1(-/-)* mice. There was no significant increase in the brain-to-plasma C_{ss} ratio when BCRP alone was absent in the *Bcrp1(-/-)* mice compared to the wild-type mice. Moreover, no significant contribution of the absence of BCRP in addition to the absence of P-gp in the increase of cediranib brain partitioning was detected when we compared *Mdr1a/b(-/-)* and *Mdr1a/b(-/-)Bcrp1(-/-)* mice.

The finding that inhibition or genetic deletion of P-gp alone or both of P-gp and BCRP is consistent in enhancing brain penetration of cediranib *in vivo*, and has significant clinical implications. It is a promising therapeutic strategy to give cediranib by coadministration with P-gp inhibitors in order to alleviate the efflux activity. This might improve the clinical efficacy of cediranib for the treatment of brain tumors.

3.5 Conclusion

In conclusion, cediranib is a substrate of active efflux transporters P-gp and BCRP *in vitro* but only P-gp plays a critical in limiting brain delivery of cediranib. The use of potent inhibitors for P-gp may be able to significantly enhance delivery and efficacy of cediranib against glioma, which might be related to the ability of cediranib to achieve therapeutic concentrations in brain tumor endothielial cells and invasive glioma cells. To deepen our insight into the effective delivery, additional studies are needed to quantitatively determine the cediranib distribution in the brain tumor endothelium.

3.6 Footnotes

We would like to thank Sagar Agarwal for his continuous help in the animal experiments. We thank Dr. Piet Borst and Dr. Schinkel from Netherlands Cancer Institute for providing the wild-type, Mdr1- and BCRP-transfected MDCKII cells. We also thank Dr. Schinkel for generously providing us Ko143, and Eli Lilly and Co. for LY335979.

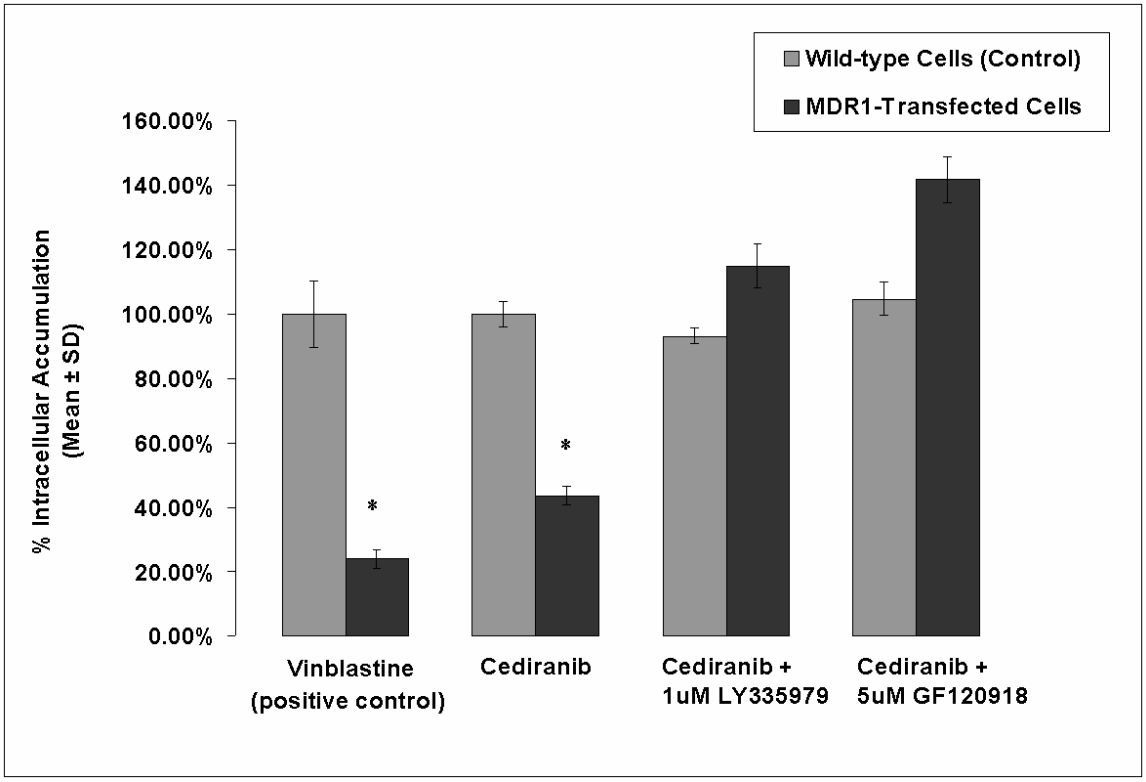

Figure 3.1.A Accumulation of cediranib in wild-type and Mdr1-transfected MDCKII cells with and without presence of the P-gp selective inhibitor, 1 μM LY335979, and the P-gp and BCRP dual inhibitor, 5 μM GF120918. ^{3}H-vinblastine accumulation was measured in wild-type and Mdr1-transfected cells as a positive control. Results are presented as mean ± SD, n=4 (*, $p < 0.05$).

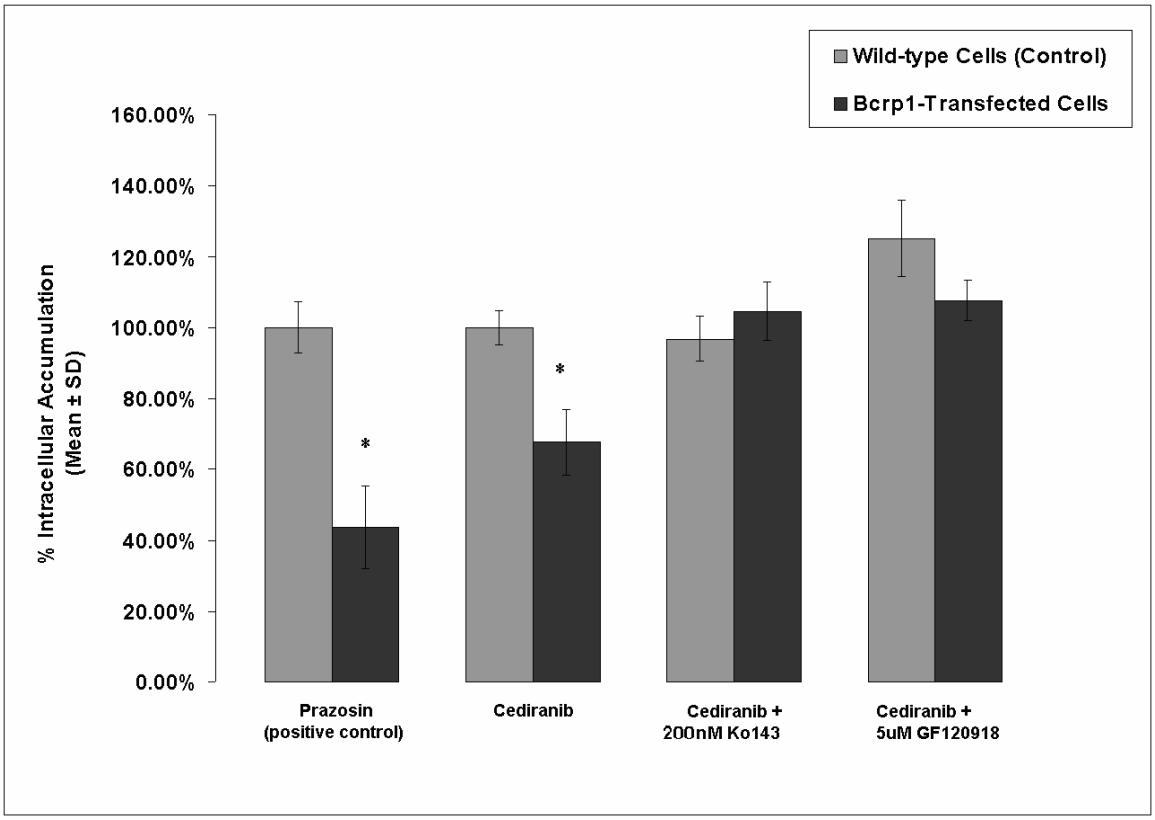

Figure 3.1.B Accumulation of cediranib in wild-type and Bcrp1-transfected MDCKII cells with and without presence of the BCRP selective inhibitor, 200 nM Ko143, and the P-gp and BCRP dual inhibitor, 5μM GF120918. ^{3}H-prazosin accumulation was measured in wild-type and Bcrp1-transfected cells as a positive control. Results are presented as mean ± SD, n=4 (*, $p < 0.05$).

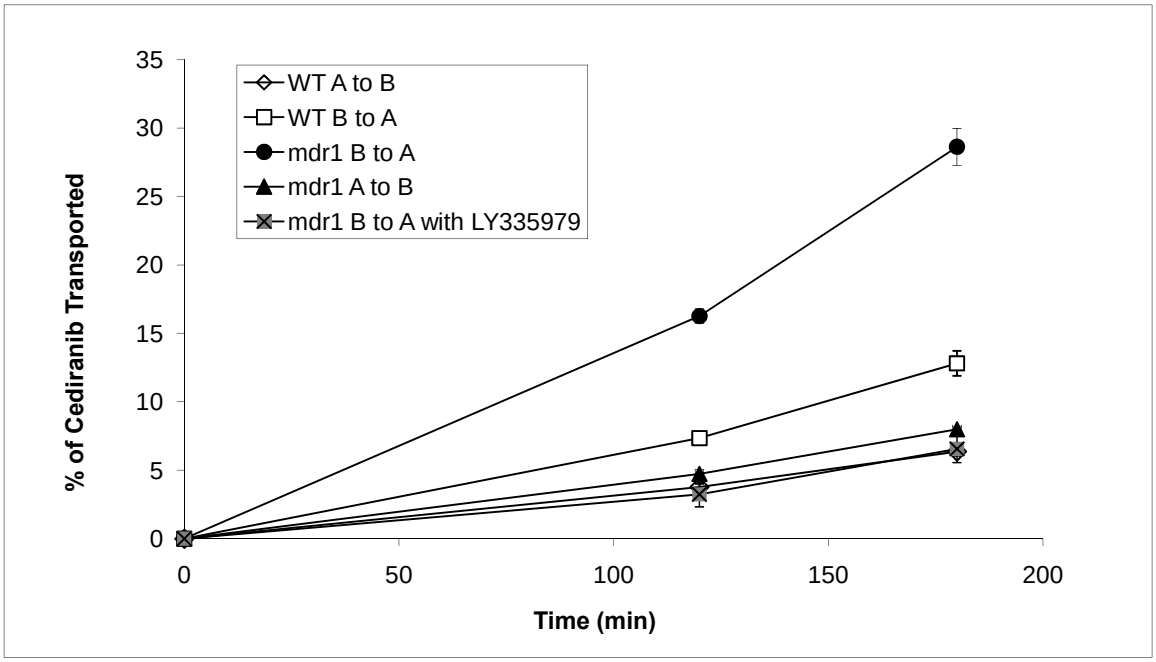

Figure 3.2 Directional flux of cediranib across MDCKII cell monolayers. (Wildtype: ◇, transport from Apical-to-Basolateral chamber; □, transport from Basolateral chamber; Mdr1-transfected: ▲, transport from Apical-to-Basolateral chamber; ●, transport from Basolateral-to-Apical chamber; ⊠, transport from Basolateral-to-Apical chamber with the treatment of LY335979.) The results are expressed as mean ± SD, n=3~4.

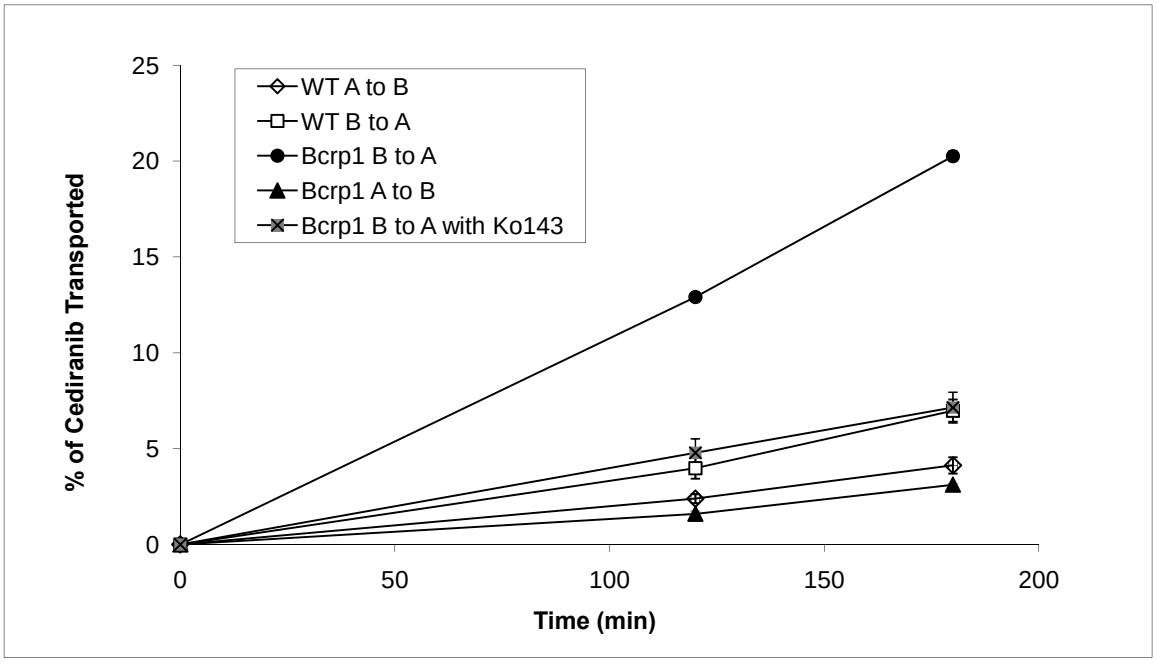

Figure 3.3 Directional flux of cediranib across MDCKII cell monolayers. (Wildtype: ◇, transport from Apical-to-Basolateral chamber; □, transport from Basolateral chamber; Bcrp1-transfected: ▲, transport from Apical-to-Basolateral chamber; ●, transport from Basolateral-to-Apical chamber; ⊠, transport from Basolateral-to-Apical chamber with the treatment of Ko143.) The results are expressed as mean ± SD, n=3~4.

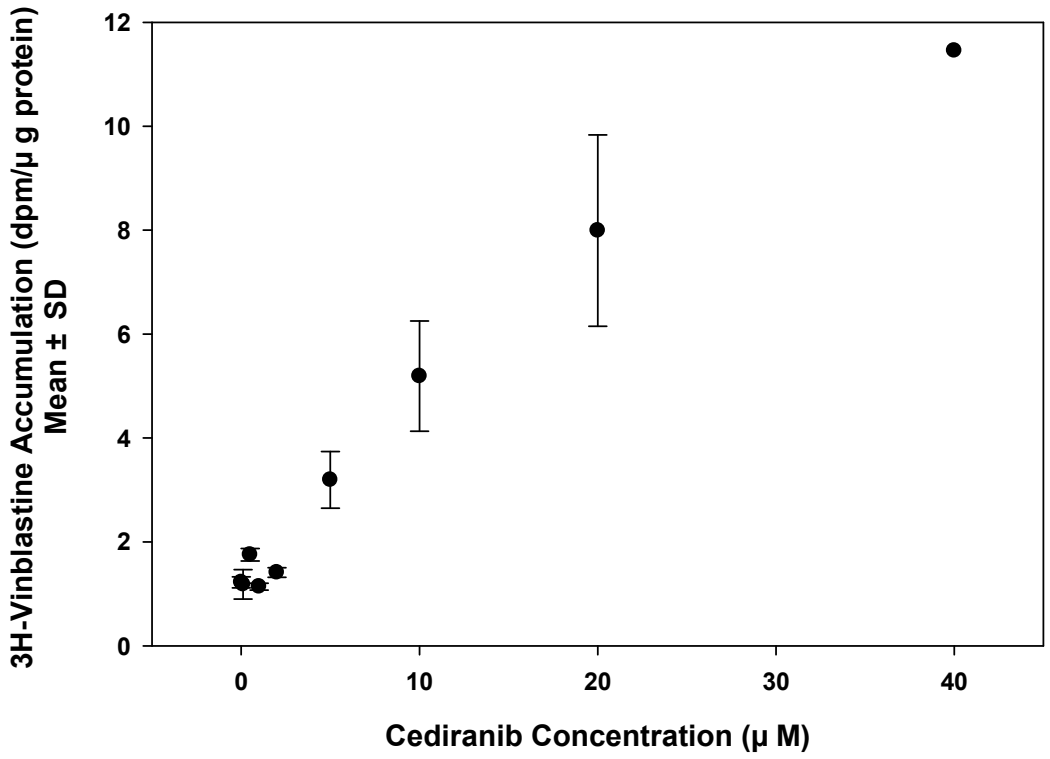

Figure 3.4.A Accumulation of ^{3}H-vinblastine in *MDR1*- transfected cells in presence of increasing concentrations of cediranib ranging from 0 to 40 µM. Results are presented as mean ± SD, n=4 (n=2 for 40 µM cediranib point).

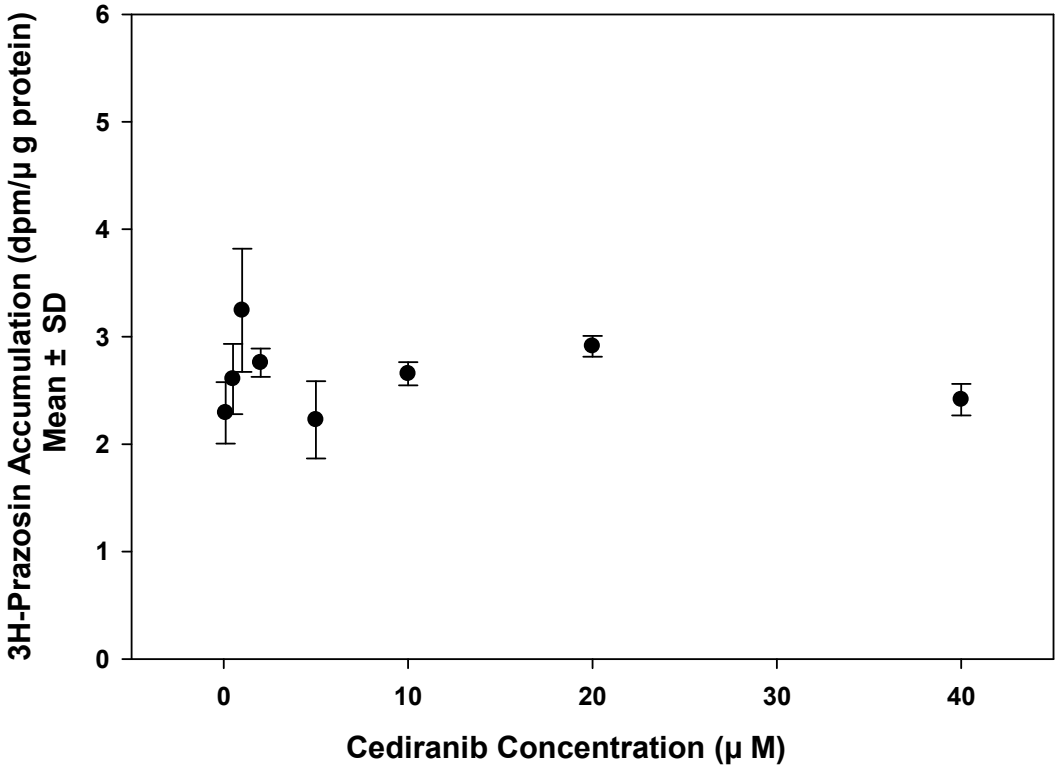

Figure 3.4.B Accumulation of ^{3}H-prazosin in *Bcrp1*- transfected cells in presence of increasing concentrations of cediranib ranging from 0 to 40 µM. Results are presented as mean ± SD, n=4.

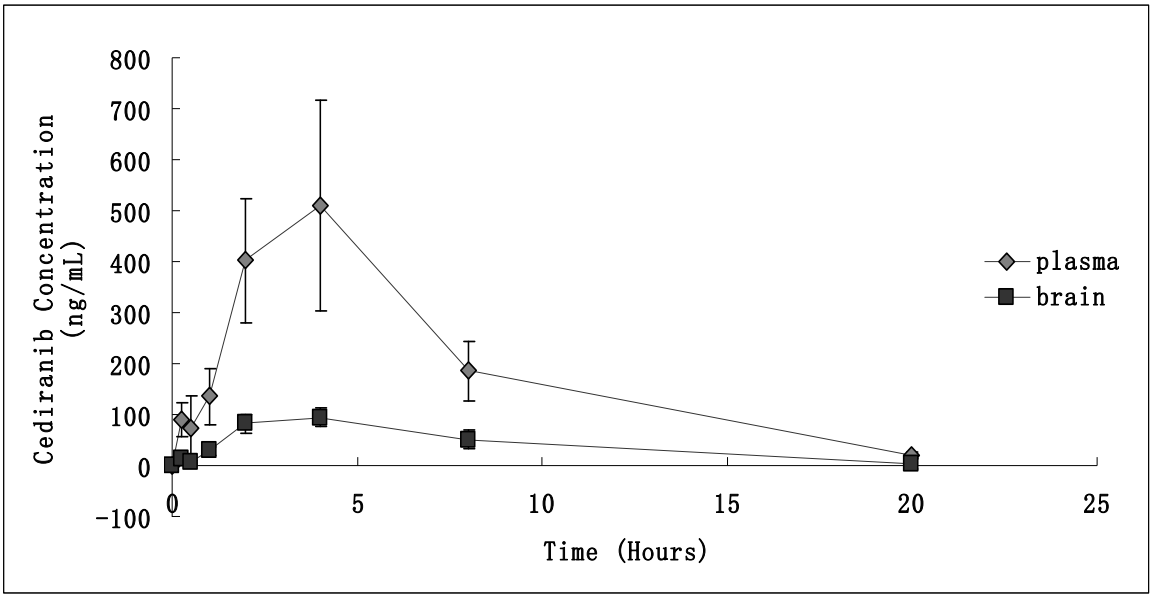

Figure 3.5.A Cediranib concentrations in wild-type mice after oral dosing (5mg/kg). For the 1-hour, 2-hour and 4-hour time points, 12 male mice were randomized, and 16 female mice were randomized for the rest of time points. (◇, cediranib concentrations in the plasma; ■ , cediranib concentrations in the brain). Results are expressed as mean ± SD, n=4.

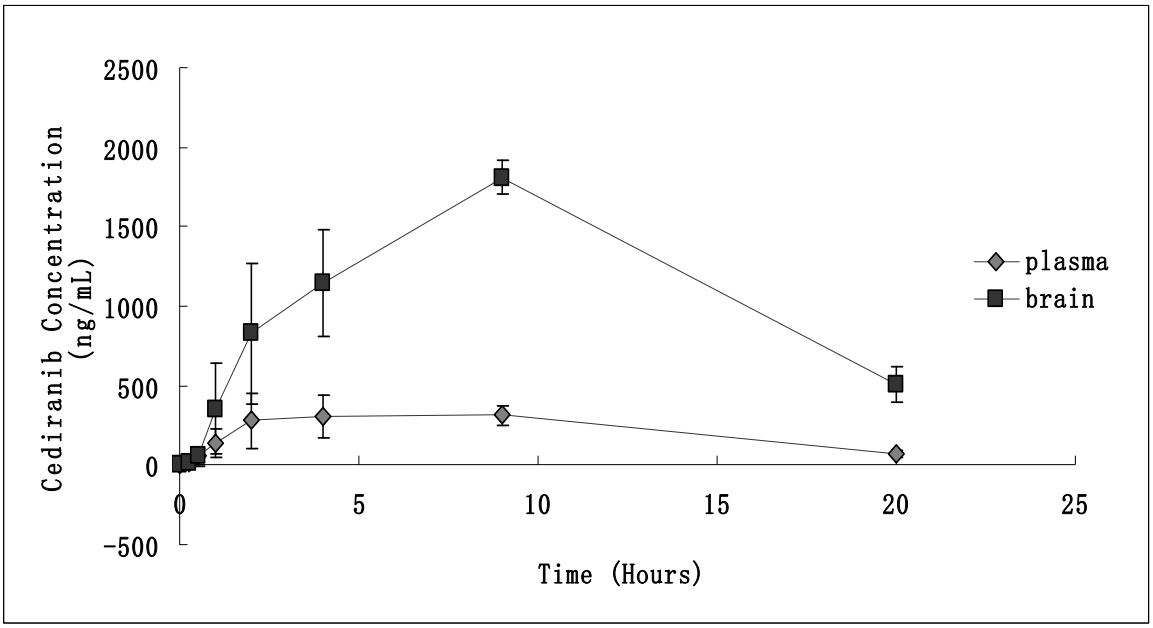

Figure 3.5.B Cediranib concentrations in Mdr1a/b(-/-) Bcrp1(-/-) mice after oral dosing (5mg/kg). For the 1-hour, 2-hour and 4-hour time points, 12 male mice were randomized, and 16 female mice were randomized for the rest of time points. (◆ , cediranib concentrations in the plasma; ■ , cediranib concentrations in the brain). Results are expressed as mean ± SD, n=4.

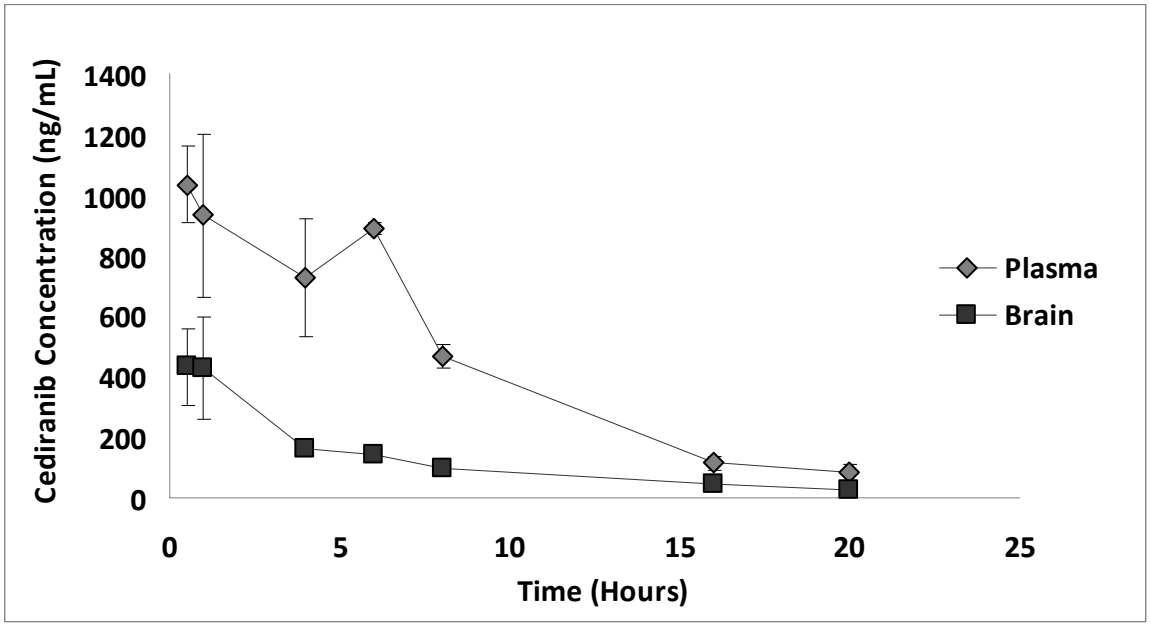

Figure 3.6.A Cediranib concentrations in wild-type mice by i.v. injection (dose = 4 mg/kg). For the 30-min and 1-hour time points, 8 female mice were randomized; for the other time points, the mice were all male. (◆, cediranib concentrations in the plasma; ■ , cediranib concentrations in the brain). Results are expressed as mean ± SD, n=4.

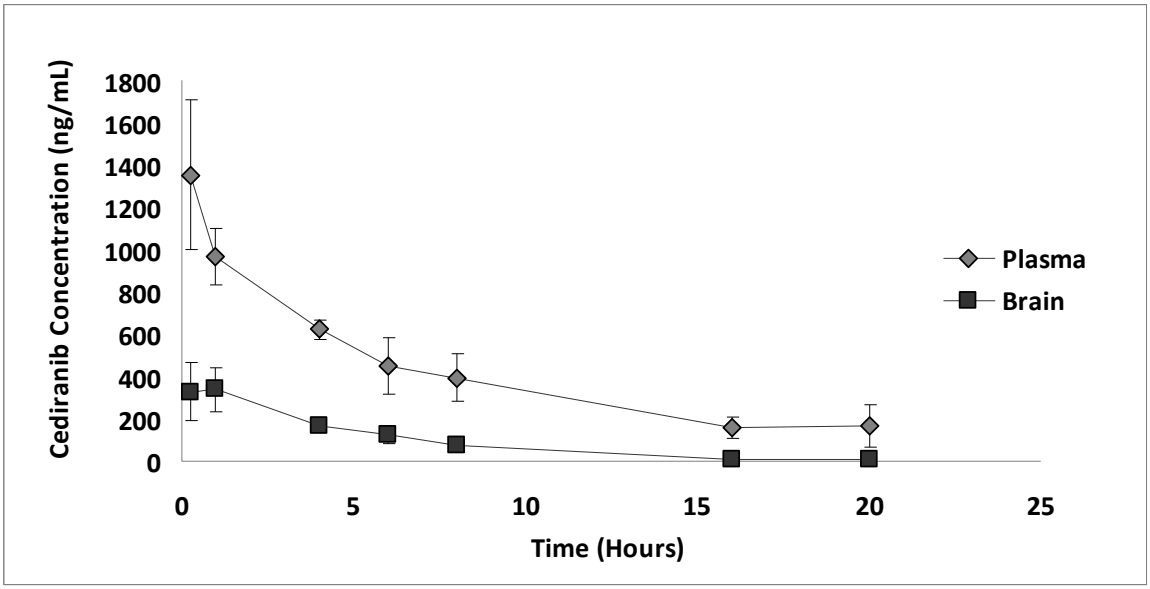

Figure 3.6.B Cediranib concentrations in Bcrp1(-/-) mice by i.v. injection (dose = 4 mg/kg). For the 15-min, 1-hour and 4-hour time points, 11 male mice were randomized; all the rest mice were female. (◆, cediranib concentrations in the plasma; ■ , cediranib concentrations in the brain). Results are expressed as mean ± SD, n=4.

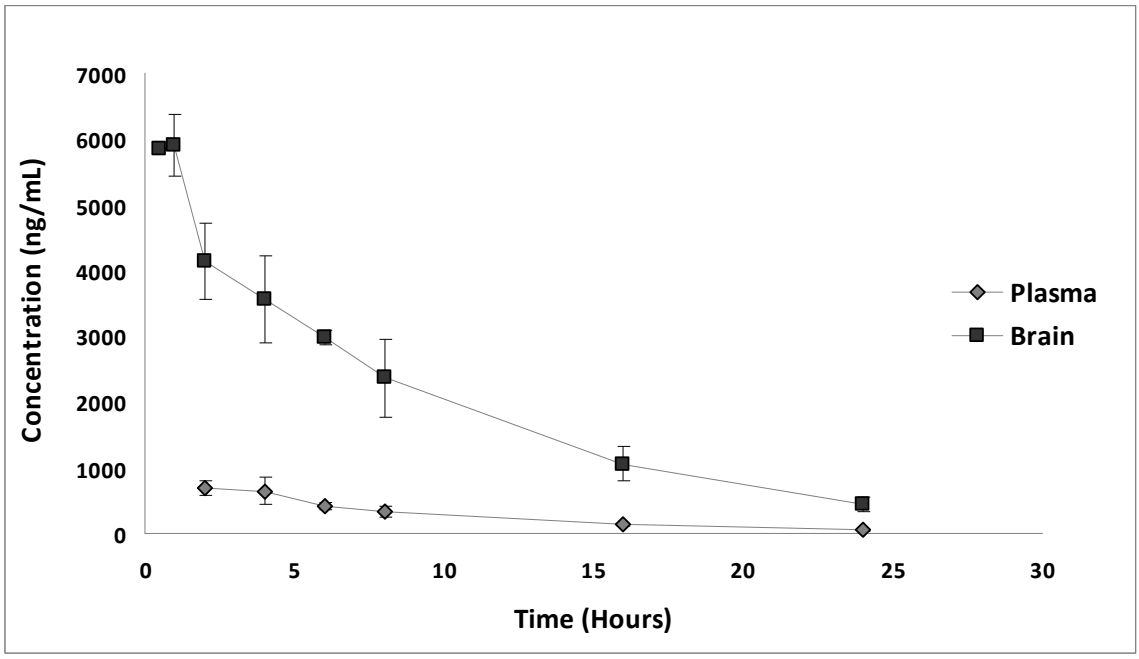

Figure 3.6.C Cediranib concentrations in Mdr1a/b(-/-) mice by i.v. injection (dose = 4 mg/kg). For the 1-hour time point, 4 male mice were randomized; for the other time points, the mice were all female. (◇, cediranib concentrations in the plasma; ■, cediranib concentrations in the brain). Results are expressed as mean ± SD, n=4.

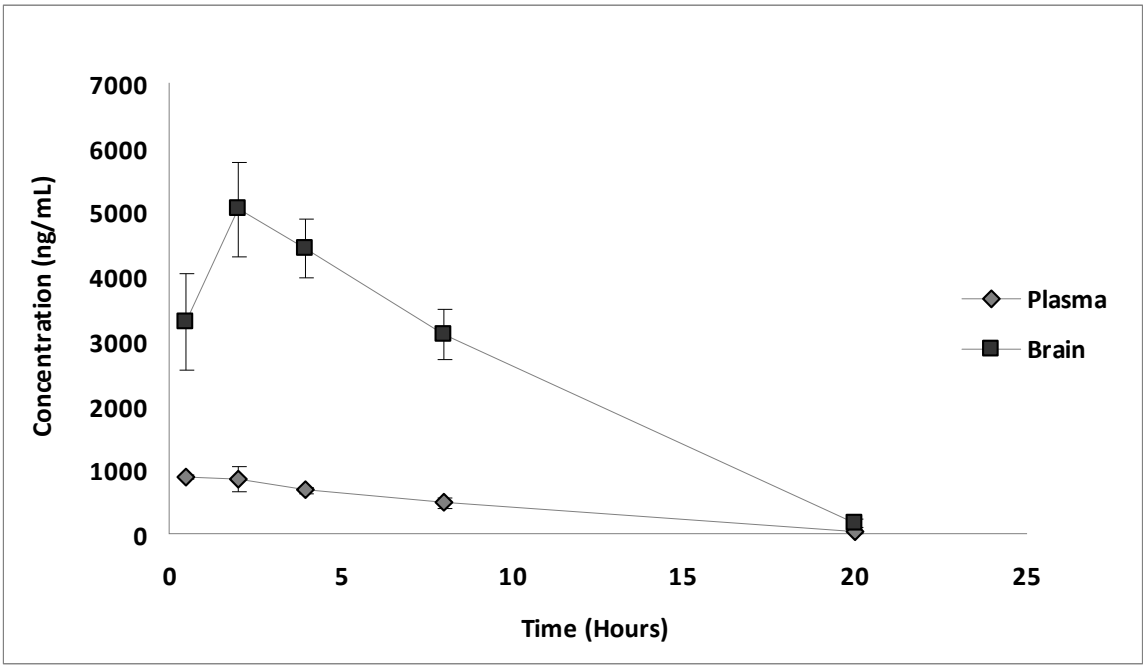

Figure 3.6.D Cediranib concentrations in Mdr1a/b(-/-)Bcrp1(-/-) mice by i.v. injection (dose = 4 mg/kg). For the 30-min, 2-hour, 4-hour and 16-hour time points, 12 male mice were randomized; all the rest mice were female. (◆ , cediranib concentrations in the plasma; ■ , cediranib concentrations in the brain). Results are expressed as mean ± SD, n=4.

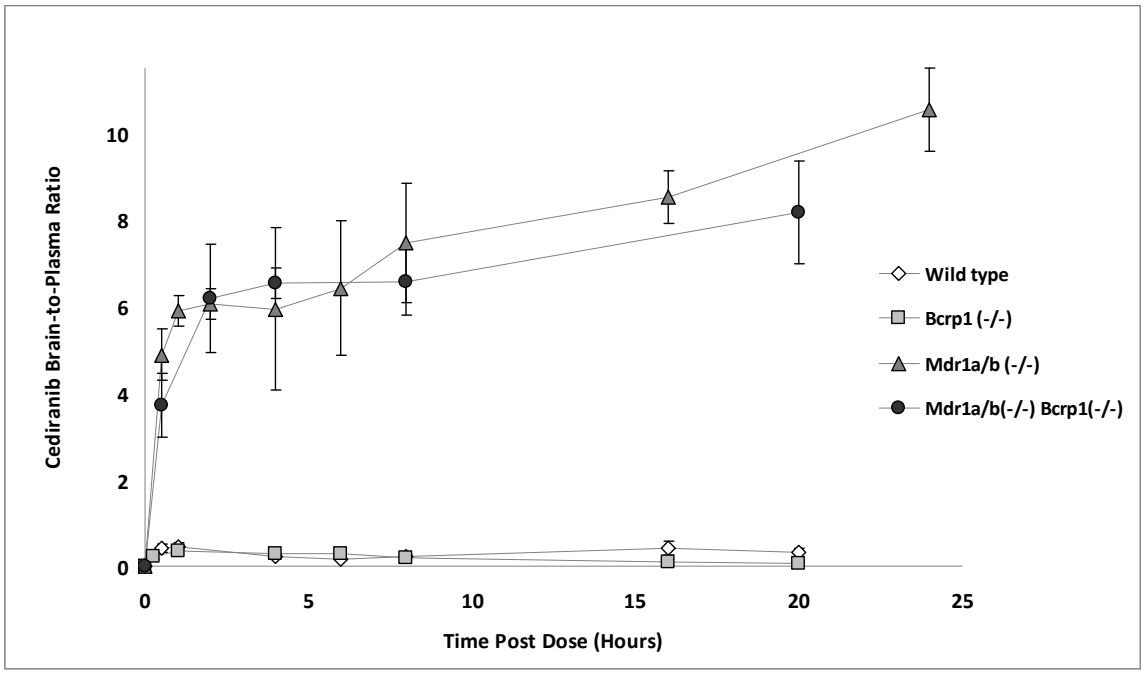

Figure 3.6.E Cediranib brain-to-plasma concentration ratio after i.v. injection (dose = 4 mg/kg). (◇ , brain-to-plasma cediranib concentration ratios in wild-type mice; ▢ , brain-to-plasma cediranib concentration ratios in *Bcrp(-/-)* mice; ▲, brain-to-plasma cediranib concentration ratios in *Mdr1a/b(-/-)* mice; ●, brain-to-plasma cediranib concentration ratios in *Mdr1a/b(-/-)Bcrp(-/-)* mice). Results are expressed as mean ± SD, n=4.

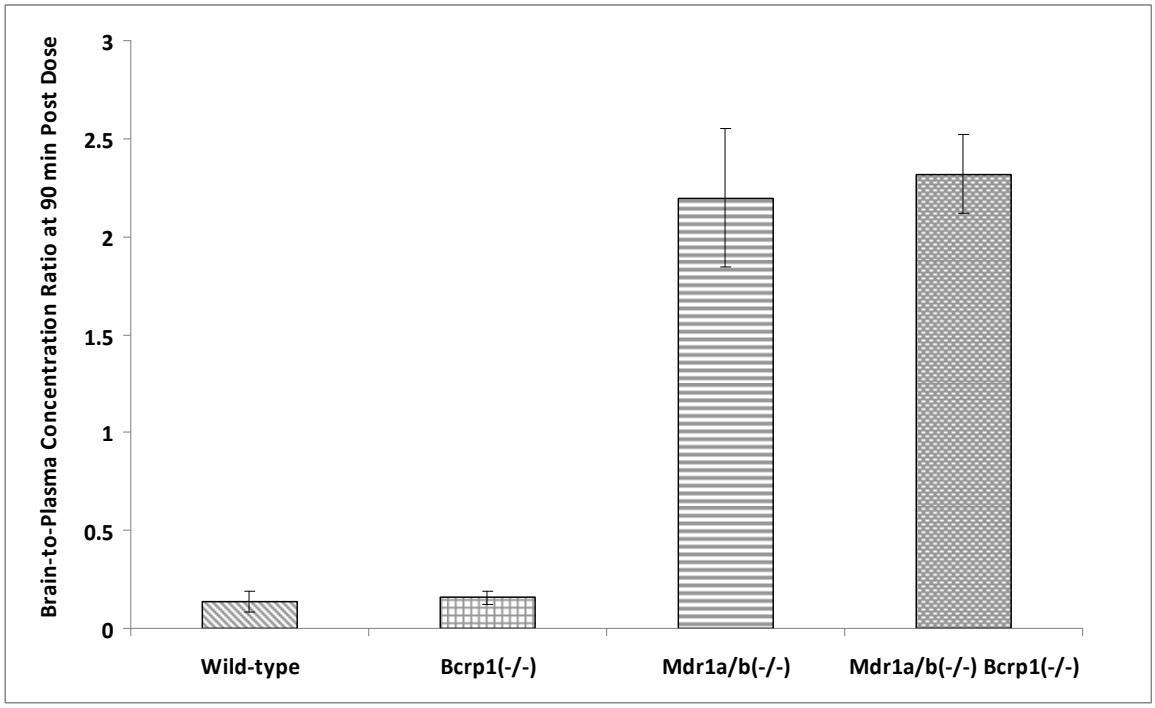

Figure 3.7.A Brain-to-plasma concentration ratios at 90 minute post oral dose of 5mg/kg cediranib into the wild-type, *Bcrp1(-/-)*, *Mdr1a/b(-/-)*, and *Mdr1a/b(-/-)Bcrp1(-/-)* mice. Wild-type mice were all female, and the gene knockout mice were all female. Results are expressed as mean ± SD, n=4.

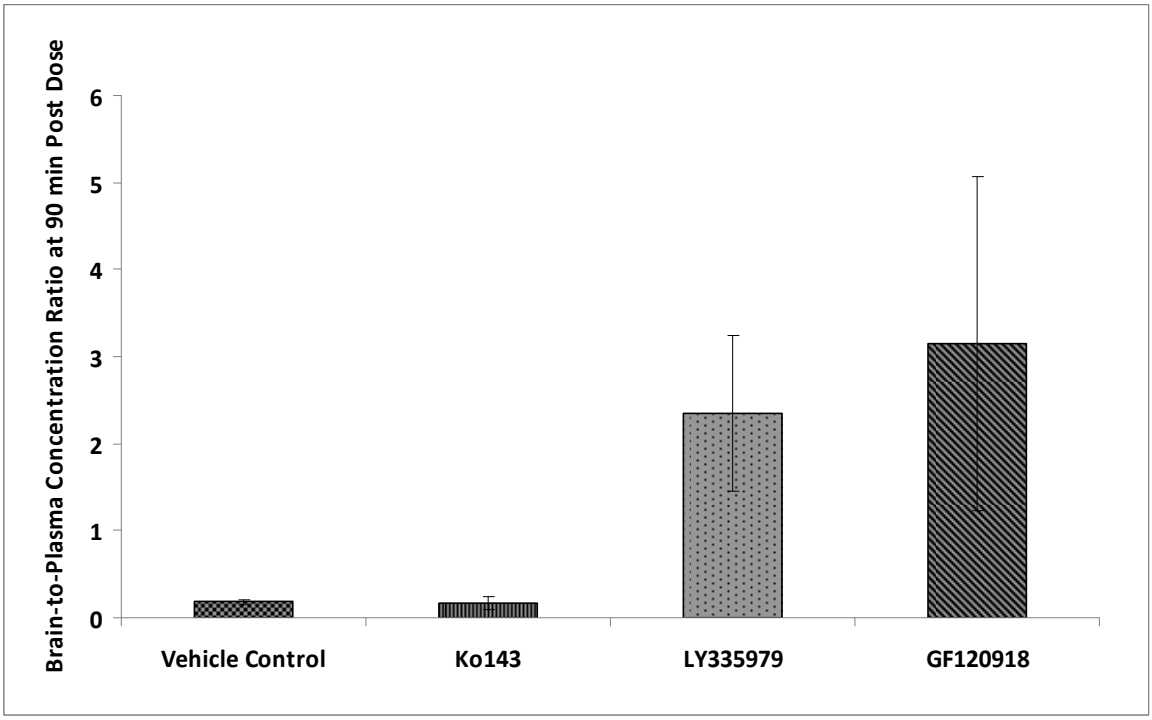

Figure 3.7.B Brain-to-plasma concentration ratios at 90 minute post oral dose of 5 mg/kg cediranib into the wild-type mice pretreated with vehicle control, 10 mg/kg BCRP inhibitor Ko143, 25 mg/kg P-gp inhibitor LY335979, and 10 mg/kg dual inhibitor GF120918. Results are expressed as mean ± SD, n=4. For the Ko143 treatment group, mice were all female; mice in all the other groups were male except that one mouse within the vehicle control group was female. The pharmacological inhibition of the transporters works consistently with the transporter-gene deletion.

Table 3-1 P_{app} of cediranib across wild-type and MDR1-transfected MDCKII cell monolayers, in the presence and absence of P-gp selective inhibitor LY335979.

	Wild-type		MDR1-transfected	
	A-to-B P_{app}	B-to-A P_{app}	A-to-B P_{app}	B-to-A P_{app}
	($\times 10^{-4}$cm/s)			
Treatment Control	3.17	3.65	3.98	8.13
1μM LY335979	-	-	-	1.79

Table 3-2 P_{app} of cediranib across wild-type and Bcrp1-transfected MDCKII cell monolayers, in the presence and absence of BCRP selective inhibitor Ko143.

	Wild-type		Bcrp1-transfected	
	A-to-B P_{app}	B-to-A P_{app}	A-to-B P_{app}	B-to-A P_{app}
	($\times 10^{-4}$cm/s)			
Treatment Control	2.04	1.98	1.50	5.94
200nM Ko143	-	-	-	2.13

Table 3-3 Plasma and brain oral non-compartmental PK parameters in wild-type and Mdr1a/b(-/-) Bcrp1(-/-) mice (n=4, respectively). Results are expressed as the estimation of the mean ± the standard error of the estimate.

Genotype	T_{max} (hour)	C_{max} (ng/mL)	F *	Plasma $AUC_{(0\text{-}20)}$ (hr*μg/mL)	Brain $AUC_{(0\text{-}20)}$ (hr*μg/mL)	Brain-to-Plasma AUC Ratio
FVB (wild-type)	4	510	0.32	3.892±0.434	0.849±0.080	0.218
Mdr1a/b(-/-) Bcrp1(-/-)	9	313	0.52	4.493±0.360	22.536±0.798	5.02

*: The bioavailability (F) was calculated based on the following equation.

$$F = \frac{Dose_{iv} \cdot AUC^{\infty}_{0,po}}{Dose_{po} \cdot AUC^{\infty}_{0,iv}}$$

Table 3-4.A One-compartment plasma PK parameters following i.v. dosing in wild-type, *Mdr1a/b (-/-)*, *Bcrp1 (-/-)* and *Mdr1a/b (-/-) Bcrp1 (-/-)* mice. Results are expressed as mean estimate ± standard error of the estimate.

Genotype	V_d (mL)	CL (mL/hr)
wild-type	81.5±5.1	7.924±0.928
Bcrp1(-/-)	70.5±4.1	11.32±1.157
Mdr1a/b(-/-)	91.6±3.7	15.97±0.921
Mdr1a/b(-/-) Bcrp1(-/-)	109.8±5.5	12.41±1.17

Table 3-4.B Brain and plasma non-compartmental PK parameters following i.v. dosing in wild-type, *Mdr1a/b (-/-)*, *Bcrp1 (-/-)* and *Mdr1a/b (-/-) Bcrp1 (-/-)* mice (n=4, respectively). Results are expressed as the estimation of the mean ± the standard error of the estimate.

Genotype	Plasma $AUC_{(0\text{-last})}$ (hr*μg/mL)	Brain $AUC_{(0\text{-last})}$ (hr*μg/mL)	Brain-to-Plasma AUC Ratio
FVB (wild-type)	9.200±0.364	2.449±0.162	0.266
Bcrp1(-/-)	8.393±0.387	1.947±0.113	0.232
Mdr1a/b(-/-)	7.640±0.243	48.185±0.807	6.31
Mdr1a/b(-/-) Bcrp1(-/-)	8.307±0.407	51.11±1.918	6.15

Table 3-5 Steady-state brain and plasma concentrations and apparent plasma cleances and the brain-to-plasma concentration ratios. Results are expressed as mean ± SD, n=4. *Bcrp1(-/-)* and *Mdr1a/b(-/-)* mice were all male; one female and three male mice were randomized within groups of the wild-type and *Mdr1a/b(-/-) Bcrp1(-/-)* mice, respectively.

Genotype	Plasma CL_{app} (mL/hr)	$C_{ss,\ plasma}$ (μg/mL)	$C_{ss,\ brain}$ (μg/gm)	Brain-to-plasma C_{ss} Ratio	K_p Ratio #
FVB (wild-type)	39.9 ± 9.6	262 ± 63	65 ± 27	0.252 ± 0.094	-
Bcrp1(-/-)	44.6 ± 12.3	237 ± 67	65 ± 22	0.274 ± 0.013	1.1
Mdr1a/b(-/-)	44.9± 16.5	243 ± 72	1264 ± 452	5.24 ± 1.10	20.8
Mdr1a/b(-/-) Bcrp1(-/-)	41.4 ± 14.5	276 ± 128	1696 ± 750	6.30± 1.23	25

[#] Kp Ratio = Ratio of steady-state brain-to-plasma concentration ratio in knockout mice to the steady-state brain-to-plasma concentration ratio in wild-type mice.

CHAPTER 4

MODELING AND SIMULATION OF BRAIN DISTRIBUTIONAL KINETICS

Accurate determination of the effect of active transport processes at the BBB on brain uptake requires complete understanding the brain distribution kinetics. The first part of this chapter employed simulation strategies to explore the relationship between the brain partitioning and the sampling time. Concentration-time profiles were simulated with a 2-compartment system (plasma and brain parenchyma). Time to achieve the distributional equilibrium was simulated in different genotypes by knocking out one or more efflux transporters. The simulation illustrated that impact of efflux transporters can be accurately estimated at the brain T_{max} and reasonably compared in the terminal elimination phase, although the latter will overestimate the true brain partition coefficient.

With the knowledge of the brain-to-plasma AUC_0^∞ ratio, a further interpretation to the magnitude of efflux transport for a substrate is through a partial-areas analysis. The second part of the chapter aimed to examine the behavior of two partial-areas analyses by simulation strategies for determining the exit rate constant from the target compartment (k_{out}), which is the sum of the rate constants for both passive diffusion and efflux transport out of the brain (Elmquist et al., 1994), and compare their accuracy of determination when differing levels of error are incorporated into the concentration data. A four-compartmental mamillary system with first-order rates between central and target compartment was simulated in order to generate concentration-time data sets in the central and target compartments with 0, 5%, 10% and 20% relative error. The results showed that both cumulative and interval partial-areas analysis work adequately well when there is no error in the concentration data. However, when error exists in the

concentration data, interval partial-areas analysis seemed more accurate regardless of robustness of linear regression. The cumulative method was robust for large nominal k_{out}; and the interval method worked better for small nominal k_{out}. It was also found that accuracy of both partial-areas analysis methods depends on experimental design – intervals of the sampling time relative to the kinetic constants when the concentrations are measured.

The third part of this chapter presents a Bayesian approach to non-compartmental analysis (NCA), which could provide not only an estimate of the complete AUC (AUC_0^∞) with its 95% confidence interval, but also accuracy and precision of the estimate of brain-to-plasma ratio of the complete AUC. Noninformative priors were assumed for all model parameters. In order to assess the prediction performance of the new method, a Monte Carlo simulation was performed using R following Bayesian estimation of the brain and plasma AUC_0^∞s and the brain-to-plasma AUC_0^∞ ratio. The coverage of Bayesian credible intervals was examined. The availability of posterior distributions of NCA parameters assessed in a serial sacrifice sampling design should allow one to statistically evaluate the precision of these predictors. We conclude with an application of the method to *in vivo* studies of brain distribution in wild-type vs. three different transporter-gene knockout mice following an intravenous injection of cediranib.

4.1 Introduction

4.1.1 Distributional kinetics of brain partitioning

For CNS compounds, it is important to get across the BBB to attain sufficient brain exposure. The brain exposure can be influenced by a number of factors, including passive membrane permeability, protein binding, ionization, metabolism at the blood-brain interface, active uptake and efflux by protein transporters at the BBB, and CSF bulk flow (Kalvass et al., 2007). Drug disposition within the brain may be evaluated by the commonly-called brain partition coefficient ($K_{p,brain}$). In order to determine $K_{p,brain}$, the true steady-state brain-to-plasma concentration ratio after constant rate infusion is desirable to measure. When the constant rate infusion technique is not feasible, there are usually two alternatives as follows in a single dose study: quantification of the brain-to-plasma ratio of AUC from time zero to infinity, and determination of the brain-to-plasma concentration ratio at a discrete time point. Since it is with less cost of labor and animals than determining the brain-to-plasma AUC ratios, many studies and publications (Chen et al., 2009; Oostendorp et al., 2009; Agarwal et al., 2010; Kodaira et al., 2010) intend to screen the P-gp- or BCRP- mediated efflux activities in different animal models via comparison of concentration ratios at a discrete time point after a single dose in the absence vs. presence of efflux activity. However, unlike the time-independent AUC ratio, brain-to-plasma concentration ratio is inherently time-dependent. After administration, the concentration ratio increases from zero to a plateau value reflecting the distributional equilibrium at which substrate concentrations in brain and plasma begin to change in parallel (Gibaldi, 1969). Thus, comparison of brain-to-plasma partitioning at any single time prior to the blood-brain distributional equilibrium may lead to an inaccurate determination of the transporter-derived effect, dependent upon sampling time, especially

when differences between the efflux clearances are significant. In order to assess the impact of efflux transport on brain distribution, it is of importance to explore the right sampling time to measure the true brain-to-plasma partitioning.

The objective of the first part of this simulation study is to explore the factors influencing the magnitude of partitioning between brain and plasma in presence vs absence of BBB efflux transporters, to develop mathematical descriptors of the relationship between brain partitioning and sampling time, and to illustrate the ideal time to fairly compare the transporter effect of different genotypes by simulation strategies. Complete understanding of distributional kinetics is important not only for designing brain uptake experiments but also for correctly interpreting measurements of the extent of transporter-derived effect.

4.1.2 Partial-areas analysis

With a knowledge of the partition coefficient ($\frac{AUC^{\infty}_{0,tissue}}{AUC^{\infty}_{0,plasma}}$), a further interpretation to the magnitude of efflux transport for a substrate is through a partial-areas analysis. As methods of measuring drug concentration at tissue sites become available and accepted, it is desirable to find a simplified and optimized method to describe the distributional kinetics between the blood or plasma and sites of extravascular measurement. Non-compartmental analysis (NCA), which was introduced in the late 1970s, provides a means of obtaining the primary pharmacokinetic parameters of a drug without the specific assumptions inherent to compartmental analysis. NCA methods are usually based on the estimation of the area under a plot of drug concentration versus time (Gibaldi and

Perrier, 1982). But non-compartmental analysis is not 'model-independent'. These methods can be applied to virtually any compartmental model (Gibaldi and Perrier, 1982). In this study, the concentration-time data were generated from a compartmental model; thus the partial-areas analysis which was used here is also called semi-NCA. This method has been used to examine the efflux kinetics of zidovudine from the cerebrospinal fluid in a study in rabbits (Sawchuk and Hedaya, 1990) and of diclofenac from synovial fluid in a human study (Elmquist et al., 1994). It has also been applied to estimate metabolite kinetics (Riad and Sawchuk, 1998). There are two ways to accomplish a partial-areas analysis for the determination of the first-order exit rate constant (k_{out}) for drug transport out of the target compartment (e.g., a site of extravascular measurement): cumulative partial-areas analysis (current work) and interval partial-areas analysis (Sawchuk and Hedaya, 1990; Elmquist et al., 1994; Riad and Sawchuk, 1998). Cumulative partial-areas analysis is based on the following linear relationship:

$$C_{t,T} = \frac{CL_{out}}{V_T}(R \cdot AUC^t_{0,C} - AUC^t_{0,T}) \qquad \text{(Equation 4-1, see Appendix I for derivation)}$$

where $C_{t,T}$ is the concentration of target compartment at time t; CL_{out} is the clearance from target compartment; V_T is the volume of target compartment; R is the partition coefficient, i.e., the ratio of the AUC in target compartment to the AUC in central compartment from time zero to infinity; $AUC^t_{0,C}$ is the cumulative area under the concentration-time curve in central compartment from time zero to the time of measurement; and $AUC^t_{0,T}$ is the cumulative area under the concentration-time curve in target compartment from time zero to the time of measurement.

Interval partial-areas analysis is based on the similar linear relationship:

$$\Delta C_T = \frac{CL_{out}}{V_T}(R \cdot AUC_{t1,C}^{t2} - AUC_{t1,T}^{t2}) \qquad \text{(Equation 4-2, see Appendix I for derivation)}$$

where ΔC_T is the difference of concentrations in target compartment between time = t1 and time = t2; $AUC_{t1,C}^{t2}$ is the interval area under the concentration-time curve in central compartment between time = t1 and time = t2; and $AUC_{t1,T}^{t2}$ is the interval area under the concentration-time curve in target compartment between time = t1 and time = t2. Both analyses are based on the assumption that CL_{out} is a constant average throughout the experiment.

The object of the second part of the present simulation study was to examine the behavior of these methods and compare their accuracy to determine k_{out}, particularly in the case when there is some error in the concentration data. The methods were evaluated for their applicability of determination of k_{out}. Statistical tests were performed to draw conclusions from simulated data that were subject to different levels of error.

4.1.3 Bayesian approach to estimate AUC and brain-to-plasma AUC ratio for sacrifice design data

As illustrated in the first part of this part, the brain-to-plasma AUC ratio is an accurate metric to reflect the brain exposure of a substrate. Nevertheless, the ability to determine the true AUC ratio will be affected by experimental error and the variation between animals. For the purpose of the first part, it was desirable to perform statistical comparison for the AUC from time zero to infinity (AUC_0^∞) ratio between different

groups/treatments. However, this was not feasible without knowing the precision of estimation for AUC_0^∞ s and their ratio. In chapter 3, we could only estimate the AUC up to the last sampling time point ($A\hat{U}C_0^t$) by Phoenix WinNonlin®, and approximately used the brain-to-plasma ratio of $A\hat{U}C_0^t$ in replacement of AUC_0^∞ ratio by assuming a small percent of extrapolated AUC (from time of the last measurable concentration to infinity). A parametric (1-α) % confidence interval of $A\hat{U}C_0^t$ could be calculated based on the standard deviation (SD) of $A\hat{U}C_0^t$ by assuming that both concentration and AUC follow normal distributions.

In order to determine the variation of AUC, it is ideal to perform intensive serial sampling in each individual subject. However, the withdrawal of a sufficient number of blood samples from individual rodents for AUC determination is restricted due to technical and cost reasons. A common scenario in preclinical pharmacokinetic studies with small animals is the use of a sparse sampling approach with few time points, in which each subject is not sampled at all time points. In this scenario, since each subject is sampled at two or more different times, the variances of data that belong to the same subject are correlated. Typically, in a serial sacrifice design (or so-called "destructive sampling"), only one sample per subject is available (Navarro-Fontestad et al., 2011). In those experimental scenarios, estimation of AUC variance is not as straightforward as that from intensive sampling design. In the present study, we will focus on the variation estimation of NCA parameters to serial sacrifice data.

In order to deal with serial sacrifice data, Bailer's method was first proposed and has been most commonly used to estimate $A\hat{U}C_0^t$ based on the linear trapezoidal rule. The corresponding Var($A\hat{U}C_0^t$) was claimed to be based on the linear relation of normally distributed sample errors of concentration at the j^{th} time point (s_j) (Bailer, 1988):

$$VAR\left[\widehat{AUC}_0^t\right] \cong \sum_j w_j^2 \frac{s_j^2}{n_j} \qquad \text{(Equation 4-3)}$$

where, n_j represents the sample size at the j^{th} time point and w_j is the sampling time intervals (Bailer, 1988):

$$w_j = \begin{cases} \frac{1}{2}(t_2 - t_1) & j=1 \\ \frac{1}{2}(t_{j+1} - t_{j-1}) & j=2,...,m\text{-}1 \\ \frac{1}{2}(t_m - t_{m-1}) & j=m \end{cases}$$

Thus, the (1-α)% confidence interval of $A\hat{U}C_0^t$ can be described as follows:

$$\widehat{AUC}_0^t \pm z_{1-\frac{\alpha}{2}} \cdot SD\left[\widehat{AUC}_0^t\right] \qquad \text{(Equation 4-4)}$$

Bailer's method depends on the assumptions that the data are normally distributed and that the variances are known (Bailer, 1988). However, the latter assumption is not statistically sound. Nedelman et al modified the Bailer's method by substituting the critical value from the standard normal distribution to the critical value from a two-tailed students t-distribution with a degrees of freedom obtained from Satterthwaite's approximation. They suggested that the sample variance $\sum_j w_j^2 \frac{s_j^2}{n_j}$ could not accurately approximate the population variance when sample sizes are not adequately large. The improved method was known as the Bailer-Satterthwaite method (Nedelman et al., 1995).

However, neither Bailer's method nor Bailer-Satterwaite method are able to obtain the variation of the AUC_0^∞, as described as follows:

$$AUC_0^\infty = AUC_0^t + \frac{C_t}{\lambda_z} \qquad \text{(Equation 4-5)}$$

In Equation 4-5, AUC_0^t denotes the AUC from time zero to the last sampling time point. C_t represents the concentration at the last sampling time point. λ_z stands for the terminal elimination rate constant usually determined by the linear regression from the logarithm of concentrations at the last 3~5 sampling points, according to the commonly used program WinNonlin® and Phoenix WinNonlin®. Nevertheless, WinNonlin® software provides only calculations of the point estimate AUC_0^∞, without approximation of its variation.

Now the question at hand is how to obtain the variation of AUC_0^∞, so that contrasts between AUC_0^∞ s can be subsequently conducted. One option to extend the Bailer's method to infinite time and construct confidence intervals for AUC_0^∞ is through Yuan's method (Yuan, 1993). Yuan's method proposed the following approximation of SD(AUC_0^∞) by assuming that all the samples are independent and the terminal rate constant λ_z is known and identical for all tested animals:

$$SD(AUC_0^\infty) = \sqrt{(1/2(t_1 - t_0)SE_0)^2 + \sum_{i=2}^{n}(1/2(t_i - t_{i-2})SE_{i-1})^2 + (1/2(t_n - t_{n-1}) + \frac{1}{\hat{\lambda}_z})^2 SE_n^2}$$

(Equation 4-6)

where SE_i is the standard error of C_i, the concentration at the i^{th} time point, and the $\hat{\lambda}_z$ is the estimated terminal rate constant. Yuan also pointed out that because of the covariance between $\hat{\lambda}_z$ and the mean concentration at the i^{th} time point, the above equation underestimated the SD(AUC_0^∞). It was proposed that one more term should be added to the variance of AUC_0^∞ if λ_z is estimated from an independent study. However, it lacks of statistical soundness and is hard to fulfill in practice. Thus, Yuan's method has some limitation inherent in its assumptions. Moreover, in some studies such as bioequivalence studies and brain uptake studies, it is usually desired to estimate the tissue-to-plasma AUC ratio ($\frac{AUC_{0,tissue}^\infty}{AUC_{0,plasma}^\infty}$) and statistically compare the AUC ratio by using the confidence interval inclusion approach. This requires more strict assumptions and complicated mathematical computation. Yuan's method does not provide solutions for those scenarios.

Note that there is a strong correlation between plasma and brain concentrations (Figure 4.1). The occurrence of plasma and brain correlation at each time point further complicates the estimation of the variability around $\frac{AUC_{0,br}^\infty}{AUC_{0,pl}^\infty}$.

Alternatively, resampling-based approaches have become an option to obtain the non-parametric confidence intervals of $A\hat{U}C_0^t$ or $A\hat{U}C_0^\infty$ via bootstrapping and jackknife (Bonate, 1998; Wolfsegger and Jaki, 2005; Jaki et al., 2009; Wolfsegger and Jaki, 2009;

Navarro-Fontestad et al., 2011). However, these approaches are time-consuming and the sample size is an issue arousing controversy.

In recent years, Bayesian approaches have been widely applied to pharmacokinetic and pharmacodynamic (PK/PD) studies (Lunn et al., 2002; Jelliffe et al., 2011). Unlike the frequentist view that the conclusions made from the current work should be independent of prior work, a Bayesian believes that existing knowledge should always be incorporated and that population parameters can be treated as random variables (not as fixed, unknown constants). According to Bayes Theorem,

$$p(\theta|y) = \frac{p(\theta, y)}{p(y)} = \frac{p(y|\theta)p(\theta)}{\int p(\theta)p(y|\theta)d\theta} \propto p(y|\theta)p(\theta) \quad \text{(Equation 4-7)}$$

In words, it says the probability of the parameter θ, given the data y, is proportional to the product of the probability of y given θ, which is also called likelihood, and the marginal probability of θ. P(θ) is called the "prior probability" in Bayesian statistics as it reflects prior beliefs about the probability of a given parameter. The prior probability allows you to estimate a parameter of interest by incorporating existing knowledge. When there is little or no prior information available, an uninformative prior can be used. P(θ|y) is usually called the "posterior probability", reflecting the belief about the parameter after collecting the data. The posterior distribution of a certain parameter is explored via the simulation-based method, with the knowledge of prior distribution of the parameter estimates and the actual data. P(y) is a normalization constant of posterior which is computable but hard to integrate. With the help of WinBUGS software, it is feasible to draw samples from posterior distribution of parameters of interest by Markov chain Monte Carlo (MCMC) sampling

methods, such as Gibbs sampling (Spiegelhalter et al., 2003). It gives us a simulation-based approach to obtain the point estimate of posterior expectation and any quantile of interest and can be applied to sparse sampling data.

The third part of this chapter presents a novel approach to NCA by Gibbs sampler, a computationally intensive Bayesian method, which provides not only the point estimate of the complete AUC with its 95% credible interval but also of the brain-to-plasma ratio of the complete AUC, and even the drug targeting index (DTI), which is defined as the ratio of brain-to-plasma AUC ratio in one genotype/treatment group vs. that in another. Since no prior information was known in our study, noninformative prior distributions were assumed for all model parameters.

4.2 Methods

4.2.1 Distributional kinetics of brain partitioning

The simulations constructed in this session were intended to illustrate the distributional kinetics of a substrate of active efflux transporters (P-gp and BCRP) during certain physiological or pharmacological conditions such as transporter deficiency or inhibition, and to guide in the design of brain uptake experiments. Transport mechanisms such as passive diffusion and active efflux transporters were examined and compared by simulating the intact BBB in wild-type mice and the less permeable BBB in various transporter knock-out genotypes.

4.2.1.1 Isee systems STELLA ®

In this study the isee systems STELLA ® software was utilized to construct a model representing a process or a system desirable to investigate. Different compartments in the body were represented by “stocks”, which were linked by distributional “flows”, which represent rates of drug distribution between compartments. Arbitrary independent model parameters were incorporated as “converters” and linked using “connectors” to an appropriate stock, flow or other converter.

Difference equations were automatically generated according to the model structure and solved by numerical approximation. In STELLA ® there are three integration methods to choose – Euler Method, Runge-Kutta 2 or Runge-Kutta 4. In this study, the Euler Method was utilized. The run time of the simulation was adjusted depending on the chosen model. Graphs and tables were automatically generated by the software to evaluate the model behavior and to examine the influence of parameters assumed in the model.

4.2.1.2 Construction of models

In this simulation, two transport mechanisms were examined – a bidirectional clearance (CL) between plasma and brain mediated by passive diffusion and a unidirectional CL from the brain to the plasma mediated by active efflux transporters, such as P-gp and BCRP. The simulation illustrated the behavior of a hypothetical P-gp and BCRP dual substrate in different mouse genotypes with respect to transporter genes – wild-type, BCRP knockout, P-gp knockout, and triple knockout mice.

Two-compartment models were built with a central compartment, representing the plasma, and a peripheral compartment, which represented the brain parenchyma (Figure 4.2). The dose was administered via intravenous bolus into the central compartment at time zero.

Since rate of distribution is dependent on CL and the concentration (C) in that compartment,

$$\text{Rate} = CL \cdot C \qquad \text{(Equation 4-8)}$$

The total flow of passive diffusion ($\text{Rate}_{\text{passive diffusion}}$) was described as follows.

$$\text{Rate}_{\text{passive diffusion}} = CL_{\text{passive diffusion}}(C_{\text{pl}} - C_{\text{br}}) \qquad \text{(Equation 4-9)}$$

$CL_{\text{passive diffusion}}$ is a constant representing the quantitative estimation of permeability and surface area product of the compound of interest, which, in this study, is assumed to be 0.5 volume unit/time for all groups of mice.

The flow mediated by active efflux transporters ($\text{Rate}_{\text{active efflux}}$) is based on equation 4-10.

$$\text{Rate}_{\text{active efflux}} = CL_{\text{active efflux}} \cdot C = \frac{T_{\max}}{K_m + C_{br}} \cdot C_{\text{br}} \qquad \text{(Equation 4-10)}$$

where $CL_{\text{active efflux}}$ is a nonlinear clearance described by a Michaelis-Menten equation; T_{max} reflects the transporter expression; and K_m represents the compound-transporter binding affinity. For triple knockout mice, since both P-gp and BCRP have been genetically deleted, we set $CL_{\text{active efflux}}$ as zero by assuming there is no other efflux transporter involved in the transport of the compound. Given the fact that the amount of P-gp protein expression at the mouse BBB vs. BCRP is 3.5:1 (Kamiie et al., 2008), we

assumed in our simulation model that T_{max} for P-gp is 140 units and for BCRP is 40 units. We also assumed that Km for both P-gp and BCRP are same (50 concentration units).

The volume of distribution was hypothetically assumed to be 100 units for the plasma compartment and 10 units for the brain compartment. Concentrations were calculated based on the amount of drug (A) in a compartment divided by the volume of distribution of that compartment.

In this model the compound's plasma and brain protein binding was assumed to be zero. The total body rate of elimination depends on the total body clearance (CL_{elim}) that includes processes, such as hepatic metabolism, hepatic clearance, and renal clearance. CL_{elim} was assumed to be 10 volume units/time.

4.2.1.3 An illustration using a cediranib study in mice

In order to evaluate the consistency of simulation with experiment results, we illustrated an example of a cediranib brain PK study described in Chapter 3. Briefly, brain concentration-time profiles of cediranib were obtained following intravenous injection into wild-type, *Mdr1a/b (-/-)*, *Bcrp1 (-/-)* and *Mdr1a/b (-/-) Bcrp1 (-/-)* mice (as shown in Figure 3.6.A~D). The influence of $CL_{active\ efflux}$ on the time to reach the concentration peak in brain and on the time to attain distributional equilibrium was examined. Based on the animal data, T_{max} was determined when the cediranib level in brain reached the peak value in each group by visual observation.

4.2.2 Partial-areas analysis

A four-compartment pharmacokinetic model with first-order rates between central and target compartment was created in STELLA ® (Figure 4.3). It was assumed that the target site is a single compartment and that there is no drug at the target site at t=0. The model parameters are listed in Table 4-1.

Before exploration of the two partial-areas analyses, we first examined the influence of parameters in non-measured compartments, i.e., exit rate constant for peripheral compartments (k1 or k3), on concentrations ($C_{t,C}$, $C_{t,T}$), AUCs ($AUC^t_{0,C}$, $AUC^t_{0,T}$) and the partial and complete AUC ratios of the target and central compartments ($AUC^t_{0,T} / AUC^t_{0,C}$ and R, respectively).

The partial AUCs at each time-point were computed by integration, and k_{out} was the slope of the linear regression line of concentrations at target compartment (Ct) versus the term (R•AUCc-AUCt) or ΔCt versus the term (R•ΔAUCc-ΔAUCt) (according to Equation 4-1 and 4-2). The estimates of k_{out} were compared with the nominal value from the model simulation, which is simply the ratio of the clearance from target compartment to the volume of target compartment, to evaluate the accuracy of the two methods. The comparisons were done when k_{out} varied from 0.02 to 2, in order to investigate the influence of the magnitude of k_{out} in the estimation behavior of the partial-areas analysis.

Performance of the two methods was also examined when there was 5%, 10% and 20% relative random error in concentrations in central compartment and target compartment. The concentration-time data with unrepeatable random error were also generated by STELLA ®. The average k_{out} (n = 20 simulations) was calculated by both methods.

The paired t-test was done to compare the accuracy of the determined k_{out} in the cases with 5%, 10% and 20% relative error. The paired t-test is generally used when the numbers of points in data sets are the same and organized in pairs, in which there is a definite relationship between each pair of data points. As a rule, scientists accept a probability of 0.05 or less as convincing evidence that a particular outcome is unlikely.

The accuracy of these two methods was also evaluated for different sampling time intervals. This study aimed to achieve a better understanding of the relationship between the sampling time interval and analytic performance of partial area analysis. Good performance of both partial-areas analyses require an accurate determination of the overall partition coefficient $\frac{AUC_{0,T}^{\infty}}{AUC_{0,C}^{\infty}}$, which warrants an investigation of the following part of this chapter.

4.2.3 Bayesian approach to estimate AUC and brain-to-plasma AUC ratio for sacrifice design data

4.2.3.1 Model specification

As with all Bayesian analyses, a full likelihood and a prior distribution for every parameter are required. Without old information, we constructed a noninformative (vague) prior distribution model for the parameters. The posterior distributions can be approximated by random draws using Gibbs sampling. Parameter mean estimate, along with standard deviation, median, and 95% confidence intervals (known as credible intervals), are calculated directly from the posterior distribution.

4.2.3.1.1 Likelihood distribution

We had two PK measurements (C_{pl} and C_{br}) on the i^{th} animal at the j^{th} sampling time. For each sampling time point, there were n animals sampled. Distributional assumption was made as log-normality regarding the individual-specific PK measurement $\vec{C}_{ij}$.

$$\ln \vec{C}_{ij} \sim MVN(\vec{\mu}_j, \Sigma_j) \qquad \text{(Equation 4-11)}$$

Or explicitly,

$$(\ln C_{pl,ij}, \ln C_{br,ij}) \sim MVN\left(\begin{bmatrix} \mu_{pl,j} \\ \mu_{br,j} \end{bmatrix}, \begin{bmatrix} \sigma^2_{pl,j} & \sigma_{br,pl,j} \\ \sigma_{pl,br,j} & \sigma^2_{br,j} \end{bmatrix}\right) \qquad \text{(Equation 4-12)}$$

where i represents the ith animal; j represents the jth time point. MVN (·, ·) denotes a two-dimensional multivariate normal distribution. μ_j stands for the true concentration mean vector at the j^{th} time point; $\vec{\mu}_j$ is a vector of two fixed effects parameters representing the mean ($\mu_{pl,j}$ and $\mu_{br,j}$) of log-transformed plasma and brain concentrations ($C_{pl,ij}$ and $C_{br,ij}$) at the j^{th} time point. Σj (2×2) is the within-animal precision matrix at time j; and σ_j denotes the variance or covariance of the plasma and brain concentrations at the jth time point. With the precision matrix, we took into account the correlation between $C_{pl,ij}$ and $C_{br,ij}$ easily, which could increase the precision of estimate.

4.2.3.1.2 Priors on parameters ($\vec{\mu}_j$ and Σj)

The prior distributions of $\mu_{pl,j}$ and $\mu_{br,j}$ were assumed as uniform distributions, for instance,

$$\mu_{pl,j} \sim Unif(-\infty,+\infty) \qquad \mu_{br,j} \sim Unif(-\infty,+\infty) \qquad \text{(Equation 4-13)}$$

Typically, prior distributions of parameters are specified for mathematical convenience in order to derive closed form posteriors. Thus, the inverse of the variance-covariance matrix (Σ^{-1}), or so-called precision matrix, was assumed to follow a 2-dimensional Wishart distribution, a probability distribution of random nonnegative-definite symmetric matrices. Therefore, the variance-covariance matrix of concentrations at time j (Σj) was assumed to follow an Inverse-Wishart distribution.

$$\Sigma_j \sim Inverse-Wishart(R,d) \qquad \text{(Equation 4-14)}$$

where R is a two-dimensional matrix called scale matrix; d is the degree of freedom. By setting a small value (e.g., 0.01) to the diagonal of R as follows, and a small number (e.g., 2) to the degree of freedom, we could also assume a minimally informative but proper Inverse-Wishart distribution.

$$R = \begin{bmatrix} 0.001 & 0 \\ 0 & 0.001 \end{bmatrix}$$

4.2.3.2 AUC estimation

The posterior distributions can be approximated by random draws using Gibbs sampling performed in WinBUGS 1.4.3 (Bayesian inference Using Gibbs Sampling), a general program for performing Bayesian inference using MCMC methods (Lunn, 2000). Since

both brain and plasma AUC_0^t can be calculated from concentrations on the basis of the trapezoidal rule, a sample from the posterior of AUC_0^t is a linear combination of the samples from the posteriors for μ_j, the mean concentrations at time *j*. According to Equation 4-5, AUC_0^∞ is a additive combination of AUC_0^{last} and C_{last}/λ_z. Thus it was desirable to determine the posterior distribution of the terminal elimination rate constant λ_z, in order to examine the posterior of AUC from the last sampling time to infinity.

4.2.3.3 Posterior distribution of terminal elimination rate constant

By assuming a first-order elimination process at terminal phase, which, in our study, was assumed to be the last three time points (t_{j*}), the terminal elimination rate constant λ_z, can be estimated using linear regression on the naturally-log-transformed concentrations, which yields a log-normal likelihood as shown in Equation 4-15.

$$\ln C_{j*} \sim N(\alpha - \beta \bullet t_{j*}, \sigma^{*2}) \qquad \text{(Equation 4-15)}$$

where $N(\cdot, \cdot)$ denotes a normal distribution with mean μ^* equal to $(\alpha - \beta \bullet t_{j*})$ and standard deviation σ^*; α is the intercept of the linear regression; and β is the slope, which equals to the terminal elimination rate constant λ_z. α and β were assumed to arise from uniform distributions:

$$\alpha \sim \text{Unif}(-\infty, +\infty) \qquad \beta \sim \text{Unif}(0, 100) \qquad \text{(Equation 4-16)}$$

Similar to the variance-covariance matrix Σj as described above, σ^{*2} was specified as an inverse-gamma prior, Inverse-Gamma (k, θ), which is the standard conjugate prior for the normal variance. To be suitable in situations with little prior knowledge, the values of k and θ were assumed as follows so that the inverse-gamma distribution is "vague":

σ^{*2} ~ Inverse-Gamma (0.01, 0.01) (Equation 4-17)

In this way, the posterior distribution of λ_z can be approximated by Gibbs sampling with the help of WinBUGS.

4.2.3.4 Model convergence

Two Markov chains of 30000 simulations were generated and the first 10000 simulations (termed "burn-in period") were discarded to get past any initial transients. From the 20000 simulations, we drew posterior inferences. Markov chain convergence was assessed by visual inspection of the trace plot (i.e., plotting the draw of the parameter against iteration number for each Markov chain), autocorrelation, and the Gelman–Rubin diagnostic for each parameter. If the model has converged, all the chains will appear to move around the parameter space and be overlapping one another in the trace plots. Autocorrelation measures dependency among sequential draws of Markov chain samples. The level of autocorrelation is desirable to decline as the number of lags in the chain increases. Moreover, once convergence is attained, within-chains and between-chains variations should coincide, so the Gelman-Rubin statistic (the red line) should approximately equal one. The green line (representing the variance between the chains) and the blue line (representing the variance within the chains) are both desirable to be stable (Brooks and Gelman, 1998).

4.2.3.5 Method validation

The performance of the Bayesian approach was verified on both simulated and real data, as outlined below.

4.2.3.5.1 Simulation

In order to validate the new method and evaluate its credible interval coverage, we applied the proposed method to 100 sets of simulated data with serial sacrifice design, and compared the obtained results with nominal values of the parameters. The experiment was simulated in R (Version 2.11.0) (R.Development.Core.Team, 2010) for 100 times. Sampling from 28 animals was simulated at 7 arbitrary time points, with 4 animals at each one, following a serial sacrifice design. The time points were 0.5, 1, 2, 4, 8, 16, 24 hr. The PK was assumed as a two-compartment model consisting of the plasma compartment and the brain compartment (Figure 4.4). An i.v. bolus dose of 1000 units was given to the plasma compartment at time zero. Arbitrary PK parameters were defined in Table 4-2. Log-normally distributed between-animal variability (5% or 20%) and proportional residual variability (CV = 5% or 20%) were incorporated. For each simulated data set, posterior means and medians of $AUC_{0,pl}^{\infty}$, $AUC_{0,pl}^{\infty}$ and $\frac{AUC_{0,br}^{\infty}}{AUC_{0,pl}^{\infty}}$ along with 95% credible interval were obtained. The results were compared to the corresponding true AUC values. The true $AUC_{0,pl}^{\infty}$ value was considered as Dose/(V_{β}•β). V_{β} and β denote the population values of total volume of distribution at terminal phase and terminal elimination rate constant, respectively. The true $AUC_{0,pl}^{\infty}$ was considered to

be the same as the true $AUC_{0,pl}^{\infty}$ as the population clearance in and out of the brain were set to be the same.

The Bayesian method was utilized to obtain the posterior distributions of three parameters – $AUC_{0,pl}^{\infty}$, $AUC_{0,pl}^{\infty}$, and $\frac{AUC_{0,br}^{\infty}}{AUC_{0,pl}^{\infty}}$ in each of the 100 simulations. For each parameter, we considered three aspects: the posterior mean, median, and the 95% credible interval. In order to assess the robustness of the Bayesian estimators, we simply calculated the average of all the 100 posterior means and posterior medians, comparing with the nominal values, and counted the proportion of nominal values falling within the Bayesian intervals. The coverage was anticipated to be close to 95%. The percentages of simulations with lower 95% credible intervals less than zero were also calculated for the purpose of validation. The method performance was assessed when data have different levels of variability (5% between-animal coefficient of variation + 5% residual error; or 20% between-animal coefficient of variation + 20% residual error), although we recognized that the variability in human data is usually much higher.

4.2.3.5.2 Model application to real data

We evaluated the applicability of the Bayesian method to the real-world experiment described in Chapter 3. Briefly, brain and plasma levels of cediranib were determined following intravenous injection into wild-type, *Mdr1a/b (-/-)*, *Bcrp1 (-/-)* and *Mdr1a/b (-/-) Bcrp1 (-/-)* mice (as shown in Figure 3.6.A~D). In this experiment, we did not know

how the error was distributed, so we assumed that concentrations followed a normal distribution. In order to explore whether absence of P-gp or BCRP changes the BBB permeability of cediranib, the brain-to-plasma partition coefficient (i.e., the brain-to-plasma ratio of AUC_0^∞) was the desirable variable to compare statistically among the four genotypes. By utilizing the Bayesian approach, the posterior mean and 95% credible interval of the complete AUC ratios in different mouse groups (genotypes) were obtained and compared with the point estimate and 95% confidence interval approximated by Yuan's method (Yuan, 1993) utilizing Equation 4-6. The Kernel density plots were obtained to evaluate the posterior distributions of parameters. In order to further evaluate the performance of Bayesian method in estimating partial AUCs, posterior means of AUC from the initial time to the last sampling time point were also obtained and compared with the estimators obtained from a commonly used program, Phoenix WinNonlin® 6.1 (Mountain View, CA), which utilizes the Bailer-Satterthwaite method (Nedelman et al., 1995; Nedelman and Jia, 1998).

4.3 Results and discussion

4.3.1 Distributional kinetics of brain partitioning

4.3.1.1 Effect of efflux clearance on the brain T_{max}

The time after a single dose when the peak concentration occurrs in the brain (T_{max}) is dependent on the clearance mediated by active efflux transporters as follows and different in every examined genotype.

$$T_{\max} = \frac{\ln(\frac{\alpha}{\beta})}{\alpha - \beta}$$ (Equation 4-18, see Appendix II for derivation)

where $\alpha + \beta = k_{in} + k_{out} + k_{e\lim}$ and $\alpha \cdot \beta = k_{out} \cdot k_{e\lim}$. k_{in} is the first-order rate constant from the plasma into the brain mediated by the passive diffusion; k_{out} is the rate constant out of the brain due to the combined effect of efflux transporter activity and passive diffusion; and k_{elim} is the elimination rate constant out of the plasma. The simulation illustrates how the change of transporter activity influences the T_{max}, which is difficult to readily ascertain from the equation.

As shown in Figure 4.5, in the wild-type mice group (WT) where both passive diffusion and P-gp- and BCRP-mediated efflux contribute to transport out of the brain, it took shortest time to achieve the peak concentration (C_{max}) in the brain compared to the other genotypes. This is because the compound was quickly excluded from the brain. In the BCRP knockout group (BCRP KO) where only P-gp was present as an efflux transporter, the efflux CL was still significant because the model was set up in such a manner that the expression of P-gp is 3.5 fold of that of BCRP (Kamiiee *et al.*, 2008). Thus it took a little longer time to attain C_{max} than the WT mice. For the same reason, the P-gp knockout group (P-gp KO), with no P-gp but BCRP activity, has longer Tmax in the brain compartment than BCRP KO. The triple knockout group (TKO) was assumed to have no efflux activity at all, where the distribution in the brain is slowest due to the only passive diffusion. Therefore, the brain concentration peak occurs at a later time than for the other

genotypes. According to the model parameters, the rank order of the brain T_{max} should be: WT < BCRP KO < P-gp KO < TKO.

At T_{max}, the clearance from the plasma into the brain mediated by the passive diffusion (CL_{in}) is at pseudo-distributional equilibrium to the clearance out of the brain (CL_{out}) due to the combined effect of efflux transporter activity and passive diffusion since rate of change in the brain concentration ($d C_{br}/d t$) is 0 at the T_{max} time point. So the T_{max} is also called the time at a transient steady state. The relationship between C_{br}/C_{pl} and $\frac{AUC_{0,br}^{\infty}}{AUC_{0,pl}^{\infty}}$ was also explored. It is anticipated that C_{br}/C_{pl} at the transient steady state would equal to the brain-to-plasma AUC from zero to infinity ratio ($\frac{AUC_{0\ br}^{\infty}}{AUC_{0\ pl}^{\infty}}$), which then would provide accurate information of brain partitioning. It reflects the overall exposure of drug in the brain relative to the level of drug in the plasma. The illustration is as shown in Figure 4.6.

The cediranib study in mice reflected the impact of efflux clearance on the brain T_{max}. As anticipated, cediranib achieved the brain T_{max} quickly in WT mice. It took significantly longer time to get to the peak in the *Mdr1a/b(-/-)Bcrp1(-/-)* mice. Data were summarized in Table 4-3. Note that in WT, *Bcrp1(-/-)*, and *Mdr1a/b(-/-)* mice, T_{max} was not an exact time but a time range because there was no significant difference between concentrations at those time points around the exact T_{max}, which made it difficult to identify the exact

T_{max} in those groups. This indicates the need for extensive sampling around T_{max} to assure an accurate determination of the brain partitioning using this method.

4.3.1.2 Brain-to-plasma concentration ratio vs time profile

A profile describing simulated C_{br}/C_{pl} ratio with respect to time was constructed (Figure 4.7). For all four genotypes, the C_{br}/C_{pl} ratio increases from zero to an constant, which is called pseudo-distributional equilibrium, or, terminal elimination phase (β phase) after a single bolus. Similar to the brain T_{max}, the time to reach distributional equilibrium varies between those mouse groups because of their different efflux clearances. It took the shortest time for the WT and the longest time for the TKO mice group to reach equilibrium. Thus, this difference makes the use of single-timepoint measurement of C_{br}/C_{pl} ratio for different genotypes misleading without knowing in what phase the samples were taken.

Once reaching the β phase, the C_{br}/C_{pl} ratio in this model is a constant independent of time which follows Equation 4-19.

$$\left(\frac{C_{br}}{C_{pl}}\right)_{\beta} = \frac{\frac{AUC^{\infty}_{0\ br}}{AUC^{\infty}_{0\ pl}}}{1-\frac{\beta}{k_{out}}} \qquad \text{(Equation 4-19, see Appendix III for derivation)}$$

where β represents the terminal-phase elimination rate constant and k_{out} represents the rate constant out of the brain mediated by efflux transporters and passive diffusion. Note that this ratio is higher than the brain-to-plasma AUC zero to infinity ratio. Therefore it

overestimates the true brain partitioning. The extent of overestimation depends on the relative magnitude of k_{out} and β. Thus, by assuming that efflux transporters do not influence the compound metabolism and excretion, it is anticipated that the β-phase C_{br}/C_{pl} ratio measured in WT mice should be closer to $\frac{AUC^{\infty}_{0\ br}}{AUC^{\infty}_{0\ pl}}$, and the brain partitioning measured in TKO mice should be more overestimated. The relationship between C_{br}/C_{pl} ratio, the partial brain-to-plasma AUC ratio, and the clearance ratio which is equal to the complete AUC ratio is illustrated in Figure 4.8. However, as a constant, the C_{br}/C_{pl} ratio at the terminal phase is reasonable to compare relative drug brain exposures and transporter activities among different genotypes.

Figure 4.9 shows the time course of brain partitioning of cediranib (C_{br}/C_{pl}) in four mouse groups. The time to reach a distributional equilibrium depends on the transporter-derived clearance. In transporter gene knockout mice, clearance out of the brain differs depending on contribution of the transporters. As shown in the profile, for the *Mdr1a/b(-/-) and Mdr1a/b(-/-) Bcrp1(-/-)* mice, since P-gp plays an dominant role, the time for C_b/C_p to reach distributional equilibrium was 2~4 hours, which was significantly longer than that for wild-type and *Bcrp1(-/-)* mice (15~30 minutes).

4.3.2 Partial area analysis

The influence of a exit rate constant from a peripheral compartment (k1 in Figure 4.3) on $C^{t}_{0,C}$, $C^{t}_{0,T}$, $AUC^{t}_{0,C}$, $AUC^{t}_{0,T}$, $AUC^{t}_{0,T} / AUC^{t}_{0,C}$, and R of the target and central

compartments was explored. It was shown that even though $C_{0,C}^{t}$, $C_{0,T}^{t}$, $AUC_{0,C}^{t}$ and $AUC_{0,T}^{t}$ changed when k1 changed (Figure 4.10~4.11), the ratio $AUC_{0,T}^{t} / AUC_{0,C}^{t}$ did not change with k1 (Figure 4.12.A), and R remained constant (Figure 4.12.B). This finding suggested that even though the partial-areas analysis is a mammillary compartment-dependent method, it does not rely on the assumption of any peripheral compartment other than the target site.

When errorless simulated concentration data were used to estimate k_{out}, both the cumulative and interval partial-areas analysis methods generated non-biased estimates (Table 4-4). However, as shown in Figure 4.13, 4.14 and 4.15, the two methods provided similar results when nominal values of k_{out} were relatively small. On the other hand, the cumulative method showed some advantage over the interval method for larger nominal values of k_{out}, because the data points tend to evenly spread out rather than form clusters from which a statistically-sound linear regression could not be done. Generally, the interval method would generate a smaller intercept for the linear regression, which ideally equals zero.

When error was added to the data, the estimated k_{out} showed increased bias in both methods as error increased. The estimated k_{out} was estimated as the slope of the linear regression line (Figures 4.16, 4.17, and 4.18). In these cases, the nominal k_{out} was 2 hr^{-1}. When there was 5%, 10% and 20% relative random error in the concentrations of both central compartment and target compartment, statistical analysis showed that the

estimated k_{out} values (mean ± SD) from cumulative method were 1.92 ± 0.12, 1.82 ± 0.33, 1.43 ± 0.28 hr^{-1} for 5%, 10%, and 20% error, respectively, and from interval method they were 2.00 ± 0.21, 2.01 ± 0.37, 1.93 ± 0.61 hr^{-1} for 5%, 10%, and 20% error, respectively (Table 4-5). These results suggested that interval method seems to be more accurate than cumulative one when error exists in the concentration-data, if only the bias of estimate with the nominal value was of interest. Results of paired t-tests (Table 4-6) showed that when error was 5%, P-value was 0.09, which meant that there was no significant difference between the estimated k_{out} from cumulative and interval methods; when error was 10%, P-value decreased to 0.04; and when error was 20%, P-value decreased to 0.00047, which meant there was significant difference between these methods. However, since the data points were in a clustered manner, the accuracy of the interval method estimate depended strongly on the largest data point at the x-axis, which might be the first few time points post dose in this i.v. bolus simulation. With that in mind, it is dangerous to make a conclusion that the interval method will provide more accurate estimate of k_{out} than the cumulative method. The advantages of one method over the other depend on the magnitude of true k_{out}. If the k_{out} is small enough to make the data points evenly spread out the x-axis, the interval method is better and more accurate. The critical magnitude of k_{out} to show a good estimate based on the interval method can be further explored in future studies.

When sampling time intervals for the concentrations in central and target compartments differed, the behaviors of cumulative and interval partial-areas analyses with 5%

concentration error were shown in Figure 4.19 and Figure 4.20. The simulated results suggested that the estimated k_{out} would be more accurate when the time interval was smaller.

4.3.3 Bayesian approach to estimate AUC and brain-to-plasma AUC ratio for sacrifice design

4.3.3.1 Simulated serial sacrifice design

Model diagnostics for one of 100 simulations were shown in Figure 4.21~4.23 as an illustration. All the three forms of diagnostic plots indicated the two Markov chains converged well. Other simulation runs converged successfully as well (diagnostics not shown).

As shown in Table 4-7, when the data had low variation (5% between-animal variability (BAV) and 5% residual error (or called within-animal variability (WAV)), both the posterior mean and median worked as a robust estimator, with the averaged values very close to the nominal population AUCs and their ratio. However, when the data had greater noise (20% BAV and 20% WAV), the posterior means of all three parameters of interest were biased. Interestingly, the averages of the 100 posterior medians of those parameters were closer to the nominal values, and they were acceptable. The results suggested that occasionally the posterior median is preferred over the mean for non-symmetric distributions, such as multimodal or skewed distributions (Bochkina and Sapatina, 2005). For purposes of prediction, the posterior mean may not always be reliable. The robustness of the posterior mean depends on the variability of the data and

the way in which samples are drew. In our study, the optimal estimator could be identified as the one with the value comparable to the point estimate provided by the Bailer's method or any other classic method.

The proportions of simulations in which the nominal population mean was covered by the 95% credible interval were also shown in Table 4-7. At all tested levels of variability, Bayesian credible interval had a good coverage (close to or above 95%). The proportion of simulations in which the lower boundary of the posterior credible interval was below zero was all zero, suggesting that the draws of samples would not give negative credible limits.

4.3.3.2 Cediranib i.v. study in mice

The Bayesian approach has been applied to the cediranib brain distribution study in wild-type and gene-knockout mice of brain efflux transporters, such as P-gp and BCRP, the details of which were described in Chapter 3. The aim of the study was to compare the cediranib brain partitioning among the genotypes in order to explore the role of brain efflux transporters in the brain penetration of cediranib. The conventional approach to estimating the complete AUC from time zero to infinity is through the Bailer-Satterthwaite method. The method can provide a point estimate of AUC_0^∞ but is not able to assess the precision of the estimation. The Bayesian method developed here could approximate the posterior distribution of any NCA parameter including AUC_0^∞ ,

$\frac{AUC^{\infty}_{0,br}}{AUC^{\infty}_{0,pl}}$ and the DTI ($\frac{\left(\frac{AUC^{\infty}_{0,br}}{AUC^{\infty}_{0,pl}}\right)_{transgenic\cdot mice}}{\left(\frac{AUC^{\infty}_{0,br}}{AUC^{\infty}_{0,pl}}\right)_{wildtype\cdot mice}}$), etc. According to the model diagnostics, there was no MCMC chain unable to converge (Figure 4.24). Based on the Bayesian simulation-based estimation, posterior distributions of the cediranib plasma and brain AUC^{∞}_{0} and their ratio from the wild-type, *Mdr1a/b(-/-)*, *Bcrp1(-/-)*, and *Mdr1a/b(-/-) Bcrp1(-/-)* mice were obtained (Figure 4.25~4.27). Figure 4.28 also illustrated the DTI of cediranib across the BBB that lacks expression of drug efflux transporters, a credible interval around which would be challenging using frequentist approaches. Thus, the biggest benefit of the Bayesian approach is the feasibility in determining the estimation precision of parameters of interest in brain uptake studies.

Table 4-8 listed the posterior means and 95% credible intervals of the complete brain and plasma AUC^{∞}_{0} and their ratios in four genotypes. This helps make a reliable conclusion that BCRP might play a small, but significant, role in excluding cediranib out of the brain, based on the fact that there was a significant difference of the brain-to-plasma AUC^{∞}_{0} ratio of cediranib between the wild-type mice and the *Bcrp1(-/-)* mice, and between the *Mdr1a/b(-/-)* and *Mdr1a/b(-/-) Bcrp1(-/-)* mice. The Bayesian estimators of the plasma and brain AUC^{∞}_{0}s were compared with the point estimate and 95% confidence interval (C.I.*), as estimated by the Bailer's approximation extended by Yuan. Yuan's method provided tighter confidence intervals than the Bayesian method. However, it is hard to

say that Yuan's method has an advantage over the Bayesian method, since Yuan's method is anticipated to underestimate the variance of AUC_0^{∞} because of its double usage of the last sampling time point for estimation of λ_z and calculation of the AUC from the last sampling time up to infinity (Yuan, 1993).

Table 4-9 shows that the Bayesian posterior estimates of partial AUC in those mice groups, which is the AUC from time zero up to the last sampling time point, were very close to the mean, SD and 95% confidence interval estimated by the Bailer-Satterthwaite method. Note that Bayesian credible intervals and frequentist confidence intervals produced from the same data set are not necessarily similar, especially if informative prior information is included in the Bayesian analysis. The reason for our comparison was simply to show that in this particular case, the noninformative Bayesian method produced approximately similar parameter estimates as the Bailer-Satterthwaite method.

Note that we compared the new approach with the conventional methods derived from the Bailer's method, such as Bailer-Satterthwaite method and Yuan's method, but we did not compare the performance of Bayesian approach with other nonparametric methods such as bootstrap and jacknife. The comparison of accuracy and precision for the Bayesian method and these nonparametric approaches may be of value in further studies.

The Bayesian approach does not rely on any compartmental assumption but it only requires the assumption that the terminal elimination rate follows first-order kinetics. The biggest advantage over other methods is that it is able to provide the precision of

$\frac{AUC^{\infty}_{0,br}}{AUC^{\infty}_{0,pl}}$ estimation easily taking into account the correlation between brain and plasma.

The limitation of this method is that the setting of the prior distribution is subjective and different priors may yield different posterior results. One of the drawbacks of using noninformative priors, e.g., the uniform prior for log-concentration means, is that there is a possibility that extremely large samples could be drawn. This might result in a poor or slow convergence, or sometimes can influence results. In the present simulation, the error at each sampling time follows a log-normal distribution (proportional to the mean value of concentrations). Thus, the concentration data were log-transformed and the entire analysis was done on a log-scale. In the animal study, the normal likelihood worked adequately well and we did not notice any significant difference between the normal likelihood and the log-normal likelihood in that case. Other appropriate assumptions of likelihood and priors are worth exploring in further studies. However, when prior knowledge is available, it is strongly recommended to incorporate informative priors into the Bayesian approach. This will help narrow down the credible intervals of the Bayesian estimate and generate a more reliable posterior distribution.

4.4 Conclusions

4.4.1 Distributional kinetics of partition coefficient

It can be concluded that the concentration-time profiles will be different in every genotype or treatment group. The time for C_{br}/C_{pl} to reach a transient steady state and to attain a pseudo-distributional equilibrium value depends on the CL mediated by efflux

transporters. Comparing C_{br}/C_{pl} at any single time point before distributional equilibrium is dangerous, especially if CLs due to efflux are quite different among genotypes or treatment groups. The true brain (or other tissues or organs) partitioning, which is described by brain-to-plasma AUC from zero to infinity ratio, can only be measured by the C_{br}/C_{pl} ratio when the C_{br}/C_{pl} ratio at the transient steady-state (brain T_{max}) in the case of single dose bolus studies. However, for comparison purposes, the efflux transport activities can also be examined by measuring the C_{br}/C_{pl} ratio at a pseudo-distributional equilibrium (terminal elimination phase), noting that at the terminal phase the true tissue partition coefficient will be overestimated. It is very possible that a single-time C_{br}/C_{pl} measurement in TKOs might require a late sampling times since the elimination out of brain is slower compared to other genotypes and the distribution into brain takes longer time to reach pseudo equilibrium.

4.4.2 Partial-areas analysis

The partial-areas analysis is a compartment-dependent method, but it is independent of the number of peripheral compartments and peripheral compartmental parameters. The estimated value of exit-rate constant from the target site by using partial-areas analysis is reliable. The cumulative method shows some advantage over the interval method for larger k_{out} values, because the data points tend to evenly spread out rather than form clusters which do not generate sound linear regression. Nevertheless, the interval method worked similar to the cumulative one for estimation of smaller nominal values of k_{out}. When concentration data have significant error, the interval partial-areas analysis can yield more accurate estimate than the cumulative one. Although the interval partial-areas

analysis has advantages over the cumulative one for accuracy, it still has to be taken into account that the linear regression behavior of the interval technique depends strongly on the data at the first few time points post i.v. dose. This requires that concentration measurement for large concentrations should be with the least error. It has also been indicated that accuracy of partial-areas analysis depends on experimental design. Both techniques work best when the time-interval for concentration measurements relative to the time constants are smallest.

4.4.3 Bayesian approach to estimate AUC and brain-to-plasma AUC ratio for sacrifice design data

Unlike the conventional frequentist approach, the Bayesian approach considers each parameter of interest as a statistical distribution with some uncertainty, rather than a known point estimate (Kitanidis, 1986). The Bayesian approach can easily estimate the variability around AUC_0^∞ without complicated mathematical computation, and make it possible to statistically compare the tissue-to-plasma ratios of AUC_0^∞ obtained following destructive sampling. Posterior distribution of other NCA parameters could be obtained in likewise fashion. When prior knowledge is available, it is strongly recommended to incorporate informative priors into the Bayesian approach, in order to obtain a more reliable posterior estimation.

4.5 Footnotes

We would like to thank Dr. Kyle Baron for his initial inspiring idea of applying Bayesian approach to NCA and his kind help in WinBUGS programming. We would also like to

express our gratitude to Wei Zhong, from Department of Biostatistics, for his help in Bayesian method development. We are also thankful for the help of Magdalena Burström, from Department of Pharmaceutical Biosciences, Uppsala University, in STELLA model building and discussion for the T_{max} simulation session.

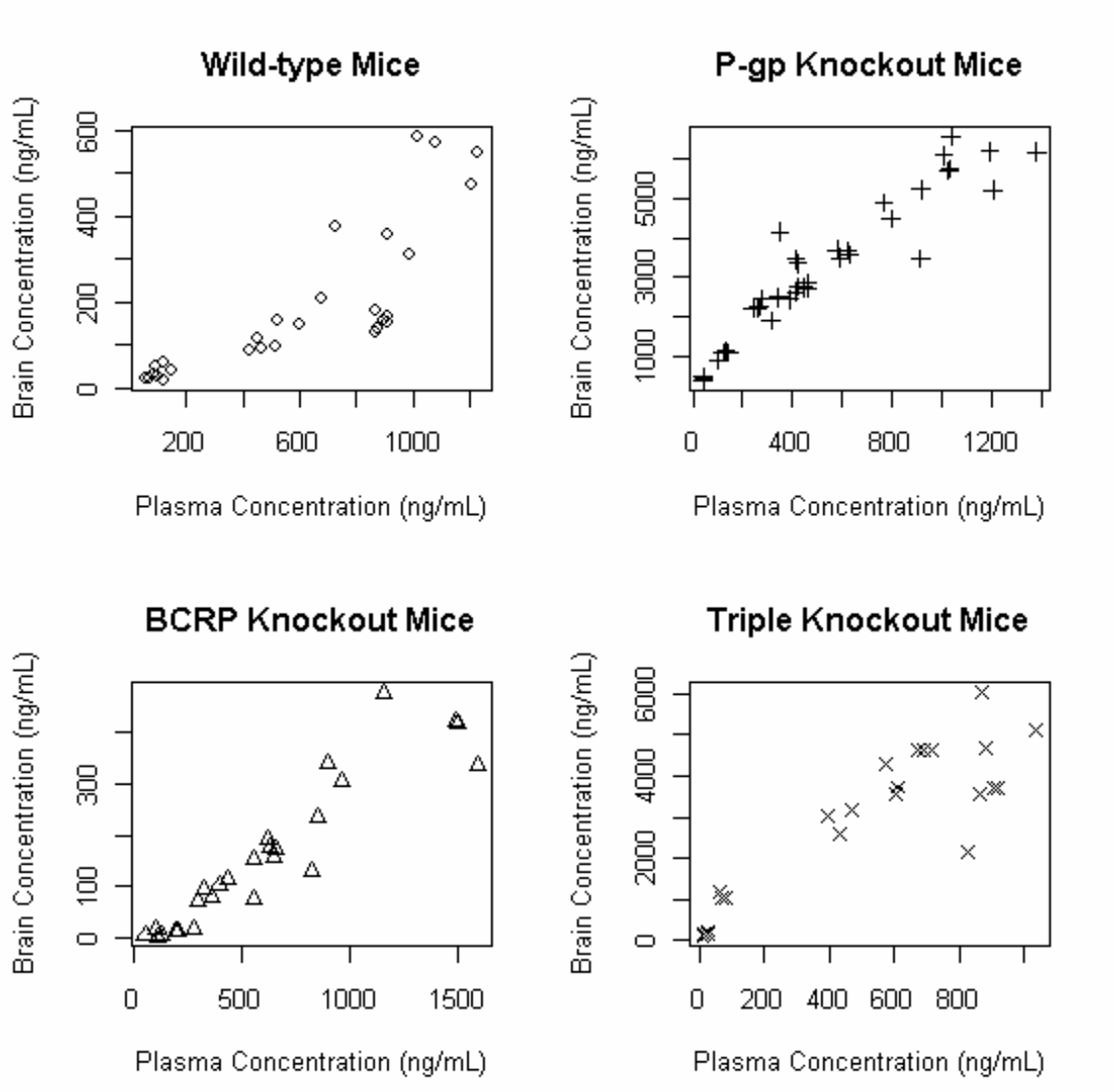

Figure 4.1 Correlation between plasma and brain concentrations after intravenous injection of 4mg/kg cediranib into four genotypes of FVB mice.

A.

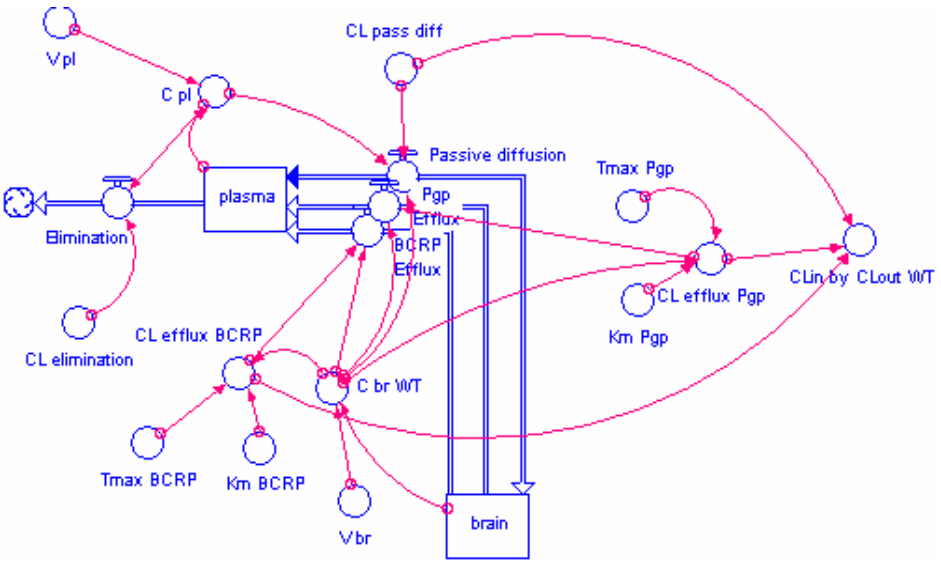
Vpl
C pl
CL pass diff
Passive diffusion
Tmax Pgp
plasma
Pgp
Efflux
BCRP
Efflux
Elimination
CL efflux Pgp
CLin by CLout WT
Km Pgp
CL elimination
CL efflux BCRP
C br WT
Tmax BCRP
Km BCRP
Vbr
brain

B.

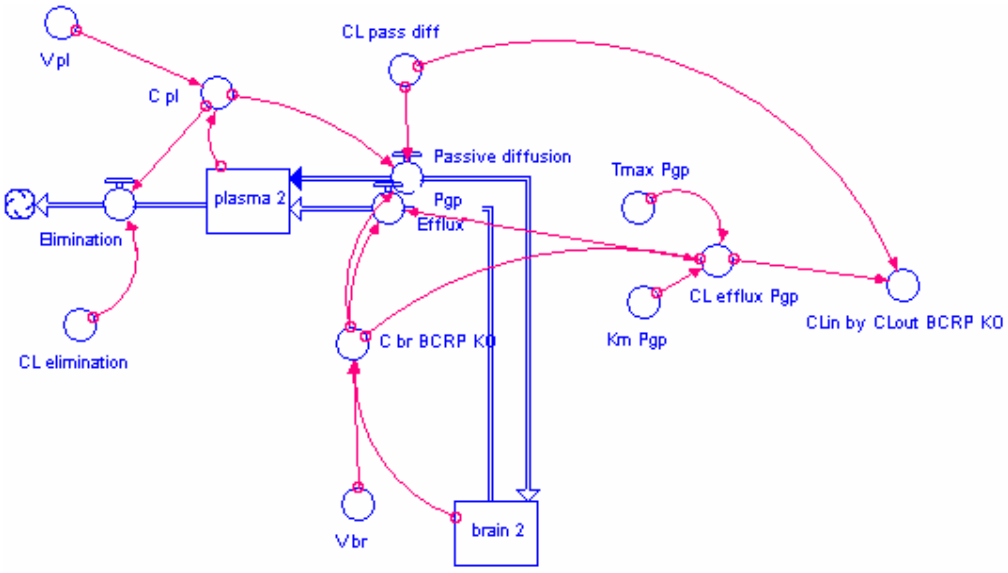
Vpl
C pl
CL pass diff
Passive diffusion
Tmax Pgp
plasma 2
Pgp
Efflux
Elimination
CL efflux Pgp
CLin by CLout BCRP KO
Km Pgp
C br BCRP KO
CL elimination
Vbr
brain 2

C.

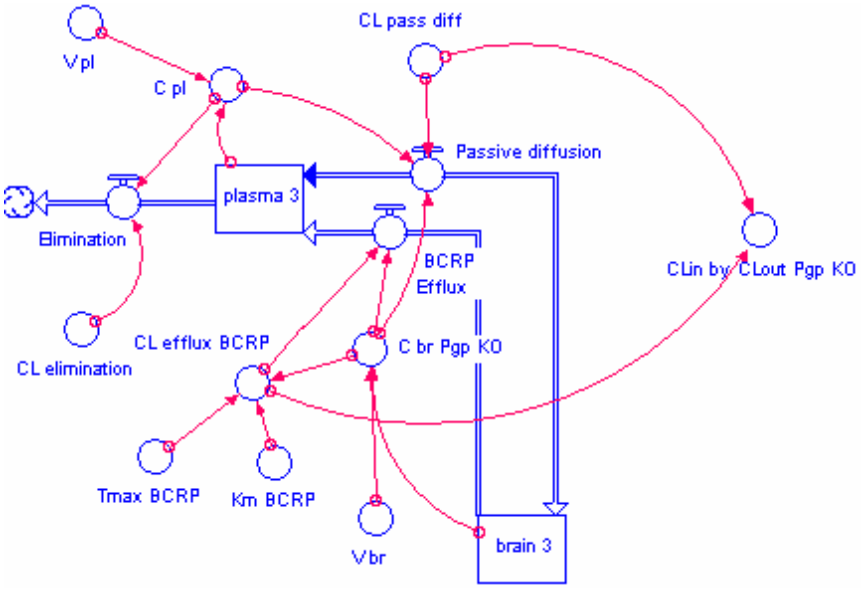

D.

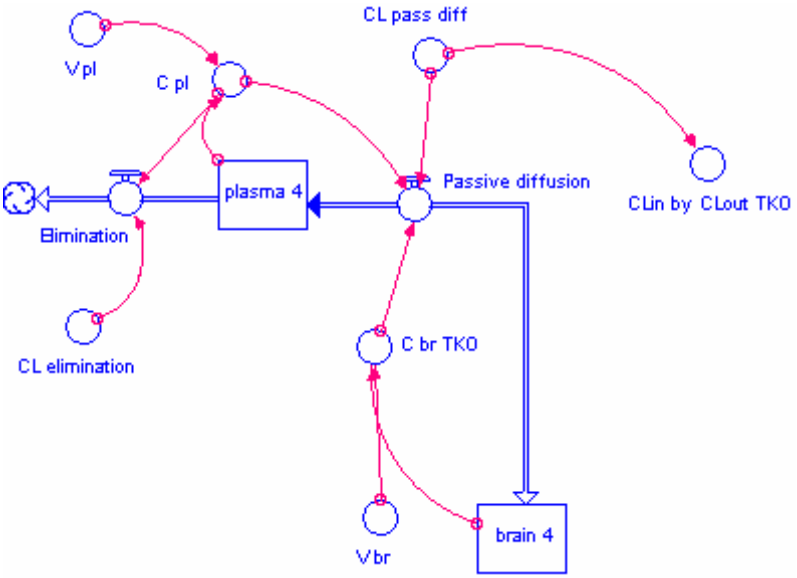

Figure 4.2 STELLA simulation model to illustrate the effect of efflux transport on brain-to-plasma partitioning in four genotypes. A. Wild-type mice (WT); B. BCRP knockout mice (BCRP KO); C. P-gp knockout mice (Pgp KO); D. Triple knockout mice (TKO).

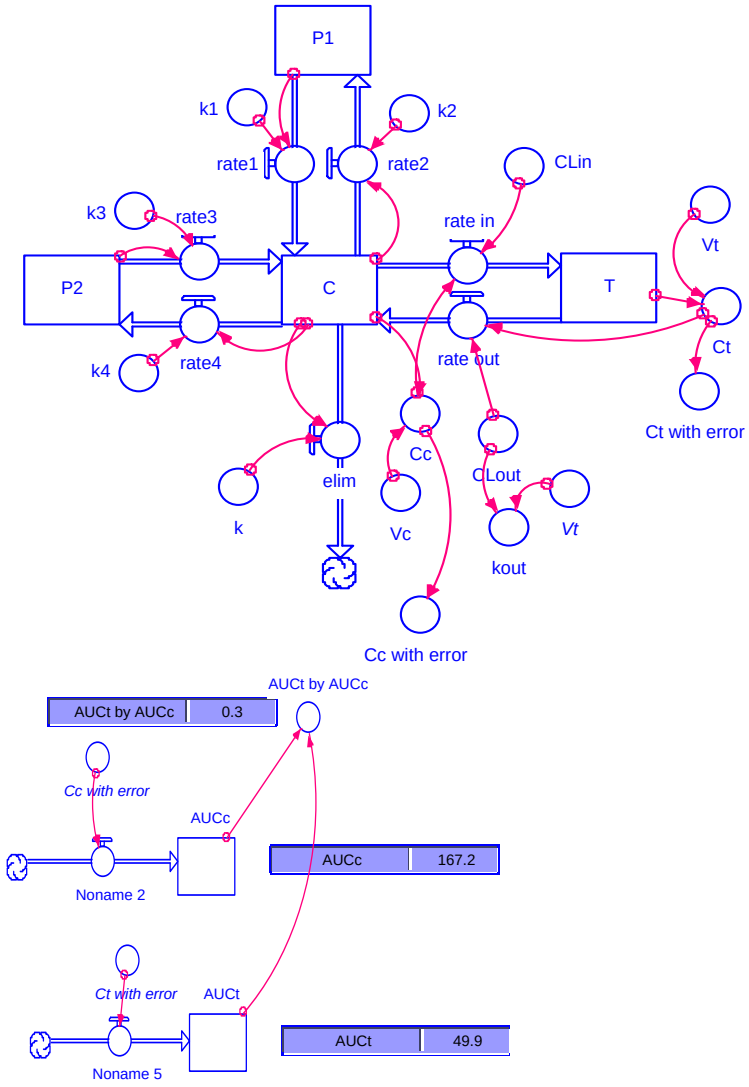

Figure 4.3 STELLA model for partial area analysis simulation

Table 4-1 Parameters of the STELLA model for partial-areas analysis

Parameter	Value
CLin	30
CLout	100
k	0.3
k1	0.3
k2	0.3
k3	0.6
k4	0.4
Vc	100
Vt	50

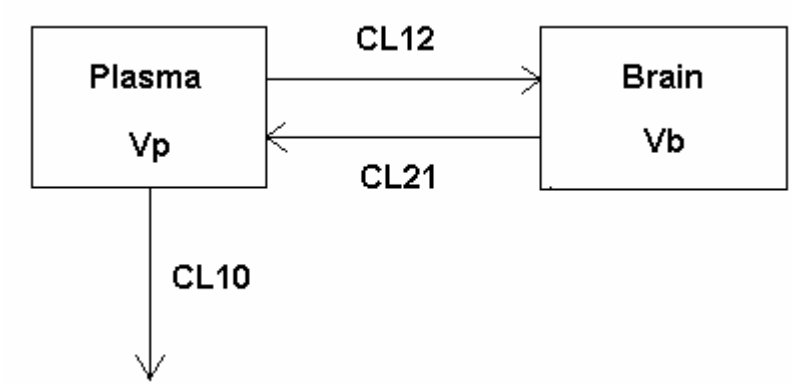

Figure 4.4 Simulated two-compartment PK model for Bayesian model validation

Table 4-2 Model parameters of the simulated two-compartment model.

Parameter	Population Parameter Value	Between-animal Variability
Vp	100	Yes
Vb	50	No
CL12	15	Yes
CL21	15	Yes
CL10	5	Yes

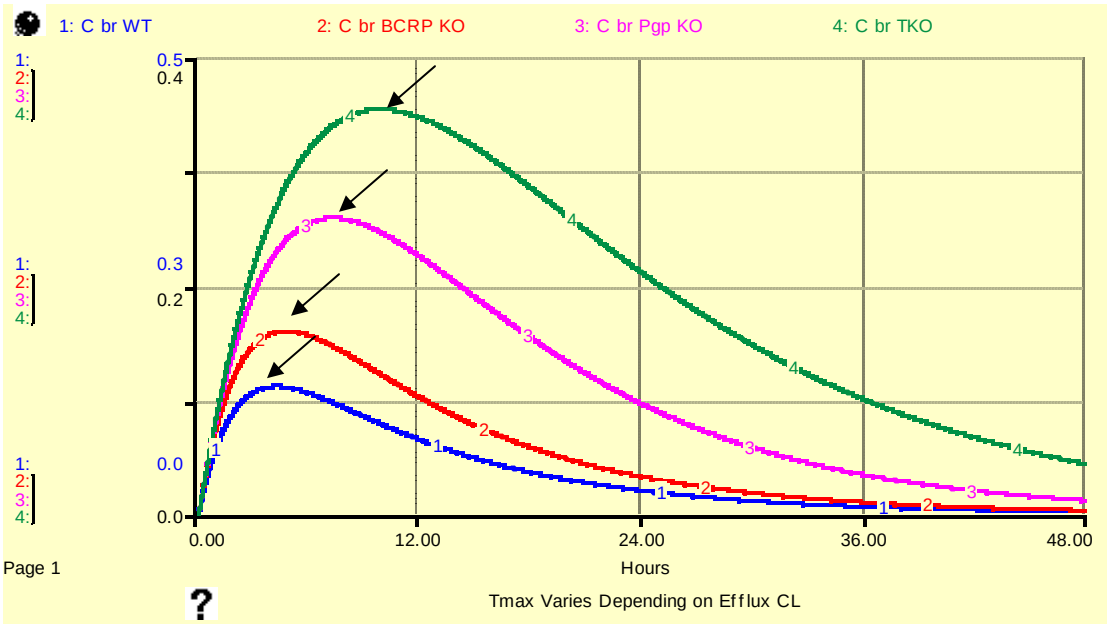

Figure 4.5 The brain concentration vs. time profiles of four genotypes. T_{max} in the brain compartment varies depending on the clearance due to active efflux transporter activity.

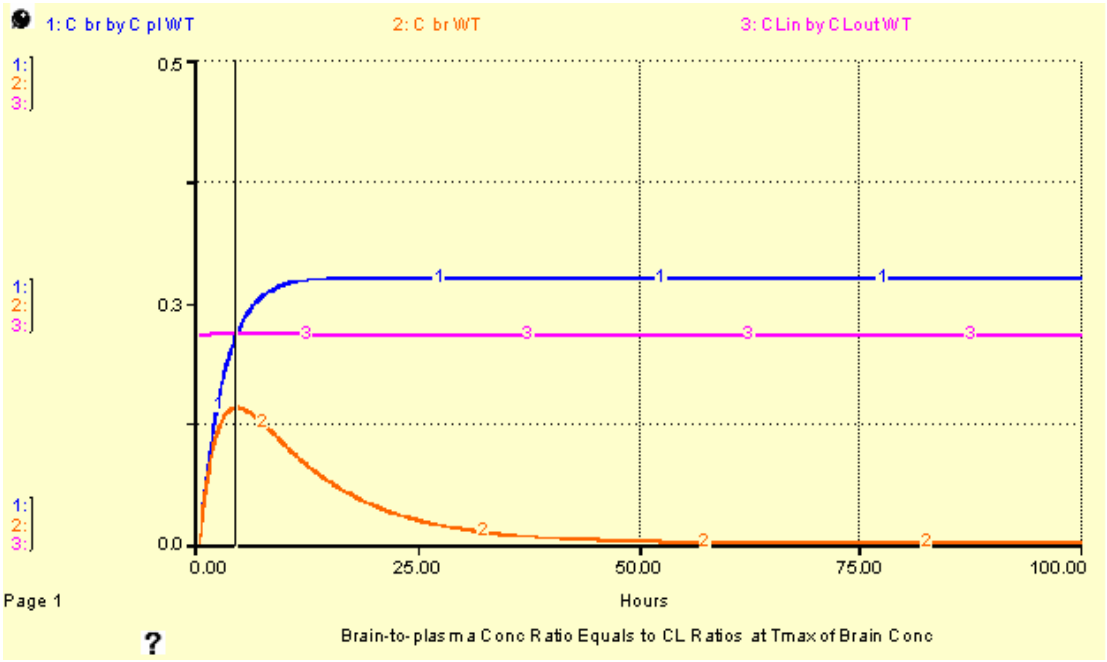

Figure 4.6 At the time when C_{brain} achieves the maximum, the C_{brain}/C_{plasma} ratio equals to the brain-to-plasma AUC zero to infinity ratio, which exactly reflects the CL_{in}/CL_{out} ratio. The profile shows the wild-type mice group (WT) as an illustration.

Table 4-3 The observed brain T_{max} in four genotypes of transporters.

Genotype	Brain Tmax (hour)
Wild-type	0.5~1
Bcrp1(-/-)	0.25~1
Mdr1a/b(-/-)	0.5~1
Mdr1a/b(-/-) Bcrp1(-/-)	2

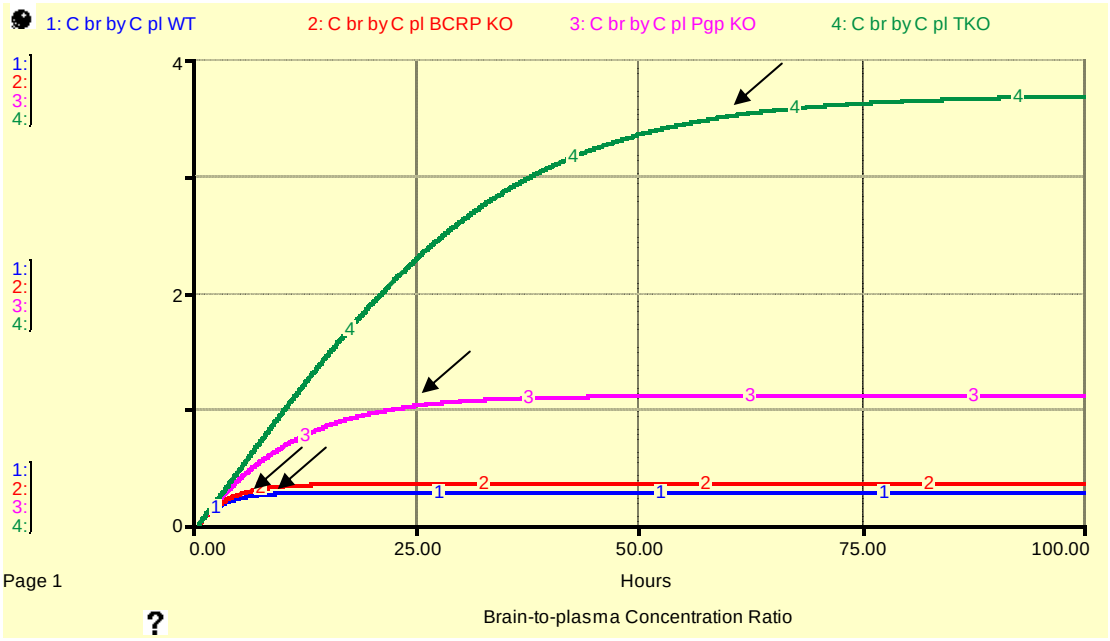

Figure 4.7 The simulated brain-to-plasma concentration ratio vs. time profiles of four genotypes.

A.

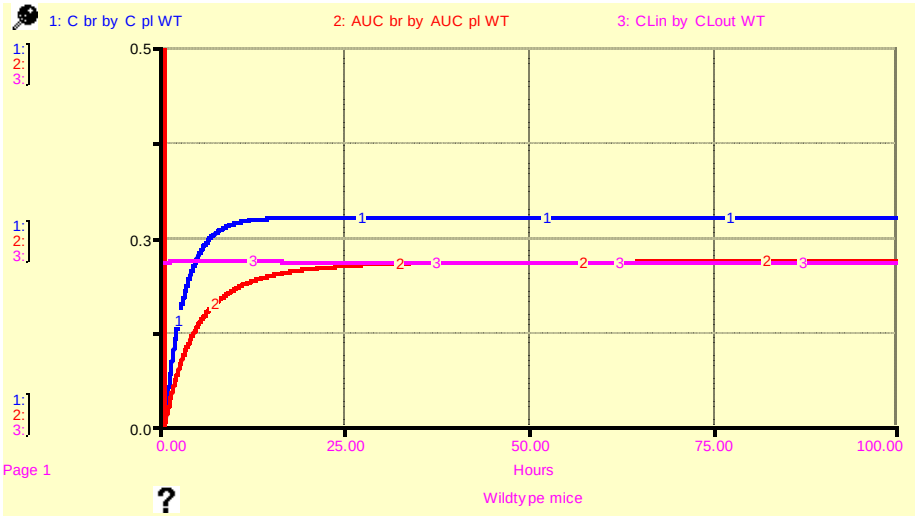
1: C br by C pl WT
2: AUC br by AUC pl WT
3: CLin by CLout WT
0.5
0.3
0.0
0.00
25.00
50.00
75.00
100.00
Page 1
Hours
Wildtype mice

B.

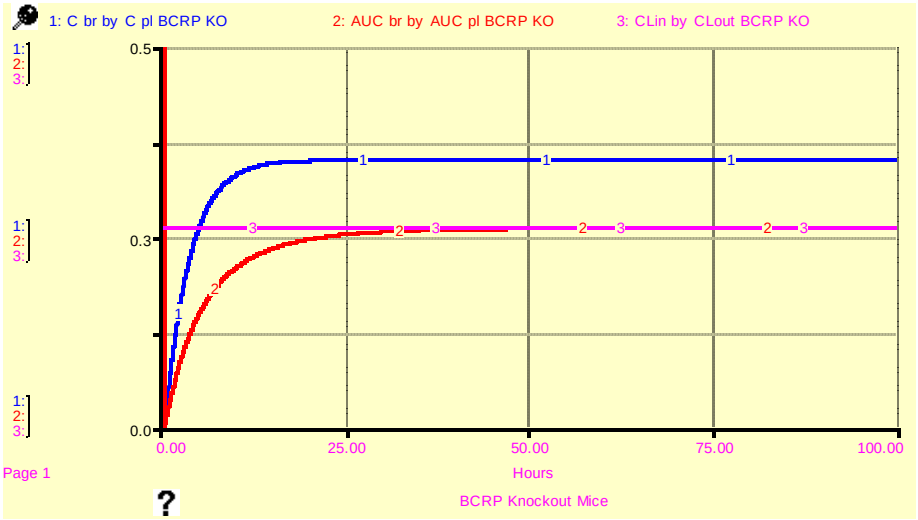
1: C br by C pl BCRP KO
2: AUC br by AUC pl BCRP KO
3: CLin by CLout BCRP KO
0.5
0.3
0.0
0.00
25.00
50.00
75.00
100.00
Page 1
Hours
BCRP Knockout Mice

C.

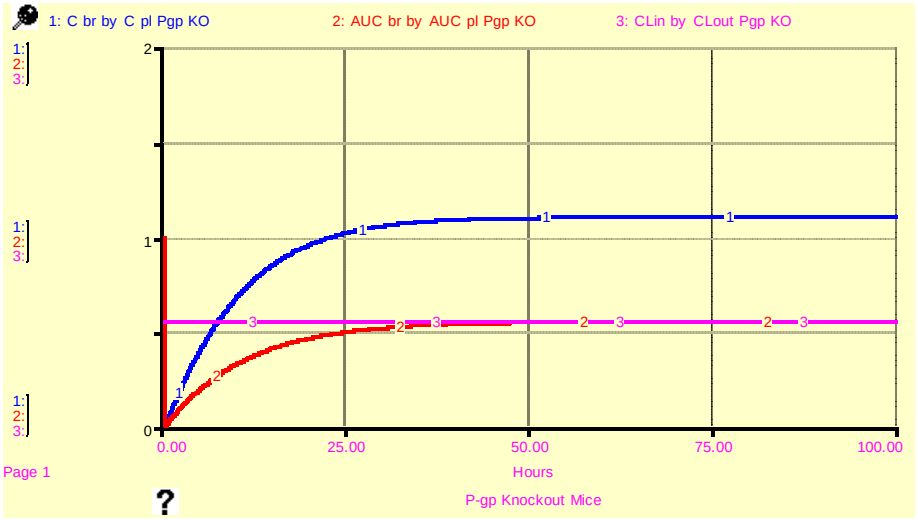

D.

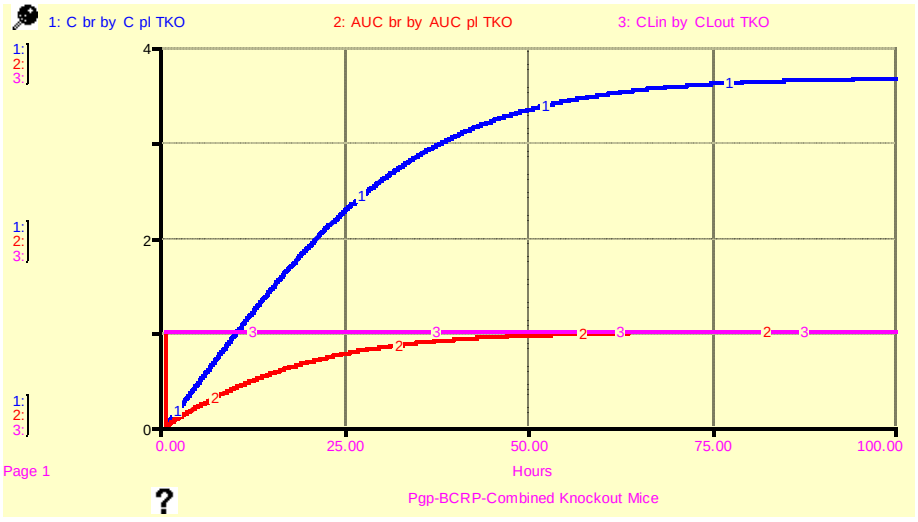

Figure 4.8 The relationship between the concentration ratio, partial AUC ratio, and clearance ratio. A. Wild-type mice (WT); B. BCRP knockout mice (BCRP KO); C. P-gp knockout mice (Pgp KO); D. Triple knockout mice (TKO).

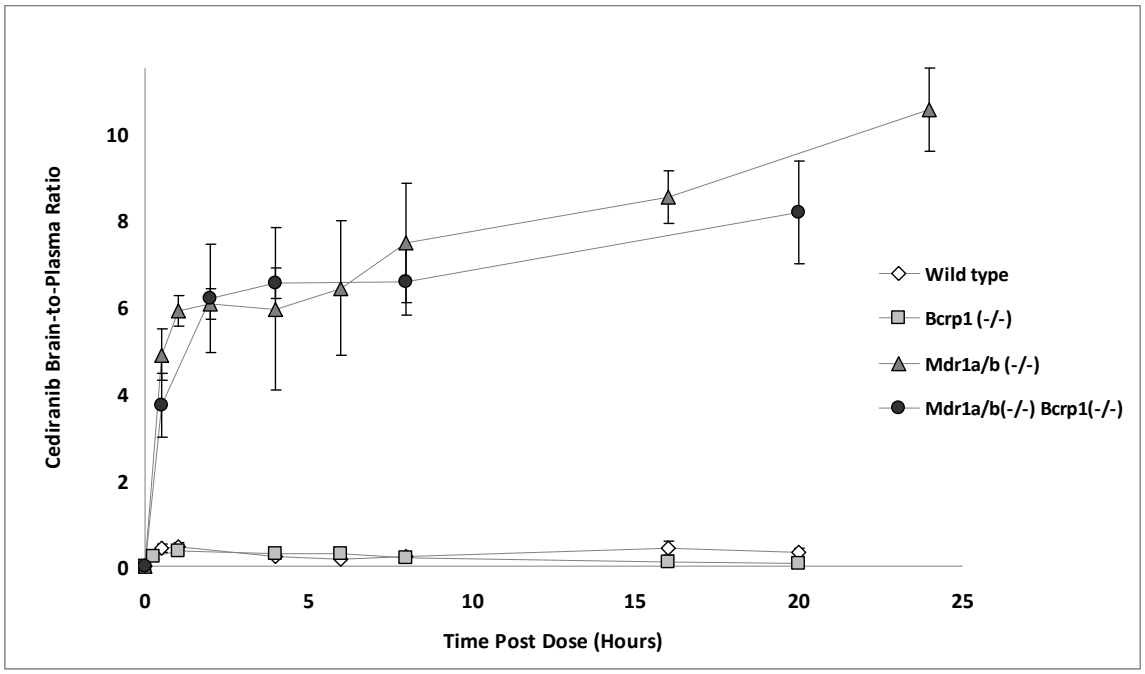

Figure 4.9 The brain-to-plasma concentration ratio vs. time profiles in a real-world experiment – cediranib brain-to-plasma concentration ratio after i.v. injection (dose = 4 mg/kg). Results are expressed as mean ± SD, n=3~4.

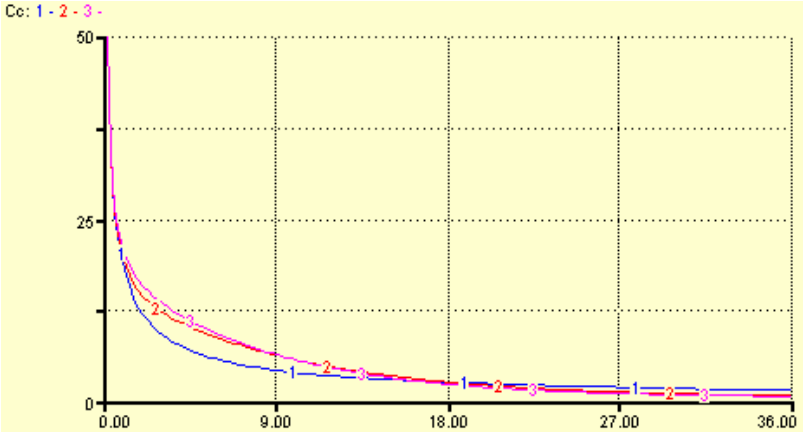

Figure 4.10.A Influence of k1 on Cc. 1: k1= 0.1, 2: k1= 0.5, 3: k1= 0.9.

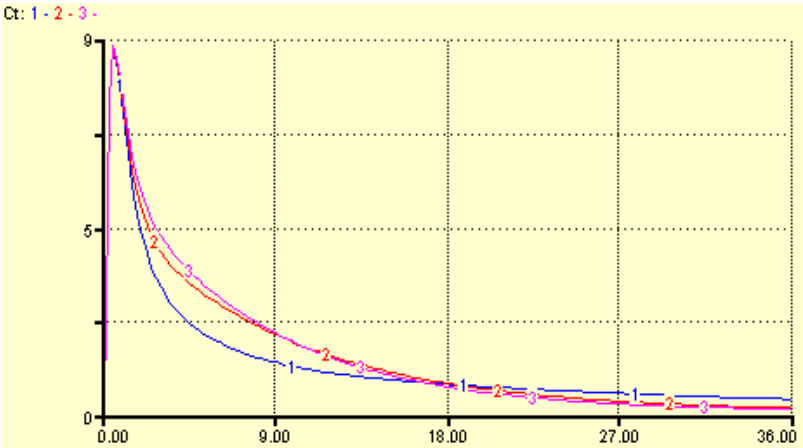

Figure 4.10.B Influence of k1 on Ct. 1: k1= 0.1, 2: k1= 0.5, 3: k1= 0.9.

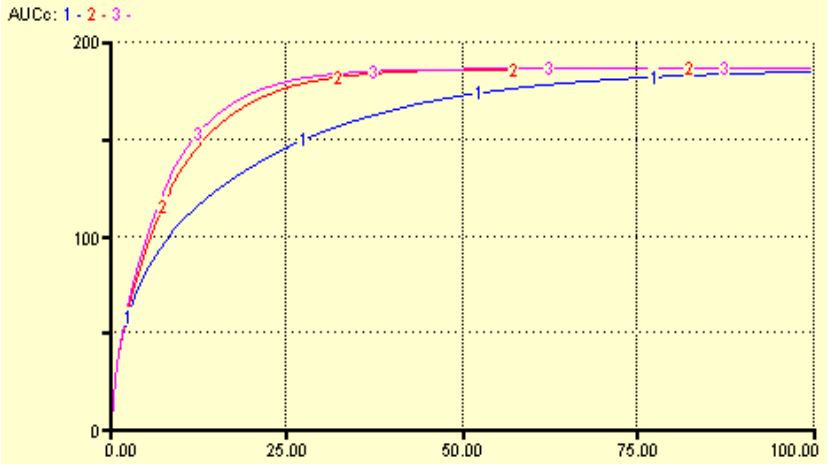

Figure 4.11.A Influence of k1 on $AUC^{t}_{0,C}$. 1: k1= 0.1, 2: k1= 0.5, 3: k1= 0.9.

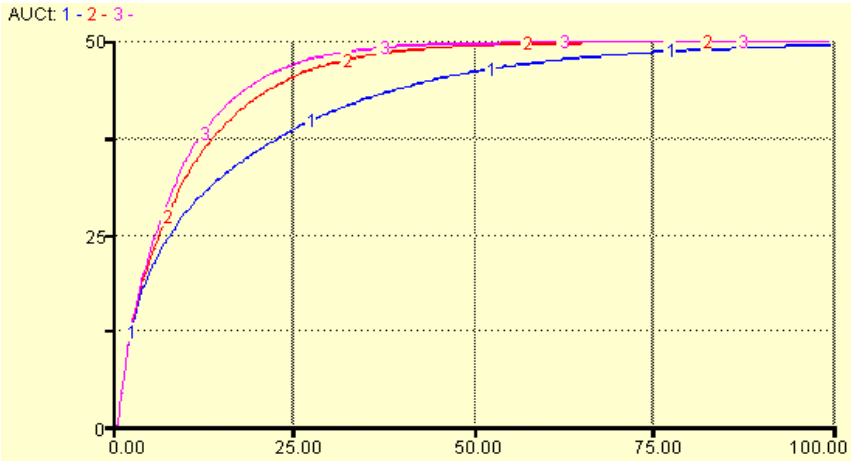

Figure 4.11.B Influence of k1 on $AUC^{t}_{0,T}$. 1: k1= 0.1, 2: k1= 0.5, 3: k1= 0.9.

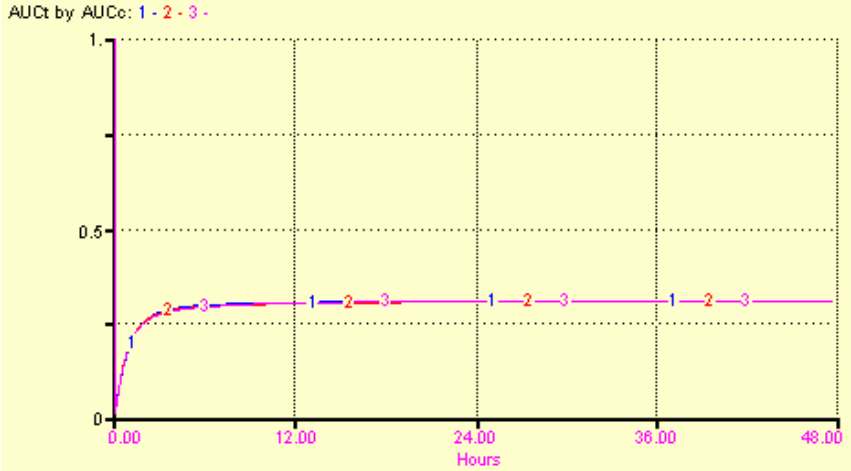

Figure 4.12.A Influence of k1 on $AUC^{t}_{0,T} / AUC^{t}_{0,C}$. 1: k1= 0.1, 2: k1= 0.5, 3: k1= 0.9.

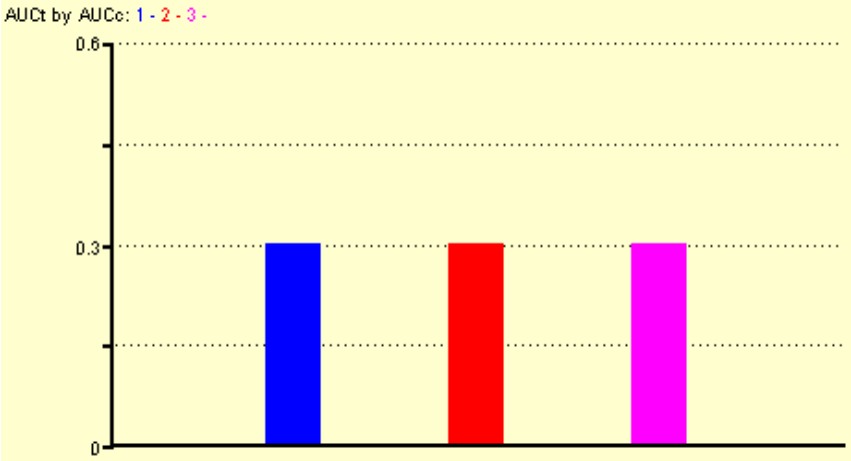

Figure 4.12.B Influence of k1 on R ($AUC^{\infty}_{0,T} / AUC^{\infty}_{0,C}$). 1: k1= 0.1, 2: k1= 0.5, 3: k1= 0.9.

Table 4-4 The estimated values of kout by the two partial-areas analysis.

Nominal k_{out} (hr^{-1})	Estimated k_{out} (hr^{-1})	
	Cumulative partial-areas analysis	Interval partial-areas analysis
2	1.9997	1.9984
0.2	0.2	0.2
0.02	0.02	0.02

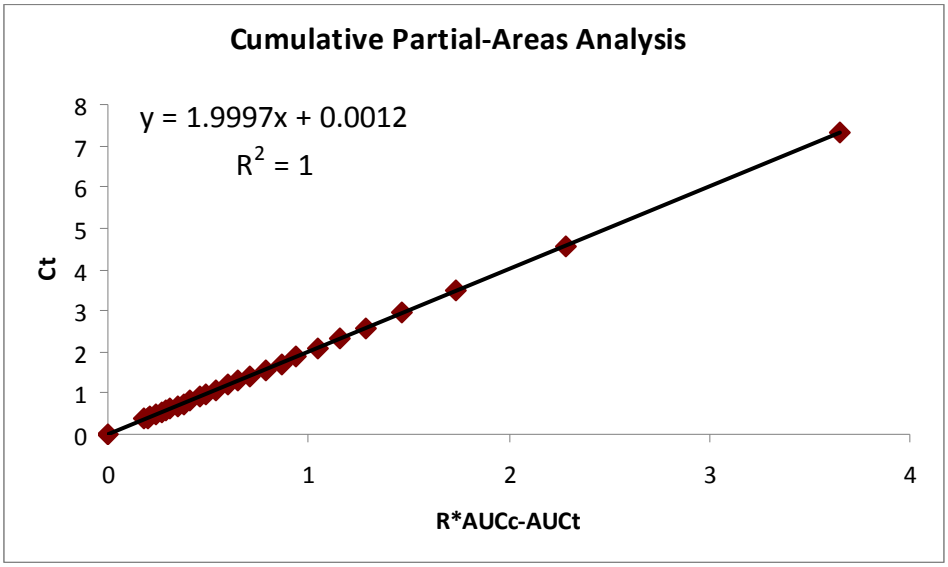

Figure 4.13.A Linear regression by cumulative partial-areas analysis when nominal k_{out} = $2hr^{-1}$

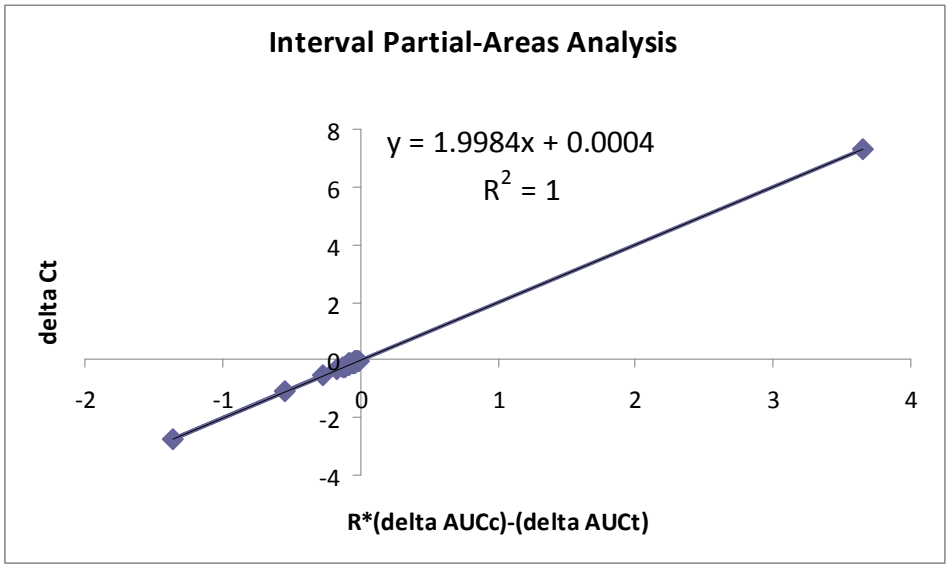

Figure 4.13.B Linear regression by interval partial-areas analysis when nominal k_{out} = $2hr^{-1}$

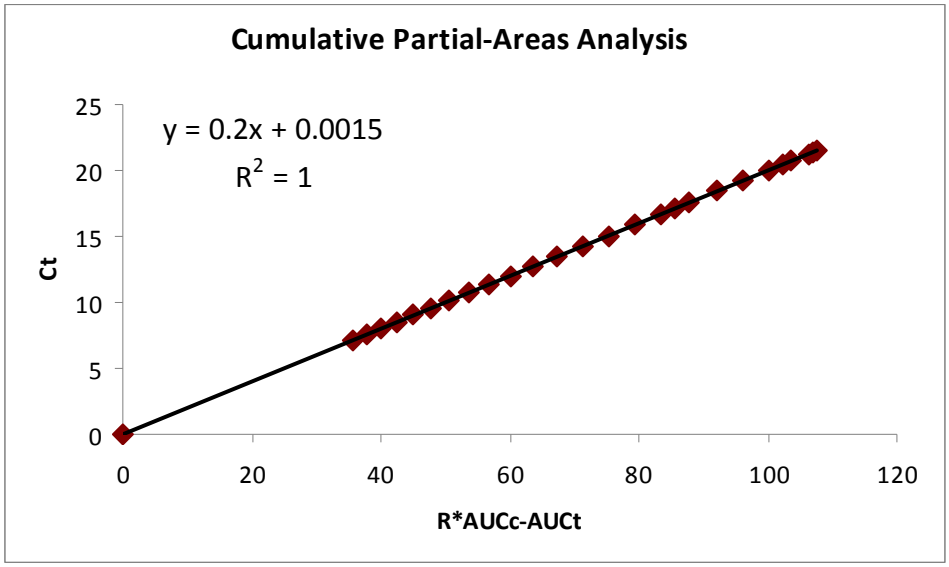

Figure 4.14.A Linear regression by cumulative partial-areas analysis when nominal k_{out} = $0.2hr^{-1}$

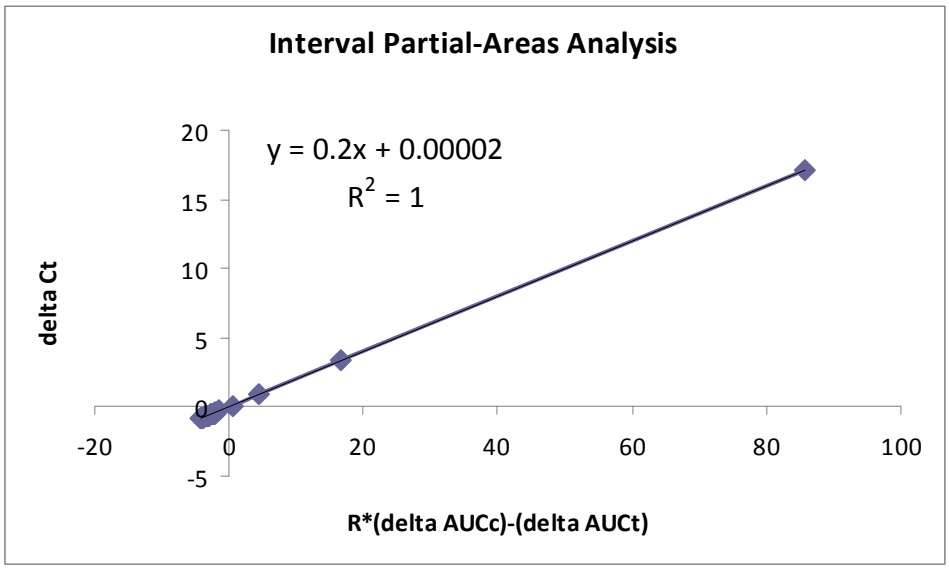

Figure 4.14.B Linear regression by interval partial-areas analysis when nominal k_{out} = $0.2hr^{-1}$

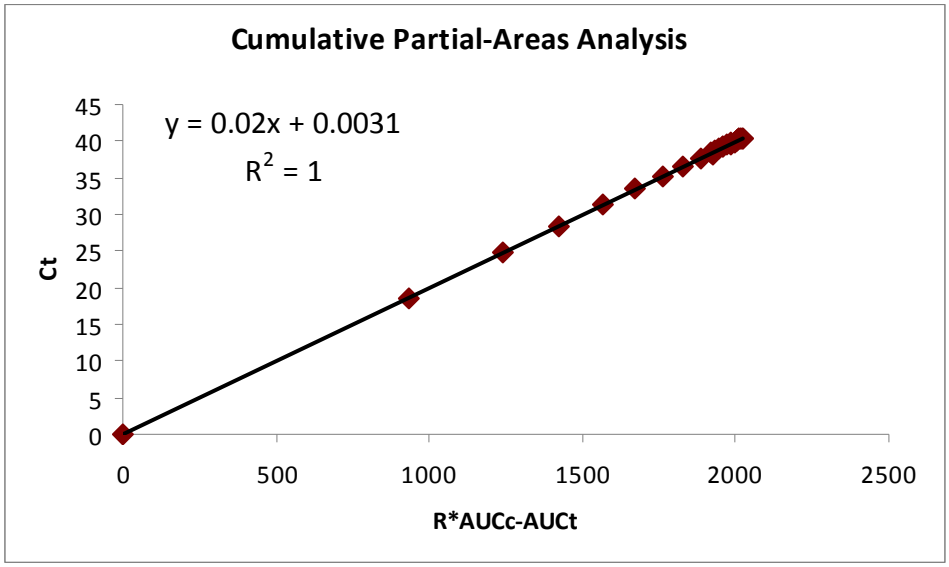

Figure 4.15.A Linear regression by cumulative partial-areas analysis when nominal k_{out} = 0.02hr^{-1}

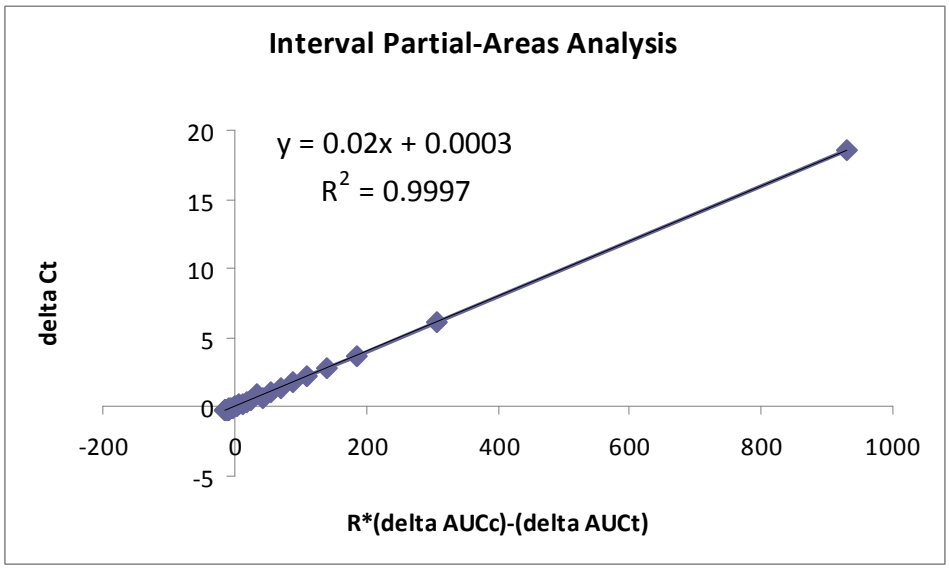

Figure 4.15.B Linear regression by interval partial-areas analysis when nominal k_{out} = 0.02hr^{-1}

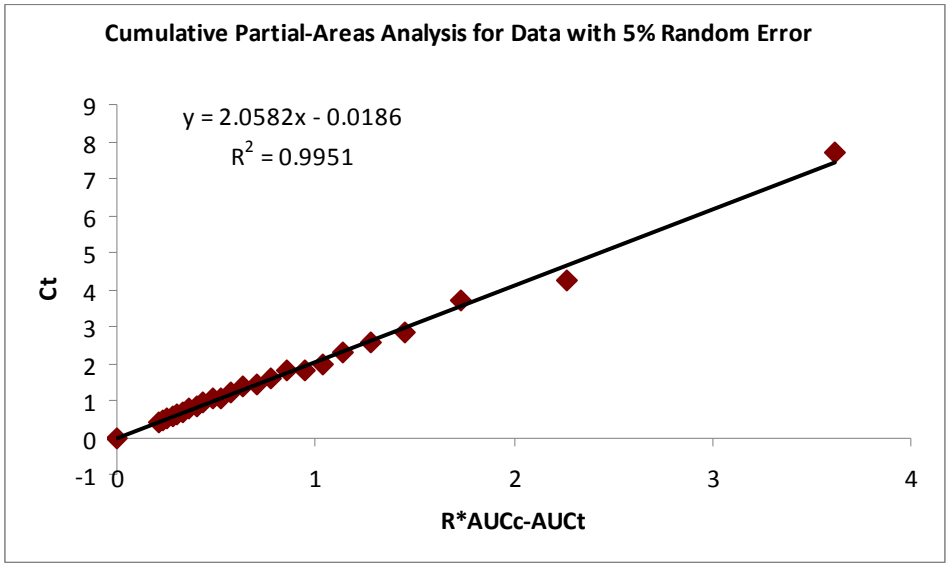

Figure 4.16.A Linear regression by cumulative partial-areas analysis when concentration data have 5% error

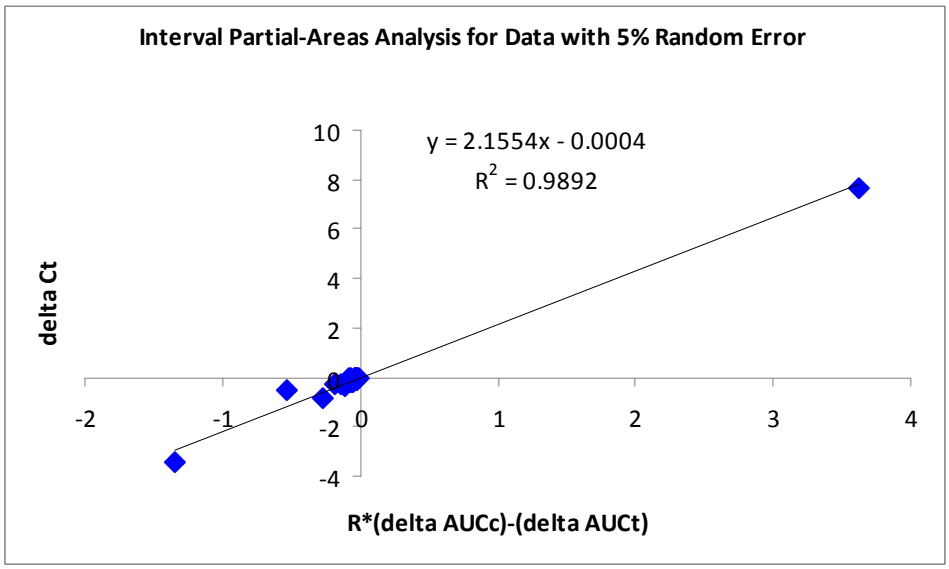

Figure 4.16.B Linear regression by interval partial-areas analysis when concentration data have 5% error

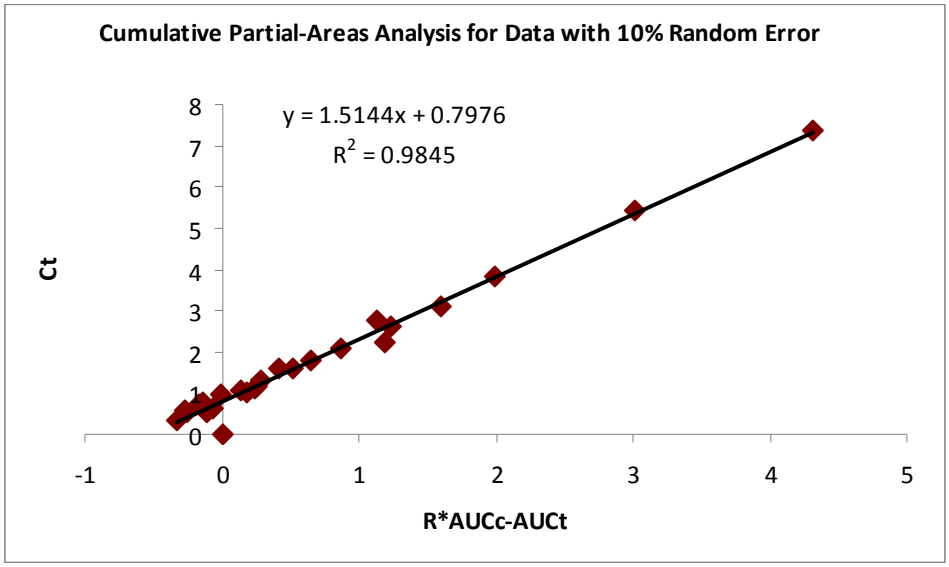

Figure 4.17.A Linear regression by cumulative partial-areas analysis when concentration data have 10% error

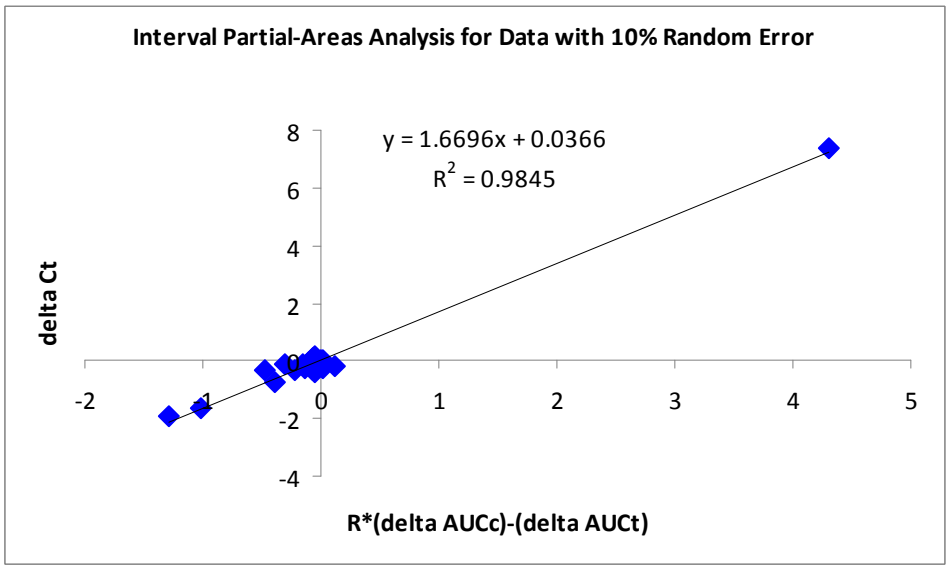

Figure 4.17.B Linear regression by interval partial-areas analysis when concentration data have 10% error

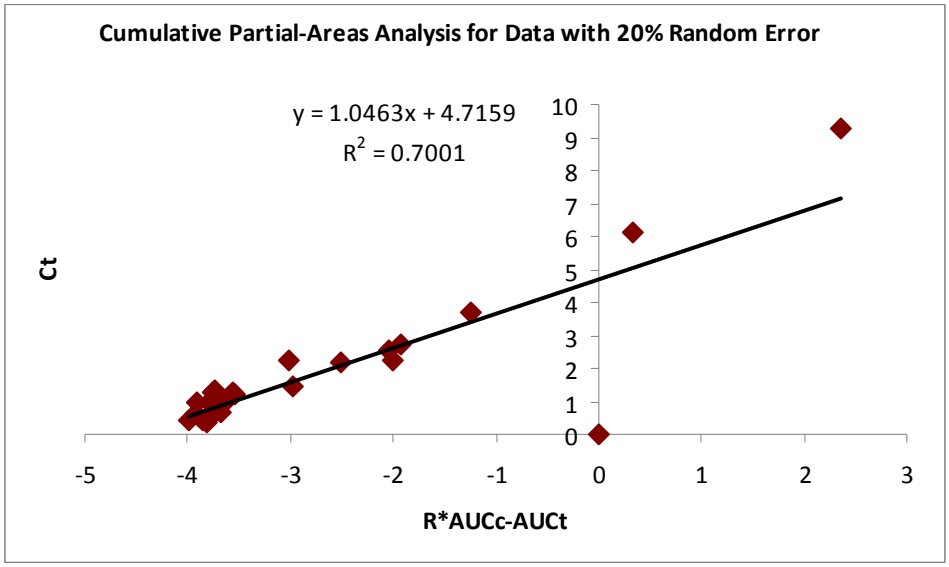

Figure 4.18.A Linear regression by cumulative partial-areas analysis when concentration data have 20% error

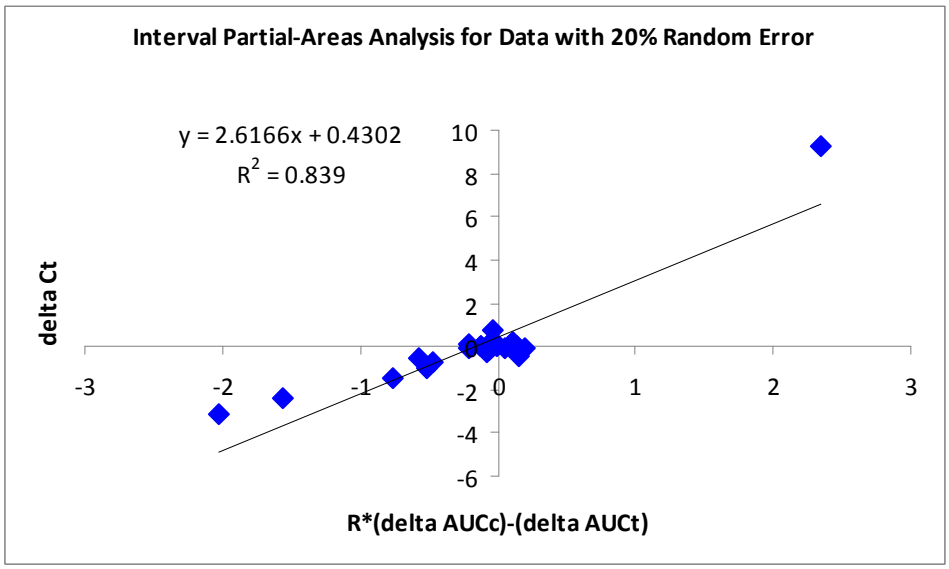

Figure 4.18.B Linear regression by interval partial-areas analysis when concentration data have 20% error

Table 4-5 Estimated values of kout by the two partial-areas analysis when concentration data had 5%, 10%, and 20% error.

Simulation No.	5% error		10% error		20% error	
	kout by cumulative partial-areas analysis	kout by interval partial-areas analysis	kout by cumulative partial-areas analysis	kout by interval partial-areas analysis	kout by cumulative partial-areas analysis	kout by interval partial-areas analysis
1	1.8868	1.9938	1.9082	1.5398	1.0463	2.6166
2	1.8535	2.132	1.5144	1.6696	1.0973	1.5407
3	2.0743	2.0369	1.6456	2.6653	1.1959	1.82
4	1.9687	1.7929	2.0847	2.2977	1.265	1.4991
5	1.8898	1.7843	2.078	2.5911	1.214	1.2814
6	2.1542	2.1779	2.1163	1.8668	1.2695	2.7409
7	2.0341	2.3574	2.063	1.9169	1.9048	2.0651
8	1.8523	1.8108	1.8313	1.6693	1.6142	1.4736
9	1.8911	1.8273	1.3384	2.1196	1.2543	1.5709
10	1.9132	2.1112	1.7765	2.003	1.6463	1.8948
11	1.8781	2.5541	2.264	1.9752	1.7522	2.7485
12	2.0952	1.9999	1.5271	1.8259	2.1791	3.4013
13	1.8673	2.0612	1.5047	1.9609	1.7039	1.9836
14	1.9536	1.9702	2.1847	2.1132	1.2149	1.2957
15	1.7598	1.7125	2.3544	2.199	1.8441	2.2404
16	2.049	1.998	1.6433	1.6267	1.0787	1.0875
17	1.7918	1.8161	2.1658	2.6684	1.0939	1.4803
18	1.9326	2.1848	1.7698	2.2782	0.9645	2.3464
19	1.6465	1.8623	1.3097	1.3329	1.4992	1.3516
20	1.9595	1.8833	1.4199	1.9295	1.6787	2.1707
Mean	1.92257	2.003345	1.82499	2.01245	1.42584	1.930455
SD	0.120838	0.210295	0.326324	0.366002	0.276202	0.609998

Table 4-6 Statistical comparison of the estimated k_{out} values by two methods when residual error was set to be 5%, 10%, and 20%.

a. t-Test: Paired two sample for means (5% error)

	Variable 1	*Variable 2*
Mean	1.92257	2.003345
Variance	0.014601907	0.04422414
Observations	20	20
Pearson Correlation	0.352426349	
Hypothesized Mean Difference	0	
df	19	
t Stat	-1.78588414	
P(T<=t) one-tail	0.045044453	
t Critical one-tail	1.729132792	
P(T<=t) two-tail	0.090088905	
t Critical two-tail	2.09302405	

** variable 1 – $\mathbf{k_{out}}$ from cumulative partial-areas analysis
variable 2 – $\mathbf{k_{out}}$ from interval partial-areas analysis

b. t-Test: Paired two sample for means (10% error)

	Variable 1	*Variable 2*
Mean	1.82499	2.01245
Variance	0.10648715	0.13395734
Observations	20	20
Pearson Correlation	0.39880091	
Hypothesized Mean Difference	0	
df	19	
t Stat	-2.2002191	
P(T<=t) one-tail	0.02018163	
t Critical one-tail	1.72913279	
P(T<=t) two-tail	0.04036327	
t Critical two-tail	2.09302405	

c. t-Test: Paired two sample for means (20% error)

	Variable 1	*Variable 2*
Mean	1.42584	1.930455
Variance	0.11718268	0.372098
Observations	20	20
Pearson Correlation	0.48572682	
Hypothesized Mean Difference	0	
df	19	
t Stat	-4.2166545	
P(T<=t) one-tail	0.00023361	
t Critical one-tail	1.72913279	
P(T<=t) two-tail	0.00046722	
t Critical two-tail	2.09302405	

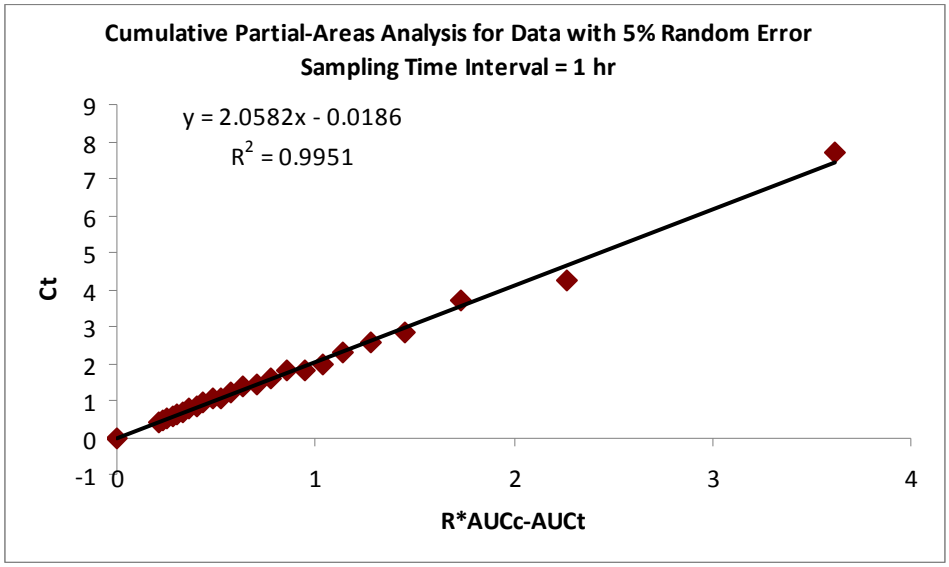

Figure 4.19.A Linear regression by cumulative partial-areas analysis when time-interval was 1 hr.

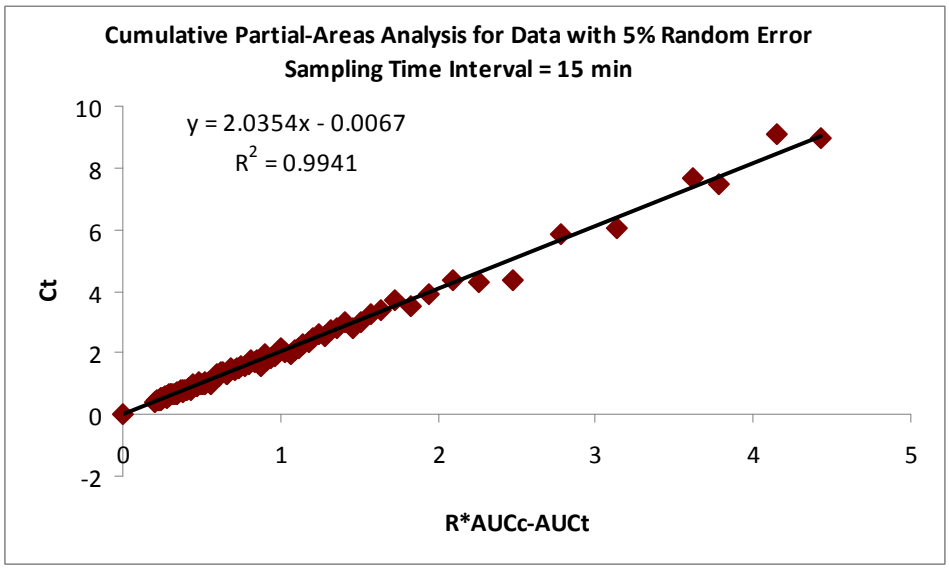

Figure 4.19.B Linear regression by cumulative partial-areas analysis when time-interval was 15 min.

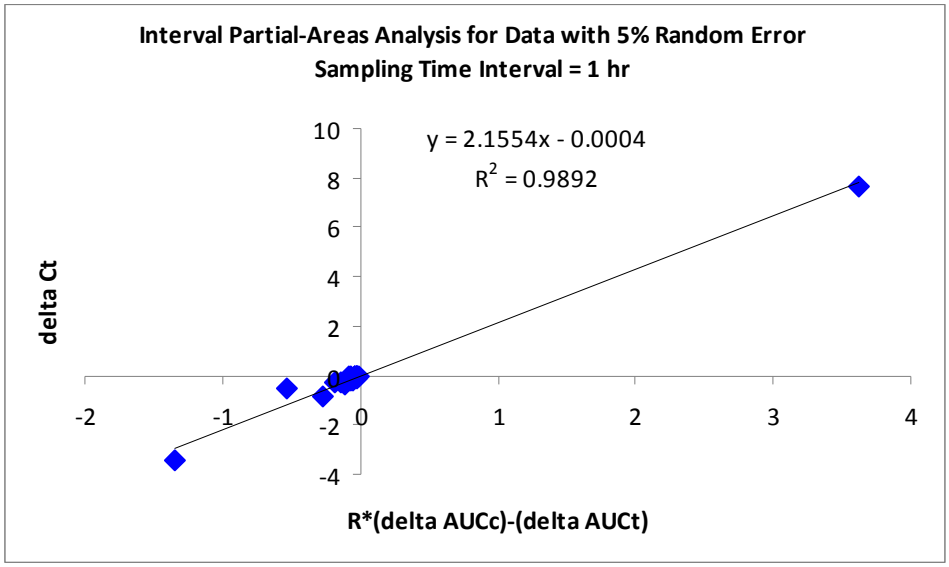

Figure 4.20.A Linear regression by interval partial-areas analysis when time-interval was 1 hr.

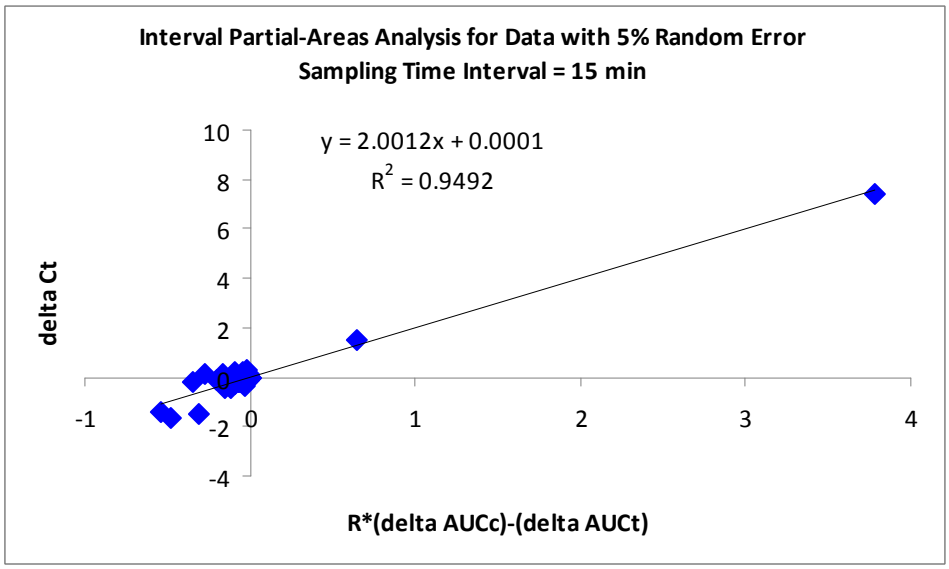

Figure 4.20.B Linear regression by interval partial-areas analysis when time-interval was 15 min.

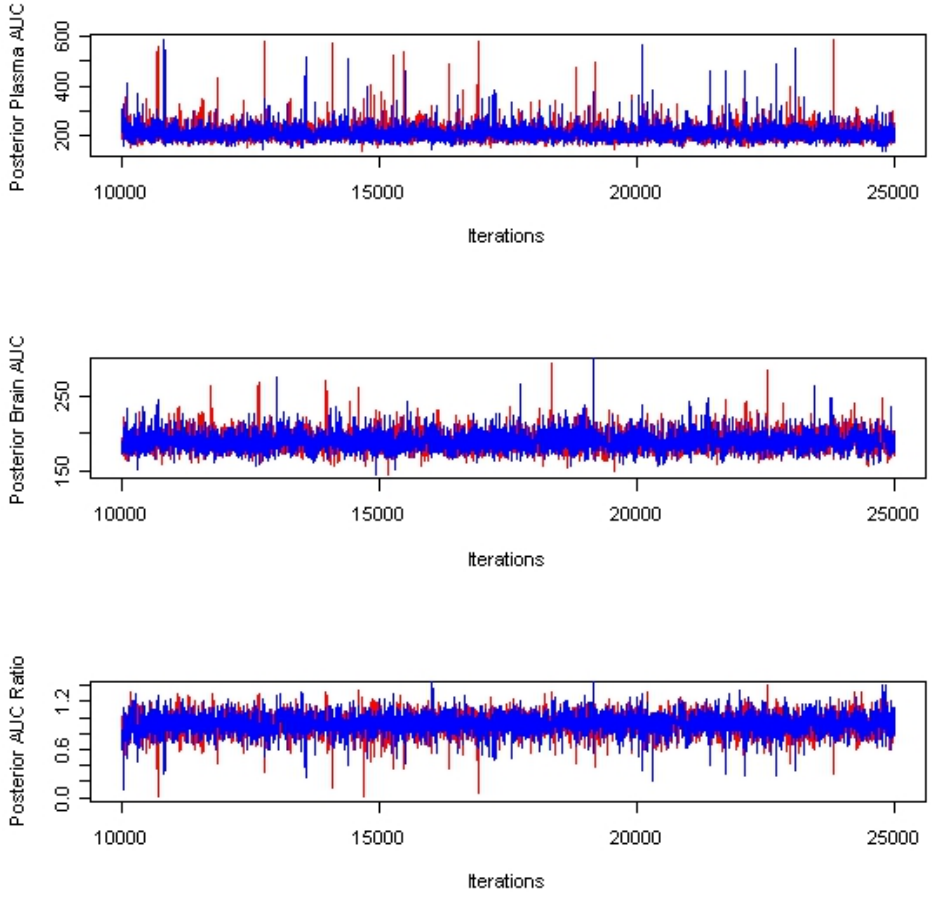

Figure 4.21 Traceplots of the posterior parameters for the simulated data (A: $AUC^{\infty}_{0,pl}$, B: $AUC^{\infty}_{0,br}$ C: $\frac{AUC^{\infty}_{0,br}}{AUC^{\infty}_{0,pl}}$). Red: chain 1; Blue: chain 2.

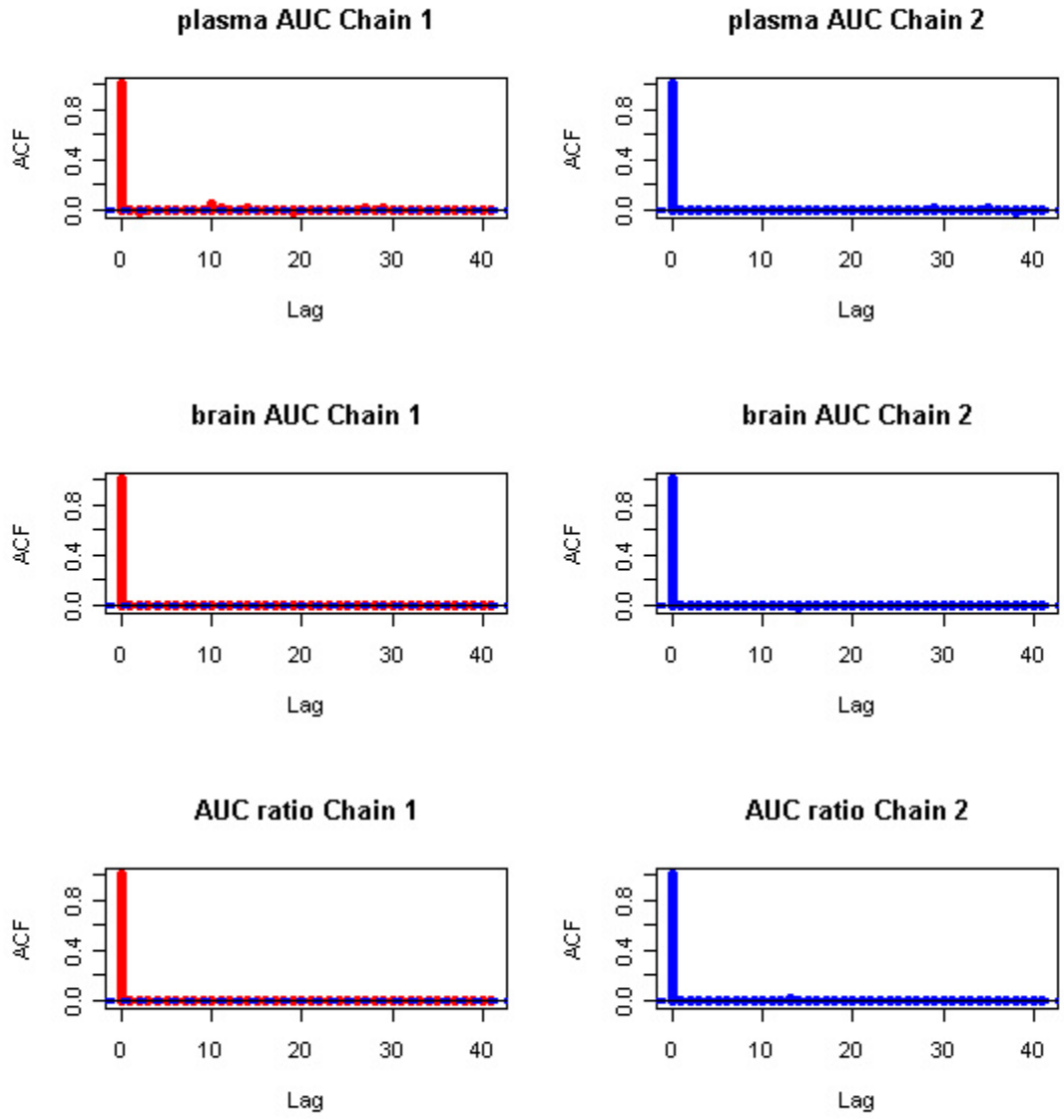

Figure 4.22 Auto-correlation plots of the posterior parameters for the simulated data ((Top panel: $AUC^{\infty}_{0,pl}$; Middle panel: $AUC^{\infty}_{0,br}$; Bottom panel: $\frac{AUC^{\infty}_{0,br}}{AUC^{\infty}_{0,pl}}$).

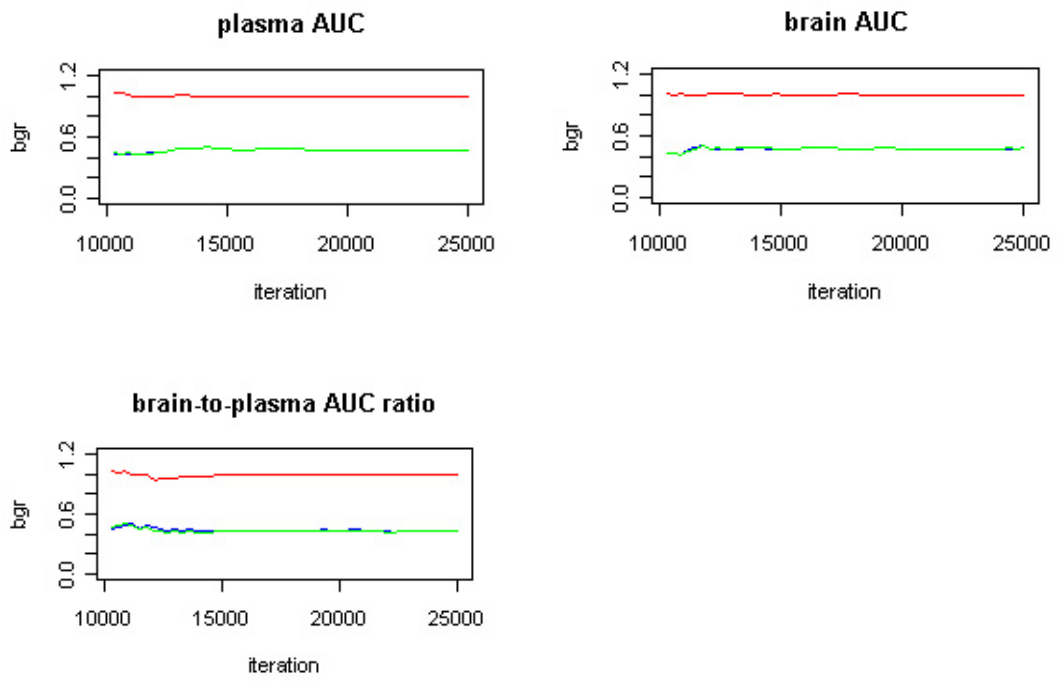

Figure 4.23 Gelman-Rubin diagnostics of the posterior parameters for the simulated data (Top left: $AUC_{0,pl}^{\infty}$; Top right: $AUC_{0,br}^{\infty}$; Bottom: $\frac{AUC_{0,br}^{\infty}}{AUC_{0,pl}^{\infty}}$).

Table 4-7 Evaluation of the robustness of posterior estimators of $AUC_{0,pl}^{\infty}$, $AUC_{0,br}^{\infty}$ and $\frac{AUC_{0,br}^{\infty}}{AUC_{0,pl}^{\infty}}$ obtained by the Bayesian approach based on 100 Monte Carlo simulations (See next page).

Simulation	Parameter	Norminal Population Mean	Averaged Posterior Mean	Avaraged Posterior Median	Probability of 95% Credible Intervals Containing the True Population Mean	Probability of Lower Credible Limit Less Than Zero
Low Variability (5% BAV + 5% WAV)	AUC pl	200.15	209.5	202.72	94%	0
	AUC br	200.15	209.38	206.69	97%	0
	AUC br / AUC pl	1	1.03	1.02	100%	0
High Variability (20% BAV + 20% WAV)	AUC pl	200.15	730.9	233.29	94%	0
	AUC br	200.15	496.84	222.79	93%	0
	AUC br / AUC pl	1	2.01	1	99%	0

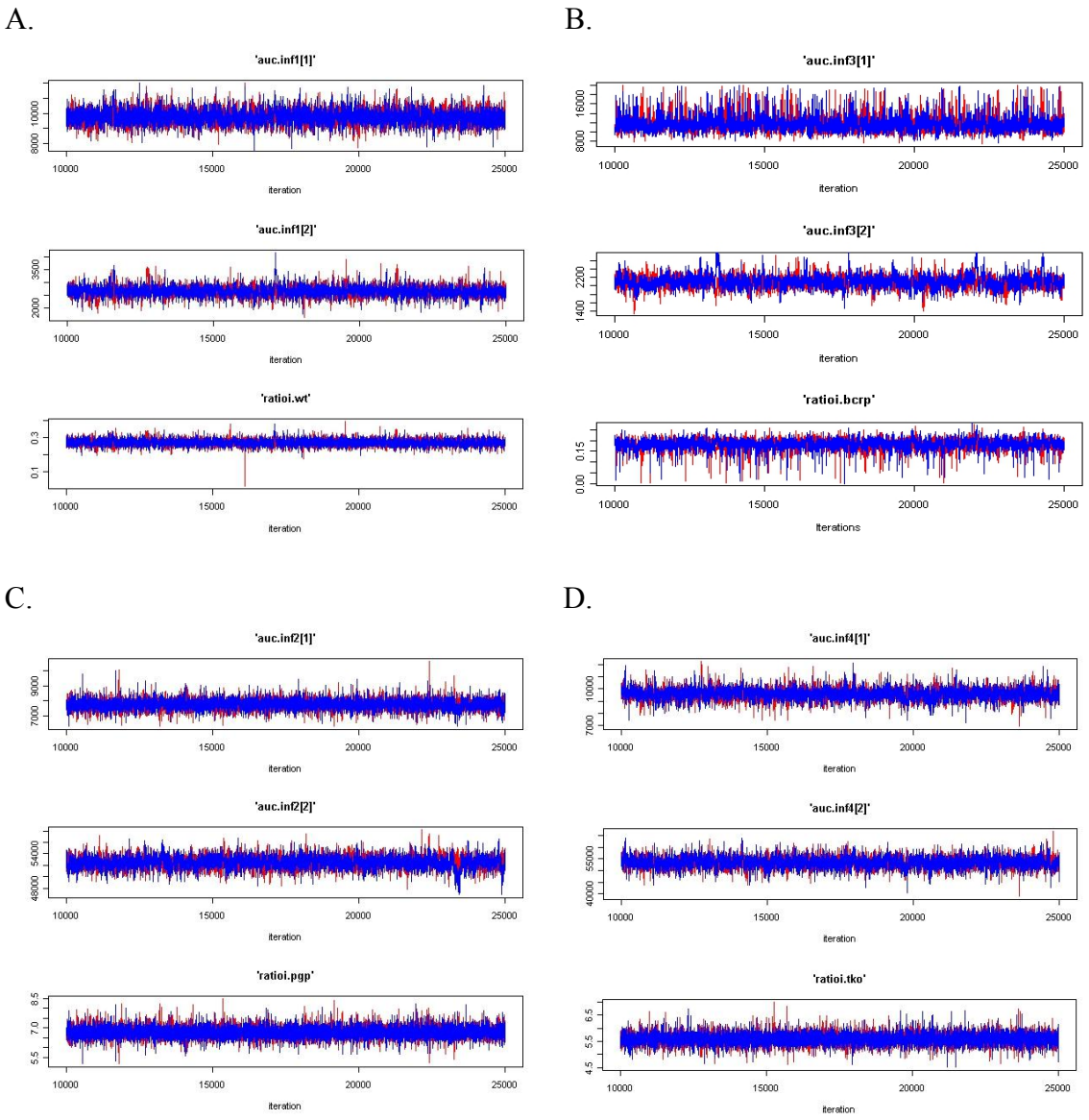

Figure 4.24 Traceplots of the posterior parameters for the FVB mice with the i.v. dose of cediranib. A. Wild-type mice; B. *Bcrp1(-/-)* mice; C. *Mdr1a/b(-/-)* mice; D. *Mdr1a/b(-/-)Bcrp1(-/-)* mice . (Top panel: $AUC_{0,pl}^{\infty}$; Middle panel: $AUC_{0,br}^{\infty}$; Bottom panel: $\frac{AUC_{0,br}^{\infty}}{AUC_{0,pl}^{\infty}}$.)

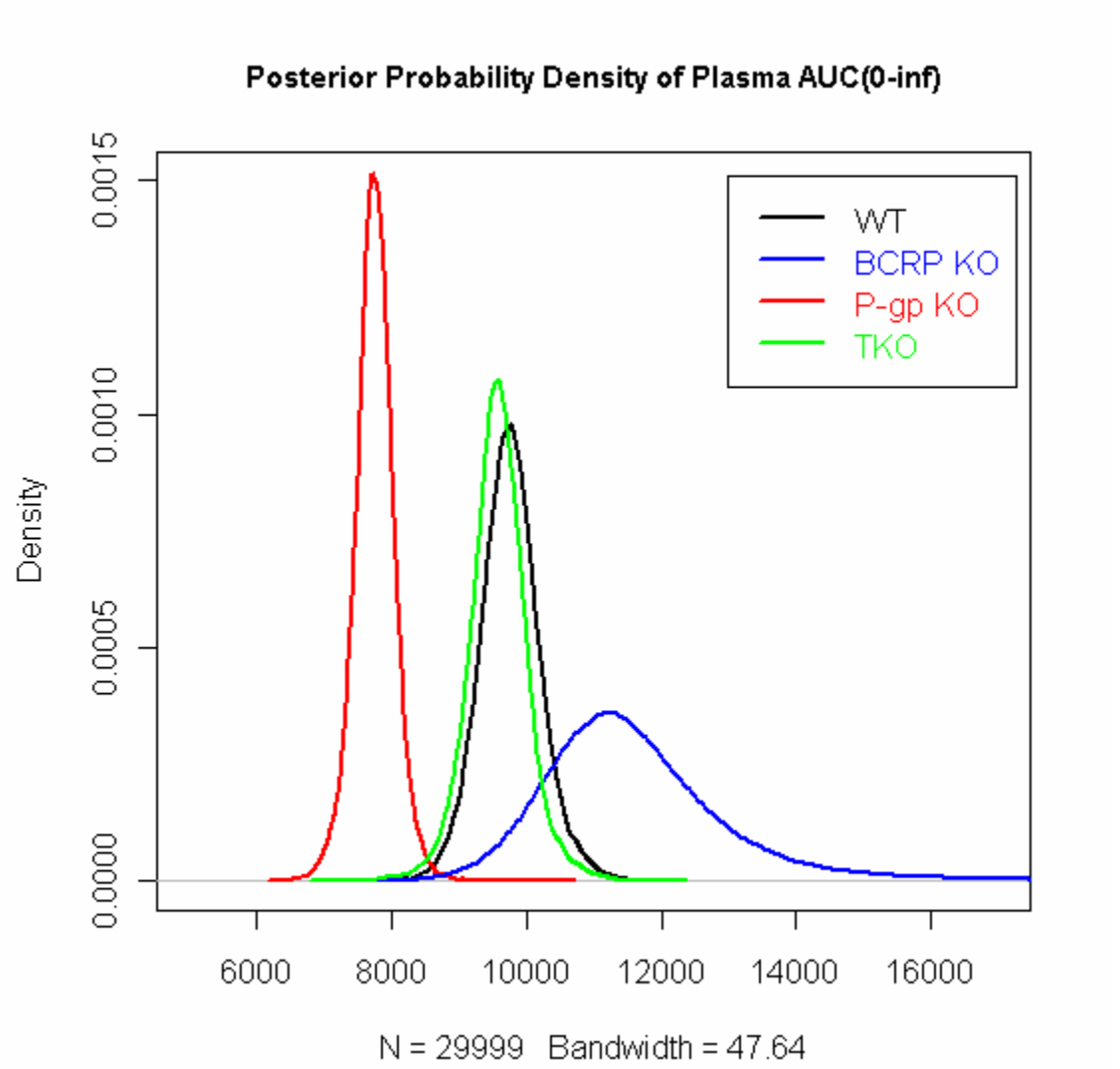

Figure 4.25 Posterior distributions of the plasma AUC_0^∞ in four genotypes of brain efflux transporters. Black: wild-type mice; Blue: *Bcrp1(-/-)* mice; Red: *Mdr1a/b(-/-)* mice; Green: *Mdr1a/b(-/-)Bcrp1(-/-)* mice.

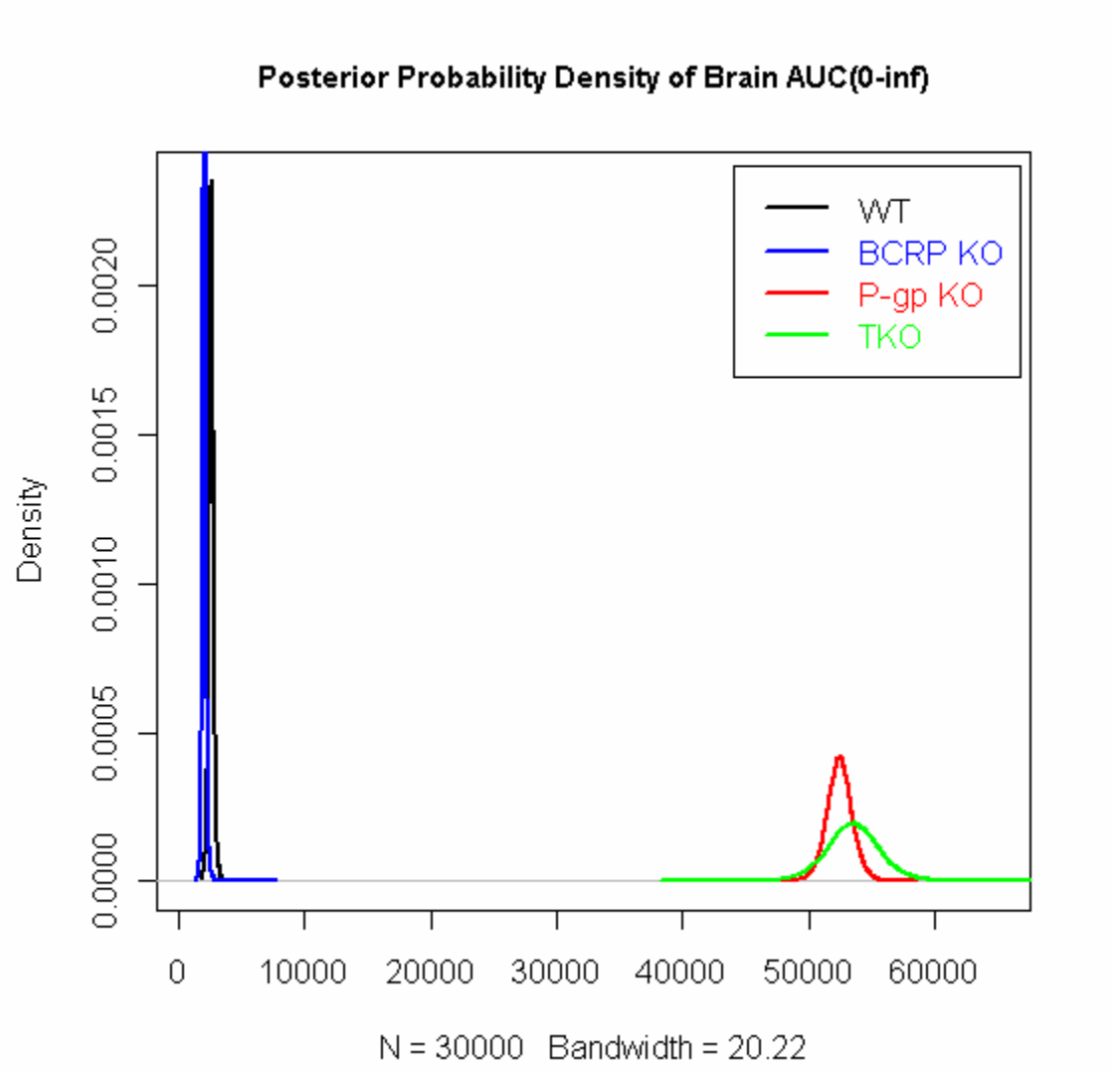

Figure 4.26 Posterior distributions of the brain AUC_0^∞ in four genotypes of brain efflux transporters. Black: wild-type mice; Blue: *Bcrp1(-/-)* mice; Red: *Mdr1a/b(-/-)* mice; Green: *Mdr1a/b(-/-)Bcrp1(-/-)* mice.

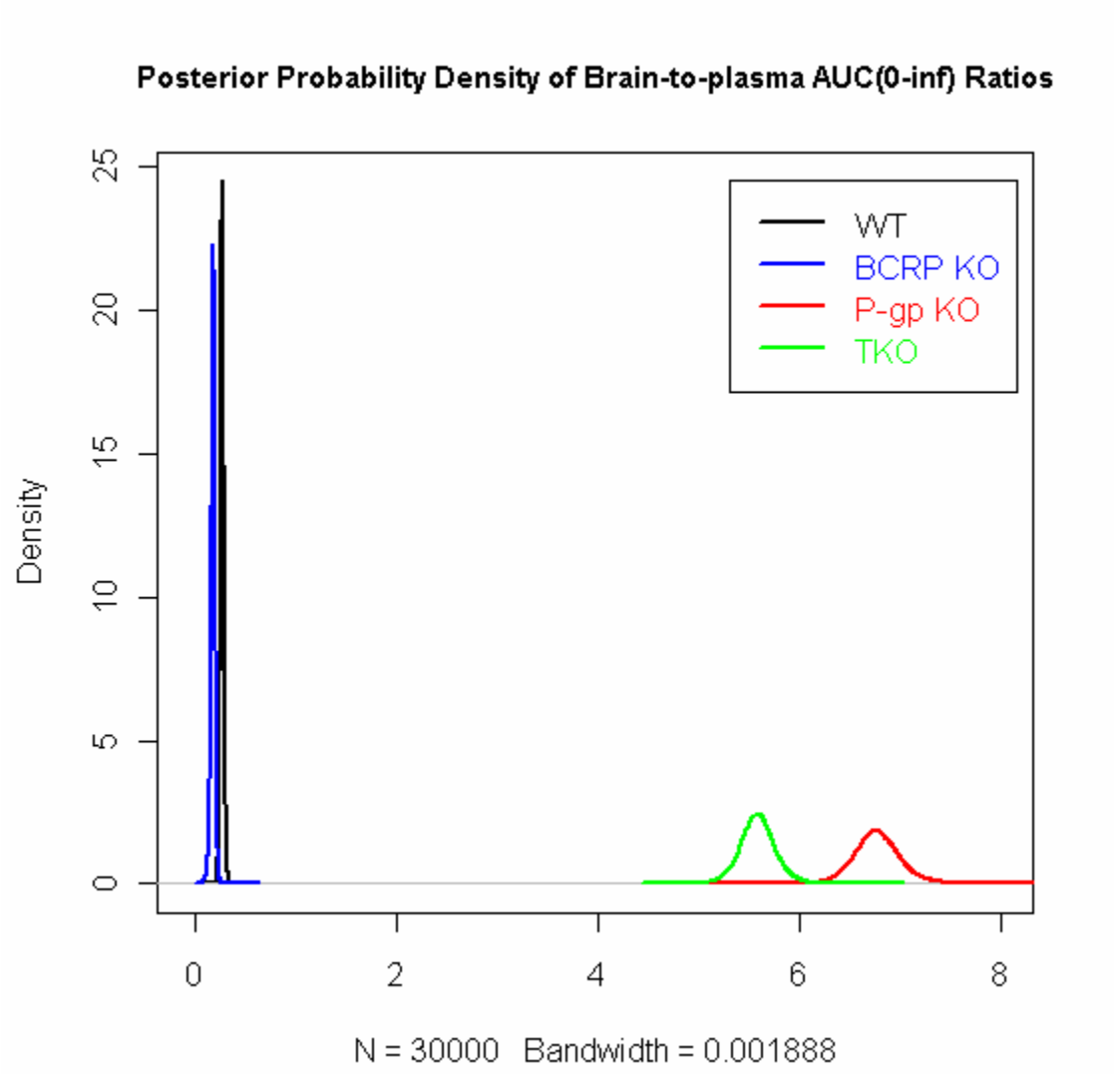

Figure 4.27 Posterior distributions of the brain-to-plasma AUC ratio ($\frac{AUC_{0,br}^{\infty}}{AUC_{0,pl}^{\infty}}$) in four genotypes of brain efflux transporters. Black: wild-type mice; Blue: *Bcrp1(-/-)* mice; Red: *Mdr1a/b(-/-)* mice; Green: *Mdr1a/b(-/-)Bcrp1(-/-)* mice.

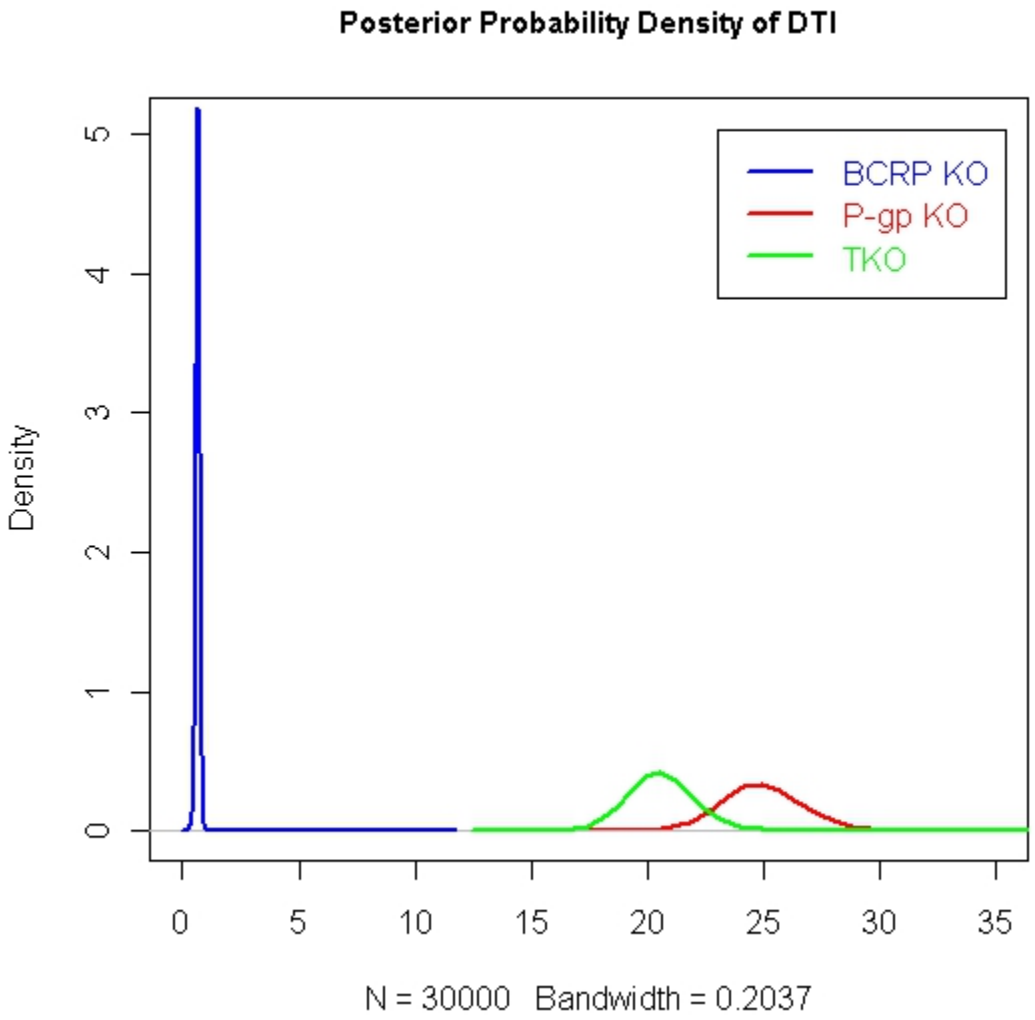

Figure 4.28 Posterior distributions of the brain drug targeting indexs (DTI) for the three transporter knockout mice. Blue: *Bcrp1(-/-)* mice; Red: *Mdr1a/b(-/-)* mice; Green: *Mdr1a/b(-/-)Bcrp1(-/-)* mice.

Table 4-8 Bayesian posterior mean and 95% credible interval (C.I.) of the plasma and brain AUC_0^{∞} s and their ratios and the comparison with the point estimate and 95% confidence interval (C.I.*) estimated by the Bailer's approximation extended by Yuan.

Parameter	Bayesian Estimator		Yuan's extention of Bailer's method	
	Mean	95% C.I.	Mean	95% C.I.*
AUC(0-inf,pl)$_{WT}$	9771	(8883, 10720)	9697	(9295, 10099)
AUC(0-inf,br)$_{WT}$	2656	(2252, 3085)	2661	(2561, 2761)
AUC(0-inf,pl)$_{BCRPKO}$	12000	(9446, 15780)	10220	(8748, 11692)
AUC(0-inf,br)$_{BCRPKO}$	2095	(1805, 2414)	1997	(1915, 2079)
AUC(0-inf,pl)$_{PgpKO}$	7754	(7140, 8351)	7785	(7558, 8012)
AUC(0-inf,br)$_{PgpKO}$	52450	(50290, 54540)	52560	(51751, 53369)
AUC(0-inf,pl)$_{TKO}$	9582	(8690, 10500)	8408	(8163, 8653)
AUC(0-inf,br)$_{TKO}$	53500	(48960, 58080)	51966	(50733, 53199)
AUC(0-inf,br)$_{WT}$/AUC(0-inf,pl)$_{WT}$	0.27	(0.24, 0.31)	0.27	-
AUC(0-inf,br)$_{BCRPKO}$/AUC(0-inf,pl)$_{BCRPKO}$	0.18	(0.13, 0.22)	0.2	-
AUC(0-inf,br)$_{PgpKO}$/AUC(0-inf,pl)$_{PgpKO}$	6.77	(6.30, 7.30)	6.75	-
AUC(0-inf,br)$_{TKO}$/AUC(0-inf,pl)$_{TKO}$	5.59	(5.22, 5.97)	6.18	-

Table 4-9 Comparisons of Bayesian posterior mean, standard deviation (SD) and 95% credible interval (C.I.) for partial AUCs (the AUC up to the last sampling time point) in four genotypes of transporters with Bailer-Satterthwaite approximation of mean, SD and 95% confidence interval (C.I.*) estimated by Phoenix WinNonlin.

Parameter	Bayesian Estimator			Bailer-Satterthwaite Estimator		
	Mean	SD	95% C.I.	Mean	SD	95% C.I.*
$AUC(0\text{-last,pl})_{WT}$	9213	419	(8386, 10090)	9200	364	(8487, 9913)
$AUC(0\text{-last,br})_{WT}$	2459	199	(2066, 2879)	2449	162	(2131, 2767)
$AUC(0\text{-last,pl})_{PgpKO}$	7384	300	(6774, 7980)	7396	243	(6920, 7872)
$AUC(0\text{-last,br})_{PgpKO}$	48150	993	(46120, 50110)	48186	807	(46604, 49768)
$AUC(0\text{-last,pl})_{BCRPKO}$	9502	639	(8240, 10830)	8393	387	(7634, 9152)
$AUC(0\text{-last,br})_{BCRPKO}$	2034	148	(1750, 2343)	1947	113	(1726, 2168)
$AUC(0\text{-last,pl})_{TKO}$	9490	442	(8603, 10410)	8307	407	(7509, 9105)
$AUC(0\text{-last,br})_{TKO}$	52710	2260	(48170, 57220)	51107	1918	(47348, 54866)

CHAPTER 5

EFFECT OF ANTI-ANGIOGENIC THERAPY ON DRUG DELIVERY TO BRAIN TUMOR SITE

The delivery of effective anti-tumor agents across an intact BBB in different regions of a brain tumor remains an important concern in the effort to treat primary brain tumors, such as glioblastoma (GBM), and secondary, metastatic brain tumors. Anti-angiogenic therapy (AAT) targeting the VEGF-mediated signaling pathway is an important component of treatment for recurrent GBM and many novel therapeutic strategies are being developed in combination with AAT as the next generation of clinical trials for GBM. However, the efficacy of combination regimens of AAT with conventional or novel therapeutics may be variably affected by AAT-mediated restoration of BBB integrity and function on brain tumor vasculature. GBM12 (a human GBM) intracranial xenografts were treated with combination AAT (e.g., avastin or cediranib) and chemotherapy (e.g., temozolomide and erlotinib) to examine drug delivery (site-specific pharmacokinetics) to the tumor core, rim and normal brain. This study helped in understanding the potential impact of AAT on brain tumor drug delivery, and may help guide the rational development of AAT combination strategies for recurrent GBM.

5.1 Introduction

For CNS therapeutic agents, access via the blood-brain barrier (BBB) is limited physically by tight junctions between endothelial cells and functionally through the activity of drug efflux pumps acting on the luminal side of the capillary endothelial cells. However, during gliomagenesis, the BBB is partially disrupted by loss of robust tight junctions between endothelial cells. There are some regions of relatively open BBB called tumor ‘core’ and other regions with an intact BBB such as tumor ‘rim’ and part of

normal brain (Agarwal et al., 2011). It is therefore essential to adequately deliver effective treatment to different regions of the brain tumor in order to prevent tumor recurrence.

Anti-angiogenic therapy (AAT) targeting the vascular endothelial growth factor (VEGF)-mediated signaling is an important component of treatment for recurrent GBM (Butowski, 2011). Many novel therapeutic strategies are being developed in combination with AAT as the next generation of clinical trials for GBM (Table 5-1). Since aberrant VEGF signaling promotes BBB disruption in GBM, anti-VEGF therapy normalizes tumor vasculature and results in a significant reduction in contrast accumulation in GBM patients (Batchelor et al., 2007; van den Bent et al., 2009). However, uptil now, few studies have examined the influence of AAT on the delivery of concomitant therapy in the treatment of glioma. These studies have all focused on the angiogenic tumor core, and have examined the tumor distribution of relatively BBB permeable drugs only, such as temozolomide. For example, recently Zhou and Gallo reported the effect of an anti-angiogenic agent sunitinib on the brain tumor distribution of temozolomide in a dose-dependent manner (Zhou and Gallo, 2009). It has been observed that low dose of sunitinib resulted in adequate normalization of tumor vasculature, determined by CD31 staining of the brain endothelial cells, to an extent that the tumor delivery of temozolomide was optimized. Despite of the encouraging result of sunitinib on temozolomide, it has been seen that there exists a converse interaction between AAT and other anti-tumor drugs. Vandetanib (ZD6474, Zactima), a tyrosine-kinase inhibitor

against VEGFR2, reduced the apoptotic effects of temozolomide in a xenograft glioma model (Claes et al., 2008). The authors here suggested that this was due to vandetanib-induced BBB normalization that limited the temozolomide tumor penetration. These data highlight a potentially complex interaction between AAT and chemotherapeutic agents with different mechanisms.

Bevacizumab (Avastin®) is a monoclonal antibody directed against the VEGF ligand, VEGF-A. Treatment with avastin can lead to normalization of tumor vasculature in GBM patients within days of starting therapy (Thompson et al., 2011). Given the clinical single agent activity and FDA approval for avastin treatment in recurrent GBM, there is significant enthusiasm for evaluating combinations of avastin with other therapeutic agents in recurrent GBM. However, the majority of avastin combination regimens being clinically tested are developed empirically without pre-clinical testing in clinically relevant orthotopic xenograft models and without consideration for the potential detrimental effect of AAT on drug delivery across a normalized BBB.

Cediranib acts intracellularly to inhibit VEGF-receptor kinase activity in endothelial cells. In a recent clinical trial, cediranib failed to demonstrate a significant survival benefit in recurrent GBM similar to avastin (T. Batchelor, 2010 Society of NeuroOncology Annual Meeting). In Chapter 3 in this thesis, we have shown approximately 20-fold higher cediranib brain distribution in MDR1a/b (P-gp) and MDR1a/b/BCRP1 triple knock-out mice as compared to wild-type mice. Moreover, co-treatment of wild-type mice with the

P-gp/BCRP1 inhibitor elacridar increases the brain to plasma ratio of cediranib by 17-fold. Thus, activity of drug efflux pumps within the BBB may account for the reduced efficacy of cediranib as compared to avastin therapy. In order to test the hypothesis, that the reduced clinical activity of cediranib is related to inadequate drug delivery to the relevant target, the effects of both avastin and cediranib were studied in the primary xenograft model of GBM.

Primary GBM xenografts were developed by directly implanting GBM tumors from patients into nude mice. These xenograft lines faithfully maintain key histologic and molecular features of the original human GBM, including elevated invasion, EGFR amplification and MGMT promoter methylation status (Giannini et al., 2005; Carlson et al., 2009). The Mayo GBM xenograft panel used in this study is recognized as a highly relevant model system for evaluating glioma biology (Giannini et al., 2005; Carlson et al., 2011).

As detailed in Table 5-1, the majority of novel therapeutic agents for GBM currently being studied in combination with AAT are at least partially excluded by the BBB, and can be broadly classified as: i) conventional cytotoxic agents, ii) molecularly targeted agents, and iii) therapeutic antibodies. Thus, it becomes imperative to explore the effect of AAT on BBB integrity, and hence drug delivery, for the rational development of AAT combination strategies for recurrent GBM. Here, in this study we have focused on the first two categories of agents and specifically evaluated the influence of AATs, such as avastin and cediranib, on tumor accumulation of a cytotoxic drug, temozolomide

(Schering-Plough Corporation, Kenilworth, NJ), and a tyrosine kinase inhibitor, erlotinib (OSI Pharmaceuticals, Inc., Melville, NY).

5.2 Material and methods

5.2.1 Chemicals and Mayo GBM xenograft model

5.2.1.1 Chemicals

Avastin was purchased from Genentech (San Francisco, CA, USA). Cediranib was procured from Selleck Chemicals LLC (Houston, TX, USA). Temozolomide and erlotinib were purchased from Toronto Research Chemicals (North York, On., Canada) and LC laboratories (Woburn, MA, USA), respectively. All other chemicals used were HPLC or reagent grade.

5.2.1.2 Mayo GBM xenograft model

Mayo GBM xenograft line (GBM12) was transduced into six week-old female nude mice with a lentiviral construct pSIN-fLuc-eGFP(enhanced green fluorecent protein) construct to provide both bioluminescent and fluorescent tumor detection. Tumor growth in the model was monitored by bioluminescence imaging. They were housed in a pathogen-free facility accredited by the Association for the Assessment and Accreditation of Laboratory Animal Care (AAALAC). This animal model was done in collaboration with Dr. Jann N. Sarkaria, from Mayo Clinic.

5.2.2 Determine the effect of anti-angiogenic treatment on drug delivery to tumor sites

Seven days after implant, mice with established intracranial tumors, as determined by luciferase imaging, were randomized into 3 groups of 12 mice each and treated for 9 days with the following regimens: 1) placebo, 2) avastin 5 mg/kg dosed twice weekly by intraperitoneal injection (i.p.), and 3) cediranib 6mg/kg dosed daily by oral gavage (p.o.). On day 9, mice were euthanized. Prior to euthanization, all mice were dosed orally with temozolomide 66 mg/kg and erlotinib 100 mg/kg. Time of dosing was recorded precisely for each mouse and dosing was staggered appropriately. For each treatment group, mice were euthanized at 1 and 4 hours post-dosing of temozolomide /erlotinib with 6 mice at each time-point. Blood was collected in heparinized (100 units/mL) tubes and centrifuged at 3500 rpm for 10 minutes at 4℃, and supernatant plasma was collected. 1 part of 0.1% formic acid was immediately added to every 5 parts of plasma. The brain was removed and frozen. Since mice were implated with intracranial tumors transducted with TurobGFP, eGFP glasses were used to define the extent of tumor (green). Normal adjacent brain was evaluated as a control. The core of tumor (bright green), rim (not so green) and contralateral hemisphere were dissected out. Samples were frozen on dry ice and stored at -80℃ until analyzed for drug levels.

5.2.3 Quantitative Analysis by Lipid Chromatography-Tandem Mass Spectrometry

The concentrations of temozolomide, erlotinib, and cediranib in mouse plasma and brain specimen were all determined by an Agilent 1200 high-performance liquid chromatography (HPLC) (Santa Clara, CA, USA) coupled with Thermo-Finnegan™ TSQ® quantum classic triple quad mass spectrometer (San Jose, CA, USA). The system included a ESI and APCI interface. Data collection and analysis was conducted with XCalibur version 2.0.7 software. Prior to analysis, frozen samples were thawed at room tempreature. 60 μL ice-cold 5% bovine serum albumin in phosphate-buffered saline was added to each of the tumor core, rim, and normal brain samples followed with homogenization using a tissue homogenizer (Fisher Scientific, Pittsburgh, PA, USA).

5.2.3.1 Temozolomide

A 50 μL aliquot of plasma and brain homogenate were spiked with a certain amount of the internal standard, d^3- temozolomide, and extracted by vigorous vortexing with 1mL acetonitrile. Samples were centrifuged at 7500 rpm for 10 mins at 4 ℃ and a volume of 750 μL of the organic layer was transferred and dried under nitrogen. Samples were reconstituted in 100 μL mobile phase and 10 μL was injected. The mobile phase was composed of 10: 90 (v/v) acetonitrile/20mM ammonium formate with 0.1% formic acid. Separation of analytes was achieved using a Phenomenex Synergi 4μ Polar – RP80A column (75 x 2.0 mm) (Torrance, CA, USA). The mobile phase flow rate was maintained at 0.25 mL/min, resulting in a run time of 7 min. Samples were analyzed using an electrospray probe with spray voltage of 4500V in the positive ionization mode. The collision energy for temozolomide was set at 7V, and 8V for internal standard, with 1.5

mTorr collision gas pressure. The transitions monitored were m/z 195 -> 138.02 for temozolomide and 198 ->137.97 for d^3- temozolomide. The two product ions were monitored with the scan width 2 m/z and scan time 0.5 s.

5.2.3.2 Erlotinib

100 µL aliquots of plasma and brain homogenate were spiked with 50ng of AG1478 as internal standard, and alkalinized by adding 100 µL of a pH 11 buffer (1 mM sodium hydroxide, 0.5 mM sodium bicarbonate). Then they were extracted by vigorous vortexing with 1 mL ethyl acetate. Samples were centrifuged at 7500 rpm for 10 mins at 4 ℃ and a volume of 750 µL of the organic layer was transferred and dried under nitrogen. Samples were reconstituted in 100 µL mobile phase and 10 µL was injected at 10ºC. The mobile phase was composed of 45/55 (v/v) acetonitrile: 20mM ammonium formate with 0.1% formic acid. Separation of analytes was achieved using an Agilent Eclipse XDB-C18 RRHT threaded column (4.6 x 50mm, 1.8 µ) (Santa Clara, CA, USA). The mobile phase flow rate was maintained at 0.25 mL/min, yielding a run time of 8 min. Samples were analyzed using an electrospray probe with spray voltage of 4500V in the positive ionization mode. The collision energy for erlotinib was set at 14V, and 9V for AG1478, with 1.5 mTorr collision gas pressure. The transitions monitored were m/z 395.1 -> 278.9 for erlotinib and 316.7 ->300.9 for AG1478. The two product ions were monitored with the scan width 1.5 m/z and scan time 0.5 s.

5.2.3.3 Cediranib

Cediranib drug levels were assessed using an LC/MS assay that was outlined in Chapter 2.

5.2.4 Statistical analysis

The drug levels of temozolomide, erlotinib and cediranib in brain vs. plasma and in tumor vs. plasma were compared between placebo vs. avastin/cediranib groups using two sample t-test (or rank sum) at a single time point.

5.3 Results

5.3.1 Effect of anti-angiogenic therapy pre-treatment on temozolomide delivery to tumor sites

As shown in Figure 5.3, at 1 hour post chemotherapy dose, brain-to-plasma ratios of temozolomide in avastin-treated groups and cediranib-treated groups were not significantly different from placebo groups. Moreover, in the placebo group, temozolomide delivery to tumor surrounding parenchyma (rim) at 1 hour post dose was not significantly different from the normal brain (contralateral hemisphere) but slightly lower than the tumor core, suggesting that in patients with recurrent GBM, even though the BBB integrity at the tumor core may be disrupted, the infiltrative tumor growth could be protected by the intact BBB at tumor surrounding parenchyma. At 4 hours post dose, however, there was no significant difference in temozolomide distributions among the tumor core, rim and normal brain in the placebo group, suggesting passive diffusion equilibrium being reached at 4 hours post dose.

At 4 hours post chemotherapy dose, brain-to-plasma ratios of temozolomide in the tumor core were on average lower (~ 0.35, which was similar to normal brain) in the avastin-treated group than the placebo group (~ 1.1). The reduced delivery of temozolomide into the tumor core suggested that avastin might limit the brain tumor delivery of BBB permeable compounds, through normalization of brain tumor vasculature. Nevertheless, following once daily cediranib pre-treatment, temozolomide delivery was unchanged (~1.1) in the normal brain and the tumor-bearing hemisphere, and not significantly different with the placebo group, indicating that treatment of cediranib may not influence temozolomide delivery to the tumor core and surrounding parenchyma.

5.3.2 Effect of anti-angiogenic therapy pre-treatment on erlotinib delivery to tumor sites

Erlotinib has been shown to be a P-gp and BCRP dual substrate (Marchetti et al., 2008; Kodaira et al., 2010). Figure 5.4 shows that for erlotinib, there was no difference in delivery at 1 hour post chemotherapy dose following avastin pre-treatment, however at 4 hours post dose, the erlotinib delivery to tumor core was reduced on average by one-half following avastin pre-treatment, suggesting that avastin might decrease the tumor delivery of erlotinib through restored tight junctions in conjuction with a restored efficient efflux by transporters.

Figure 5.4 also shows that there was no site-difference in erlotinib delivery at either 1 hour or 4 hours post chemotherapy dose following once daily cediranib pre-treatment,

suggesting that treatment of cediranib may not influence erlotinib delivery to the tumor core and surrounding parenchyma.

5.3.3 Effect of cediranib pre-treatment on its own delivery to tumor sites

Since cediranib itself is mainly a P-gp substrate (see Chapter 3), the influence of cediranib pre-treatment on its own delivery to brain tumors was examined. Figure 5.5 shows that at 1 hour post dose, the brain-to-plasma concentration of cediranib in the tumor core was on average 0.54, however, the cediranib distribution in tumor core was on average reduced by one-half to 0.27 at 4 hours post dose while the cediranib levels in the tumor rim and the normal brain remained unchanged (~0.4). This suggested that as a VEGFR pan-inhibitor, cediranib might to some extent restore the efflux by P-gp and hence reduce its own delivery to brain tumors. Activity of drug efflux transporters such as P-gp within the BBB may account for the reduced efficacy of cediranib even if the BBB has been disrupted in GBM. However, due to the large variability within the preliminary data, further studies need to be done to confirm this hypothesis.

5.4 Discussion

Normalization of the brain tumor vasculature with AAT reinforces the disrupted BBB enhancing blood flow. Thus, delivery of drugs that are typically more permeable in the intact BBB could be enhanced, due to their ability to diffuse transcellularly across an intact barrier. However, it has been observed that avastin reduced the tumoral delivery of temozolomide, suggesting that AAT can influence drug delivery through different

mechanisms rather than simply changes in perfusion. Surprisingly, there was no similar impact of once daily treatment of cediranib on temozolomide brain delivery as avastin. One of possible reasons might be that cediranib is less efficacious than avastin in patients with recurrent GBM in that cediranib may restore the P-gp efflux and hence limit its own delivery to brain tumors, yielding a reduced AAT efficacy.

Since VEGFR2 signaling through Src and PKC-beta suppresses Pgp expression and/or activity in brain capillary endothelial cells, AAT through inhibition of VEGFR2 can lead to increased Pgp expression and possibly higher levels of drug exclusion from the endothelial cells (Liu et al., 2009; Hawkins et al., 2010). Therefore, besides of restoring tight junction integrity, AAT is likely to increase efflux pump activity within the brain capillary endothelium, and hence, drugs that are limited by efficient efflux transporters may have their delivery to the tumor diminished as the vasculature normalizes, due to lack of permeability through passive diffusion and a restored efficient efflux by transporters. Our observations showed that the delivery of erlotinib into brain tumors following avastin pre-treatment and the delivery of cediranib into brain tumors following its own pre-treatment were both on average reduced by one-half. These results were consistent with previous studies in our lab on brain tumor delivery of dasatinib, another P-gp and BCRP dual substrate (Chen et al., 2009), that upon avastin treatment, dasatinib brain-to-plasma ratios were unchanged in the normal brain, but significantly lower in the tumor-bearing hemisphere (40% with avastin vs. 130% with placebo).

However, it is unclear why the once daily treatment of cediranib, a VEGFR2 inhibitor, did not have a similar impact on erlotinib delivery as avastin, but might have an influence on its own delivery. One possible explanation is that the reduced delivery of erlotinib by avastin might be mainly due to normalization of the tumor vasculature such as the reformed tight junctions, rather than the restoration of P-gp efflux mediated by VEGFR2 inhibition. Because of the restored P-gp efflux, cediranib might limit its own delivery to brain tumors, yielding a reduced efficacy of restoring disrupted tight junctions. Further studies need to be conducted to explore other possible mechanisms in the future.

Another observed phenomenon, the reason for which remains unclear, was that in the placebo group, erlotinib delivery to the tumor core, rim and normal brain was not significantly different at either 1 hour or 4 hours post dose. According to the hypothesis, the BBB at tumor core is broken down during gliomagenesis, hence, the delivery of erlotinib into the tumor core should have been higher than other sites. This observation requires further studies to confirm this result.

5.5 Conclusion

In summary, anti-angiogenic therapy mediated restoration of BBB integrity could significantly decrease delivery of chemotherapy, such as temozolomide and erlotinib, to the brain tumor, leading to reduced efficacy. Changes in perfusion may not be at play in influencing drug delivery, but vessel permeability may change delivery for compounds of varying permeability across the intact BBB. Cediranib may be less efficacious than

avastin in patients with recurrent GBM in that cediranib may limit its own delivery to brain tumors, yielding a reduced AAT efficacy.

5.6 Footnotes

We would like to thank Dr. Sarkaria's laboratory from Mayo Clinic, for the animal model and their help in designing and conducting animal studies. We thank Sagar Agarwal and Dr. Rajendar Mittapalli for their kind help with analytical analysis of temozolomide and erlotinib.

Table 5-1 List of agents being studied in combination with avastin in GBM clinically.

i) Cytotoxic		**ii) Small molecule inhibitors**		**iii) Antibodies**
	Efflux substrate?		Efflux substrate?	
temozolomide	None	erlotinib	P-gp and BCRP1	Cetuximab
lomustine	None	dasatinib	P-gp and BCRP1	Neuradiab
Carmustine	None	tandutinib	P-gp and BCRP1	RO5323441
irinotecan	P-gp and BCRP1	enzastaurin	unknown	AMG386
topotecan	P-gp and BCRP1	RO4929097 (GSI)	unknown	AMB102
etoposide	P-gp and BCRP1	temsirolimus	P-gp	
		everolimus	P-gp	
		bortezomib	P-gp	
		cediranib	P-gp and BCRP1	
		vorinostat	None	
		sorafinib	P-gp and BCRP1	
		sunitinib	P-gp and BCRP1	
		imatinib	P-gp and BCRP1	

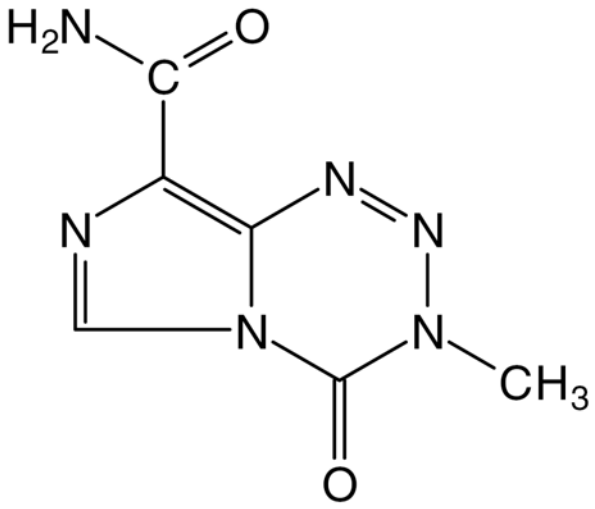

Figure 5.1 Chemical structure of temozolomide, an alkylating agent

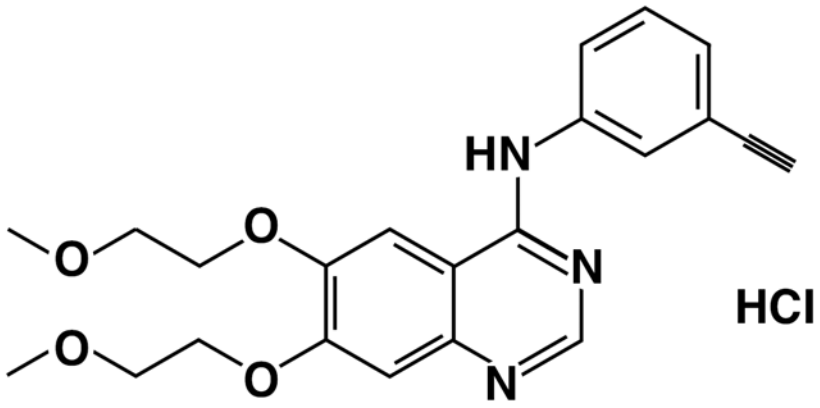

Figure 5.2 Chemical structure of erlotinib, a selective tyrosine kinase inhibitor against EGFR

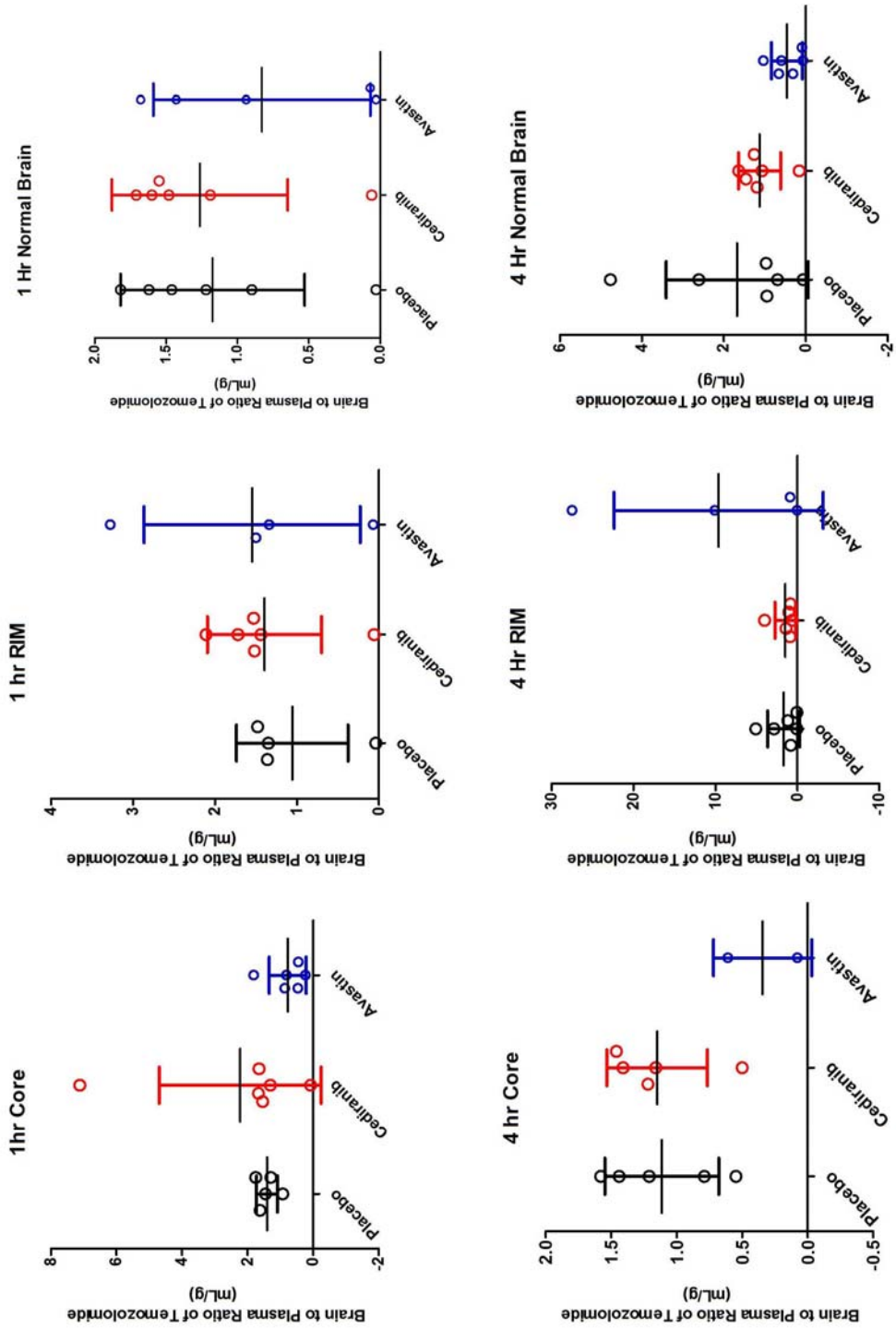

Figure 5.3 Impact of AATs (cediranib and avastin) on temozolomide uptake into tumor core, rim, and normal brain at 1 hour and 4 hours post dose of temozolomide.

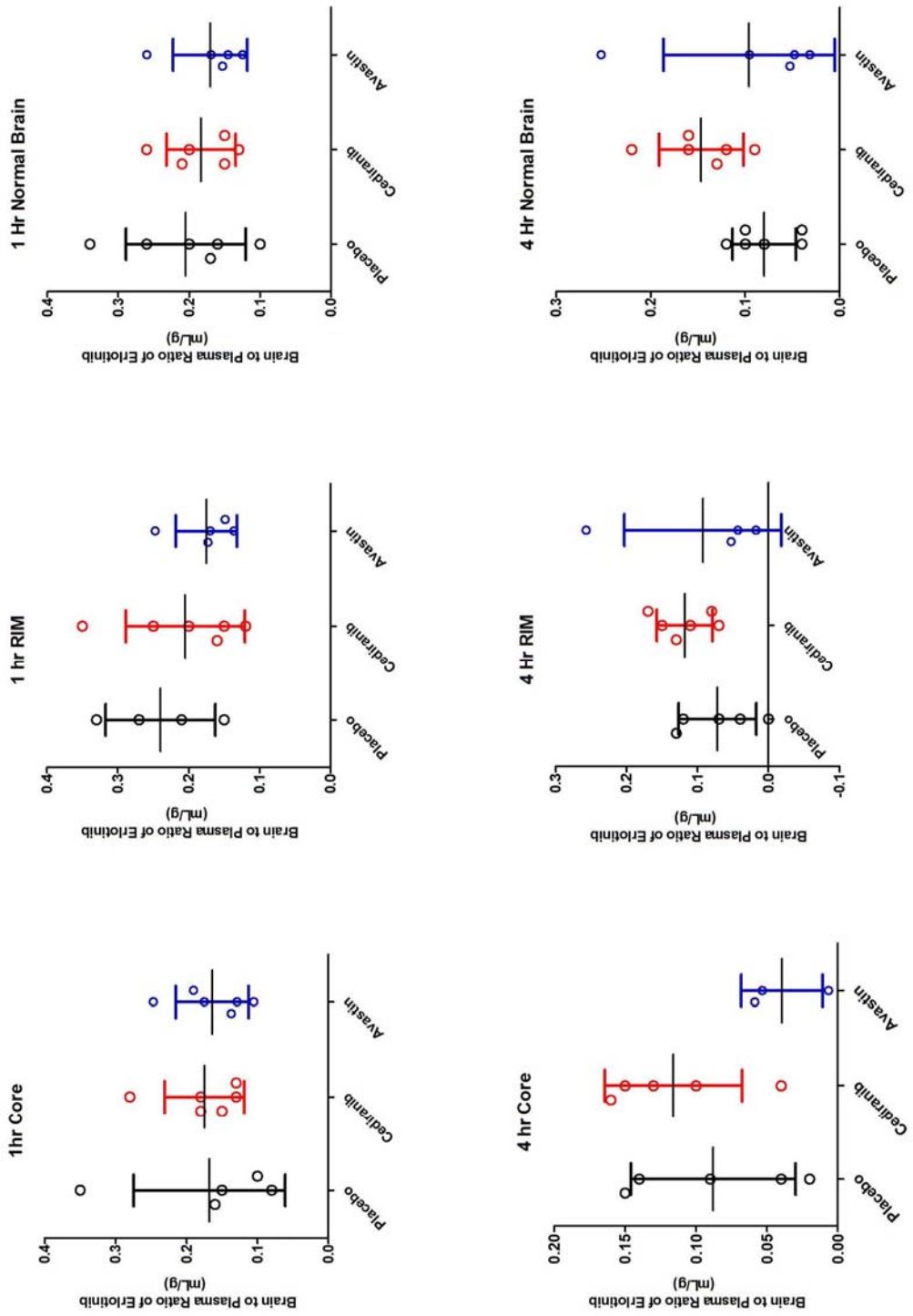

Figure 5.4 Impact of AATs (cediranib and avastin) on erlotinib uptake into tumor core, rim, and normal brain at 1 hour and 4 hours post dose of erlotinib.

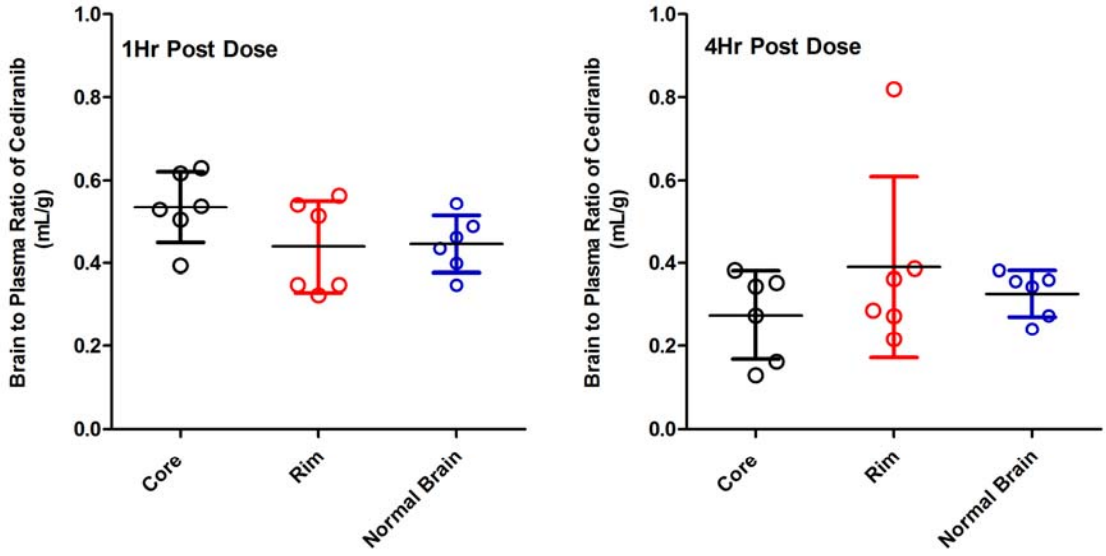

Figure 5.5 Impact of once daily treatment of cediranib on its own uptake into tumor core, rim, and normal brain at 1 hour and 4 hours post dose.

CHAPTER 6

RECAPITULATION

Glioblastoma multiforme (GBM) is the most common and fatal primary brain tumor, the treatment of which is a challenge due to the high relapse rate. Despite aggressive treatments, relapse occurs within virtually all GBM, and only 25% of patients survive over 2 years (Stupp et al., 2007). Glioma cells evade treatment through migration to normal brain parenchyma. The invasive growth pattern of glioblastoma (GBM) gives rise to salellite lesions shielded by an intact blood-brain barrier (BBB) in areas away from the boundary of surgical resection and eventually causes glioma recurrence. Therefore, novel therapies capable of targeting invasive GBM cell populations are needed. In addition to the high invasiveness, endothelial proliferation is another defining feature of GBM. Vascular endothelial growth factor (VEGF) and its receptor VEGFR are highly expressed in GBM and correlated to tumor malignancy (Carlson et al., 2007). Thus, brain vascular endothelium has been suggested as a target for anti-angiogenic agents for the treatment of recurrent GBM (Hormigo et al., 2011). Anti-angiogenic therapies (AATs) function to promote normalization of tumor vasculature and hence significantly reduce cerebral edema.

Although the demonstrable clinical achievements with the current generation of VEFG pathway inhibitors establish a milestone for angiogenesis research, these AATs have shown in some cases to produce temporary efficacy or no objective clinical benefit to block tumor progression (Bergers and Hanahan, 2008). Failure of a variety of VEGF pathway inhibitiors, including bevacizumab and small molecule tyrosine kinase inhibitors, to show clinical benefit is counterintuitive to the proposition that VEGF is a key mediator

of angiogenesis (Carmeliet, 2005), a characterastic of GBM. Other than intrinsic resistance to AATs, some adaptive mechanisms have been hypothesized for the evasive resistance to AATs, including compensatory upregulation of alternative pro-angiogenic signaling pathways, recruitment of bone marrow derived vascular progenitor cells, and increased tumor cell invasiveness by inhibition of angiogenesis (Bergers and Hanahan, 2008; Rahman et al., 2010). For instance, Norden, Zuniga and Iwamoto et al. reported that it is more likely that glioma recurrence after bevacizumab therapy is distant to the primary tumor location and exhibits diffuse patterns (Norden et al., 2008; Iwamoto et al., 2009; Zuniga et al., 2009). A recent study (Pope et al., 2011) demostrated that before initiation of bevacizumab treatment, 72% of patients followed by combination treatment of temozolomide and radiotherapy had local recurrent GBM, with 7% diffuse, 2.4% distant and 8% multifocal recurrence. However, after bevacizumab therapy, there was no change in disease pattern within 82% of patients, but 16% of patients who had local glioma recurrence converted to a diffuse pattern (Chamberlain et al., 2010).

Cediranib, an anti-angiogenic molecularly-targeted tyrosine kinase inhibitor (TKI) of pan-VEGFRs, has shown great improvement in both glioma vessel structure and function after monotherapy as soon as one day after treatment initiation (Batchelor et al., 2007). Since cediranib has a variety of additional kinase targets, such as PDGFRs and c-Kit, it may provide more therapeutic benefit than just anti-angiogenesis (Bergers and Hanahan, 2008). However, more and more studies showed that cediranib has anti-angiogenic effect

but not anti-tumor effect (Batchelor et al., 2007; Kamoun et al., 2009), which may be one of the reasons for the limited clinical benefit of cediranib.

Since GBM can be treated as a whole brain disease, the delivery of possibly effective anti-tumor agents, such as cediranib, in different regions of a brain tumor is an important concern in the effort to treat brain tumors. P-glycoprotein (P-gp) and breast cancer resistance protein (BCRP), the important drug exclusion systems at the BBB, have been shown to limit brain penetration of various chemotherapeutics including a variety of TKIs. Despite the permeable vasculature in the tumor core, the intact BBB in the tumor rim and in the normal brain still presents an intact barrier for the drugs that target the invasive GBM cell populations, due to high expression of these efflux transporters. Interaction with these active efflux transporters may limit cediranib brain distribution and result in poor efficacy in treatment of brain tumors such as GBM. The limited delivery of cediranib to different regions of brain tumor may be another possible reason for the poor effectiveness seen in GBM.

Last but not least, beneficial effects of anti-angiogesis encourage the application of combination therapies of anti-angiogenic agents and chemotherapies for anti-cancer treatment. However, it is unclear how one therapy modality may influence the delivery and hence efficacy of another. Two competing effects of AATs on the efficacy of concurrently used chemotherapies have been hypothesized. One suggests that improved vasculature could improve delivery of chemotherapy agents to poorly perfused regions

within the tumor and therefore result in an enhanced delivery. The other hypothesizes that the restored BBB integrity could limit delivery to the tumor cells for drugs that do not cross the BBB readily.

The ultimate objective of the work addressed in this thesis is to improve the molecularly-targeted tumor delivery of cediranib and to provide insight into proper strategies for administration of effective cediranib treatment and combination therapy.

Initial studies, as outlined in chapter 3, focused on investigation of effect of efflux transporters present at the BBB on the brain penetration of cediranib. Cediranib is different from some other TKIs in that although both P-gp and BCRP were involved in restricting the intracellular accumulation of cediranib, P-gp played a predominant role in excluding cediranib out of the brain. This was examined by comparing brain partitioning of cediranib in *Mdr1a/b (-/-)*, *Bcrp1 (-/-)* and *Mdr1a/b (-/-) Bcrp1 (-/-)* mice with the relevant wild-type strain. We further examined this by concurrent administration of transporter selective and combined inhibitors along with cediranib. These studies confirmed the results from transgenic mice models and provided conclusive evidence for the dominant role of P-gp in preventing cediranib across the BBB.

Since elimination half-life appears to be relevant to efficacy of AATs (Cai et al., 2011), in our preclinical PK studies, it was suggested that cediranib had an approximate half-life of 7 hours in mice, implying the necessity of daily administration. Additionally, the time

to reach the brain concentration peak (T_{max}) for different genotypes of transporters varied because of the different efflux clearance out of the brain. The influence of efflux clearance on T_{max} and the time to achieve steady state of the brain-to-plasma partition coefficient was further investigated by simulation strategies in chapter 4.

We next examined the analysis of brain distributional kinetics. Our simulations in chapter 4 illustrated that impact of efflux transporters can be reasonably estimated at the brain T_{max} or in the terminal elimination phase, although the latter will overestimate the true brain partitioning. Partial area analysis can also be used to intepret the maginitude of efflux transport for a substrate. Performances of cumulative and interval partial-areas analyses were evaluated. Furthermore, since the ability to determine the true brain-to-plasma AUC_0^∞ ratio, the accurate metric to reflect the brain exposure of a substrate, is affected by experimental error and the variation between animals, a Baysian approach was proposed and utilized to determine the variation of brain-to-plasma AUC_0^∞ ratio under a serial sacrifice study design.

The final preliminary study, described in chapter 5, investigated the influence of AAT (bevacizumab and cediranib) on the tumor delivery of both traditional chemotherapy (such as temozolomide) and molecularly-targeted agents (such as erlotinib) using a xenograft GBM model. The eGFP-transducted tumor allows dissection of the brain into the following regions: 1) tumor core, 2) rim and 3) normal tissues. Our preliminary data showed that AAT-mediated restoration of BBB integrity by cediranib or bevacizumab

could decrease the tumor site delivery of both temozolomide and erlotinib, and even the delivery of cediranib itself, making its own anti-angiogenic efficacy reduced over time.

Future work will examine the distribution of cediranib within the brain vascular endothelial cells with and without the presence of drug efflux transporters. It would be interesting to investigate the distribution of cediranib in the endothelium in the tumor core and in other regions with an intact BBB. Further studies are also needed to confirm our conclusion of the effect of AATs on limiting the delivery of chemotherapeutics to tumor sites. The efficacy (changes in pharmacodynamic endpoints and overall survival) of combination anti-angiogenic therapy and traditional (such as temozolomide) and investigational (such as other TKIs) chemotherapy against GBM is also desirable to be examined in the future.

BIBLIOGRAPHY

References for Chapter 1

Agarwal S, Sane R, Gallardo JL, Ohlfest JR and Elmquist WF (2010) Distribution of gefitinib to the brain is limited by P-glycoprotein (ABCB1) and breast cancer resistance protein (ABCG2)-mediated active efflux. *J Pharmacol Exp Ther* 334:147-155.

Agarwal S, Sane R, Oberoi R, Ohlfest JR and Elmquist WF (2011a) Delivery of molecularly targeted therapy to malignant glioma, a disease of the whole brain. *Expert Rev Mol Med* 13:e17.

Agarwal S, Sane R, Ohlfest JR and Elmquist WF (2011b) The role of the breast cancer resistance protein (ABCG2) in the distribution of sorafenib to the brain. *J Pharmacol Exp Ther* 336:223-233.

Bahr O, Rieger J, Duffner F, Meyermann R, Weller M and Wick W (2003) P-glycoprotein and multidrug resistance-associated protein mediate specific patterns of multidrug resistance in malignant glioma cell lines, but not in primary glioma cells. *Brain Pathol* 13:482-494.

Ban Y and Rizzolo LJ (2000) Differential regulation of tight junction permeability during development of the retinal pigment epithelium. *Am J Physiol Cell Physiol* 279:C744-750.

Batchelor TT, Duda DG, di Tomaso E, Ancukiewicz M, Plotkin SR, Gerstner E, Eichler AF, Drappatz J, Hochberg FH, Benner T, Louis DN, Cohen KS, Chea H, Exarhopoulos A, Loeffler JS, Moses MA, Ivy P, Sorensen AG, Wen PY and Jain RK (2010) Phase II study of cediranib, an oral pan-vascular endothelial growth factor receptor tyrosine kinase inhibitor, in patients with recurrent glioblastoma. *J Clin Oncol* 28:2817-2823.

Batchelor TT, Sorensen AG, di Tomaso E, Zhang WT, Duda DG, Cohen KS, Kozak KR, Cahill DP, Chen PJ, Zhu M, Ancukiewicz M, Mrugala MM, Plotkin S, Drappatz J, Louis DN, Ivy P, Scadden DT, Benner T, Loeffler JS, Wen PY and Jain RK (2007) AZD2171, a pan-VEGF receptor tyrosine kinase inhibitor, normalizes tumor vasculature and alleviates edema in glioblastoma patients. *Cancer Cell* 11:83-95.

Beaulieu E, Demeule M, Ghitescu L and Beliveau R (1997) P-glycoprotein is strongly expressed in the luminal membranes of the endothelium of blood vessels in the brain. *Biochem J* 326 (Pt 2):539-544.

Benyahia B, Huguet S, Decleves X, Mokhtari K, Criniere E, Bernaudin JF, Scherrmann JM and Delattre JY (2004) Multidrug resistance-associated protein MRP1 expression in human gliomas: chemosensitization to vincristine and etoposide by indomethacin in human glioma cell lines overexpressing MRP1. *J Neurooncol* 66:65-70.

Bergers G and Hanahan D (2008) Modes of resistance to anti-angiogenic therapy. *Nat Rev Cancer* 8:592-603.

Brave SR, Ratcliffe K, Wilson Z, James NH, Ashton S, Wainwright A, Kendrew J, Dudley P, Broadbent N, Sproat G, Taylor S, Barnes C, Silva JC, Farnsworth CL, Hennequin L, Ogilvie DJ, Jurgensmeier JM, Shibuya M, Wedge SR and Barry ST (2011) Assessing the activity of cediranib, a VEGFR-2/3 tyrosine kinase inhibitor, against VEGFR-1 and members of the structurally related PDGFR family. *Mol Cancer Ther* 10:861-873.

Breedveld P, Pluim D, Cipriani G, Wielinga P, van Tellingen O, Schinkel AH and Schellens JH (2005) The effect of Bcrp1 (Abcg2) on the in vivo pharmacokinetics and brain penetration of imatinib mesylate (Gleevec): implications for the use of breast cancer resistance protein and P-glycoprotein inhibitors to enable the brain penetration of imatinib in patients. *Cancer Res* 65:2577-2582.

Cai J, Han S, Qing R, Liao D, Law B and Boulton ME (2011) In pursuit of new anti-angiogenic therapies for cancer treatment. *Front Biosci* 16:803-814.

Carmeliet P and Jain RK (2000) Angiogenesis in cancer and other diseases. *Nature* 407:249-257.

Chamberlain MC (2011) Bevacizumab for the treatment of recurrent glioblastoma. *Clin Med Insights Oncol* 5:117-129.

Chen Y, Agarwal S, Shaik NM, Chen C, Yang Z and Elmquist WF (2009) P-glycoprotein and breast cancer resistance protein influence brain distribution of dasatinib. *J Pharmacol Exp Ther* 330:956-963.

Choucair AK, Levin VA, Gutin PH, Davis RL, Silver P, Edwards MS and Wilson CB (1986) Development of multiple lesions during radiation therapy and chemotherapy in patients with gliomas. *J Neurosurg* 65:654-658.

Colgan OC, Collins NT, Ferguson G, Murphy RP, Birney YA, Cahill PA and Cummins PM (2008) Influence of basolateral condition on the regulation of brain microvascular endothelial tight junction properties and barrier function. *Brain Res* 1193:84-92.

Cordon-Cardo C, O'Brien JP, Casals D, Rittman-Grauer L, Biedler JL, Melamed MR and Bertino JR (1989) Multidrug-resistance gene (P-glycoprotein) is expressed by endothelial cells at blood-brain barrier sites. *Proc Natl Acad Sci U S A* 86:695-698.

Dai H, Marbach P, Lemaire M, Hayes M and Elmquist WF (2003) Distribution of STI-571 to the brain is limited by P-glycoprotein-mediated efflux. *J Pharmacol Exp Ther* 304:1085-1092.

Davis FG, Kupelian V, Freels S, McCarthy B and Surawicz T (2001) Prevalence estimates for primary brain tumors in the United States by behavior and major histology groups. *Neuro Oncol* 3:152-158.

de Vries NA, Zhao J, Kroon E, Buckle T, Beijnen JH and van Tellingen O (2007) P-glycoprotein and breast cancer resistance protein: two dominant transporters working together in limiting the brain penetration of topotecan. *Clin Cancer Res* 13:6440-6449.

Dean M, Fojo T and Bates S (2005) Tumour stem cells and drug resistance. *Nat Rev Cancer* 5:275-284.

Decleves X, Fajac A, Lehmann-Che J, Tardy M, Mercier C, Hurbain I, Laplanche JL, Bernaudin JF and Scherrmann JM (2002) Molecular and functional MDR1-Pgp and MRPs expression in human glioblastoma multiforme cell lines. *Int J Cancer* 98:173-180.

Demeule M, Regina A, Annabi B, Bertrand Y, Bojanowski MW and Beliveau R (2004) Brain endothelial cells as pharmacological targets in brain tumors. *Mol Neurobiol* 30:157-183.

Demeule M, Regina A, Jodoin J, Laplante A, Dagenais C, Berthelet F, Moghrabi A and Beliveau R (2002) Drug transport to the brain: key roles for the efflux pump P-glycoprotein in the blood-brain barrier. *Vascul Pharmacol* 38:339-348.

Diestra JE, Scheffer GL, Catala I, Maliepaard M, Schellens JH, Scheper RJ, Germa-Lluch JR and Izquierdo MA (2002) Frequent expression of the multi-drug resistance-associated protein BCRP/MXR/ABCP/ABCG2 in human tumours detected by the BXP-21 monoclonal antibody in paraffin-embedded material. *J Pathol* 198:213-219.

Du R, Lu KV, Petritsch C, Liu P, Ganss R, Passegue E, Song H, Vandenberg S, Johnson RS, Werb Z and Bergers G (2008) HIF1alpha induces the recruitment of bone marrow-derived vascular modulatory cells to regulate tumor angiogenesis and invasion. *Cancer Cell* 13:206-220.

Fidler IJ, Yano S, Zhang RD, Fujimaki T and Bucana CD (2002) The seed and soil hypothesis: vascularisation and brain metastases. *Lancet Oncol* 3:53-57.

Fischer I, Gagner JP, Law M, Newcomb EW and Zagzag D (2005) Angiogenesis in gliomas: biology and molecular pathophysiology. *Brain Pathol* 15:297-310.

Friedman HS, Prados MD, Wen PY, Mikkelsen T, Schiff D, Abrey LE, Yung WK, Paleologos N, Nicholas MK, Jensen R, Vredenburgh J, Huang J, Zheng M and Cloughesy T (2009) Bevacizumab alone and in combination with irinotecan in recurrent glioblastoma. *J Clin Oncol* 27:4733-4740.

Gagner JP, Law M, Fischer I, Newcomb EW and Zagzag D (2005) Angiogenesis in gliomas: imaging and experimental therapeutics. *Brain Pathol* 15:342-363.

Gerstner ER, Duda DG, di Tomaso E, Ryg PA, Loeffler JS, Sorensen AG, Ivy P, Jain RK and Batchelor TT (2009) VEGF inhibitors in the treatment of cerebral edema in patients with brain cancer. *Nat Rev Clin Oncol* 6:229-236.

Gilbertson RJ and Rich JN (2007) Making a tumour's bed: glioblastoma stem cells and the vascular niche. *Nat Rev Cancer* 7:733-736.

Giri N, Shaik N, Pan G, Terasaki T, Mukai C, Kitagaki S, Miyakoshi N and Elmquist WF (2008) Investigation of the role of breast cancer resistance protein (Bcrp/Abcg2)

on pharmacokinetics and central nervous system penetration of abacavir and zidovudine in the mouse. *Drug Metab Dispos* 36:1476-1484.

Goellner EM, Grimme B, Brown AR, Lin YC, Wang XH, Sugrue KF, Mitchell L, Trivedi RN, Tang JB and Sobol RW (2011) Overcoming temozolomide resistance in glioblastoma via dual inhibition of NAD+ biosynthesis and base excision repair. *Cancer Res* 71:2308-2317.

Haseloff RF, Blasig IE, Bauer HC and Bauer H (2005) In search of the astrocytic factor(s) modulating blood-brain barrier functions in brain capillary endothelial cells in vitro. *Cell Mol Neurobiol* 25:25-39.

Hawkins BT and Davis TP (2005) The blood-brain barrier/neurovascular unit in health and disease. *Pharmacol Rev* 57:173-185.

Hawkins BT, Sykes DB and Miller DS (2010) Rapid, reversible modulation of blood-brain barrier P-glycoprotein transport activity by vascular endothelial growth factor. *J Neurosci* 30:1417-1425.

Hoeben A, Landuyt B, Highley MS, Wildiers H, Van Oosterom AT and De Bruijn EA (2004) Vascular endothelial growth factor and angiogenesis. *Pharmacol Rev* 56:549-580.

Hormigo A, Ding BS and Rafii S (2011) A target for antiangiogenic therapy: vascular endothelium derived from glioblastoma. *Proc Natl Acad Sci U S A* 108:4271-4272.

Huang H, Held-Feindt J, Buhl R, Mehdorn HM and Mentlein R (2005) Expression of VEGF and its receptors in different brain tumors. *Neurol Res* 27:371-377.

Huber JD, Egleton RD and Davis TP (2001) Molecular physiology and pathophysiology of tight junctions in the blood-brain barrier. *Trends Neurosci* 24:719-725.

Jain RK, di Tomaso E, Duda DG, Loeffler JS, Sorensen AG and Batchelor TT (2007) Angiogenesis in brain tumours. *Nat Rev Neurosci* 8:610-622.

Kamiie J, Ohtsuki S, Iwase R, Ohmine K, Katsukura Y, Yanai K, Sekine Y, Uchida Y, Ito S and Terasaki T (2008) Quantitative atlas of membrane transporter proteins: development and application of a highly sensitive simultaneous LC/MS/MS method combined with novel in-silico peptide selection criteria. *Pharm Res* 25:1469-1483.

Kamoun WS, Ley CD, Farrar CT, Duyverman AM, Lahdenranta J, Lacorre DA, Batchelor TT, di Tomaso E, Duda DG, Munn LL, Fukumura D, Sorensen AG and Jain RK (2009) Edema control by cediranib, a vascular endothelial growth factor receptor-targeted kinase inhibitor, prolongs survival despite persistent brain tumor growth in mice. *J Clin Oncol* 27:2542-2552.

Kawahara M, Sakata A, Miyashita T, Tamai I and Tsuji A (1999) Physiologically based pharmacokinetics of digoxin in mdr1a knockout mice. *J Pharm Sci* 88:1281-1287.

Kodaira H, Kusuhara H, Ushiki J, Fuse E and Sugiyama Y (2010) Kinetic analysis of the cooperation of P-glycoprotein (P-gp/Abcb1) and breast cancer resistance protein (Bcrp/Abcg2) in limiting the brain and testis penetration of erlotinib, flavopiridol, and mitoxantrone. *J Pharmacol Exp Ther* 333:788-796.

Kuratsu J, Itoyama Y, Uemura S and Ushio Y (1989) [Regrowth patterns of glioma--cases of glioma regrew away from the original tumor]. *Gan No Rinsho* 35:1255-1260.

Kusuhara H and Sugiyama Y (2001a) Efflux transport systems for drugs at the blood-brain barrier and blood-cerebrospinal fluid barrier (Part 1). *Drug Discov Today* 6:150-156.

Kusuhara H and Sugiyama Y (2001b) Efflux transport systems for drugs at the blood-brain barrier and blood-cerebrospinal fluid barrier (Part 2). *Drug Discov Today* 6:206-212.

Lee YJ, Kusuhara H, Jonker JW, Schinkel AH and Sugiyama Y (2005) Investigation of efflux transport of dehydroepiandrosterone sulfate and mitoxantrone at the mouse blood-brain barrier: a minor role of breast cancer resistance protein. *J Pharmacol Exp Ther* 312:44-52.

Levin VA (1980) Relationship of octanol/water partition coefficient and molecular weight to rat brain capillary permeability. *J Med Chem* 23:682-684.

Liu H, Yang H, Wang D, Liu Y, Liu X, Li Y, Xie L and Wang G (2009) Insulin regulates P-glycoprotein in rat brain microvessel endothelial cells via an insulin receptor-mediated PKC/NF-kappaB pathway but not a PI3K/Akt pathway. *Eur J Pharmacol* 602:277-282.

Loscher W and Potschka H (2005) Blood-brain barrier active efflux transporters: ATP-binding cassette gene family. *NeuroRx* 2:86-98.

Ma J, Pulfer S, Li S, Chu J, Reed K and Gallo JM (2001) Pharmacodynamic-mediated reduction of temozolomide tumor concentrations by the angiogenesis inhibitor TNP-470. *Cancer Res* 61:5491-5498.

Masi A, Becchetti A, Restano-Cassulini R, Polvani S, Hofmann G, Buccoliero AM, Paglierani M, Pollo B, Taddei GL, Gallina P, Di Lorenzo N, Franceschetti S, Wanke E and Arcangeli A (2005) hERG1 channels are overexpressed in glioblastoma multiforme and modulate VEGF secretion in glioblastoma cell lines. *Br J Cancer* 93:781-792.

Mentlein R, Forstreuter F, Mehdorn HM and Held-Feindt J (2004) Functional significance of vascular endothelial growth factor receptor expression on human glioma cells. *J Neurooncol* 67:9-18.

Mohri M, Nitta H and Yamashita J (2000) Expression of multidrug resistance-associated protein (MRP) in human gliomas. *J Neurooncol* 49:105-115.

Mrugala MM, Kesari S, Ramakrishna N and Wen PY (2004) Therapy for recurrent malignant glioma in adults. *Expert Rev Anticancer Ther* 4:759-782.

Newlands ES, Blackledge GR, Slack JA, Rustin GJ, Smith DB, Stuart NS, Quarterman CP, Hoffman R, Stevens MF, Brampton MH and et al. (1992) Phase I trial of temozolomide (CCRG 81045: M&B 39831: NSC 362856). *Br J Cancer* 65:287-291.

Pan G, Giri N and Elmquist WF (2007) Abcg2/Bcrp1 mediates the polarized transport of antiretroviral nucleosides abacavir and zidovudine. *Drug Metab Dispos* 35:1165-1173.

Pardridge WM (1998) CNS drug design based on principles of blood-brain barrier transport. *J Neurochem* 70:1781-1792.

Polli JW, Humphreys JE, Harmon KA, Castellino S, O'Mara MJ, Olson KL, John-Williams LS, Koch KM and Serabjit-Singh CJ (2008) The role of efflux and uptake transporters in [N-{3-chloro-4-[(3-fluorobenzyl)oxy]phenyl}-6-[5-({[2-

(methylsulfonyl)ethy l]amino}methyl)-2-furyl]-4-quinazolinamine (GW572016, lapatinib) disposition and drug interactions. *Drug Metab Dispos* 36:695-701.

Polli JW, Olson KL, Chism JP, John-Williams LS, Yeager RL, Woodard SM, Otto V, Castellino S and Demby VE (2009) An unexpected synergist role of P-glycoprotein and breast cancer resistance protein on the central nervous system penetration of the tyrosine kinase inhibitor lapatinib (N-{3-chloro-4-[(3-fluorobenzyl)oxy]phenyl}-6-[5-({[2-(methylsulfonyl)ethy l]amino}methyl)-2-furyl]-4-quinazolinamine; GW572016). *Drug Metab Dispos* 37:439-442.

Prewett M, Huber J, Li Y, Santiago A, O'Connor W, King K, Overholser J, Hooper A, Pytowski B, Witte L, Bohlen P and Hicklin DJ (1999) Antivascular endothelial growth factor receptor (fetal liver kinase 1) monoclonal antibody inhibits tumor angiogenesis and growth of several mouse and human tumors. *Cancer Res* 59:5209-5218.

Rahman R, Smith S, Rahman C and Grundy R (2010) Antiangiogenic therapy and mechanisms of tumor resistance in malignant glioma. *J Oncol* 2010:251231.

Reardon DA, Turner S, Peters KB, Desjardins A, Gururangan S, Sampson JH, McLendon RE, Herndon JE, 2nd, Jones LW, Kirkpatrick JP, Friedman AH, Vredenburgh JJ, Bigner DD and Friedman HS (2011) A review of VEGF/VEGFR-targeted therapeutics for recurrent glioblastoma. *J Natl Compr Canc Netw* 9:414-427.

Rubenstein JL, Kim J, Ozawa T, Zhang M, Westphal M, Deen DF and Shuman MA (2000) Anti-VEGF antibody treatment of glioblastoma prolongs survival but results in increased vascular cooption. *Neoplasia* 2:306-314.

Sasaki T, Tanno S, Shibukawa K, Osanai S, Kawabe J and Ohsaki Y (2008) Administration of VEGF receptor tyrosine kinase inhibitor increases VEGF production causing angiogenesis in human small-cell lung cancer xenografts. *Int J Oncol* 33:525-532.

Sathornsumetee S (2011) Therapeutic Strategies to Target Multiple Kinases in Glioblastoma. *Anticancer Agents Med Chem*.

Sathornsumetee S and Reardon DA (2009) Targeting multiple kinases in glioblastoma multiforme. *Expert Opin Investig Drugs* 18:277-292.

Sathornsumetee S, Reardon DA, Desjardins A, Quinn JA, Vredenburgh JJ and Rich JN (2007) Molecularly targeted therapy for malignant glioma. *Cancer* 110:13-24.

Sathornsumetee S and Rich JN (2007) Antiangiogenic therapy in malignant glioma: promise and challenge. *Curr Pharm Des* 13:3545-3558.

Schinkel AH and Jonker JW (2003) Mammalian drug efflux transporters of the ATP binding cassette (ABC) family: an overview. *Adv Drug Deliv Rev* 55:3-29.

Schinkel AH, Smit JJ, van Tellingen O, Beijnen JH, Wagenaar E, van Deemter L, Mol CA, van der Valk MA, Robanus-Maandag EC, te Riele HP and et al. (1994) Disruption of the mouse mdr1a P-glycoprotein gene leads to a deficiency in the blood-brain barrier and to increased sensitivity to drugs. *Cell* 77:491-502.

Schinkel AH, Wagenaar E, Mol CA and van Deemter L (1996) P-glycoprotein in the blood-brain barrier of mice influences the brain penetration and pharmacological activity of many drugs. *J Clin Invest* 97:2517-2524.

Sharma PS, Sharma R and Tyagi T (2011) VEGF/VEGFR Pathway Inhibitors as Anti-Angiogenic Agents: Present and Future. *Curr Cancer Drug Targets*.

Sharom FJ (2008) ABC multidrug transporters: structure, function and role in chemoresistance. *Pharmacogenomics* 9:105-127.

Sikkema AH, de Bont ES, Molema G, Dimberg A, Zwiers PJ, Diks SH, Hoving EW, Kamps WA, Peppelenbosch MP and den Dunnen WF (2011) VEGFR-2 signalling activity in paediatric pilocytic astrocytoma is restricted to tumour endothelial cells. *Neuropathol Appl Neurobiol*.

Silbergeld DL and Chicoine MR (1997) Isolation and characterization of human malignant glioma cells from histologically normal brain. *J Neurosurg* 86:525-531.

Sorensen AG, Batchelor TT, Zhang WT, Chen PJ, Yeo P, Wang M, Jennings D, Wen PY, Lahdenranta J, Ancukiewicz M, di Tomaso E, Duda DG and Jain RK (2009) A "vascular normalization index" as potential mechanistic biomarker to predict survival after a single dose of cediranib in recurrent glioblastoma patients. *Cancer Res* 69:5296-5300.

Stupp R, Hegi ME, Mason WP, van den Bent MJ, Taphoorn MJ, Janzer RC, Ludwin SK, Allgeier A, Fisher B, Belanger K, Hau P, Brandes AA, Gijtenbeek J, Marosi C,

Vecht CJ, Mokhtari K, Wesseling P, Villa S, Eisenhauer E, Gorlia T, Weller M, Lacombe D, Cairncross JG and Mirimanoff RO (2009) Effects of radiotherapy with concomitant and adjuvant temozolomide versus radiotherapy alone on survival in glioblastoma in a randomised phase III study: 5-year analysis of the EORTC-NCIC trial. *Lancet Oncol* 10:459-466.

Stupp R, Mason WP, van den Bent MJ, Weller M, Fisher B, Taphoorn MJ, Belanger K, Brandes AA, Marosi C, Bogdahn U, Curschmann J, Janzer RC, Ludwin SK, Gorlia T, Allgeier A, Lacombe D, Cairncross JG, Eisenhauer E and Mirimanoff RO (2005) Radiotherapy plus concomitant and adjuvant temozolomide for glioblastoma. *N Engl J Med* 352:987-996.

Takano S, Yoshii Y, Kondo S, Suzuki H, Maruno T, Shirai S and Nose T (1996) Concentration of vascular endothelial growth factor in the serum and tumor tissue of brain tumor patients. *Cancer Res* 56:2185-2190.

Tang SC, Lagas JS, Lankheet NA, Poller B, Hillebrand MJ, Rosing H, Beijnen JH and Schinkel AH (2011) Brain accumulation of sunitinib is restricted by P-glycoprotein (ABCB1) and breast cancer resistance protein (ABCG2) and can be enhanced by oral elacridar and sunitinib coadministration. *Int J Cancer*.

Theeler BJ and Groves MD (2011) High-grade gliomas. *Curr Treat Options Neurol* 13:386-399.

van Asperen J, Schinkel AH, Beijnen JH, Nooijen WJ, Borst P and van Tellingen O (1996) Altered pharmacokinetics of vinblastine in Mdr1a P-glycoprotein-deficient Mice. *J Natl Cancer Inst* 88:994-999.

Vredenburgh JJ, Desjardins A, Herndon JE, 2nd, Marcello J, Reardon DA, Quinn JA, Rich JN, Sathornsumetee S, Gururangan S, Sampson J, Wagner M, Bailey L, Bigner DD, Friedman AH and Friedman HS (2007) Bevacizumab plus irinotecan in recurrent glioblastoma multiforme. *J Clin Oncol* 25:4722-4729.

Vredenburgh JJ, Desjardins A, Reardon DA, Peters KB, Herndon JE, 2nd, Marcello J, Kirkpatrick JP, Sampson JH, Bailey L, Threatt S, Friedman AH, Bigner DD and Friedman HS (2011) The addition of bevacizumab to standard radiation therapy

and temozolomide followed by bevacizumab, temozolomide, and irinotecan for newly diagnosed glioblastoma. *Clin Cancer Res* 17:4119-4124.

Wachsberger PR, Lawrence RY, Liu Y, Xia X, Andersen B and Dicker AP (2011) Cediranib enhances control of wild type EGFR and EGFRvIII-expressing gliomas through potentiating temozolomide, but not through radiosensitization: implications for the clinic. *J Neurooncol*.

Weil RJ, Palmieri DC, Bronder JL, Stark AM and Steeg PS (2005) Breast cancer metastasis to the central nervous system. *Am J Pathol* 167:913-920.

Wong ET, Hess KR, Gleason MJ, Jaeckle KA, Kyritsis AP, Prados MD, Levin VA and Yung WK (1999) Outcomes and prognostic factors in recurrent glioma patients enrolled onto phase II clinical trials. *J Clin Oncol* 17:2572-2578.

Wurdinger T and Tannous BA (2009) Glioma angiogenesis: Towards novel RNA therapeutics. *Cell Adh Migr* 3:230-235.

Yang JJ, Milton MN, Yu S, Liao M, Liu N, Wu JT, Gan L, Balani SK, Lee FW, Prakash S and Xia CQ (2010) P-glycoprotein and breast cancer resistance protein affect disposition of tandutinib, a tyrosine kinase inhibitor. *Drug Metab Lett* 4:201-212.

Zhang J, Zhao P, Fu Z, Chen X, Liu N, Lu A, Li R, Shi L, Pu P, Kang C and You Y (2008) Glioma cells enhance endothelial progenitor cell angiogenesis via VEGFR-2, not VEGFR-1. *Oncol Rep* 20:1457-1463.

Zhao R, Raub TJ, Sawada GA, Kasper SC, Bacon JA, Bridges AS and Pollack GM (2009) Breast cancer resistance protein interacts with various compounds in vitro, but plays a minor role in substrate efflux at the blood-brain barrier. *Drug Metab Dispos* 37:1251-1258.

Zhou S, Schuetz JD, Bunting KD, Colapietro AM, Sampath J, Morris JJ, Lagutina I, Grosveld GC, Osawa M, Nakauchi H and Sorrentino BP (2001) The ABC transporter Bcrp1/ABCG2 is expressed in a wide variety of stem cells and is a molecular determinant of the side-population phenotype. *Nat Med* 7:1028-1034.

References for Chapter 2

Batchelor TT, Duda DG, Di Tomaso E, Ancukiewicz M, Plotkin SR, Gerstner E, Eichler AF, Drappatz J, Hochberg FH, Benner T, Louis DN, Cohen KS, Chea H, Exarhopoulos A, Loeffler JS, Moses MA, Ivy P, Sorensen AG, Wen PY and Jain RK (2010) Phase II Study of Cediranib, an Oral Pan-Vascular Endothelial Growth Factor Receptor Tyrosine Kinase Inhibitor, in Patients With Recurrent Glioblastoma. *Journal of Clinical Oncology* **28**:2817-2823.

Dietrich J, Wang D and Batchelor TT (2009) Cediranib: profile of a novel anti-angiogenic agent in patients with glioblastoma. *Expert Opin Investig Drugs* **18**:1549-1557.

Lenz EM, Spear M, Drake C, Pollard CR, Ward M, Schulz-Utermoehl T and Harrison M Characterisation and identification of the human N+-glucuronide metabolite of cediranib. *J Pharm Biomed Anal* **53**:526-536.

Medinger M, Esser N, Zirrgiebel U, Ryan A, Jurgensmeier JM and Drevs J (2009) Antitumor and antiangiogenic activity of cediranib in a preclinical model of renal cell carcinoma. *Anticancer Res* **29**:5065-5076.

Sharma PS, Sharma R and Tyagi T (2011) VEGF/VEGFR Pathway Inhibitors as Anti-Angiogenic Agents: Present and Future. *Curr Cancer Drug Targets* **11**:624-653.

Siemann DW, Brazelle WD and Jurgensmeier JM (2009) The vascular endothelial growth factor receptor-2 tyrosine kinase inhibitor cediranib (Recentin; AZD2171) inhibits endothelial cell function and growth of human renal tumor xenografts. *Int J Radiat Oncol Biol Phys* **73**:897-903.

Takeda M, Arao T, Yokote H, Komatsu T, Yanagihara K, Sasaki H, Yamada Y, Tamura T, Fukuoka K, Kimura H, Saijo N and Nishio K (2007) AZD2171 shows potent antitumor activity against gastric cancer over-expressing fibroblast growth factor receptor 2/keratinocyte growth factor receptor. *Clin Cancer Res* **13**:3051-3057.

Wedge SR, Kendrew J, Hennequin LF, Valentine PJ, Barry ST, Brave SR, Smith NR, James NH, Dukes M, Curwen JO, Chester R, Jackson JA, Boffey SJ, Kilburn LL, Barnett S, Richmond GH, Wadsworth PF, Walker M, Bigley AL, Taylor ST,

Cooper L, Beck S, Jurgensmeier JM and Ogilvie DJ (2005) AZD2171: a highly potent, orally bioavailable, vascular endothelial growth factor receptor-2 tyrosine kinase inhibitor for the treatment of cancer. *Cancer Res* **65**:4389-4400.

References for Chapter 3

Agarwal S, Sane R, Gallardo JL, Ohlfest JR and Elmquist WF (2010a) Distribution of gefitinib to the brain is limited by P-glycoprotein (ABCB1) and breast cancer resistance protein (ABCG2)-mediated active efflux. *J Pharmacol Exp Ther* **334**:147-155.

Agarwal S, Sane R, Ohlfest JR and Elmquist WF (2010b) The role of the breast cancer resistance protein (ABCG2) in the distribution of sorafenib to the brain. *J Pharmacol Exp Ther* **336**:223-233.

Agarwal S, Sane R, Oberoi R, Ohlfest JR and Elmquist WF (2011) Delivery of molecularly targeted therapy to malignant glioma, a disease of the whole brain. *Expert Rev Mol Med* 13:e17.

Batchelor TT, Duda DG, di Tomaso E, Ancukiewicz M, Plotkin SR, Gerstner E, Eichler AF, Drappatz J, Hochberg FH, Benner T, Louis DN, Cohen KS, Chea H, Exarhopoulos A, Loeffler JS, Moses MA, Ivy P, Sorensen AG, Wen PY and Jain RK (2010) Phase II study of cediranib, an oral pan-vascular endothelial growth factor receptor tyrosine kinase inhibitor, in patients with recurrent glioblastoma. *J Clin Oncol* **28**:2817-2823.

Batchelor TT, Sorensen AG, di Tomaso E, Zhang WT, Duda DG, Cohen KS, Kozak KR, Cahill DP, Chen PJ, Zhu M, Ancukiewicz M, Mrugala MM, Plotkin S, Drappatz J, Louis DN, Ivy P, Scadden DT, Benner T, Loeffler JS, Wen PY and Jain RK (2007) AZD2171, a pan-VEGF receptor tyrosine kinase inhibitor, normalizes tumor vasculature and alleviates edema in glioblastoma patients. *Cancer Cell* **11**:83-95.

Breedveld P, Pluim D, Cipriani G, Wielinga P, van Tellingen O, Schinkel AH and Schellens JH (2005) The effect of Bcrp1 (Abcg2) on the in vivo pharmacokinetics and brain penetration of imatinib mesylate (Gleevec): implications for the use of breast cancer resistance protein and P-glycoprotein inhibitors to enable the brain penetration of imatinib in patients. *Cancer Res* **65**:2577-2582.

Carmeliet P and Jain RK (2000) Angiogenesis in cancer and other diseases. *Nature* **407**:249-257.

Chen Y, Agarwal S, Shaik NM, Chen C, Yang Z and Elmquist WF (2009) P-glycoprotein and breast cancer resistance protein influence brain distribution of dasatinib. *J Pharmacol Exp Ther* **330**:956-963.

Dai H, Marbach P, Lemaire M, Hayes M and Elmquist WF (2003) Distribution of STI-571 to the brain is limited by P-glycoprotein-mediated efflux. *J Pharmacol Exp Ther* **304**:1085-1092.

de Vries NA, Zhao J, Kroon E, Buckle T, Beijnen JH and van Tellingen O (2007) P-glycoprotein and breast cancer resistance protein: two dominant transporters working together in limiting the brain penetration of topotecan. *Clin Cancer Res* **13**:6440-6449.

Demeule M, Regina A, Annabi B, Bertrand Y, Bojanowski MW and Beliveau R (2004) Brain endothelial cells as pharmacological targets in brain tumors. *Mol Neurobiol* **30**:157-183.

Giri N, Shaik N, Pan G, Terasaki T, Mukai C, Kitagaki S, Miyakoshi N and Elmquist WF (2008) Investigation of the role of breast cancer resistance protein (Bcrp/Abcg2) on pharmacokinetics and central nervous system penetration of abacavir and zidovudine in the mouse. *Drug Metab Dispos* **36**:1476-1484.

Herold-Mende C, Steiner HH, Andl T, Riede D, Buttler A, Reisser C, Fusenig NE and Mueller MM (1999) Expression and functional significance of vascular endothelial growth factor receptors in human tumor cells. *Lab Invest* **79**:1573-1582.

Hong X, Jiang F, Kalkanis SN, Zhang ZG, Zhang X, Zheng X, Mikkelsen T, Jiang H and Chopp M (2007) Decrease of endogenous vascular endothelial growth factor may not affect glioma cell proliferation and invasion. *J Exp Ther Oncol* **6**:219-229.

Hormigo A, Ding BS and Rafii S (2011) A target for antiangiogenic therapy: vascular endothelium derived from glioblastoma. *Proc Natl Acad Sci U S A* **108**:4271-4272.

Huang H, Held-Feindt J, Buhl R, Mehdorn HM and Mentlein R (2005) Expression of VEGF and its receptors in different brain tumors. *Neurol Res* **27**:371-377.

Kamiie J, Ohtsuki S, Iwase R, Ohmine K, Katsukura Y, Yanai K, Sekine Y, Uchida Y, Ito S and Terasaki T (2008) Quantitative atlas of membrane transporter proteins:

development and application of a highly sensitive simultaneous LC/MS/MS method combined with novel in-silico peptide selection criteria. *Pharm Res* **25**:1469-1483.

Kamoun WS, Ley CD, Farrar CT, Duyverman AM, Lahdenranta J, Lacorre DA, Batchelor TT, di Tomaso E, Duda DG, Munn LL, Fukumura D, Sorensen AG and Jain RK (2009) Edema control by cediranib, a vascular endothelial growth factor receptor-targeted kinase inhibitor, prolongs survival despite persistent brain tumor growth in mice. *J Clin Oncol* **27**:2542-2552.

Kodaira H, Kusuhara H, Ushiki J, Fuse E and Sugiyama Y (2010) Kinetic analysis of the cooperation of P-glycoprotein (P-gp/Abcb1) and breast cancer resistance protein (Bcrp/Abcg2) in limiting the brain and testis penetration of erlotinib, flavopiridol, and mitoxantrone. *J Pharmacol Exp Ther* **333**:788-796.

Kuratsu J, Itoyama Y, Uemura S and Ushio Y (1989) [Regrowth patterns of glioma--cases of glioma regrew away from the original tumor]. *Gan No Rinsho* **35**:1255-1260.

Lee YJ, Kusuhara H, Jonker JW, Schinkel AH and Sugiyama Y (2005) Investigation of efflux transport of dehydroepiandrosterone sulfate and mitoxantrone at the mouse blood-brain barrier: a minor role of breast cancer resistance protein. *J Pharmacol Exp Ther* **312**:44-52.

Lucio-Eterovic AK, Piao Y and de Groot JF (2009) Mediators of glioblastoma resistance and invasion during antivascular endothelial growth factor therapy. *Clin Cancer Res* **15**:4589-4599.

Mentlein R, Forstreuter F, Mehdorn HM and Held-Feindt J (2004) Functional significance of vascular endothelial growth factor receptor expression on human glioma cells. *J Neurooncol* **67**:9-18.

Morelli MP, Brown AM, Pitts TM, Tentler JJ, Ciardiello F, Ryan A, Jurgensmeier JM and Eckhardt SG (2009) Targeting vascular endothelial growth factor receptor-1 and -3 with cediranib (AZD2171): effects on migration and invasion of gastrointestinal cancer cell lines. *Mol Cancer Ther* **8**:2546-2558.

Oostendorp RL, Buckle T, Beijnen JH, van Tellingen O and Schellens JH (2009) The effect of P-gp (Mdr1a/1b), BCRP (Bcrp1) and P-gp/BCRP inhibitors on the in vivo absorption, distribution, metabolism and excretion of imatinib. *Invest New Drugs* **27**:31-40.

Polli JW, Humphreys JE, Harmon KA, Castellino S, O'Mara MJ, Olson KL, John-Williams LS, Koch KM and Serabjit-Singh CJ (2008) The role of efflux and uptake transporters in [N-{3-chloro-4-[(3-fluorobenzyl)oxy]phenyl}-6-[5-({[2-(methylsulfonyl)ethy l]amino}methyl)-2-furyl]-4-quinazolinamine (GW572016, lapatinib) disposition and drug interactions. *Drug Metab Dispos* **36**:695-701.

Polli JW, Olson KL, Chism JP, John-Williams LS, Yeager RL, Woodard SM, Otto V, Castellino S and Demby VE (2009) An unexpected synergist role of P-glycoprotein and breast cancer resistance protein on the central nervous system penetration of the tyrosine kinase inhibitor lapatinib (N-{3-chloro-4-[(3-fluorobenzyl)oxy]phenyl}-6-[5-({[2-(methylsulfonyl)ethy l]amino}methyl)-2-furyl]-4-quinazolinamine; GW572016). *Drug Metab Dispos* **37**:439-442.

Prewett M, Huber J, Li Y, Santiago A, O'Connor W, King K, Overholser J, Hooper A, Pytowski B, Witte L, Bohlen P and Hicklin DJ (1999) Antivascular endothelial growth factor receptor (fetal liver kinase 1) monoclonal antibody inhibits tumor angiogenesis and growth of several mouse and human tumors. *Cancer Res* **59**:5209-5218.

Ramalingam SS, Belani CP, Mack PC, Vokes EE, Longmate J, Govindan R, Koczywas M, Ivy SP, Gandara DR (2010) Phase II study of Cediranib (AZD 2171), an inhibitor of the vascular endothelial growth factor receptor, for second-line therapy of small cell lung cancer (National Cancer Institute #7097). *Journal of thoracic oncology* **8**:1279-1284.

Sasaki T, Tanno S, Shibukawa K, Osanai S, Kawabe J and Ohsaki Y (2008) Administration of VEGF receptor tyrosine kinase inhibitor increases VEGF production causing angiogenesis in human small-cell lung cancer xenografts. *Int J Oncol* **33**:525-532.

Satoh T, Yamaguchi K, Boku N, Okamoto W, Shimamura T, Yamazaki K, Shi X, Mishima H (2011) Phase I results from a two-part Phase I/II study of cediranib in combination with mFOLFOX6 in Japanese patients with metastatic colorectal cancer. *Investigational new drugs*.

Sharma PS, Sharma R and Tyagi T (2011) VEGF/VEGFR Pathway Inhibitors as Anti-Angiogenic Agents: Present and Future. *Curr Cancer Drug Targets*.

Siemann DW, Norris CM, Ryan A and Shi W (2009) Impact of tumor cell VEGF expression on the in vivo efficacy of vandetanib (ZACTIMA; ZD6474). *Anticancer Res* **29**:1987-1992.

Sikkema AH, de Bont ES, Molema G, Dimberg A, Zwiers PJ, Diks SH, Hoving EW, Kamps WA, Peppelenbosch MP and den Dunnen WF (2011) VEGFR-2 signalling activity in paediatric pilocytic astrocytoma is restricted to tumour endothelial cells. *Neuropathol Appl Neurobiol*.

Silbergeld DL and Chicoine MR (1997) Isolation and characterization of human malignant glioma cells from histologically normal brain. *J Neurosurg* **86**:525-531.

Tang SC, Lagas JS, Lankheet NA, Poller B, Hillebrand MJ, Rosing H, Beijnen JH and Schinkel AH (2011) Brain accumulation of sunitinib is restricted by P-glycoprotein (ABCB1) and breast cancer resistance protein (ABCG2) and can be enhanced by oral elacridar and sunitinib coadministration. *Int J Cancer*.

Zhao R, Raub TJ, Sawada GA, Kasper SC, Bacon JA, Bridges AS and Pollack GM (2009) Breast cancer resistance protein interacts with various compounds in vitro, but plays a minor role in substrate efflux at the blood-brain barrier. *Drug Metab Dispos* **37**:1251-1258.

References for Chapter 4

Agarwal S, Sane R, Gallardo JL, Ohlfest JR and Elmquist WF (2010) Distribution of gefitinib to the brain is limited by P-glycoprotein (ABCB1) and breast cancer resistance protein (ABCG2)-mediated active efflux. *J Pharmacol Exp Ther* **334**:147-155.

Bailer AJ (1988) Testing for the equality of area under the curves when using destructive measurement techniques. *J Pharmacokinet Biopharm* **16**:303-309.

Bochkina N and Sapatina T (2005) On The Posterior Median Estimators Of Possibly Sparse Sequences. *Ann. Inst. Statist. Math.* **57**:315-351.

Bonate PL (1998) Coverage and precision of confidence intervals for area under the curve using parametric and non-parametric methods in a toxicokinetic experimental design. *Pharm Res* **15**:405-410.

Brooks SP and Gelman A (1998) Alternative Methods for Monitoring Convergence of Iterative Simulations. *Journal of Computational and Graphical Statistics* **7**:434-455.

Chen Y, Agarwal S, Shaik NM, Chen C, Yang Z and Elmquist WF (2009) P-glycoprotein and breast cancer resistance protein influence brain distribution of dasatinib. *J Pharmacol Exp Ther* **330**:956-963.

Elmquist WF, Chan KK and Sawchuk RJ (1994) Transsynovial drug distribution: synovial mean transit time of diclofenac and other nonsteroidal antiinflammatory drugs. *Pharm Res* **11**:1689-1697.

Gibaldi M (1969) Effect of mode of administration on drug distribution in a two-compartment open system. *J Pharm Sci* **58**:327-331.

Gibaldi M and Perrier D (1982) *Pharmacokinetics*. Dekker, New York.

Jaki T, Wolfsegger MJ and Ploner M (2009) Confidence intervals for ratios of AUCs in the case of serial sampling: a comparison of seven methods. *Pharm Stat* **8**:12-24.

Jelliffe R, Neely M, Schumitzky A, Bayard D, Van Guilder M, Botnen A, Bustad A, Laing D, Yamada W, Bartroff J and Tatarinova T (2011) Nonparametric population modeling and Bayesian analysis. *Pharmacol Res*.

Kalvass JC, Maurer TS and Pollack GM (2007) Use of plasma and brain unbound fractions to assess the extent of brain distribution of 34 drugs: comparison of unbound concentration ratios to in vivo p-glycoprotein efflux ratios, in *Drug Metab Dispos* pp 660-666.

Kamiie J, Ohtsuki S, Iwase R, Ohmine K, Katsukura Y, Yanai K, Sekine Y, Uchida Y, Ito S and Terasaki T (2008) Quantitative atlas of membrane transporter proteins: development and application of a highly sensitive simultaneous LC/MS/MS method combined with novel in-silico peptide selection criteria. *Pharm Res* **25**:1469-1483.

Kitanidis P (1986) Parameter Uncertainty in Estimation of Spatial Functions: Bayesian Analysis. *Water Resources Research* **22**:499-507.

Kodaira H, Kusuhara H, Ushiki J, Fuse E and Sugiyama Y (2010) Kinetic analysis of the cooperation of P-glycoprotein (P-gp/Abcb1) and breast cancer resistance protein (Bcrp/Abcg2) in limiting the brain and testis penetration of erlotinib, flavopiridol, and mitoxantrone. *J Pharmacol Exp Ther* **333**:788-796.

Lunn DJ, Best N, Thomas A, Wakefield J and Spiegelhalter D (2002) Bayesian analysis of population PK/PD models: general concepts and software. *J Pharmacokinet Pharmacodyn* **29**:271-307.

Lunn DJ, Thomas, A., Best, N., and Spiegelhalter, D. (2000) WinBUGS -- a Bayesian modelling framework: concepts, structure, and extensibility. *Statistics and Computing* **10**:325-337.

Navarro-Fontestad C, Gonzalez-Alvarez I, Fernandez-Teruel C, Bermejo M and Casabo VG (2011) A new mathematical approach for the estimation of the AUC and its variability under different experimental designs in preclinical studies. *Pharm Stat*.

Nedelman JR, Gibiansky E and Lau DT (1995) Applying Bailer's method for AUC confidence intervals to sparse sampling. *Pharm Res* **12**:124-128.

Nedelman JR and Jia X (1998) An extension of Satterthwaite's approximation applied to pharmacokinetics. *J Biopharm Stat* **8**:317-328.

Oostendorp RL, Buckle T, Beijnen JH, van Tellingen O and Schellens JH (2009) The effect of P-gp (Mdr1a/1b), BCRP (Bcrp1) and P-gp/BCRP inhibitors on the in

vivo absorption, distribution, metabolism and excretion of imatinib. *Invest New Drugs* **27**:31-40.

R.Development.Core.Team (2010) *R: A language and environment for statistical computing*. R Foundation for Statistical Computing, Vienna, Austria.

Riad LE and Sawchuk RJ (1998) A partial area difference analysis for estimating elimination rate constants and distribution volumes of metabolites. *J Pharm Sci* **87**:769-773.

Sawchuk RJ and Hedaya MA (1990) Modeling the enhanced uptake of zidovudine (AZT) into cerebrospinal fluid. 1. Effect of probenecid. *Pharm Res* **7**:332-338.

Spiegelhalter D, Thomas A, Best N and Lunn D (2003) *WinBUGS Version 1.4 User Manual*. Medical Research Council Biostatistics Unit, Cambridge.

Wolfsegger MJ and Jaki T (2005) Estimation of AUC from 0 to Infinity in Serial Sacrifice Designs. *J Pharmacokinet Pharmacodyn* **32**:757-766.

Wolfsegger MJ and Jaki T (2009) Non-compartmental estimation of pharmacokinetic parameters in serial sampling designs. *J Pharmacokinet Pharmacodyn* **36**:479-494.

Yuan J (1993) Estimation of variance for AUC in animal studies. *J Pharm Sci* **82**:761-763.

References for Chapter 5

Agarwal S, Sane R, Oberoi R, Ohlfest JR and Elmquist WF (2011) Delivery of molecularly targeted therapy to malignant glioma, a disease of the whole brain. *Expert Rev Mol Med* **13**:e17.

Batchelor TT, Sorensen AG, di Tomaso E, Zhang WT, Duda DG, Cohen KS, Kozak KR, Cahill DP, Chen PJ, Zhu M, Ancukiewicz M, Mrugala MM, Plotkin S, Drappatz J, Louis DN, Ivy P, Scadden DT, Benner T, Loeffler JS, Wen PY and Jain RK (2007) AZD2171, a pan-VEGF receptor tyrosine kinase inhibitor, normalizes tumor vasculature and alleviates edema in glioblastoma patients. *Cancer Cell* **11**:83-95.

Butowski N (2011) Anti-angiogenic therapy in glioma. *Clin Transl Oncol* **13**:294-300.

Carlson BL, Grogan PT, Mladek AC, Schroeder MA, Kitange GJ, Decker PA, Giannini C, Wu W, Ballman KA, James CD and Sarkaria JN (2009) Radiosensitizing effects of temozolomide observed in vivo only in a subset of O6-methylguanine-DNA methyltransferase methylated glioblastoma multiforme xenografts. *Int J Radiat Oncol Biol Phys* **75**:212-219.

Carlson BL, Pokorny JL, Schroeder MA and Sarkaria JN (2011) Establishment, Maintenance and in vitro and in vivo Applications of Primary Human Glioblastoma Multiforme (GBM) Xenograft Models for Translational Biology Studies and Drug Discovery. *Curr Protoc Pharmacol* **52**:1-14.

Chen Y, Agarwal S, Shaik NM, Chen C, Yang Z and Elmquist WF (2009) P-glycoprotein and breast cancer resistance protein influence brain distribution of dasatinib. *J Pharmacol Exp Ther* **330**:956-963.

Claes A, Wesseling P, Jeuken J, Maass C, Heerschap A and Leenders WP (2008) Antiangiogenic compounds interfere with chemotherapy of brain tumors due to vessel normalization. *Mol Cancer Ther* **7**:71-78.

Giannini C, Sarkaria JN, Saito A, Uhm JH, Galanis E, Carlson BL, Schroeder MA and James CD (2005) Patient tumor EGFR and PDGFRA gene amplifications retained in an invasive intracranial xenograft model of glioblastoma multiforme. *Neuro Oncol* **7**:164-176.

Hawkins BT, Sykes DB and Miller DS (2010) Rapid, reversible modulation of blood-brain barrier P-glycoprotein transport activity by vascular endothelial growth factor. *J Neurosci* **30**:1417-1425.

Kodaira H, Kusuhara H, Ushiki J, Fuse E and Sugiyama Y (2010) Kinetic analysis of the cooperation of P-glycoprotein (P-gp/Abcb1) and breast cancer resistance protein (Bcrp/Abcg2) in limiting the brain and testis penetration of erlotinib, flavopiridol, and mitoxantrone. *J Pharmacol Exp Ther* **333**:788-796.

Liu H, Yang H, Wang D, Liu Y, Liu X, Li Y, Xie L and Wang G (2009) Insulin regulates P-glycoprotein in rat brain microvessel endothelial cells via an insulin receptor-mediated PKC/NF-kappaB pathway but not a PI3K/Akt pathway. *Eur J Pharmacol* **602**:277-282.

Marchetti S, de Vries NA, Buckle T, Bolijn MJ, van Eijndhoven MA, Beijnen JH, Mazzanti R, van Tellingen O and Schellens JH (2008) Effect of the ATP-binding cassette drug transporters ABCB1, ABCG2, and ABCC2 on erlotinib hydrochloride (Tarceva) disposition in in vitro and in vivo pharmacokinetic studies employing Bcrp1-/-/Mdr1a/1b-/- (triple-knockout) and wild-type mice. *Mol Cancer Ther* **7**:2280-2287.

Thompson EM, Frenkel EP and Neuwelt EA (2011) The paradoxical effect of bevacizumab in the therapy of malignant gliomas. *Neurology* **76**:87-93.

van den Bent MJ, Vogelbaum MA, Wen PY, Macdonald DR and Chang SM (2009) End point assessment in gliomas: novel treatments limit usefulness of classical Macdonald's Criteria. *J Clin Oncol* **27**:2905-2908.

Zhou Q and Gallo JM (2009) Differential effect of sunitinib on the distribution of temozolomide in an orthotopic glioma model. *Neuro Oncol* **11**:301-310.

References for Chapter 6

Batchelor TT, Sorensen AG, di Tomaso E, Zhang WT, Duda DG, Cohen KS, Kozak KR, Cahill DP, Chen PJ, Zhu M, Ancukiewicz M, Mrugala MM, Plotkin S, Drappatz J, Louis DN, Ivy P, Scadden DT, Benner T, Loeffler JS, Wen PY and Jain RK (2007) AZD2171, a pan-VEGF receptor tyrosine kinase inhibitor, normalizes tumor vasculature and alleviates edema in glioblastoma patients. *Cancer Cell* **11**:83-95.

Bergers G and Hanahan D (2008) Modes of resistance to anti-angiogenic therapy. *Nat Rev Cancer* **8**:592-603.

Cai J, Han S, Qing R, Liao D, Law B and Boulton ME (2011) In pursuit of new anti-angiogenic therapies for cancer treatment. *Front Biosci* **16**:803-814.

Carlson MR, Pope WB, Horvath S, Braunstein JG, Nghiemphu P, Tso CL, Mellinghoff I, Lai A, Liau LM, Mischel PS, Dong J, Nelson SF and Cloughesy TF (2007) Relationship between survival and edema in malignant gliomas: role of vascular endothelial growth factor and neuronal pentraxin 2. *Clin Cancer Res* **13**:2592-2598.

Carmeliet P (2005) VEGF as a key mediator of angiogenesis in cancer. *Oncology* **69 Suppl 3**:4-10.

Chamberlain MC, Lassman AB and Iwamoto FM (2010) Patterns of relapse and prognosis after bevacizumab failure in recurrent glioblastoma. *Neurology* **74**:1239-1241.

Hormigo A, Ding BS and Rafii S (2011) A target for antiangiogenic therapy: vascular endothelium derived from glioblastoma. *Proc Natl Acad Sci U S A* **108**:4271-4272.

Iwamoto FM, Abrey LE, Beal K, Gutin PH, Rosenblum MK, Reuter VE, DeAngelis LM and Lassman AB (2009) Patterns of relapse and prognosis after bevacizumab failure in recurrent glioblastoma. *Neurology* **73**:1200-1206.

Kamoun WS, Ley CD, Farrar CT, Duyverman AM, Lahdenranta J, Lacorre DA, Batchelor TT, di Tomaso E, Duda DG, Munn LL, Fukumura D, Sorensen AG and Jain RK (2009) Edema control by cediranib, a vascular endothelial growth factor

receptor-targeted kinase inhibitor, prolongs survival despite persistent brain tumor growth in mice. *J Clin Oncol* **27**:2542-2552.

Norden AD, Young GS, Setayesh K, Muzikansky A, Klufas R, Ross GL, Ciampa AS, Ebbeling LG, Levy B, Drappatz J, Kesari S and Wen PY (2008) Bevacizumab for recurrent malignant gliomas: efficacy, toxicity, and patterns of recurrence. *Neurology* **70**:779-787.

Pope WB, Xia Q, Paton VE, Das A, Hambleton J, Kim HJ, Huo J, Brown MS, Goldin J and Cloughesy T (2011) Patterns of progression in patients with recurrent glioblastoma treated with bevacizumab. *Neurology* **76**:432-437.

Rahman R, Smith S, Rahman C and Grundy R (2010) Antiangiogenic therapy and mechanisms of tumor resistance in malignant glioma. *J Oncol* **2010**:251231.

Stupp R, Hegi ME, Gilbert MR and Chakravarti A (2007) Chemoradiotherapy in malignant glioma: standard of care and future directions. *J Clin Oncol* **25**:4127-4136.

Zuniga RM, Torcuator R, Jain R, Anderson J, Doyle T, Ellika S, Schultz L and Mikkelsen T (2009) Efficacy, safety and patterns of response and recurrence in patients with recurrent high-grade gliomas treated with bevacizumab plus irinotecan. *J Neurooncol* **91**:329-336.

Appendix I

Partial Area Analyses

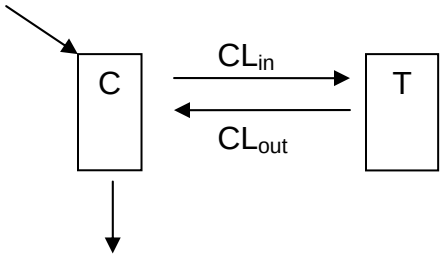

The block schematic diagram above represents a tissue distribution model with intravenous bolus. For simplicity, a two-compartment model was proposed. CL's represent the corresponding clearances in and out of the tissue compartment (T). On the basis of mass balance principles, we can get the following differential equation:

$$V_T \cdot \frac{dC_T}{dt} = CL_{in} \cdot C_C - CL_{out} \cdot C_T \qquad \text{Equation 1}$$

1) Cumulative partial area analysis

Integrating both sides of Equation 1 from time zero to infinity, we get,

$$V_T \cdot \int_0^\infty C_T = CL_{in} \cdot \int_0^\infty C_C \cdot dt - CL_{out} \cdot \int_0^\infty C_T \cdot dt$$

$$0 = CL_{in} \cdot AUC_{0,C}^{\infty} - CL_{out} \cdot AUC_{0,T}^{\infty}$$

Thus,

$$CL_{in} \cdot AUC_{0,C}^{\infty} = CL_{out} \cdot AUC_{0,T}^{\infty}$$

Let R denote the AUC ratio, then

$$R = \frac{AUC_{0,T}^{\infty}}{AUC_{0,C}^{\infty}} = \frac{CL_{in}}{CL_{out}} \qquad \text{Equation 2}$$

Integrating both sides of Equation 1 from time zero to a certain time, t, we get,

$$V_T \cdot \int_0^t C_T = CL_{in} \cdot \int_0^t C_C \cdot dt - CL_{out} \cdot \int_0^t C_T \cdot dt$$

$$V_T \cdot C_{t,T} = CL_{in} \cdot AUC_{0,C}^t - CL_{out} \cdot AUC_{0,T}^t$$

$$C_{t,T} = \frac{CL_{in}}{V_T} \cdot AUC_{0,C}^t - \frac{CL_{out}}{V_T} \cdot AUC_{0,T}^t$$

According to Equation 2, $CL_{in} = R \cdot CL_{out}$, thus

$$C_{t,T} = \frac{CL_{out}}{V_T} \cdot R \cdot AUC_{0,C}^t - \frac{CL_{out}}{V_T} \cdot AUC_{0,T}^t$$

Therefore,

$$C_{t,T} = \frac{CL_{out}}{V_T} \cdot \left(R \cdot AUC_{0,C}^t - AUC_{0,T}^t\right) \qquad \text{Equation 4-1}$$

2) Interval partial area analysis

Integrating both sides of Equation 1 for a certain time interval from t1 to t2, we get,

$$V_T \cdot \int_{t1}^{t2} C_T = CL_{in} \cdot \int_{t1}^{t2} C_C \cdot dt - CL_{out} \cdot \int_{t1}^{t2} C_T \cdot dt$$

$$V_T \cdot \Delta C_T = CL_{in} \cdot AUC_{t1,C}^{t2} - CL_{out} \cdot AUC_{t1,T}^{t2}$$

$$\Delta C_T = \frac{CL_{in}}{V_T} \cdot AUC_{t1,C}^{t2} - \frac{CL_{out}}{V_T} \cdot AUC_{t1,T}^{t2}$$

Since $CL_{in} = R \cdot CL_{out}$,

$$\Delta C_T = \frac{CL_{out}}{V_T} \cdot R \cdot AUC_{t1,C}^{t2} - \frac{CL_{out}}{V_T} \cdot AUC_{t1,T}^{t2}$$

Therefore,

$$\Delta C_T = \frac{CL_{out}}{V_T} \cdot \left(R \cdot AUC_{t1,C}^{t2} - AUC_{t1,T}^{t2}\right) \qquad \text{Equation 4-2}$$

Appendix II

Derivation of Time to Attain Peak Concentration in the Brain

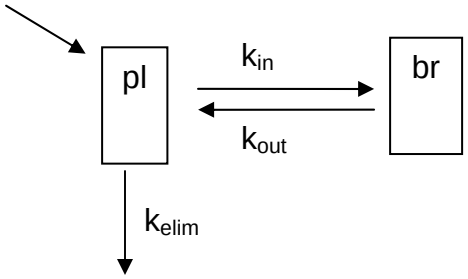

The block schematic diagram above represents a two compartment pharmacokinetic model consisting of a central compartment of plasma (pl) and a brain compartment (br). The drug is administered intravenously into the plasma compartment at time zero. k's represent the corresponding rate constant. Based on this model, two differential equations can be generated as follows:

$$V_{pl} \cdot \frac{dC_{pl}}{dt} = -k_{in} \cdot C_{pl} \cdot V_{pl} - k_{e\lim} \cdot C_{pl} \cdot V_{pl} + k_{out} \cdot C_{br} \cdot V_{br} \qquad \text{Equation 1}$$

$$V_{br} \cdot \frac{dC_{br}}{dt} = k_{in} \cdot C_{pl} \cdot V_{pl} - k_{out} \cdot C_{br} \cdot V_{br} \qquad \text{Equation 2}$$

Laplace transform of Equation 1 is as below:

$$V_{pl} \cdot S \cdot \overline{C_{pl}} - Dose = -k_{in} \cdot V_{pl} \cdot \overline{C_{pl}} - k_{e\lim} \cdot V_{pl} \cdot \overline{C_{pl}} + k_{out} \cdot V_{br} \cdot \overline{C_{br}}$$

$$V_{pl} \cdot \left(S + k_{in} + k_{e\lim}\right) \cdot \overline{C_{pl}} - k_{out} \cdot V_{br} \cdot \overline{C_{br}} = Dose \qquad \text{Equation 3}$$

Laplace transform of Equation 2 is as below:

$$V_{br} \cdot S \cdot \overline{C_{br}} = k_{in} \cdot V_{pl} \cdot \overline{C_{pl}} - k_{out} \cdot V_{br} \cdot \overline{C_{br}}$$

$$V_{br} \cdot \left(S + k_{out}\right) \cdot \overline{C_{br}} - k_{in} \cdot V_{pl} \cdot \overline{C_{pl}} = 0$$

$$\overline{C_{pl}} = \frac{V_{br} \cdot (S + k_{out}) \cdot \overline{C_{br}}}{V_{pl} \cdot k_{in}} \qquad \text{Equation 4}$$

Solve Equation 3 and 4 for $\overline{C_{br}}$:

$$\overline{C_{br}} = \frac{Dose \cdot k_{in}}{V_{br} \cdot \left[S^2 + S \cdot (k_{in} + k_{out} + k_{e\lim}) + k_{out} \cdot k_{e\lim}\right]} = \frac{Dose \cdot k_{in}}{(S + \alpha)(S + \beta) \cdot V_{br}} \qquad \text{Equation 5}$$

where, $\alpha + \beta = k_{in} + k_{out} + k_{e\lim}$ and $\alpha \cdot \beta = k_{out} \cdot k_{e\lim}$.

Solve Equation 5 by Hidden-Hand method, we get the expression of C_{br}:

$$C_{br} = \frac{Dose \cdot k_{in}}{V_{br} \cdot (\alpha - \beta)} \left(e^{-\beta \cdot t} - e^{-\alpha \cdot t}\right) \qquad \text{Equation 6}$$

At the time to attain the peak concentration at the brain compartment (T_{max}), the rate of change in brain concentration is zero. Thus,

$$\frac{dC_{br}}{dt} = \frac{Dose \cdot k_{in}}{V_{br} \cdot (\alpha - \beta)} \left[(-\beta) \cdot e^{-\beta \cdot T_{\max}} - (-\alpha) \cdot e^{-\alpha \cdot T_{\max}}\right] = 0$$

Therefore,

$$\alpha \cdot e^{-\alpha \cdot T_{\max}} - \beta \cdot e^{-\beta \cdot T_{\max}} = 0$$

$$\frac{\alpha}{\beta} = \frac{e^{-\beta \cdot T_{\max}}}{e^{-\alpha \cdot T_{\max}}}$$

$$T\max = \frac{\ln\left(\frac{\alpha}{\beta}\right)}{\alpha - \beta} \qquad \text{Equation 4-18}$$

Appendix III

Derivation of Terminal Phase Brain-to-Plasma Concentration Ratio

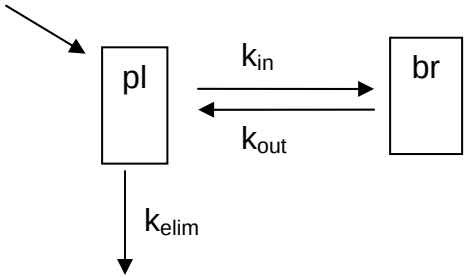

The block schematic diagram above represents a two compartment pharmacokinetic model consisting of a central compartment of plasma (pl) and a brain compartment (br). The drug is administered intravenously into the plasma compartment at time zero. k's represent the corresponding rate constant. Based on this model, two differential equations can be generated as follows:

$$V_{pl} \cdot \frac{dC_{pl}}{dt} = -k_{in} \cdot C_{pl} \cdot V_{pl} - k_{e\lim} \cdot C_{pl} \cdot V_{pl} + k_{out} \cdot C_{br} \cdot V_{br} \qquad \text{Equation 1}$$

$$V_{br} \cdot \frac{dC_{br}}{dt} = k_{in} \cdot C_{pl} \cdot V_{pl} - k_{out} \cdot C_{br} \cdot V_{br} \qquad \text{Equation 2}$$

Laplace transform of Equation 1 is as below:

$$V_{pl} \cdot S \cdot \overline{C_{pl}} - Dose = -k_{in} \cdot V_{pl} \cdot \overline{C_{pl}} - k_{e\lim} \cdot V_{pl} \cdot \overline{C_{pl}} + k_{out} \cdot V_{br} \cdot \overline{C_{br}}$$

$$V_{pl} \cdot \left(S + k_{in} + k_{e\lim}\right) \cdot \overline{C_{pl}} - k_{out} \cdot V_{br} \cdot \overline{C_{br}} = Dose \qquad \text{Equation 3}$$

Laplace transform of Equation 2 is as below:

$$V_{br} \cdot S \cdot \overline{C_{br}} = k_{in} \cdot V_{pl} \cdot \overline{C_{pl}} - k_{out} \cdot V_{br} \cdot \overline{C_{br}}$$

$$V_{br} \cdot \left(S + k_{out}\right) \cdot \overline{C_{br}} - k_{in} \cdot V_{pl} \cdot \overline{C_{pl}} = 0$$

$$\overline{C_{pl}} = \frac{V_{br} \cdot (S + k_{out}) \cdot \overline{C_{br}}}{V_{pl} \cdot k_{in}} \qquad \text{Equation 4}$$

Solve Equation 3 and 4 for $\overline{C_{br}}$:

$$\overline{C_{br}} = \frac{Dose \cdot k_{in}}{V_{br} \cdot \left[S^2 + S \cdot (k_{in} + k_{out} + k_{e\lim}) + k_{out} \cdot k_{e\lim}\right]} = \frac{Dose \cdot k_{in}}{(S + \alpha)(S + \beta) \cdot V_{br}} \qquad \text{Equation 5}$$

where, $\alpha + \beta = k_{in} + k_{out} + k_{e\lim}$ and $\alpha \cdot \beta = k_{out} \cdot k_{e\lim}$.

Solve Equation 3 and 4 for $\overline{C_{pl}}$:

$$\overline{C_{pl}} = \frac{Dose \cdot k_{in}}{(S + \alpha)(S + \beta) \cdot V_{br}} \cdot \frac{V_{br} \cdot (S + k_{out})}{V_{pl} \cdot k_{in}} = \frac{Dose \cdot (S + k_{out})}{(S + \alpha)(S + \beta) \cdot V_{pl}} \qquad \text{Equation 6}$$

Solve Equation 5 and 6 by Hidden-Hand method, we get:

$$C_{br} = \frac{Dose \cdot k_{in}}{V_{br} \cdot (\alpha - \beta)} \left(e^{-\beta \cdot t} - e^{-\alpha \cdot t}\right) \qquad \text{Equation 7}$$

$$C_{pl} = \frac{Dose}{V_{pl} \cdot (\alpha - \beta)} \left[(k_{out} - \beta) e^{-\beta \cdot t} - (\alpha - k_{out}) e^{-\alpha \cdot t}\right] \qquad \text{Equation 8}$$

At terminal phase of elimination, the absorption phase is gone, so

$$C_{br,\beta} = \frac{Dose \cdot k_{in}}{V_{br} \cdot (\alpha - \beta)} \cdot e^{-\beta \cdot t} \qquad \text{Equation 9}$$

$$C_{pl,\beta} = \frac{Dose}{V_{pl} \cdot (\alpha - \beta)} \cdot (k_{out} - \beta) e^{-\beta \cdot t} \qquad \text{Equation 10}$$

$$\left(\frac{C_{br}}{C_{pl}}\right)_{\beta} = \frac{\frac{Dose \cdot k_{in}}{V_{br} \cdot (\alpha - \beta)} \cdot e^{-\beta \cdot t}}{\frac{Dose}{V_{pl} \cdot (\alpha - \beta)} \cdot (k_{out} - \beta) e^{-\beta \cdot t}} = \frac{k_{in} \cdot V_{pl}}{V_{br} \cdot (k_{out} - \beta)} = \frac{k_{in} \cdot V_{pl}}{V_{br} \cdot k_{out} \left(1 - \frac{\beta}{k_{out}}\right)}$$

Since $k_{in} \cdot V_{pl}$ =CL_{in}

$k_{out} \cdot V_{br}$ =$\mathrm{CL_{out}}$

$$\left(\frac{C_{br}}{C_{pl}}\right)_{\beta} = \frac{\frac{CL_{in}}{CL_{out}}}{1-\frac{\beta}{k_{out}}}$$ Equation 11

According to Equation 2,

$$V_{br} \cdot dC_{br} = k_{in} \cdot V_{pl} \cdot C_{pl} \cdot dt - k_{out} \cdot V_{br} \cdot C_{br} \cdot dt$$

Integrate it from time zero to infinity, and we get:

$$V_{br} \cdot \int_0^{\infty} dC_{br} = k_{in} \cdot V_{pl} \cdot \int_0^{\infty} C_{pl} \cdot dt - k_{out} \cdot V_{br} \cdot \int_0^{\infty} C_{br} \cdot dt$$

$$0 = CL_{in} \cdot AUC_{0,pl}^{\infty} - CL_{out} \cdot AUC_{0,br}^{\infty}$$

Thus,

$$\frac{CL_{in}}{CL_{out}} = \frac{AUC_{0,br}^{\infty}}{AUC_{0,pl}^{\infty}}$$ Equation 12

So we get $\left(\frac{C_{br}}{C_{pl}}\right)_{\beta} = \frac{\frac{AUC_{0,br}^{\infty}}{AUC_{0,pl}^{\infty}}}{1-\frac{\beta}{k_{out}}}$ Equation 4-19